

Ph.D. Program in Civil, Chemical and Environmental Engineering
Curriculum in Chemical, Materials and Process Engineering



Department of Civil, Chemical and Environmental Engineering
Polytechnic School, University of Genoa, Italy



**Measurement of Physical Properties of Different Solutions and
Investigation of Their Performance as a Solvent for CO₂ Capture**

Rouzbeh Ramezani

Measurement of Physical Properties of Different Solutions
and
Investigation of Their Performance as a Solvent for CO₂ Capture

BY

ROUZBEH RAMEZANI

*Dissertation discussed in partial fulfillment of
the requirements for the Degree of*

DOCTOR OF PHILOSOPHY

*Civil, Chemical and Environmental Engineering
curriculum in Chemical, Materials and Process Engineering,
Department of Civil, Chemical and Environmental Engineering, University of Genoa, Italy*



November, 2019

Adviser(s):

Prof. Renzo Di Felice – Department of Civil, Chemical and Environmental Engineering, University of Genoa

External Reviewers:

Prof. Laura A. Pellegrini – Department of Chemistry, Materials and Chemical Engineering, Politecnico di Milano

Prof. Mohammad Abu Zahra – Department of Chemical Engineering, Khalifa University of Science and Technology

Examination Committee:

Prof. Antonio Barbucci – Department of Civil, Chemical and Environmental Engineering, University of Genoa

Prof. Camilla Costa – Department of Chemistry and Industrial Chemistry, University of Genoa

Prof. Cristiano Nicoletta – Department of Civil and Industrial Engineering, University of Pisa

Ph.D. program in Civil, Chemical and Environmental Engineering

Curriculum in Chemical, Materials and Process Engineering,

Cycle XXXII

ABSTRACT

Industrial activities such as natural gas purification and fossil-fueled power plants emit high quantities of carbon dioxide (CO₂), which is the most significant greenhouse gas and has a significant impact on climate change. The most industrially practiced technology for CO₂ capture is absorption into various types of amines, particularly monoethanolamine (MEA). However, these absorbents have a limited CO₂ absorption capacity, suffer from solvent losses due to the high volatility in the stripping column, have a high energy consumption in the regeneration step, and are corrosive. Therefore, there is a motivation in finding new alternative absorbents to improve the absorption performance and make post-combustion technology more economical. In this work, after a prescreening, several chemical absorbents including 2-((2-aminoethyl)amino)ethanol (AEEA), methyldiethanolamine (MDEA), piperazine (PZ), triethylenetetramine (TETA), 2-methylpiperazine (2-MPZ), 2-Amino-2-methyl-1-propanol (AMP), monoethanolamine (MEA), trisodium phosphate (TSP), potassium carbonate (K₂CO₃), potassium salts of sarcosine (K-Sar), lysine (K-Lys), glycine (K-Gly), proline (K-Pro), alanine (K-Ala) and serine (K-Ser) were selected based on their chemical structure and also their potential for industrial application. The use of blended absorbents to develop a new solvent with various advantages is considered a suitable method to improve the CO₂ absorption. In this regard, blend solutions of K₂CO₃/TSP with amine additives, MDEA + Lys and MEA + Lys were suggested as absorbent and their CO₂ absorption performance was investigated. Several equipment including stirred cell reactor, Ubbelohde viscometer, Gay-Lussac pycnometer, Benchtop pH meter, Metrohm Autolab were used in this work to study of CO₂ absorption different solutions. Experiment measurements were performed at temperatures between 298 and 323 K, CO₂ partial pressures up to 500 kPa and various concentrations of solvent. Density, viscosity, corrosion rate and as well as pH of solvents were measured. The CO₂ loading capacity of solvent was also determined and the results were compared with other conventional solvents such MEA and MDEA. In addition, the effect of temperature, concentration, pressure and additive type on CO₂ loading capacity of solution was evaluated and explained in details. Reaction mechanism between CO₂ and different solvents was studied and equilibrium constants of reactions were obtained. Then, a thermodynamic model based

on the modified Kent-Eisenberg theory was successfully developed using MATLAB software to predict experimental CO₂ loading data. CO₂ absorption heat was another important parameter of solvent which was reported in this work. Heat of CO₂ absorption of all of blend solutions was estimated using the Gibbs-Helmholtz method and compared with other absorbents. The absorption rate of CO₂ in solvents was measured experimentally using a fall in pressure method. Furthermore, characterization and kinetics of the reaction of CO₂ with solvents was studied and described in detail using zwitterion mechanism. In order to study reaction kinetics, it was necessary to obtain several physical properties of solvents. Therefore, the values of the liquid mass transfer coefficient, overall mass transfer coefficient, Henry's constant, CO₂ and N₂O diffusivity were calculated. The kinetics parameters of each solvent such as Hatta number, enhancement factor, the reaction rate constant, reaction order and activation energy were found and a rate model was developed to describe the experimental absorption rate data. Finally, toxicity of different amines and amino acids was studied and discussed. In this work, 18 blended solutions including 2 inorganic solvents, 5 cyclic diamines, 1 primary amine, 1 tertiary amine, 1 sterically hindered amines, 6 amino acid salts as solvent for CO₂ capture from flue gas were screened in terms of density, viscosity, kinetics, absorption heat, CO₂ loading capacity, toxicity and corrosion rate, and the results were explained in details in next sections. The objectives of this work are, a) to develop of novel solvents for CO₂ capture, b) to measure chemical and physical properties of solvents, c) to understand the fundamental thermodynamic behavior associated with the CO₂ absorption in solvent, d) to evaluate potential of different solutions as solvent for CO₂ capture.

INDEX

List of Tables.....	7
List of Figures.....	9
Thesis objectives and outline.....	15
1. Introduction.....	16
1.1. Global warming and CO ₂ emission.....	16
1.2. Capture technologies.....	16
1.2.1. Post-combustion.....	17
1.2.2. Pre-combustion.....	18
1.2.3. Oxy-combustion.....	18
1.3. CO ₂ capture using chemical solvent.....	19
1.4. Types of solvents.....	20
1.4.1. Amino acids.....	21
1.4.1.1. CO ₂ loading capacity of amino acids.....	23
1.4.1.2. Cyclic capacity of amino acids.....	26
1.4.1.3. Density and viscosity of amino acids.....	28
1.4.1.4. pKa of amino acids.....	29
1.4.1.5. Reactivity of amino acids with CO ₂	29
1.4.1.6. Surface tension of amino acids.....	32
1.4.1.7. Heat of CO ₂ absorption of amino acids.....	34
1.4.1.8. Precipitation of amino acids.....	35
1.4.1.9. Degradation of amino acids.....	35
1.4.1.10. Corrosion rate of amino acids.....	36
1.4.2. Inorganic solvents.....	36
1.4.3. Sterically hindered amines.....	37
1.4.4. Cyclic diamines and polyamines.....	37
1.4.5. Primary amines.....	37
1.4.6. Secondary amines.....	38
1.4.7. Tertiary amines.....	38
1.4.8. Ionic liquid.....	39

1.4.9. Blended solvents.....	39
2. Reaction mechanism.....	41
2.1. Reaction mechanism between CO ₂ and amino acids.....	41
2.2. Reaction mechanism between CO ₂ and MEA.....	42
2.3. Reaction mechanism between CO ₂ and PZ.....	42
2.4. Reaction mechanism between CO ₂ and AEEA.....	43
2.5. Reaction mechanism between CO ₂ and MDEA	43
2.6. Reaction mechanism between CO ₂ and TSP.....	43
2.7. Reaction mechanism between CO ₂ and TETA.....	44
2.8. Reaction mechanism between CO ₂ and AMP.....	44
2.9. Reaction mechanism between CO ₂ and DETA.....	44
2.10. Reaction mechanism between CO ₂ and 2MPZ.....	44
2.11. Reaction mechanism between CO ₂ and K ₂ CO ₃	44
3. Experimental section.....	46
3.1. Materials.....	46
3.2. Experimental gas-liquid contactors.....	48
3.2.1. Stirred cell reactor apparatus.....	49
3.2.1.1. CO ₂ loading capacity measurement.....	50
3.2.1.2. CO ₂ absorption rate measurement.....	51
3.3. Density and viscosity measurement.....	51
3.4. Absorption heat measurement.....	51
3.5. pH measurement.....	52
3.6. Corrosion rate.....	52
4. Results and discussion.....	53
4.1. Preliminary reliability test.....	53
4.2. Absorption characterization of CO ₂ in TSP solution.....	53
4.2.1. CO ₂ loading capacity of TSP	53
4.3. Absorption characterization of CO ₂ in TSP + amine additives.....	56
4.3.1. CO ₂ loading capacity of TSP + additive (1)	56
4.3.2. Absorption rate of CO ₂ in TSP + additive (1)	64

4.3.3. CO ₂ loading capacity of TSP + additive (2)	66
4.3.4. Absorption rate of CO ₂ in TSP + additive (2)	70
4.3.5. Corrosion rate of TSP + additive solution.....	72
4.3.6. Solvent toxicity.....	73
4.4. Absorption characterization of CO ₂ in K ₂ CO ₃ + AEEA, Ala, Ser.....	74
4.4.1. CO ₂ loading capacity of K ₂ CO ₃ + AEEA, Ala, Ser.....	74
4.4.2. Absorption rate of CO ₂ in K ₂ CO ₃ + AEEA, Ala, Ser.....	77
4.4.3. Heat of CO ₂ absorption of K ₂ CO ₃ + AEEA, Ala, Ser.....	80
4.5. Absorption characterization of CO ₂ in K ₂ CO ₃ + 2MPZ.....	85
4.5.1. CO ₂ loading capacity of K ₂ CO ₃ + 2MPZ.....	85
4.5.2. Density and viscosity of K ₂ CO ₃ + 2MPZ.....	86
4.5.3. Diffusivity of CO ₂ in K ₂ CO ₃ + 2MPZ.....	87
4.5.4. Kinetics study of CO ₂ absorption in K ₂ CO ₃ + 2MPZ.....	89
4.6. Absorption characterization of CO ₂ in MEA + K-Lys.....	94
4.6.1. CO ₂ loading capacity of MEA + K-Lys.....	95
4.6.2. Density and viscosity of MEA + K-Lys.....	98
4.6.3. Diffusivity of CO ₂ in MEA + K-Lys.....	100
4.6.4. Kinetics study of CO ₂ absorption in MEA + K-Lys.....	101
4.6.5. Heat of CO ₂ absorption of MEA + K-Lys.....	107
4.7. Absorption characterization of CO ₂ in MDEA + K-Lys.....	108
4.7.1. CO ₂ loading capacity of MDEA + K-Lys.....	108
4.7.2. Density, viscosity and pH of MDEA + K-Lys.....	113
4.7.3. Diffusivity of CO ₂ in MDEA + K-Lys.....	115
4.7.4. Kinetics study of CO ₂ absorption in MDEA + K-Lys.....	116
4.7.5. Heat of CO ₂ absorption of MDEA + K-Lys.....	129
4.8. Absorption characterization of CO ₂ in MEA + Sugar.....	130
4.8.1. Density of MEA + Sugar.....	131
4.8.2. Viscosity of MEA + Sugar.....	135
4.8.3. Overall mass transfer coefficient of MEA + Sugar.....	141
5. Thermodynamic modeling of CO ₂ absorption	148

5.1. Thermodynamic modeling of CO ₂ absorption in MEA.....	148
5.2. Thermodynamic modeling of CO ₂ absorption in K-Lys.....	152
5.3. Thermodynamic modeling of CO ₂ absorption in MEA + K-Lys.....	157
5.4. Thermodynamic modeling of CO ₂ absorption in MDEA + PZ.....	161
6. Conclusion and recommendation for further work.....	165
List of symbols.....	169
List of publications.....	172
References.....	173

List of Tables

Table 1.1: Chemical structure of amino acids.....	22
Table 1.2: Experimental results for CO ₂ loading capacity of different amino acid salt solutions.....	23
Table 1.3: Chemical structure of primary amines.....	38
Table 1.4: Chemical structure of secondary amines.....	38
Table 1.5: Chemical structure of tertiary amines.....	39
Table 3.1: Description of chemical samples used in present work.....	47
Table 3.2: Heat of CO ₂ absorption in aqueous solutions of MEA, DEA and MDEA.....	52
Table 4.1: CO ₂ loading capacity of TSP solution at 313.15 K and different concentrations.....	55
Table 4.2: CO ₂ loading capacity of TSP solution at 323.15 K and different concentrations.....	55
Table 4.3: CO ₂ loading capacity of 2.5 kmol/m ³ TSP solution at different temperatures.....	55
Table 4.4: CO ₂ loading capacity of TSP + TETA solution.....	56
Table 4.5: CO ₂ loading capacity of TSP + K-Gly solution.....	57
Table 4.6: CO ₂ loading capacity of TSP + AMP solution.....	57
Table 4.7: CO ₂ loading capacity of TSP + 2-MPZ solution.....	58
Table 4.8: CO ₂ loading capacity of TSP + K-Pro solution.....	58
Table 4.9: CO ₂ loading capacity of TSP + K-Lys solution at 313.15 K.....	66
Table 4.10: CO ₂ loading capacity of TSP + PZ solution at 313.15 K.....	67
Table 4.11: CO ₂ loading capacity of TSP + AEEA solution at 313.15 K.....	67
Table 4.12: CO ₂ loading capacity of TSP + K-Sar solution at 313.15 K.....	67
Table 4.13: CO ₂ loading capacity of TSP + MDEA solution at 313.15 K.....	67
Table 4.14: CO ₂ loading capacity of K ₂ CO ₃ + AEEA solution at 313.15 K.....	75
Table 4.15: CO ₂ loading capacity of K ₂ CO ₃ + K-Ala solution at 313.15 K.....	75
Table 4.16: CO ₂ loading capacity of K ₂ CO ₃ + K-Ser solution at 313.15 K.....	75
Table 4.17: Value of absorption rate of CO ₂ in 2 M K ₂ CO ₃ + 0.1 M additive.....	77
Table 4.18: Value of absorption rate of CO ₂ in 2 M K ₂ CO ₃ + 0.2 M additive.....	78
Table 4.19: Value of absorption rate of CO ₂ in 2 M K ₂ CO ₃ + 0.3 M additive.....	78
Table 4.20: Heat of CO ₂ absorption in solution of 2 M K ₂ CO ₃ + 0.1 M additive.....	81
Table 4.21: Heat of CO ₂ absorption in solution of 2 M K ₂ CO ₃ + 0.2 M additive.....	81
Table 4.22: Heat of CO ₂ absorption in solution of 2 M K ₂ CO ₃ + 0.3 M additive.....	81

Table 4.23: CO ₂ loading capacity of K ₂ CO ₃ + (0.1-0.5) M 2MPZ solution at 313.15 K.....	85
Table 4.24: Comparison of experimental and literature data of density and viscosity of pure water.....	86
Table 4.25: Density and viscosity of 2 M K ₂ CO ₃ + (0.1-0.5) M 2MPZ solutions.....	86
Table 4.26: The diffusivity of CO ₂ in 2 M K ₂ CO ₃ + (0.1-0.5) M 2MPZ solutions.....	88
Table 4.27: CO ₂ loading capacity of 2 M MEA + (0.2-0.5) M K-Lys solution at 303 K.....	95
Table 4.28: CO ₂ loading capacity of 2 M MEA + (0.2-0.5) M K-Lys solution at 313 K.....	95
Table 4.29: CO ₂ loading capacity of 2 M MEA + (0.2-0.5) M K-Lys solution at 323 K.....	95
Table 4.30: Comparison of experimental data of density and viscosity of MEA and water with literature.....	99
Table 4.31: Density and viscosity of solution of 2 M MEA + (0.2-0.5) M K-Lys.....	99
Table 4.32: The diffusivity of CO ₂ in solutions 2 M MEA + (0.2-0.5) M K-Lys.....	101
Table 4.33: Kinetic data for the CO ₂ + MEA + K-Lys system.....	106
Table 4.34: CO ₂ loading capacity of MDEA + K-Lys solution at 298.15.....	109
Table 4.35: CO ₂ loading capacity of MDEA + K-Lys solution at 303.15.....	109
Table 4.36: CO ₂ loading capacity of MDEA + K-Lys solution at 313.15.....	109
Table 4.37: The values of density and viscosity of MDEA and water.....	113
Table 4.38: Density and viscosity of MDEA + K-Lys solution at 298-313 K.....	113
Table 4.39: The pH of solutions of MDEA and MDEA + K-Lys before absorption at 298-313 K.....	115
Table 5.1: The equilibrium constants of K ₁ to K ₅ for Eqs. (121-125).....	150
Table 5.2: The equilibrium constants of K ₁ to K ₄ for Eqs. (153-156).....	154
Table 5.3: Model parameters fitted in Eq. (120) for the equilibrium constants K ₁ and K ₂	159

List of Figures

Figure 1.1: Proportional emissions of greenhouse gases to the atmosphere.....	16
Figure 1.2: Carbon capture and storage technology.....	17
Figure 1.3: Schematic diagram of post-combustion capture.....	17
Figure 1.4: Schematic diagram of pre-combustion capture.	18
Figure 1.5: Schematic diagram of oxy-combustion capture.....	19
Figure 1.6: Process flow diagram for CO ₂ absorption with chemical absorbent.....	20
Figure 1.7: The CO ₂ loading capacity of different amino acid salt solutions and MEA at 313 K.....	26
Figure 1.8: Values of cyclic capacity of CO ₂ in solutions of amino acid.....	28
Figure 1.9: pKa values of amino acid salts at 298 K in diluted solutions.....	29
Figure 1.10: Reaction rate constant expressions for CO ₂ reacting with amino acid salt solutions.....	31
Figure 1.11: Overall kinetic constants for CO ₂ absorption in amino acid salt solutions at 298 K.....	32
Figure 1.12: Comparison of surface tension of 1 M amino acid salt solutions with MEA and water.....	33
Figure 3.1: Schematic diagram of the vapor-liquid equilibrium equipment.....	50
Figure 4.1: Comparison of experimental CO ₂ loading data of MEA obtained in this work with literature at 313 K.....	53
Figure 4.2: CO ₂ loading capacity of TSP solution at 313.15 K and different concentrations.....	54
Figure 4.3: CO ₂ loading capacity of TSP solution at 323.15 K and different concentrations.....	54
Figure 4.4: The effect of addition of different additives on CO ₂ loading of TSP at 313.15 K and mole fraction 0.2.....	60
Figure 4.5: The effect of addition of different additives on CO ₂ loading of TSP at 313.15 K and mole fraction 0.3.....	60
Figure 4.6: The effect of addition of different additives on CO ₂ loading of TSP at 313.15 K and mole fraction 0.4.....	61
Figure 4.7: The effect of temperature and 2MPZ mole fraction on CO ₂ loading capacity of TSP + 2MPZ solution.....	61
Figure 4.8: The effect of temperature and TETA mole fraction on CO ₂ loading capacity of TSP + TETA solution.....	62
Figure 4.9: The effect of temperature and AMP mole fraction on CO ₂ loading capacity of TSP + AMP solution.....	62
Figure 4.10: The effect of temperature and K-Pro mole fraction on CO ₂ loading capacity of TSP + K-Pro solution.....	63
Figure 4.11: The effect of temperature and K-Gly mole fraction on CO ₂ loading capacity of TSP + K-Gly solution.....	63

Figure 4.12: The effect of addition of additives to TSP solution on the CO ₂ absorption rate at 313.15 K and additive mole fraction 0.2.....	65
Figure 4.13: The effect of addition of additives to TSP solution on the CO ₂ absorption rate at 313.15 K and additive mole fraction 0.3.....	65
Figure 4.14: The effect of addition of additives to TSP solution on the CO ₂ absorption rate at 313.15 K and additive mole fraction 0.4.....	66
Figure 4.15: The effect of addition of additives on CO ₂ loading of TSP at 313.15 K and mole fraction 0.2.....	68
Figure 4.16: The effect of addition of additives on CO ₂ loading of TSP at 313.15 K and mole fraction 0.4.....	69
Figure 4.17: The effect of addition of additives on CO ₂ loading of TSP at 313.15 K and mole fraction 0.5.....	69
Figure 4.18: The effect of addition of additives on the CO ₂ absorption rate of TSP at 313.15 K and additive mole fraction 0.2.....	70
Figure 4.19: The effect of addition of additives on the CO ₂ absorption rate of TSP at 313.15 K and additive mole fraction 0.4.....	71
Figure 4.20: The effect of addition of additives on the CO ₂ absorption rate of TSP at 313.15 K and additive mole fraction 0.5.....	71
Figure 4.21: Comparison of corrosion rate between MEA and TSP+ amine additives at 313.15 K.....	73
Figure 4.22: Values of toxicity of different types of chemical absorbents.....	74
Figure 4.23: The values of CO ₂ loading capacity of 2 M K ₂ CO ₃ + 0.1 M additive at 313.15 K.....	76
Figure 4.24: The values of CO ₂ loading capacity of 2 M K ₂ CO ₃ + 0.2 M additive at 313.15 K.....	76
Figure 4.25: The values of CO ₂ loading capacity of 2 M K ₂ CO ₃ + 0.3 M additive at 313.15 K.....	77
Figure 4.26: The effect of addition of 0.1 M additives on CO ₂ absorption rate of K ₂ CO ₃ at 313.15 K.....	79
Figure 4.27: The effect of addition of 0.2 M additives on CO ₂ absorption rate of K ₂ CO ₃ at 313.15 K.....	79
Figure 4.28: The effect of addition of 0.3 M additives on CO ₂ absorption rate of K ₂ CO ₃ at 313.15 K.....	80
Figure 4.29: The effect of temperature on CO ₂ absorption rate of K ₂ CO ₃ + AEEA solution.....	80
Figure 4.30: Heat of CO ₂ absorption in solution of 2 M K ₂ CO ₃ + 0.1 M additive.....	82
Figure 4.31: Heat of CO ₂ absorption in solution of 2 M K ₂ CO ₃ + 0.2 M additive.....	83
Figure 4.32: Heat of CO ₂ absorption in solution of 2 M K ₂ CO ₃ + 0.3 M additive.....	83
Figure 4.33: Comparison of heat of CO ₂ absorption of K ₂ CO ₃ + additive with the other absorbents.....	84
Figure 4.34: CO ₂ loading capacity of K ₂ CO ₃ + (0.1-0.5) M 2MPZ at 313.15 K.....	85
Figure 4.35: Density of 2 M K ₂ CO ₃ + (0.1–0.5) M 2MPZ solutions.....	87
Figure 4.36: Viscosity of 2 M K ₂ CO ₃ + (0.1–0.5) M 2MPZ solutions.....	87
Figure 4.37: The diffusivity of CO ₂ in 2 M K ₂ CO ₃ + (0.1-0.5) M 2MPZ solutions.....	89

Figure 4.38: The absorption rate of CO ₂ in 2 M K ₂ CO ₃ + (0.1–0.5) M 2MPZ solutions.....	92
Figure 4.39: Plot of log (k _{app}) versus log of concentration of 2MPZ.....	93
Figure 4.40: Arrhenius plot for the CO ₂ + K ₂ CO ₃ + 2MPZ system.....	93
Figure 4.41: Effect of 2MPZ concentration on Ha and Ei at 303 K for K ₂ CO ₃ + 2MPZ system.....	94
Figure 4.42: Partial pressure of CO ₂ as a function of CO ₂ loading capacity of 2 M MEA + 0.2 K-Lys solution.....	96
Figure 4.43: Partial pressure of CO ₂ as a function of CO ₂ loading capacity of 2 M MEA + 0.3 K-Lys solution.....	96
Figure 4.44: Partial pressure of CO ₂ as a function of CO ₂ loading capacity of 2 M MEA + 0.4 K-Lys solution.....	97
Figure 4.45: Partial pressure of CO ₂ as a function of CO ₂ loading capacity of 2 M MEA + 0.5 K-Lys solution.....	97
Figure 4.46: The effect of addition of K-Lys on CO ₂ loading capacity of MEA solution.....	97
Figure 4.47: Comparison of CO ₂ loading of solution of MEA + K-Lys with the other solvents at 313.15 K.....	98
Figure 4.48: Density of solution of MEA blended with K-Lys as a function of K-Lys concentration.....	99
Figure 4.49: Viscosity of solution of MEA blended with K-Lys as a function of K-Lys concentration.....	100
Figure 4.50: The diffusion coefficients of CO ₂ in MEA + K-Lys solution.....	101
Figure 4.51: The CO ₂ absorption rate in MEA + K-Lys at different temperatures and concentrations.....	104
Figure 4.52: Plot of the apparent reaction rate constant versus K-Lys concentration.....	104
Figure 4.53: Plot of the log(k _{app}) versus log of concentration of K-Lys.....	105
Figure 4.54: Arrhenius plot for the CO ₂ + MEA + K-Lys system.....	105
Figure 4.55: Effect of K-Lys concentration on Ha and E _∞ at 313 K for MEA + K-Lys system.....	106
Figure 4.56: Comparison of the overall reaction rate constant of MEA + K-Lys with other blended systems at 313 K.....	107
Figure 4.57: Comparison of heat of CO ₂ absorption of MEA + K-Lys solution with the other absorbents.....	108
Figure 4.58: CO ₂ loading of 1.5 M MDEA + 0.2 M K-Lys solution.....	110
Figure 4.59: CO ₂ loading of 1.5 M MDEA + 0.35 M K-Lys solution.....	110
Figure 4.60: CO ₂ loading of 1.5 M MDEA + 0.5 M K-Lys solution.....	111
Figure 4.61: The effect of concentration of K-Lys on CO ₂ loading capacity of MDEA at 313.15 K.....	111
Figure 4.62: CO ₂ loading capacity of MDEA + K-Lys and other blended solutions at 313 K.....	112
Figure 4.63 Comparison of CO ₂ loading capacity of chemical solvents studied in this work at 313.15 K.....	112
Figure 4.64: The density of 20 wt% MDEA + 10 wt% K-Lys solution after absorption at 298-313 K.....	114

Figure 4.65: The viscosity of 20 wt% MDEA + 10 wt% K-Lys solution after absorption at 298-313 K.....	114
Figure 4.66: The pH of 20 wt% MDEA + 10 wt% K-Lys solution after absorption at 298-313 K.....	115
Figure 4.67: Diffusivity of CO ₂ in MDEA + K-Lys as a function of K-Lys concentration.....	116
Figure 4.68: Comparison of the second-order rate constant calculated in this work with those obtained in the literature.....	118
Figure 4.69: Pressure decay during CO ₂ absorption in solutions of a) 1.5 M MDEA; b) 0.2 M K-Lys; c) 1.5 M MDEA + 0.2 M K-Lys.....	119
Figure 4.70: CO ₂ absorption flux vs. absorption time at different CO ₂ partial pressures for a) 1.5 M MDEA; b) 0.2 M K-Lys; c) 1.5 M MDEA + 0.2 M K-Lys.....	120
Figure 4.71: CO ₂ absorption flux vs. CO ₂ loading at different CO ₂ partial pressures for a) 1.5 M MDEA; b) 0.2 M K-Lys; c) 1.5 M MDEA + 0.2 M K-Lys.....	121
Figure 4.72: The effect of temperature on absorption flux of CO ₂ in MDEA + K-Lys solution, a) P _{CO2} vs. time; b) flux vs. time and c) flux vs. CO ₂ loading.....	122
Figure 4.73: Comparison of performance of CO ₂ absorption rate in different solutions at P _{CO2} =50 kPa, a) P _{CO2} vs. t ; b) flux vs. t and c) flux vs. CO ₂ loading.....	123
Figure 4.74: Comparison of performance of CO ₂ absorption rate in different solutions at P _{CO2} =200 kPa, a) P _{CO2} vs. t ; b) flux vs. t and c) flux vs. CO ₂ loading.....	124
Figure 4.75: Comparison of performance of CO ₂ absorption rate in different solutions at P _{CO2} =350 kPa, a) P _{CO2} vs. t ; b) flux vs. t and c) flux vs. CO ₂ loading.....	125
Figure 4.76: Comparison of performance of CO ₂ absorption rate in different solutions at P _{CO2} =500 kPa, a) P _{CO2} vs. t ; b) flux vs. t and c) flux vs. CO ₂ loading.....	126
Figure 4.77: Comparison of experimental and predicted enhancement factor for CO ₂ absorption in MDEA and K-Lys solutions.....	127
Figure 4.78: Comparison of experimental and predicted CO ₂ absorption flux in MDEA solution.....	128
Figure 4.79: Comparison of experimental and predicted CO ₂ absorption flux in K-Lys solution.....	128
Figure 4.80: Comparison of experimental and predicted pressure decay for CO ₂ absorption in K-Lys solution.....	129
Figure 4.81: Comparison of heat of CO ₂ absorption of MDEA + K-Lys solution with the other absorbents.....	129
Figure 4.82 Comparison of heat of CO ₂ absorption of chemical solvent studied in this work.....	130
Figure 4.83: Density of unloaded and CO ₂ loaded MEA solution at different temperatures.....	131
Figure 4.84: Density of unloaded and CO ₂ loaded MEA + 3wt% sugar solution at different temperatures.....	131

Figure 4.85: Density of unloaded and CO ₂ loaded MEA + 6wt% sugar solution at different temperatures.....	132
Figure 4.86: Density of unloaded and CO ₂ loaded MEA + 10wt% sugar solution at different temperatures.....	132
Figure 4.87: Density of unloaded and CO ₂ loaded MEA + 20wt% sugar solution at different temperatures.....	133
Figure 4.88: The effect of addition of sugar on density of MEA solution at 25 °C.....	133
Figure 4.89: The effect of addition of sugar on density of MEA solution at 40 °C.....	134
Figure 4.90: The effect of addition of sugar on density of MEA solution at 50 °C.....	134
Figure 4.91: The effect of addition of sugar on density of MEA solution at 60 °C.....	135
Figure 4.92: The effect of addition of sugar on density of MEA solution at 70 °C.....	135
Figure 4.93: Viscosity of unloaded and CO ₂ loaded MEA solution at different temperatures.....	136
Figure 4.94: Viscosity of unloaded and CO ₂ loaded MEA + 3wt% sugar solution at different temperatures.....	136
Figure 4.95: Viscosity of unloaded and CO ₂ loaded MEA + 6wt% sugar solution at different temperatures.....	137
Figure 4.96: Viscosity of unloaded and CO ₂ loaded MEA + 10wt% sugar solution at different temperatures.....	137
Figure 4.97: Viscosity of unloaded and CO ₂ loaded MEA + 20wt% sugar solution at different temperatures.....	138
Figure 4.98: The effect of addition of sugar on viscosity of MEA solution at 25 °C.....	138
Figure 4.99: The effect of addition of sugar on viscosity of MEA solution at 40 °C.....	139
Figure 4.100: The effect of addition of sugar on viscosity of MEA solution at 50 °C.....	139
Figure 4.101: The effect of addition of sugar on viscosity of MEA solution at 60 °C.....	140
Figure 4.102: The effect of addition of sugar on viscosity of MEA solution at 70 °C.....	140
Figure 4.103: Schematic diagram of the string of discs contactor.....	141
Figure 4.104: Comparison of overall mass transfer coefficient obtained in this work with literature.....	142
Figure 4.105: The overall mass transfer coefficient as a function of temperature at unloaded solutions..	143
Figure 4.106: The overall mass transfer coefficient as a function of temperature at CO ₂ loading of 0.1.....	143
Figure 4.107: The overall mass transfer coefficient as a function of temperature at CO ₂ loading of 0.2.....	144

Figure 4.108: The overall mass transfer coefficient as a function of temperature at CO ₂ loading of 0.3.....	144
Figure 4.109: The overall mass transfer coefficient as a function of temperature at CO ₂ loading of 0.4.....	145
Figure 4.110: The effect of temperature and CO ₂ loading on overall mass transfer coefficient of MEA.....	145
Figure 4.111: The effect of temperature and CO ₂ loading on overall mass transfer coefficient of MEA+3wt% sugar.....	146
Figure 4.112: The effect of temperature and CO ₂ loading on overall mass transfer coefficient of MEA+6wt% sugar.....	146
Figure 4.113: The effect of temperature and CO ₂ loading on overall mass transfer coefficient of MEA+10wt% sugar.....	147
Figure 4.114: The effect of temperature and CO ₂ loading on overall mass transfer coefficient of MEA+20wt% sugar.....	147
Figure 5.1: Experimental CO ₂ loading of MEA solution compared with model predicted results.....	151
Figure 5.2: The profile of concentration of liquid-phase species in 2.5 M MEA solution.....	152
Figure 5.3: Comparison of experimental CO ₂ loading capacity of K-Lys and model results.....	154
Figure 5.4: Comparison of modeling results between presented model in this work and model presented by in the literature.....	155
Figure 5.5: The profile of concentration of liquid-phase species in 0.5 M K-Lys solution.....	156
Figure 5.6: The profile of concentration of liquid-phase species in 2.5 M K-Lys solution.....	156
Figure 5.7: Model predicted pH of 2.5 M K-Lys solution at 313.15 K.....	157
Figure 5.8: Comparison of experimental CO ₂ loading capacity of 2 M MEA + (0.2-0.5) M K-Lys and model results at different temperatures.....	160
Figure 5.9: The profile of concentration of liquid-phase species in 2 M MEA + 0.5 M K-Lys solution.....	161
Figure 5.10: The profile of concentration of liquid-phase species in 0.84 M MDEA solution.....	163
Figure 5.11: The profile of concentration of liquid-phase species in 0.12 M PZ solution.....	163
Figure 5.12: The profile of concentration of liquid-phase species in 0.84 M MDEA + 0.12 M PZ solution.....	164

Thesis objectives and outline

The selection of a suitable chemical solvent plays a critical role in CO₂ absorption process because the performance of process is significantly dependent on the behavior of the solvent. Monoethanolamine as the most popular solvent in chemical absorption presents several weaknesses, which limits its industrial application. Therefore, a need exists to find more energy efficient and environmentally friendly solvents. This thesis focuses on the development of new chemical solvents for post-combustion CO₂ capture process. To achieve this goal, the physicochemical properties of different types of amine solutions were measured and their CO₂ absorption performance was studied experimentally and theoretically. The chapters of this thesis are organized as follows:

Chapter 1 provides a brief introduction of CO₂ absorption using different technologies. In addition, the main categories of solvents include inorganic absorbents, ionic liquids, alkanolamines, amino acids, cyclic amines and sterically hindered amines was explained in this chapter and their advantages and disadvantages were discussed. The most recent information available in the literature on the potential of using amino acids as a solvent for CO₂ was also reviewed.

Chapter 2 mainly focuses on the reaction mechanism between CO₂ and different chemical solvents.

Chapter 3 introduces different experimental equipment used in this work as well as calculation method for determining physicochemical properties of amine solutions.

Chapter 4 presents absorption characterization of CO₂ in different solvents. The density, viscosity, CO₂ loading capacity, corrosion rate, pH, CO₂ absorption heat, CO₂ diffusivity, CO₂ physical solubility, toxicity, absorption rate and kinetics of CO₂ absorption were measured experimentally, and the results were reported in several tables and figures.

Chapter 5 describes thermodynamic models which were used to predict experimental data obtained in this work.

Chapter 6 summarizes the conclusions from all chapters and gives suggestions for the future work.

INTRODUCTION

1.1. Global warming and CO₂ emission

Nowadays, the earth's rising temperature, due to increasing greenhouse gas emissions from large sources such as fossil fuel power plants, is one of the most important environmental concerns [1]. As shown in Figure 1.1, carbon dioxide (CO₂) emission as an important greenhouse gas is considered to play a major role in climate change, particularly in global warming [2]. The stronger storms, loss of animal and plant habitats, increase in sea level and extreme weather are another environmental issues regarding increasing atmospheric concentration of CO₂ [3]. Hence, CO₂ removal from industrial processes is essential in order to reduce the impacts of greenhouse gases significantly.

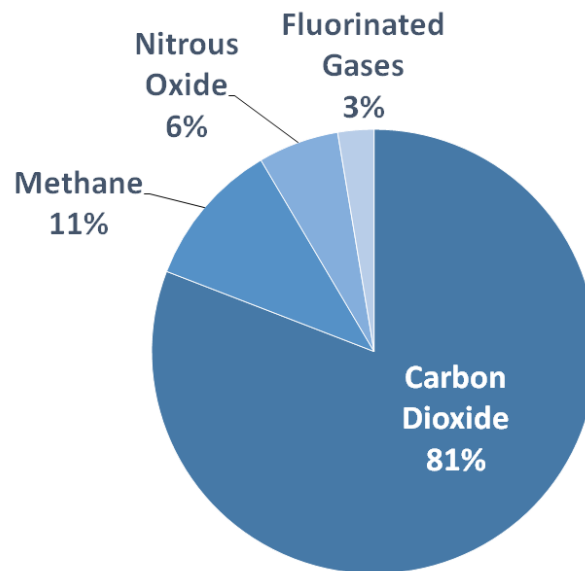


Figure 1.1 Proportional emissions of greenhouse gases to the atmosphere [4]

1.2. Capture technologies

Carbon capture and storage (CCS) is one of the most efficient methods which is applied in the industrial sector and in power generation, and can capture up to 90% of the CO₂ emissions produced from the fossil fuel combustion [5]. As can be seen in Figure 1.2, CCS consists of three main parts including CO₂ absorption, transporting the CO₂ by pipeline or ship, and storing the CO₂. CO₂ capture from power plants can be technically applied by three main technologies including post-combustion CO₂ capture, oxy-combustion and pre-combustion [6].

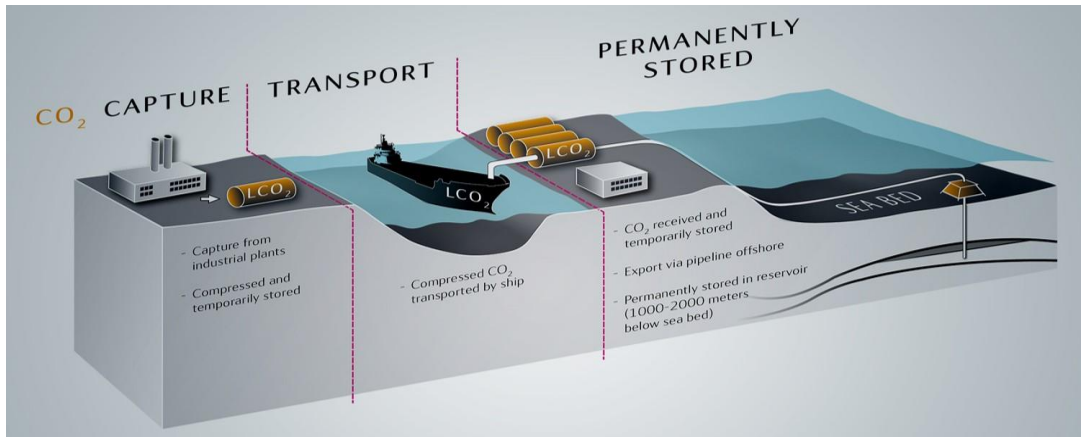


Figure 1.2 Carbon capture and storage technology [7]

1.2.1. Post-combustion

According to Figure 1.3, this technology uses a chemical solvent to absorb CO₂ directly from flue gas which released from fuel combustion in air. Post-combustion capture is widely employed due to its high capture efficiency and scale-up feasibility, and includes several technologies such as cryogenic method, membrane separation process, physical and chemical absorption and physical adsorption [8]. However, low concentration of CO₂ in flue gas is a challenge in this absorption process [9].

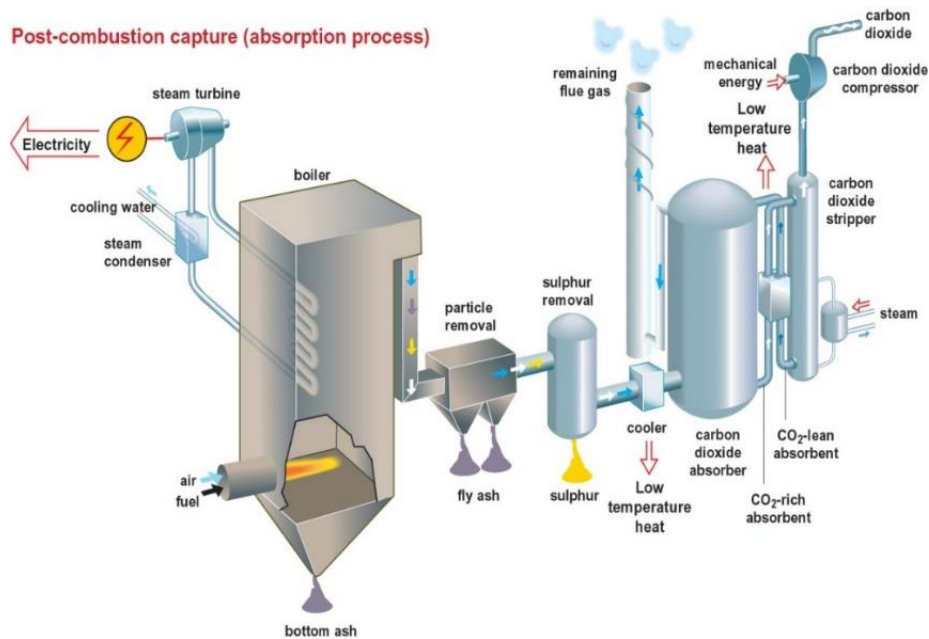


Figure 1.3 Schematic diagram of post-combustion capture [10]

1.2.2. Pre-combustion

Pre-combustion is relatively new technology associated with carbon capture, and is more complex than post-combustion which leads to a higher capital cost. In this approach CO_2 is recovered from a stream before burning the fuel. The advantages of this process are high energy efficiency and high concentration of CO_2 [8]. A schematic representation of this technology is shown in Figure 1.4.

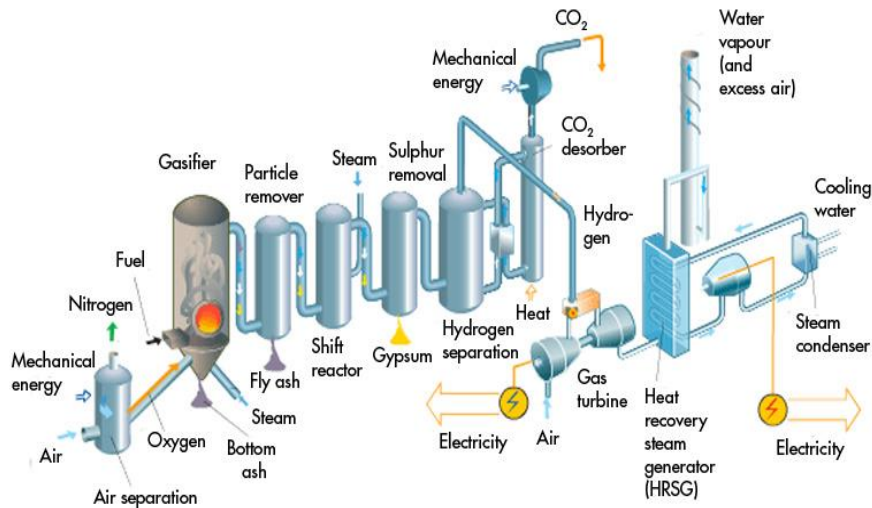


Figure 1.4 Schematic diagram of pre-combustion capture [11]

1.2.3. Oxy-combustion

This technology as given in Figure 1.5 is based on burning the fuel with oxygen instead of air. The drawbacks of this process are high SO_2 concentration in the flue gas, high cost of air separation step and special construction materials requirement for boiler [9].

Each of these three technologies has its own advantages and disadvantages. The choice of the suitable technology depends on the several factors such as gas composition, gas impurities specification and configuration of the actual plant. Pre-combustion can be applied in natural gas combined cycle power generation. However, the required additional investment cost for the syngas generation makes pre-combustion capture from an economic point of view, less attractive compared to the post combustion capture route using chemical solvents [6]. At the moment, post-combustion carbon capture (PCC) is the only industrial CO_2 capture technology being demonstrated at full commercial scale. The post-combustion technologies are cheaper and simpler to be integrated, therefore most of studies and

investment in NGCC focused on post-combustion technologies. This work focuses on post-combustion CO₂ capture technology using chemical solvent.

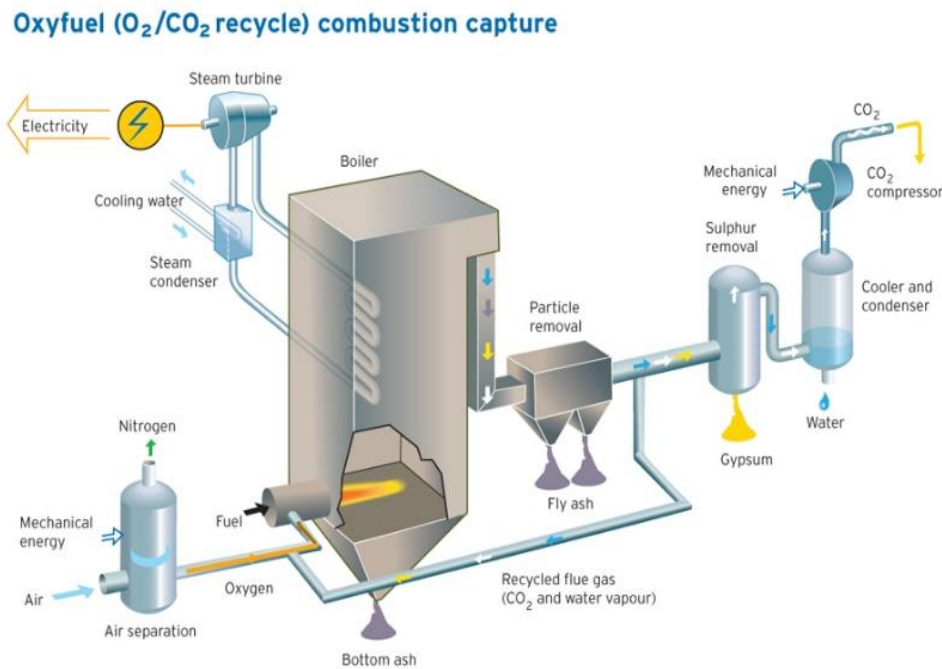


Figure 1.5 Schematic diagram of oxy-combustion capture [11]

1.3. CO₂ capture using Chemical Solvent

CO₂ capture using chemical solvent is the most attractive technology because of its advantages, including its compatibility with the low partial pressure of CO₂ in flue gas and its applicability to the current operating facilities [12]. In this process, flue gas including around 15 % CO₂ is introduced to the bottom of absorption column while reactive solvent is pumped to the top of the column as presented in Figure 1.6. During contact between flue gas and chemical solvent, CO₂ reacts and is absorbed in the solution at 313 K and clean gas leaves absorber. Then, solvent containing CO₂ is fed to desorption column. The solvent is regenerated at temperature around 393 K and the lean solvent again is pumped back to absorption column for another round of absorption [13].

Monoethanolamine (MEA) solution is the most popular chemical solvent for the uptake of CO₂ due to fast reaction kinetics with CO₂, high alkalinity and low cost [14]. However, MEA has several operational issues, including high thermal degradation, low CO₂ loading capacity, corrosion of equipment, solvent loss and high energy consumption for regenerating which leads to a high cost of CO₂ capture process [15]. Other chemical solvents such as methyldiethanolamine (MDEA) and diethanolamine (DEA) solutions have also been used for CO₂ capture but they suffered from similar limitations.

Therefore, the development of new absorbents with desired properties and high performance for CO₂ capture is one of the most effective methods to minimize the cost and penalty in the power plant efficiency, and make the process both more economical efficient as well as environmental safe [16].

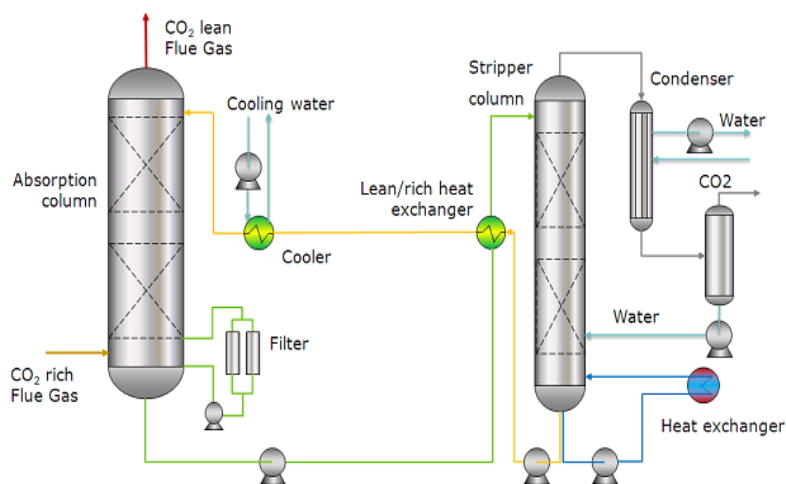


Figure 1.6 Process flow diagram for CO₂ absorption with chemical absorbent [17]

1.4. Types of solvents

The selection of an appropriate absorbent is one of the main challenges in CO₂ absorption process because efficiency and economics of a commercial scale operation depends on solvent characteristics [18]. To be selected as a solvent, it needs to satisfy several desired properties, including high CO₂ loading capacity, fast kinetics with CO₂, low volatility and viscosity, high chemical and thermal stability, low heat of absorption, high CO₂ selectivity, less toxicity and corrosive [19].

Fast reaction kinetics between CO₂ and solvent is necessary because of its relation with height of the absorber tower. A high absorption rate leads to smaller absorber size and thereby lowering the capital investment cost [20]. CO₂ cyclic capacity of solvent is another important parameter which should be considered during solvent selection. A solvent with high cyclic capacity needs lower circulation rate, thus reducing the size and cost of heat exchanger [21]. Energy requirement for regeneration of solvent accounts for about 70% of the overall operating cost [10]. Therefore, that is so important to select an absorbent with low heat of CO₂ absorption to minimize the energy cost of the process [22].

Before applying a new solvent on pilot plant scale, its corrosion rate needs to be evaluated. The corrosion problem has a major effect on the gas absorption process economy because it causes production losses and decreases equipment life time [23]. Foaming, oxidation, thermal degradation, toxicity and volatility are other challenges when implementing chemical absorption with solvent. These solvent limitations can reduce absorption efficiency, equipment life time and impact directly on the plant's economy [24,25].

The main categories of solvents include inorganic absorbents, ionic liquids, alkanolamines, amino acids, cyclic amines and sterically hindered amines which will be explained in the next sections.

1.4.1. Amino acids

An alternative to the use of alkanolamines based solvents are amino acids. Amino acid salt solutions gained interest as solvent because of their advantages over amines such as low volatility, less toxicity, high surface tension as well as being more environmentally friendly [26].

There are 20 common amino acids which are classified into four different groups including cyclic amino acid (proline, 4-hydroxyproline), sterically hindered amino acids (alanine, serine), poly amino acids (asparagine, glutamine, arginine) and linear amino acids (lysine, glycine, taurine) [27]. Chemical structures of amino acids were given in Table 1.1.

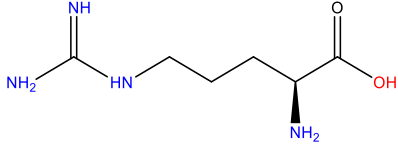
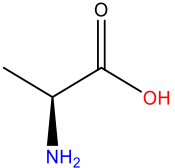
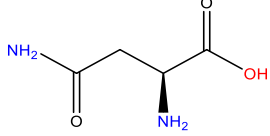
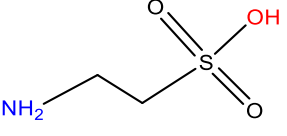
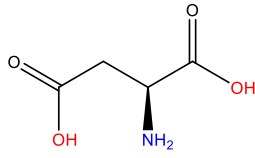
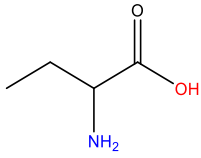
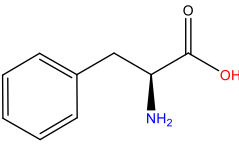
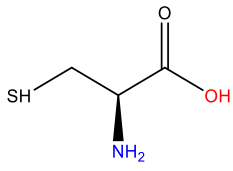
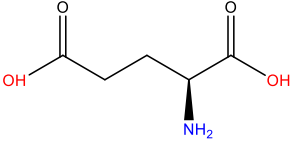
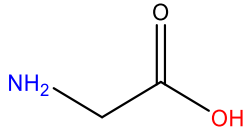
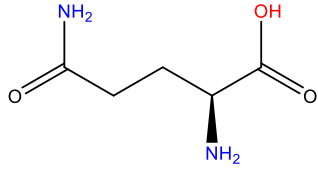
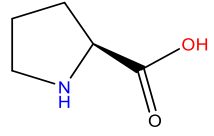
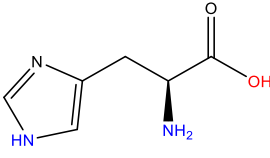
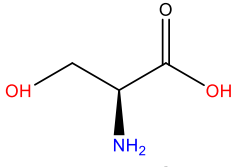
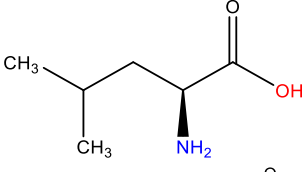
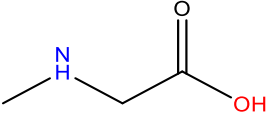
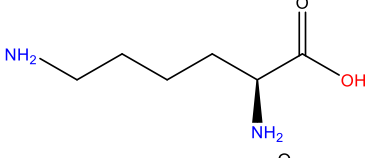
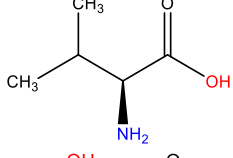
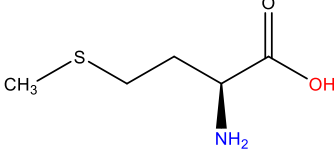
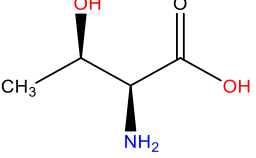
Although amino acid salt solutions are becoming an attractive candidate for CO₂ capture due to their favorable properties, but they still have their own drawback. The challenge associated with amino acid salts is formation of solid product when react with CO₂, especially at high concentration.

The precipitation could cause several operational problems such as fouling and plugging of equipment in the CO₂ capture processes [28]. This drawback limits their application as a single solvent for CO₂ capture at a commercial scale. Addition of amino acids to other amines with low concentration could be a suitable strategy to address this issue, while maintaining the good performance of amino acids.

Several researchers investigated performance of potassium salt of amino acids as absorbent for CO₂ capture. In this section, a comprehensive review of using amino acids as absorbent was provided and their various properties in terms of CO₂ loading capacity, cyclic capacity, density, viscosity, pKa, CO₂ physical solubility, CO₂ diffusivity, kinetic study, reaction rate constant, surface tension, heat of CO₂ absorption, precipitation, solvent degradation and corrosion rate were discussed.

This investigation of different amino acids can be useful for choosing the most appropriate amino acid.

Table 1.1 Chemical structure of amino acids

Amino acid	Molecular Structure	Amino acid	Molecular Structure
Arginine (Arg)		Alanine (Ala)	
Asparagine (Asp)		Taurine (Tau)	
Aspartic acid (Asp acid)		α -Aminobutyric acid (α -ABA)	
Phenylalanine (Phe)		Cysteine (Cys)	
Glutamic acid (Glu acid)		Glycine (Gly)	
Glutamine (Glu)		Proline (Pro)	
Histidine (His)		Serine (Ser)	
Leucine (Leu)		Sarcosine (Sar)	
Lysine (Lys)		Valine (Val)	
Methionine (Met)		Threonine (Thr)	

1.4.1.1. CO₂ loading capacity of amino acids

The CO₂ loading capacity of a solvent which is defined as the number of absorbed CO₂ moles per mole of solvent, is one of the most important parameters of an absorbent in the CO₂ capture process. CO₂ loading data at different temperatures, pressures and solvent concentrations are critical to develop an optimal capture process and helpful in selection of an appropriate solvent [29]. Many publications reported CO₂ loading capacity of amino acid salt solutions at different experimental conditions as listed in Table 1.2.

Table 1.2 Experimental results for CO₂ loading capacity of different amino acid salt solutions.

Solution	T (K)	Concentration	P_{CO₂} (kPa)	CO₂ loading	Ref.
N-Gly	303 - 323	10 - 30 wt%	0.1 - 200	0.17 - 1.07	[34]
K-Gly	293 - 351	0.1 - 3 M	0.1 - 100	0.1 - 1.4	[35]
K-Thr	313	1 M	1 - 42	0.1 - 0.8	[35]
K-Asp	313 - 353	8.5 - 34 wt%	5 - 950	0.17 - 1.22	[36]
K-Glu	313 - 353	9.2 - 36.8 wt%	5 - 950	0.28 - 1.44	[36]
K-Pro	285, 323	0.5 - 3 M	0 - 70	0.5 - 0.9	[37]
K-Lys	313, 333	2.27 M	0.1 - 18	0.88 - 1.12	[15]
N-Phe	303 - 333	10 - 25 wt%	200 - 2500	0.2 - 1.8	[29]
K-Phe	303 - 333	10 - 25 wt%	200 - 2500	0.2 - 1.9	[31]
K-Tau	333 - 373	2 - 6 M	1 - 100	0.1 - 1.1	[33]
N-Ala	303 - 333	10 - 30 wt%	200 - 2500	0.3 - 1.8	[30]
K-Ser	313 - 373	14.3 wt%	0.1 - 433	0.03 - 0.99	[38]

For example, Aftab et al. [30] measured CO₂ loading capacity of 10-30 wt% sodium alaninate (N-Ala) at temperatures of 303 to 333 K and high CO₂ partial pressures. It was found that enhancing N-Ala concentration from 10 to 30 wt% and temperature led to a decrease in CO₂ loading capacity. In addition, the authors compared CO₂ loading capacity of 30 wt% N-Ala solution with MEA, 2-amino-2-methyl-1,3-propanediol (AMPD) and sodium glycinate (N-Gly) at the same concentration and 313.15 K, and observed that N-Ala has higher CO₂ loading capacity than others at CO₂ partial pressures higher than 15 kPa. They explained that the better performance of N-Ala is due to unstable carbamate formation between CO₂ and N-Ala solution.

In another study, Garg et al. [29,31] added sodium hydroxide and potassium hydroxide to phenylalanine in order to prepare sodium and potassium salts of phenylalanine, respectively. They discovered that potassium salt of phenylalanine (K-Phe) showed a better performance than sodium salt of phenylalanine (N-Phe). Moreover, their results showed that 25 wt% K-Phe exhibits higher CO₂ loading capacity than 30 wt% MEA, but lower than 30 wt% MDEA.

The authors also claimed that N-Phe can be considered as an attractive solvent at high partial pressure of CO₂. They explained that unstable carbamate formation as a result of the reaction of sodium salt of phenylalanine with CO₂ is converted to bicarbonate and free amine molecules which leads to high CO₂ loading capacity.

Likewise, Kumar et al. [32] and Wei et al. [33] investigated the CO₂ loading capacity of potassium taurate (K-Tau) at temperatures 298-373 K using stirred-cell reactor. According to their results, the partial pressure of CO₂ increases when concentration of K-Tau decreases from 6 molar to 2 molar due to fewer free K-Tau molecules in lower concentrations.

Subsequently, CO₂ loading capacity data in solutions of N-Gly and potassium glycinate (K-Gly) were published by several researchers. For example, Song et al. [34] compared 10 wt% N-Gly solution with MEA, AMPD and triisopropanolamine (TIPA) at the same concentration and at 313 K. Their results revealed that the CO₂ loading capacity in N-Gly is the highest as compared with the solvents studied. In addition, they indicated that there was no change in the net amount of CO₂ absorbed by N-Gly when the concentration was increased from 20 wt% to 30 wt%.

Potassium salts of asparagine (K-Asp) and glutamine (K-Glu) are another two amino acids that were evaluated by Chen et al. [36] at temperatures and CO₂ partial pressures of 313-353 K and 5-950 kPa, respectively. Their experimental results showed that the CO₂ loading capacity of K-Asp and K-Glu decreases when temperature increases from 313 to 353 K due to the exothermic nature of CO₂ absorption. They also compared the absorption performance of CO₂ in K-Glu solution with two conventional alkanolamines at 313.15 K. Their comparison demonstrated that CO₂ loading in 18 wt% K-Glu was higher than 30 wt% MDEA and 30 wt% 2-amino-2-methyl-1-propanol (AMP). Moreover, CO₂ loading capacity was found to be the same for 17 wt% K-Asp and 16 wt% K-Tau solutions as well as 18 wt% K-Glu and 11 wt% K-Gly solutions.

Majchrowicz et al. [37] obtained CO₂ loading capacity of potassium proline (K-Pro). They observed that CO₂ partial pressure has a positive effect on CO₂ loading capacity of the solution due to the increase in the concentration gradient. In addition, a comparison between K-Pro and MEA solutions showed that K-Pro solution has a higher CO₂ loading capacity than MEA only at low partial pressure of CO₂.

Solutions of potassium serinate (K-Ser) and potassium threonate (K-Thr) were proposed by Song et al. [38] and Portugal et al. [35], respectively. According to their observations, 14.3 wt% K-Ser solution has better CO₂ loading capacity than 15 wt% MEA at CO₂ partial pressures above 10 kPa and 313.15 K while at high temperatures and low CO₂ partial pressure, MEA shows a much better performance.

Kang et al. [40] selected 4 molar potassium sarcosinate (K-Sar) solution as an absorbent for CO₂ capture and studied its performance at temperatures 313, 333 and 353 K using a vapor-liquid equilibrium apparatus. It was found that K-Sar presents the lowest CO₂ loading capacity when compared to K-Ala and

K-Ser solutions at a CO₂ partial pressure of 15 kPa. This weak performance of K-Sar in comparison to other two amino acid salts is due to its lower basicity ($pK_b = 11.64$) than serine ($pK_b = 9.15$) and alanine ($pK_b = 9.69$).

CO₂ loading experiments in potassium lysinate (K-Lys) solutions were carried out by several researchers [15,42]. The results showed that there is no difference between CO₂ loading capacity of 33 wt% and 41 wt% K-Lys. Therefore, the selection of a suitable concentration in this case is necessary to save material cost.

Additionally, K-Lys presented a higher CO₂ loading capacity than K-Pro and MEA solutions which can be explained due to their difference in pH of solution and molecular structure. K-Lys has two amino groups which are involved in the reaction with CO₂ while K-Pro and MEA have only one amino group. In addition, K-Lys solution also has higher pH than K-Pro solution, thus K-Lys is more basic than K-Pro. Since carbamate stability decreases with basicity of α -amino group, greater CO₂ loading capacity is expected [15].

Chang and et al. [41] observed that potassium aminobutyrate (K-ABA) solution shows different behaviors at different partial pressures of CO₂. When partial pressure of CO₂ is high, CO₂ loading of 13 wt% K-ABA solution is greater than 15 wt% MEA and 14 wt% K-Pro at 313.15 K.

However, K-ABA solution absorbs less CO₂ than K-Pro in low partial pressure. The authors explained that this better performance of K-ABA solution is due to bicarbonate formation during reaction with CO₂ while K-Pro produces stable carbamate. Based on the review above, it was found that amino acid solutions have different behaviors at different experimental conditions.

In order to have a better analysis of performance of amino acids in terms of CO₂ loading capacity, a comprehensive comparison between CO₂ loading capacity of potassium and sodium salts of various types of amino acids and MEA solution was carried out at 313.15 K and a wide range of CO₂ partial pressures as presented in Figure 1.7.

It can clearly be seen that K-Lys and K-Glu have the highest CO₂ loading capacity among all amino acid salt solutions. This can be explained by the fact that these two amino acids contain two amino groups in their structures which can absorb more CO₂ during reaction [15].

Serine, glycine and asparagine are other amino acids which exhibit high CO₂ loading capacity due to more amine functional groups than other amino acids. Serine as a primary amino acid provides easier access of CO₂ to its nitrogen atom [38].

This figure also shows that K-ABA, K-Sar and K-Pro have approximately the same CO₂ loading capacity. Proline as a secondary amino acid has an amino group and a distinctive structure of a five-membered ring [39].

It was found that potassium salt of glycine and phenylalanine has a better absorption performance than sodium salt of glycine and phenylalanine. K-Thr and K-Sar solutions indicated the lowest CO₂ loading capacity among the amino acids studied.

Based on the analysis above, most amino acid salt solutions have higher CO₂ loading capacity than MEA solution which makes them attractive solvents for CO₂ capture in terms of CO₂ absorption capacity. Among these amino acids, potassium salts of lysine and glutamine with a higher CO₂ loading capacity could be promising alternatives to MEA solutions.

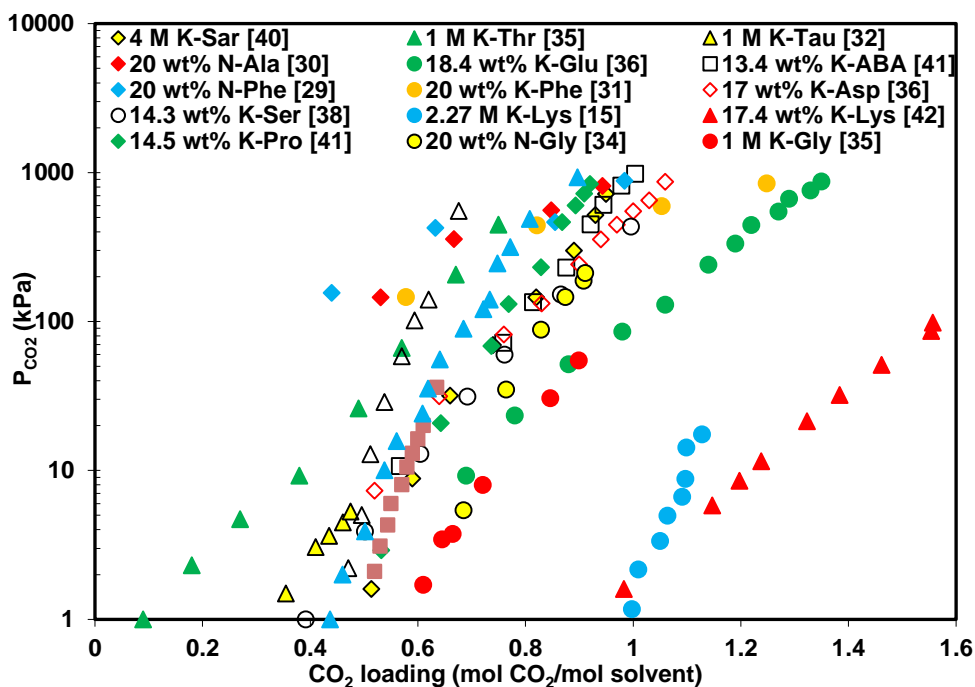


Figure 1.7 The CO₂ loading capacity of different amino acid salt solutions and MEA at 313 K.

1.4.1.2. Cyclic capacity of amino acids

Another important parameter that needs to be considered is cyclic capacity. A solvent with high cyclic capacity is favorable to CO₂ capture because it reduces the size of the column due to reduced absorbent circulation flow rate, thereby reducing process costs [9]. Values of CO₂ cyclic capacity can be calculated from the difference between the CO₂ loading capacity of solvent after absorption (α_{abs}) and the CO₂ loading of solvent after desorption (α_{des}) according to Eq. (1):

$$\alpha_{\text{cyc}} = \alpha_{\text{abs}} - \alpha_{\text{des}} \quad (1)$$

Song et al. [27] reported values of cyclic capacity of some amino acids at absorption and desorption temperatures of 313.15 K and 353.15 K, respectively. They concluded that smaller distances between amino and carboxyl groups and bulkier substituted groups lead to an enhancement of cyclic capacity. In addition, the authors studied the effect of the addition of 0.1 molar piperazine to 1 molar K-Ala, K-Ser

and K-ABA solutions and observed that an enhancement in net cyclic capacity (mol CO₂/mol solvent) from 0.535 to 0.606 for K-Ala, 0.54 to 0.609 for K-ABA and 0.558 to 0.631 for K-Ser solutions. These blend solutions also showed a higher net cyclic capacity than 1 molar MEA solution (0.483 mol CO₂/mol solvent). The strong bonds between CO₂ and MEA which cause a difficult desorption process is the reason for lower cyclic capacity of MEA in comparison with amino acid salt solutions.

Aronu et al. [44] investigated cyclic capacity of 2.5 molar K-Sar solution and compared the results with 2.5 molar MEA solution. It was found that K-Sar has a lower cyclic capacity in comparison with MEA due to the lower equilibrium temperature sensitivity of K-Sar.

CO₂ cyclic capacity of K-Lys at absorption temperature of 313.15 K and desorption temperature of 379.15 K was studied by Zhao et al. [45]. They used two methods, including equilibrium-based and continuous absorption-desorption cycles to calculate cyclic capacity. The findings of their study showed a high cyclic capacity equal to 0.71 (mol CO₂/mol solvent) for 30 wt% K-Lys, which is comparable with 30 wt% MEA solution which is 0.3 (mol CO₂/mol solvent). Moreover, according to their results, cyclic capacity values obtained using a continuous-cycle method are lower than values obtained using the equilibrium-based method due to unlimited time to reach equilibrium.

Bian et al. [46] evaluated the cyclic capacity of 27.5 wt% potassium salt of proline at absorption and desorption temperatures of 298.15 K and 383.15 K, respectively, and concluded that K-Pro has a higher cyclic capacity ($\alpha_{cyc} = 0.37$) than 30 wt% MEA solution ($\alpha_{cyc} = 0.3$). The values of cyclic capacity of several amino acid was reported by Aronu et al. [44] and Zhao et al. [45].

A comparison between CO₂ loading capacity of different amino acid salts and MEA solution was given in Figure 1.8. As can be observed from this figure, the highest and the lowest cyclic capacities among amino acids were attained for K-Lys and K-Sar solutions, respectively. This shows a poor desorption performance for K-Sar which leads to a higher regeneration cost. Although the cyclic capacities of K-Arg, K-Ser and K-Asp were lower than K-Lys, these amino acids indicated better cyclic capacity than the others. K-Arg exhibits the best cyclic capacity among these three amino acids because of its structure. The presence of two primary and two secondary amino groups in its structure make arginine an interesting amino acid in terms of cyclic capacity and CO₂ loading capacity. The K-Ser might be a better choice than K-Asp because serine presents larger values of cyclic capacity and CO₂ loading capacity. Figure 1.8 also shows that K-Tau has a higher cyclic capacity than K-Gly due to the presence of bulky sulfonic groups in the structure of taurine compared to the carboxylic group of glycine [27]. In addition, K-Glu and K-Ala have the same cyclic capacity equal to 0.535 (mol CO₂/mol amine).

As an overall conclusion, potassium salts of lysine, arginine, serine and asparagine offer much better performance than MEA in terms of cyclic capacity which is favorable to CO₂ capture, and thus may be more cost saving than others in industrial application.

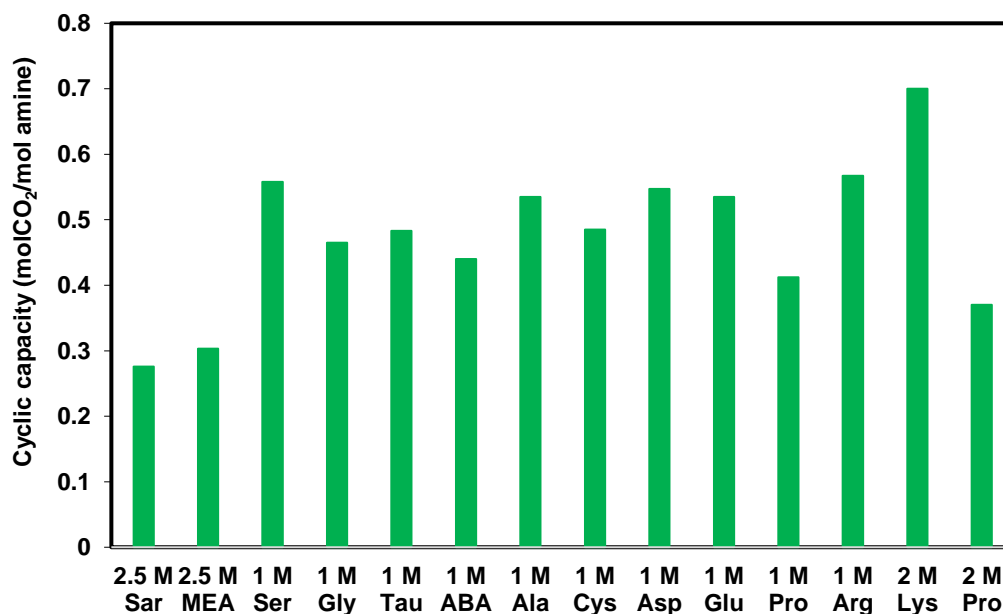


Figure 1.8 Values of cyclic capacity of CO₂ in solutions of amino acid [44,45]

1.4.1.3. Density and viscosity of amino acids

The values of density and viscosity of amino acid salt solutions are necessary for the design of gas-liquid contactors in the absorption process [47]. In the last few years, many researchers have measured the density and viscosity of amino acid salt solutions at different temperatures and concentrations.

Garg et al. [48] showed that density reduces with a rise in temperature. The space between amino acid molecules increases at higher temperatures while the mass stays constant, thus decreasing the density.

It was also found that the density increases when increasing the concentration of amino acids because of the higher availability of amino acids molecules [49].

Shaikh et al. [50] investigated the effect of temperature on viscosity of amino acid salt solutions and concluded that the viscosity decreases with increasing temperature. This effect can be explained due to a decrease in the internal resistance of molecules at high temperature. In addition, the viscosity of amino acids increases as concentration increases. The reason is that as the concentration increases collisions between the molecules increase due to the availability of a higher number of molecules [51].

Since viscosity affects mass transfer, amino acid salt solutions with low viscosity benefit from the diffusion coefficient of CO₂ in the liquid phase, which results in low mass transfer resistance. In addition, future work should focus on density and viscosity of CO₂ loaded amino acid salt solutions.

1.4.1.4. pKa of amino acids

The dissociation constant (pKa) is another parameter of solvent that should be taken into consideration because of its effect on the reaction kinetics of CO₂ with solvent [52]. The values of pKa of several amino acids along with MEA solution at temperature of 298.15 K are presented in Figure 1.9. As can be seen in this figure, most amino acid salt solutions have a greater pKa than MEA which shows high reactivity of the amino group in their structure with CO₂. Therefore, this factor can be useful during amino acid selection for CO₂ absorption.

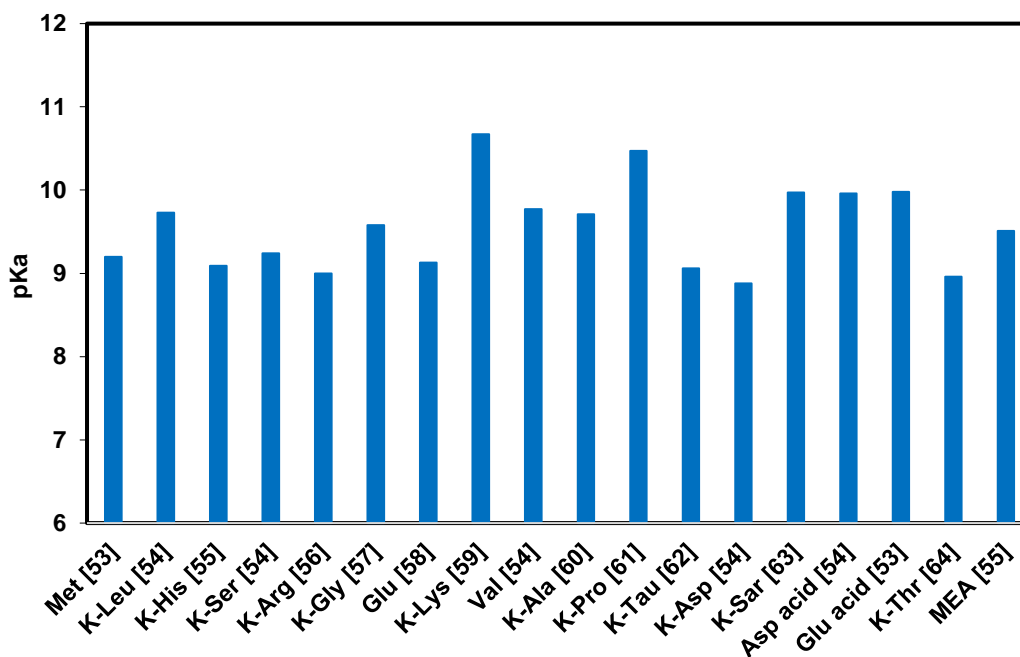


Figure 1.9 pKa values of amino acid salts at 298 K in diluted solutions.

1.4.1.5. Reactivity of amino acids with CO₂

An ideal solvent for CO₂ capture should have a faster absorption rate because it leads to shorter column sizes, thus reducing the capital cost of the absorber [59]. The most widely used techniques to investigate reaction kinetics of CO₂ with chemical absorbents are the string of discs contactor (SDC), wetted-wall column (WWC), stirred-cell reactor (SCR) and stopped-flow technique [65]. Many researchers used these techniques to study the kinetics of the CO₂ absorption in amino acid salt solutions.

Mahmud et al. [66] measured the rate of CO₂ absorption in potassium salts of arginine, sarcosine and glycine at temperatures of 293 to 313 K, concentrations of 0.05 to 2 molar and using the stopped flow technique. Reaction order with respect to K-Gly, K-Sar and K-Arg was found to be 1, 1.22 and 1.2, respectively, which means zwitterion formation is rate-determining. It was also found that the effect of hydroxyl ion in the formation of carbamate for K-Gly + CO₂ and K-Arg + CO₂ systems is negligible while this effect is significant for K-Sar + CO₂ system.

Guo et al. [67] determined kinetics data of CO₂ absorption in 0.5 to 2 molar K-Gly solution using the stopped flow technique and wetted-wall column. They concluded that absorption rate using the stopped flow technique shows slower values in comparison with wetted-wall column.

A string of disks contactor was used by Aronu et al. [68] to study reaction kinetics between CO₂ and K-Sar at temperatures of 298 to 333 K and where the concentration was varied between 1 and 4 M. It was found that the reaction order varies from 1.25 to 1.81 when the concentration of K-Sar increases.

The kinetics of CO₂ absorption in histidine at temperatures and concentrations ranging from 298 to 333 K and 0.2 to 2 M, respectively, using a wetted-wall column were investigated by Shen et al. [55]. The findings of this study showed that K-his has a faster CO₂ absorption rate than MEA solution but lower than K-Lys, K-Sar, K-Pro and K-Gly solutions. The reaction order was also found to be between 1.22 and 1.45 with activation energy equal to 25 kJ/mol.

Kim et al. [60] studied CO₂ absorption rate in 1 to 3 molar K-Ala solution using stirred-cell reactor. The authors observed absorption rate increases as the temperature and concentration of amino acid increases.

Wei et al. [33] proposed potassium salt of taurine and evaluated its absorption rate performance at temperatures up to 353 K using a wetted wall column. They reported values of reaction order with respect to K-Tau and activation energy equal to 1 and 50.5 kJ/mol, respectively. In addition, the overall mass transfer coefficient was measured and the effect of temperature, concentration and CO₂ loading was studied. According to them, the overall mass transfer coefficient increased with temperature and K-Tau concentration while it decreased as CO₂ loading increased. The reduction of overall mass transfer coefficient with CO₂ loading is due to a reduction in free taurate molecules available to react with CO₂. K-Tau solution also showed a faster reaction rate with CO₂ at high temperatures in comparison with MEA solution.

In another study, termolecular and zwitterion reaction mechanisms were used by Sodiq et al. [75] to analyze CO₂ absorption kinetics in sodium salts of proline and taurine solution using the stopped flow technique. The zwitterion formation was found to be the rate-determining step during reaction with CO₂. They also indicated that N-Pro has a faster reaction rate with CO₂ than N-Tau solution.

Portugal et al. [64] measured CO₂ absorption rate in K-Thr at temperatures from 293 to 313 K using a stirred-cell reactor. It was found that K-The exhibits a faster reaction rate than diethanolamine (DEA) but slower than K-Gly.

Kinetics measurement of CO₂ absorption in 0.25 to 2 molar K-Lys and at temperatures of 298 to 333 were performed by Shen et al. [59]. The authors demonstrated that K-Lys has a higher chemical reactivity with CO₂ than K-Pro, K-Sar and MEA solutions. The reaction order was found to be between 1.36 and 1.54 with respect to K-Lys with means zwitterion deprotonation steps are not much faster than the zwitterion formation step.

Song et al. [27] studied absorption and desorption rate performance of several amino acids based on their molecular structure. They categorized amino acids into four groups, including sterically hindered amino acids, poly amino acids, cyclic amino acids and linear amino acids. They concluded that a slower absorption rate and faster desorption rate can be achieved for linear amino acids with smaller distances between amino and carboxyl groups and bulkier substituted groups. The sterically hindered amino acids also showed a slow absorption rate and high desorption rate due to the bulkier substituent group that exhibited stronger steric repulsion. The presence of carbonyl oxygen in structure of di-amino acids leads to a faster desorption rate and slower absorption rate. Moreover, the slow desorption rate and fast absorption rate were explained due to the protruding structures of the cyclic amino acids.

The Arrhenius curves of the reaction rate constants between CO_2 and different amino acid salts were shown in Figure 1.10. In addition, a comparison between absorption rate performance of different amino acids is necessary in order to better understand the results in the literature. Therefore, overall reaction rate constant (K_{ov}) as a function of amino acid concentration at 298.15 K is shown in Figure 1.11. As illustrated in this figure, lysine and sarcosine present the fastest reaction kinetics while taurine shows the slowest reaction rate among all amino acids. Although proline, arginine and glycine indicate a lower absorption rate than lysine and sarcosine, their CO_2 absorption rate performance is much better than other amino acids. Arginine has a molecular structure similar to primary amines, and therefore is expected to have a fast reaction rate. It can also be seen that all amino acids except taurine and alanine have better reactivity with CO_2 than MEA at concentrations higher than 1 molar. In summary, potassium salts of lysine, sarcosine and proline are the most promising amino acids for CO_2 capture from the perspective of reaction kinetics.

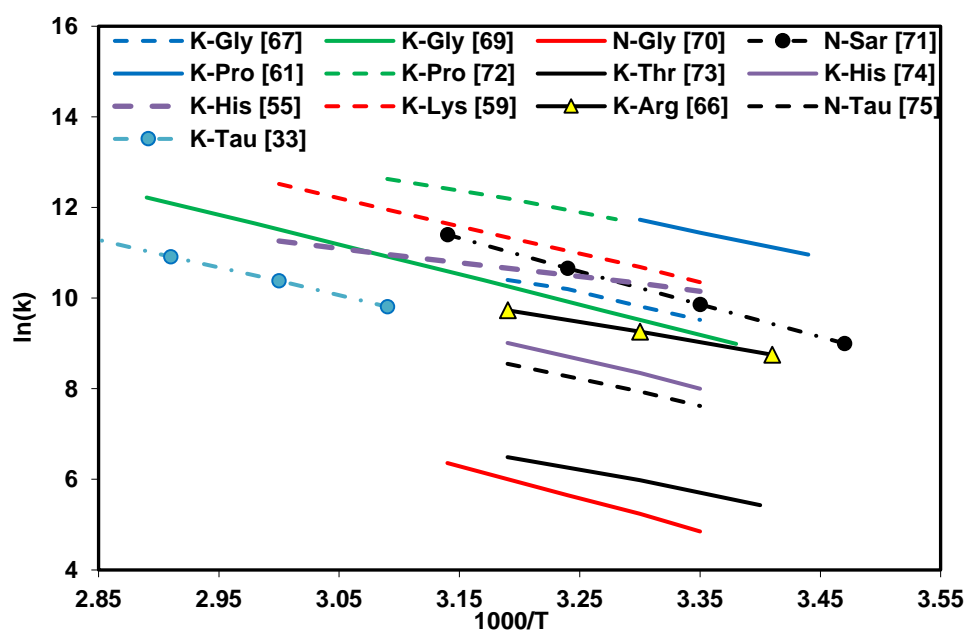


Figure 1.10 Reaction rate constant expressions for CO_2 reacting with amino acid salt solutions.

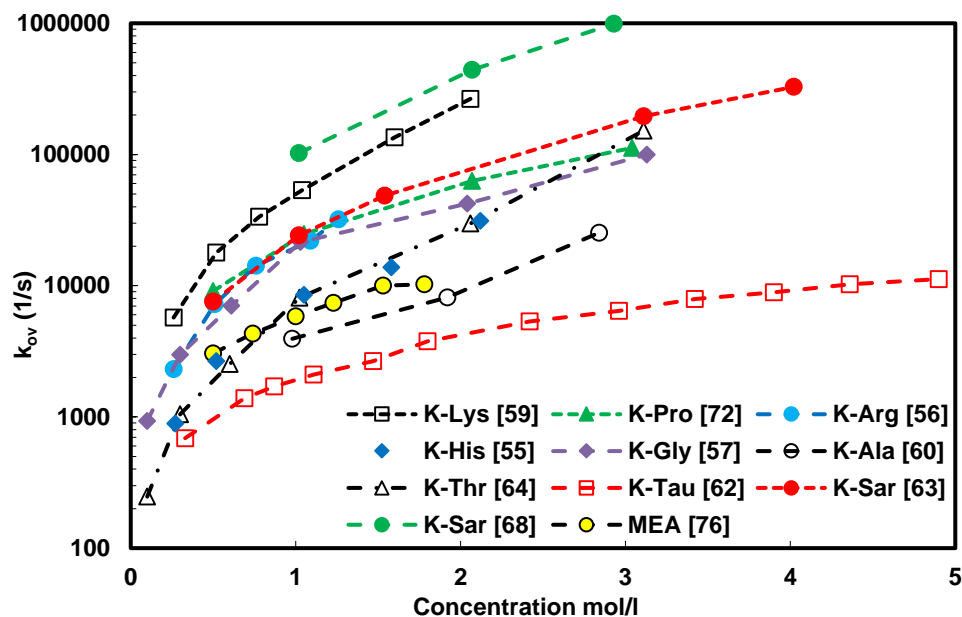


Figure 1.11 Overall kinetic constants for CO₂ absorption in amino acid salt solutions at 298 K.

1.4.1.6. Surface tension of amino acids

High surface tension of amino acids due to their ionic nature is one of the advantages which makes them an attractive absorbent in membrane gas absorption processes because it can avoid pore wetting at the membrane contactor [27]. Since surface tension affects the effective mass transfer area in a packed column, it is necessary to study this parameter at different experimental conditions.

Song et al. [27,38] measured surface tension of several amino acids using a commercial bubble pressure meter at a temperature and concentration of 298.15 K and 2.5 M, respectively. In addition, they added piperazine (PZ) to alanine and serine, and found that the addition of PZ to amino acids decreases their surface tension.

Lee et al. [77] determined surface tension of 10 to 50 wt% N-Gly solution using an automated tensiometer. The results showed that surface tension increases with a rise in concentration of amino acid.

Surface tension of glycine, sarcosine and taurine at 298.15 K were investigated by Park et al. [78]. Their results showed that these three amino acids have higher surface tension than MEA and pure water. They also studied the effect of addition of PZ to taurine and glycine and observed that surface tension decreases with the addition of piperazine to amino acids.

He et al. [79] reported the surface tension of some amino acids at temperatures of 298, 313, 328 and 343 K and concentration of 1 M. According to their results, surface tension of potassium salts of proline, glycine, arginine and sarcosine decreases as temperatures increases from 298 to 343 K.

The surface tensions of 5-25 wt% potassium salt of phenylalanine at temperatures of 298-343 K were determined by Garg et al. [48]. They observed higher values of surface tension for K-Phe when

concentration increases from 5wt% to 25wt%. This effect can be explained by the fact that hydroxyl ions in amino acid salt solution cause the stability of the surface tension to increase with increasing concentration.

A comparison between surface tension of amino acids with water and MEA solution was presented in Figure 1.12. The results demonstrated that K-Gly and K-Pro have the highest and lowest surface tension among amino acids.

Although the surface tension of taurine and alanine is lower than glycine, they showed good performance when compared with other amino acids. It can also be observed that potassium salts of glycine, taurine, alanine, threonine and sarcosine have higher surface tension than water while the surface tension of arginine, phenylalanine and proline were found to be lower than water.

In addition, Figure 1.12 demonstrates that temperature has a negative effect on surface tension. Molecules of water and amino acid salts tend to move apart at high temperature, which causes a weakening of hydrogen bonding. Therefore, surface tension decreases with temperature [48] which can help in finding a suitable absorbent with high surface tension performance at high temperature for the gas absorption process.

From the surface tension point of view, amino acids would be the right choice due to much higher surface tension than MEA which makes them a promising alternative to MEA in a membrane contactor with negligible wetting problem.

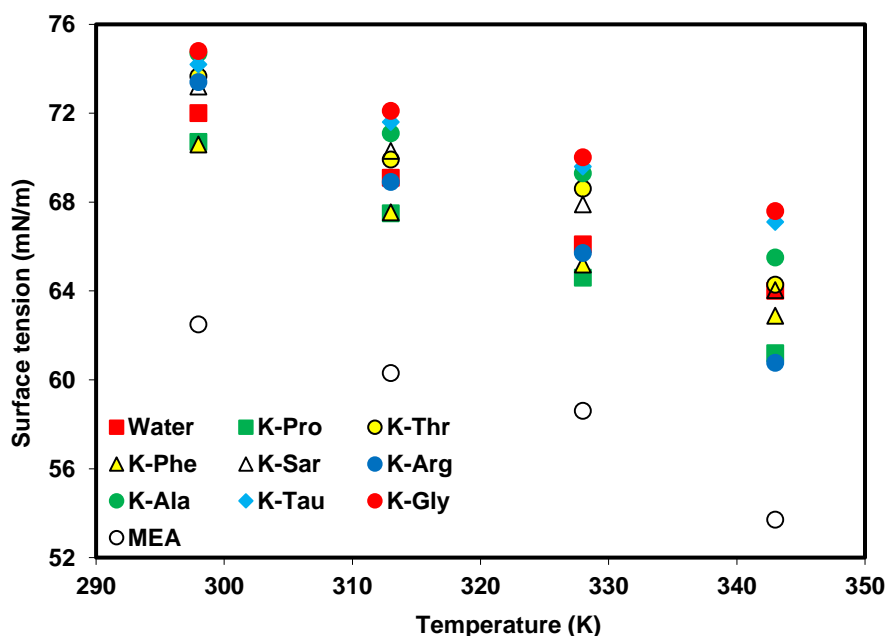


Figure 1.12 Comparison of surface tension of 1 M amino acid salt solutions with MEA and water. Data taken from [27,48,79]

1.4.1.7. Heat of CO₂ absorption of amino acids

The greatest challenge in CO₂ capture using MEA solution is high energy consumption during regeneration of solvent [80]. The reason is that MEA solution as a primary alkanolamine reacts with CO₂ and forms primary stable carbamate which needs high energy for regeneration. Therefore, an important requirement of a CO₂ chemical absorbent is a lower energy requirement for regeneration which leads to reducing total operation costs [81].

Zhao et al. [82] estimated the heat of CO₂ absorption for potassium salt of lysine using the Gibbs-Helmholtz equation and concluded that 20-30wt% K-Lys exhibits a lower absorption heat (55-70 kJ/mol) in comparison with 30 wt% MEA solution (84.5 kJ/mol).

In another study [45], they determined the absorption heat for 32 wt% K-Lys solution at different values of CO₂ loading using a calorimeter. It was found that the heat of CO₂ absorption decreases with increasing CO₂ loading capacity and reaches an absorption heat of about 60 kJ/mol at CO₂ loading equal to 1.2 (mol CO₂/mol solvent). This result can be explained mainly due to the fact that at high CO₂ loading, physical absorption dominates, and bicarbonate is formed that leads to a reduction in heat of CO₂ absorption.

Aronu et al. [83] calculated absorption heat of 3.5 molar potassium salt of sarcosine at CO₂ loading of 0.2 (mol CO₂/mol solvent) and compared it with 30 wt% MEA solution at the same CO₂ loading capacity. According to their work, K-Sar showed absorption heat of 66.7 kJ/mol which is less than MEA with absorption heat 84.5 kJ/mol.

Majchrowicz et al. [37] measured CO₂ solubility of 0.5 molar K-Pro and determined its heat of absorption at CO₂ loading of 0.8 (mol CO₂/mol solvent) using experimental solubility data and the Gibbs-Helmholtz equation. Absorption heat of CO₂ was found to be 54.3 kJ/mol.

Salazar et al. [84] investigated performance of 10 wt% N-Gly solution in terms of absorption heat using a calorimeter and observed N-Gly with absorption heat of 72.5 kJ/mol has a better performance than MEA in terms of absorption heat.

A differential reaction calorimeter was used by Lim et al. [39] in order to study absorption heat of 2.5 molar K-Pro and 2.5 molar K-Ala at temperatures of 298 and 313 K. They reported that absorption heat at 298 K was found to be 53.26 and 90.2 kJ/mol for K-Ala and K-Pro while at 313 K absorption heat was found to be 66.13 and 86.17 kJ/mol for K-Ala and K-Pro, respectively.

Based on their results, K-Ala solution as a sterically hindered amino acid offers lower absorption heat in comparison with K-Pro that can be explained due to unstable carbamate formation. According to the results above, potassium salts of alanine, sarcosine and proline exhibit much lower absorption heat than MEA solution, which makes them an interesting energy-efficient alternative to MEA. Although, some

amino acids showed a lower CO₂ absorption heat than MEA, more work is needed to confirm the better performance of amino acids than other absorbents.

1.4.1.8. Precipitation of amino acids

Although amino acids present many advantages, they also have their own limitations. Amino acids precipitate at high concentrations or high CO₂ loading during CO₂ absorption which causes damage to absorption plant and also reduces mass transfer [28]. However, low concentration of amino acid salts does not produce precipitates.

Aronu et al. [85], Majchrowicz et al. [86] and Rabensteiner et al. [87] showed that precipitation occurs at concentrations higher than 3.5 molar for K-Pro, 4 molar for K-Sar and 30 wt% for K-Gly, respectively.

Kumar [88] studied the effect of precipitation on CO₂ loading capacity on K-Tau at temperatures of 298.15 K to 313.15 K, and observed that precipitation starts at concentrations ≥ 2 molar K-Tau solution and moderate CO₂ loading. They also found that precipitation of the reaction product can be expected to increase the CO₂ loading capacity of K-Tau solution.

Song et al. [38] mentioned that there was no precipitate during CO₂ absorption for 41 wt% K-Lys and 14.3 wt% K-Ser, respectively. Based on the results of precipitation, although precipitation in amino acid salt solutions during CO₂ absorption presents several problems, high CO₂ loading and low regeneration energy were also observed with precipitation. Therefore, more investigation should be performed on the precipitation range of amino acids to use its advantages and minimize its limitations.

1.4.1.9. Degradation of amino acids

Thermal and oxidative degradation are important issues in gas absorption from flue gases because they cause solvent loss, environmental problems and increased corrosion rate [89].

Zhao et al. [45] investigated thermal and oxidative degradation of potassium salt of lysine at 383 and 423 K under static N₂ and O₂ exposure conditions for 15 days. They concluded that K-Lys has high resistance to thermal degradation and less solvent loss than MEA solution.

Aldenkamp et al. [90] investigated degradation performance of K-Gly solution and observed a significant degradation for K-Gly solution at 393 K.

Huang et al. [89] evaluated thermal degradation of several amino acid salt solutions, including N-Sar, N-Gly and N-Ala at temperatures up to 418 K. Their results revealed that tested amino acids have faster degradation rate in comparison with MEA. It was also found that sodium salts of sarcosine and alanine present the slowest and fastest degradation.

Epp et al. [91] measured oxidative degradation of K-Gly solution and found that K-Gly shows less resistance to oxidative degradation when compared to MEA.

Moioli et al. [92] compared the performance of K-Tau as a solvent with MEA and observed much lower degradation rate for K-Tau in comparison with MEA. Studies on the degradation of amino acid salts during CO₂ absorption are rare in the literature, and thus more experiments on the degradation of amino acids are necessary to make a better judgment about them.

1.4.1.10. Corrosion rate of amino acids

Corrosion is a serious problem in gas absorption units because it reduces the equipment life and thus increases capital costs [23]. Since amino acid salt solutions are still new absorbents for CO₂ capture, investigation and experimental data on corrosion rate of amino acids are very scarce in the literature.

Mazinani et al. [93] measured the corrosion rate of K-Lys solution without dissolved CO₂ at concentrations of 0.5, 1.5 and 2.5 molar using electrochemical technique. It was found that the corrosion rate increases from 0.0008 to 0.012 mm/yr as concentration of K-Lys increases from 0.5 to 2.5 molar.

In another study [94], they proposed a blend solution of N-Gly + MEA as a solvent and evaluated its corrosion rate at 308 K. According to their findings, the addition of N-Gly to MEA accelerate the corrosion rate.

Ahn et al. [95] determined the corrosion rate of K-Gly and K-Tau solutions and studied the effect of temperature, CO₂ loading capacity and concentration on corrosion rate. They concluded that with an increasing concentration of amino acid, the corrosion rate of K-Tau increases while the corrosion rate of K-Gly decreases. Potassium salt of taurine indicated a lower corrosion rate when compared to MEA. In addition, they observed the fastest corrosion rate at high temperature and CO₂ loading capacity.

The corrosion rate experiments of MDEA + arginine solution were carried out by Talkhan et al. [96] at a temperature range 293 to 323 K using a three-electrode electrochemical glass cell. The results indicated that the addition of arginine to MDEA decreases the corrosion rate. This trend can be explained by the inhibition effect of arginine. Arginine as an amino acid acts as an inhibitor and reduces the corrosion rate of a blend solution.

The negative and positive effect of amino acids on corrosion rate shows that more investigation on corrosion behavior of amino acids is still required.

1.4.2. Inorganic solvents

Few inorganic solvents proved to have a good potential for absorbing acidic gases. Trisodium phosphate (TSP) and potassium carbonate (K₂CO₃) as inorganic solvents have some benefits in comparison to alkanolamines such as less solvent loss, lower toxicity, high stability towards thermal degradation, better resistance to degradation in the presence of oxygen and weak corrosivity [97].

Due to these favorable properties, they may be a feasible solvent for CO₂ absorption. It was estimated that inorganic solvents such as TSP and K₂CO₃ require less energy for regeneration around 37% of MEA [97]. In addition, potassium carbonate is able to absorb other components such as SO_x and NO_x existing in flue gas [98]. The most important advantage of potassium carbonate is lower regeneration energy in comparison with MEA, which means more efficient and economical regeneration process. However, the main drawback associated with using K₂CO₃ and TSP is their slow absorption rate with CO₂ [20]. In the industrial application, to solve this problem, these solvents are usually mixed with an additive to enhance the CO₂ absorption rate.

Thus, many researchers investigated the effect of the addition of additives to K₂CO₃ and TSP in their studies. Generally, these promoters can be classified into three main categories, including inorganic, organic and enzymatic promoters. There is always a motivation in finding better promoters to enhance the CO₂ absorption rate. To the best of our knowledge, there is limited information on the absorption characterization of CO₂ into TSP solutions. So far, only published experimental data for the solubility of CO₂ in aqueous solutions of the TSP has been presented by Balsora and Mondal [99]. They measured the CO₂ solubility in TSP and showed that TSP has a high CO₂ loading capacity and can be used as a promising alternative absorbent for CO₂ capture.

1.4.3. Sterically hindered amines

Absorbents in this category such as 2-amino-2-ethyl-1,3-propanediol (AEPD), 2-amino-2-methyl-1,3-propanediol (AMPD) and 2-amino-2-methylpropanol (AMP) have one or more substituents attached to the α -carbon which lead to higher CO₂ capacity as well as lower the heat of absorption. However, its absorption rate with CO₂ is slow, but still is faster than tertiary amines such as MDEA. Xu et al. [100] measured reaction kinetics between CO₂ and AMP solution at different temperatures and concentrations.

1.4.4. Cyclic diamines and polyamines

Another category of amines are cyclic diamine and polyamines which have more than two amino groups in their structure. They present high CO₂ capacity and absorption rate in comparison with amines with one amino group. Examples include diethylenetriamine (DETA), 2-aminoethylamino-ethanol (AEEA), triethylenetetramine (TETA), piperazine (PZ), 1-methylpiperazine (1MPZ) and 2-methylpiperazine (2MPZ). Several researchers investigated their performance as absorbent for CO₂ absorption [101,102].

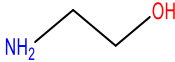
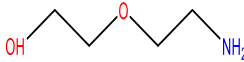
1.4.5. Primary amines

According to the number of carbons bonded to the nitrogen atom, alkanolamines are classified as primary, secondary and tertiary amine. Monoethanolamine and diglycolamine (DGA) as primary alkanolamines

have one carbon bonded to the nitrogen as given in Table 1.3. MEA has been used extensively in many CO₂ capture processes because of its low solvent cost and fast reaction kinetic [14]. However, MEA has several disadvantages such as low CO₂ absorption capacity, thermal or chemical degradation, high regeneration energy requirement and corrosive [15]. Since MEA has a fast reactivity with CO₂, some researchers added MEA as a rate promoter to other solvents in order to improve absorption rate.

As an example, Thee et al. [103] used 5 and 10 wt% MEA as a promoter for potassium carbonate. The results revealed that CO₂ absorption rate in K₂CO₃ + MEA solution is higher than potassium carbonate. The absorption rate of CO₂ in the blend solution of 2-amino-2-hydroxymethyl-1,3-propanediol (AHPD) and MEA was measured by Muraleedharan et al. [104] at 303, 313 and 323 K. Their results indicate that MEA can increase the absorption rate of CO₂ in AHPD solution.

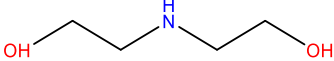
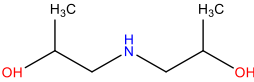
Table 1.3 Chemical structure of primary amines

Amine	Molecular Structure	Amine	Molecular Structure
MEA		DGA	

1.4.6. Secondary amines

Secondary alkanolamines such as diethanolamine (DEA) and diisopropanolamine (DIPA) have two carbons bonded to the nitrogen (Table 1.4). DEA and DIPA solutions react with CO₂ and form carbamates. Although their reactivity with CO₂ is slower than primary amines, they have faster absorption rate when compared to tertiary amines. The less corrosive, lower vapour pressure, lower regeneration energy requirement and greater selectivity of H₂S toward CO₂, are other advantages of DEA and DIPA in comparison to primary amines such as MEA [105]. Camacho et al. [106] examined reaction kinetics in DIPA solution using a stirred tank reactor at temperatures from 288 K to 313 K.

Table 1.4 Chemical structure of secondary amines

Amine	Molecular Structure	Amine	Molecular Structure
DEA		DIPA	

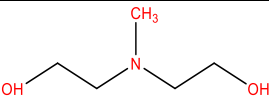
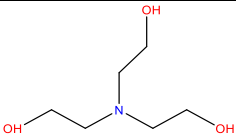
1.4.7. Tertiary amines

This category of solvents has no carbamate product when they react with CO₂. Instead, they facilitate the CO₂ hydrolysis reaction to form bicarbonates. Methyldiethanolamine (MDEA) and triethanolamine (TEA) are examples of this group of absorbents. The bicarbonate formation leads to a lower energy consumption for regeneration which is one of the main advantages of tertiary amines [107]. In addition,

less degradation and corrosivity as well as good selectivity for H₂S removal make them attractive absorbent for CO₂ capture.

However, similar to other absorbent, they have their own limitation. Slow absorption rate with CO₂ in comparison to primary and secondary amines is a challenge for this group of solvents. Liao et al. [108] selected MEA as rate promoters to add to MDEA solution, respectively. It was discovered that MEA enhanced the reaction kinetics between CO₂ and MDEA. Chemical structure of MDEA and TEA were given in Table 1.5.

Table 1.5 Chemical structure of tertiary amines

Amine	Molecular Structure	Amine	Molecular Structure
MDEA		TEA	

1.4.8. Ionic liquid

Solutions of ionic liquids as a new type of green solvent are considered as attractive solvent because of their unique characteristics such as negligible vapour pressures and high thermal stability. Similar to other category of solvents, ionic liquid also have their own limitations, including high cost and viscosity [109]. The CO₂ absorption performance in 1-butyl-3-methylimidazolium glycinate solution was studied by Wu et al. [110]. Based on their observation, 1-butyl-3-methylimidazolium glycinate showed faster absorption rate than DEA, but slower than MEA solution.

1.4.9. Blended solvents

Since a single solvent will rarely be optimal with regard to all the solvent factors, blend of two solvents with various advantages can be a suitable technique to produce a better absorbent with desired properties for CO₂ capture. Simplicity, reproducibility, commercial benefits, the desired properties and cost reduction are the most important advantages of solvent blend systems [19].

Garg et al. [47] determined density and viscosity of a mixture of 2-piperidineethanol (2-PE), as an amine, and sarcosine as an amino acid. They found that with an increasing concentration of sarcosine in blended solution, density increases while viscosity decreases.

Mondal et al. [18] studied reaction kinetics between CO₂ and HMDA + sodium glycinate solution using a stirred cell reactor at temperatures of 313, 323 and 333 K. Their results showed that the addition of sodium glycinate to HMDA has a positive effect of reaction rate.

Kang et al. [40] carried out CO₂ loading measurements in PZ + potassium alaninate solution using stirred cell reactor at a temperature rang from 313 to 333 K. According to their observation CO₂ loading capacity of PZ + K-Ala solution decreases as temperature increases.

Talkhan et al. [96] evaluated corrosion rate of CO₂ absorption in blend solution of MDEA + arginine and studied the effect of temperature and concentration on corrosion rate. They found that arginine acts as an inhibitor. In addition, corrosion rate decreases when arginine was added to the amine solution.

Kumar Dash et al. [111] assessed the impact of piperazine on the absorption rate of CO₂ into 2-amino-2-methyl-1-propanol (AMP) solutions at temperatures of 303, 313 and 323 K. It was discovered that the mixed solution has a much higher CO₂ absorption rate than that of pure AMP.

In a very recent time, Fu et al. [112] investigated viscosity and solubility of CO₂ in MEA activated 2-diethylaminoethanol (DEAE) aqueous solution at three different temperatures (303, 313, and 323 K). According to their findings, CO₂ loading capacity of mixture MEA and DEAE is higher than pure MEA.

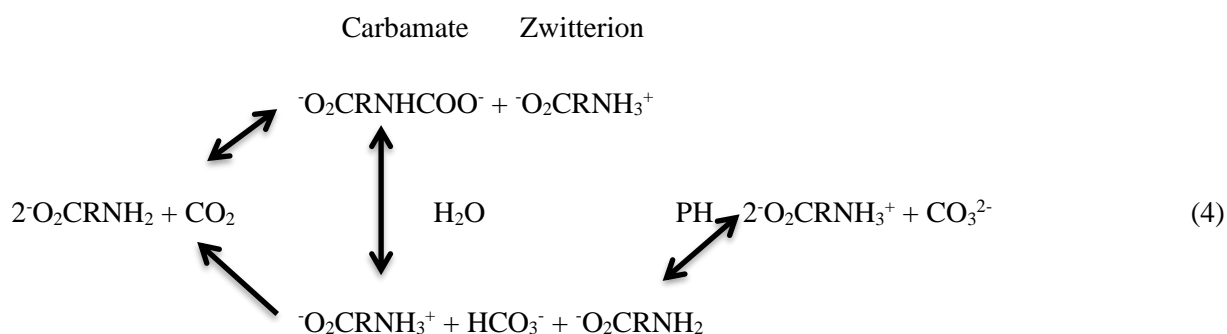
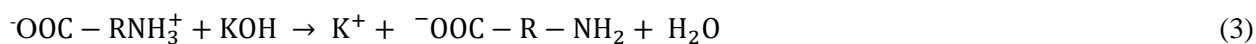
Based on analysis above, it is obvious that each category of solvents has own advantages and disadvantages. These drawbacks of solvents lead to high cost of CO₂ capture and hinders the conventional post-combustion process from being used for industrial applications. To develop a more economical and energy-efficient CO₂ capture technology, it is therefore essential to discover the new solvent systems. The main objective of the present work is to develop a new chemical solvent with better CO₂ absorption performance in comparison with conventional amines such as MEA and MDEA.

REACTION MECHANISM

Modeling of the absorption process using aqueous amine solutions and deduction of characteristic solvent parameters require the knowledge of CO₂ absorption-reaction mechanisms taking place for the different types of amine solutions. In this regard, the various reaction mechanisms (zwitterion, termolecular, and base-catalyzed hydration) have been extensively studied in the literature.

2.1. Reaction mechanism between CO₂ and amino acids

Amino acids such as lysine and sarcosine exist in three different states, which includes: a) the acidic state, b) the unstable zwitterion state, c) and the deprotonated zwitterion state. When amino acids are dissolved in water, the unstable zwitterion state will exist. The acidic state and the unstable zwitterion state are not active to react with CO₂. Only the deprotonated zwitterion state can react with CO₂ [113]. This state is achieved by the reaction with a strong base, such as potassium hydroxide (KOH). When KOH is added to an amino acid, the deprotonated state is obtained, which is able to react with CO₂ [114].



Other chemical reactions taking place in the liquid phase are:

Hydration of CO₂:



Carbonate formation reaction:



Dissociation of water:



2.2. Reaction mechanism between CO₂ and MEA

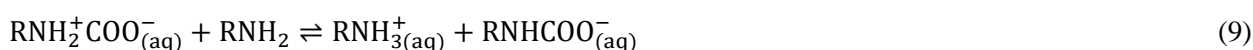
The reactions between CO₂ and MEA solution have been described by zwitterion mechanism; namely introduced by Danckwerts [115]. The zwitterion mechanism consists of the formation of a complex called a zwitterion, followed by the deprotonation of the zwitterion by a base.

The chemical reaction of aqueous MEA solution as a primary alkanolamine and CO₂ takes place through Eqs. (8-13):

Zwitterion formation from MEA (RNH₂) and CO₂ reaction:



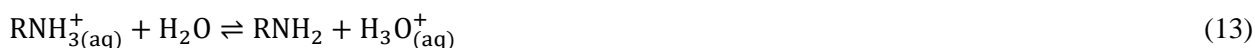
Carbamate formation by deprotonation of the zwitterion:



Carbamate reversion to bicarbonate (hydrolysis reaction):



Dissociation of protonated MEA:



2.3. Reaction mechanism between CO₂ and PZ

There is a symmetrical diamino cyclic structure in the piperazine molecule as a secondary amine. Based on the study by Bishnoi et al. [116] and Ermatchkov et al. [117], the following reactions are considered in the liquid phase:

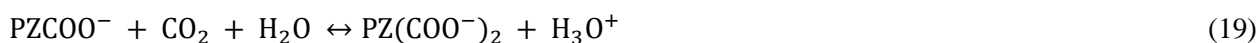
Piperazine protonation:



Piperazine deprotonation:



Carbamate formation:



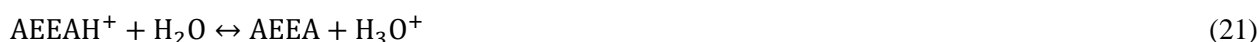
Manocarbamate protonation:



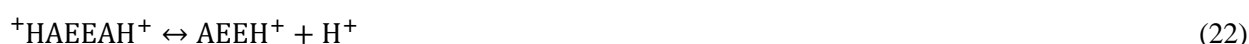
2.4. Reaction mechanism between CO₂ and AEEA

Since AEEA has both primary and secondary amine groups in its structure, and both of them may react in the aqueous phase, the chemistry of the reactions is very complex. The system gives rise to a large number of possible chemical reactions and formed species [118].

Dissociation of protonated AEEA:



Dissociation of diprotonated AEEA:



Two different carbamate ($\text{AEEACOO}_\text{P}^-$, $\text{AEEACOO}_\text{S}^-$) formation reactions are possible for AEEA.

Formation of carbamate from primary group to form primary carbamate ($\text{AEEACOO}_\text{P}^-$):



Formation of carbamate from secondary group to form secondary carbamate ($\text{AEEACOO}_\text{S}^-$):



Dissociation of carbamates:



Formation of dicarbamate:



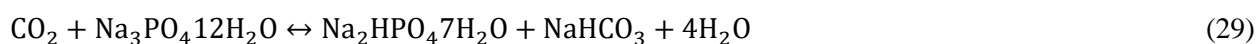
2.5. Reaction mechanism between CO₂ and MDEA

Tertiary amines such as TEA and MDEA do not react directly with CO₂. Donaldson and Nguyen [119] proposed base-catalyzed hydration mechanism for MDEA + CO₂ + H₂O system. According to their mechanism, MDEA acts as a base that catalyzes the hydration of CO₂. The only reaction MDEA is subjected to its protonation.



2.6. Reaction mechanism between CO₂ and TSP

Balsora and Mondal [99] showed that the overall reaction between trisodium phosphate and CO₂ can be represented as:



2.7. Reaction mechanism between CO₂ and TETA

Amann et al. [120] only considered an overall reaction to explain the CO₂ reaction with TETA (R₁ = C₂H₄) because the chemistry of the reactions is complex.



2.8. Reaction mechanism between CO₂ and AMP

Reaction mechanism between CO₂ and AMP as a primary sterically hindered amine is similar to primary and secondary alkanolamines. The only difference is that the carbamate generated from the reaction of AMP with CO₂ is not stable because of its high branches [107]. Pei et al. [121] represented the overall CO₂ reaction mechanism with AMP (RNH₂), (where, R=C(CH₃)₂CH₂OH) can be followed:



2.9. Reaction mechanism between CO₂ and DETA

The chemical reactions during the absorption of CO₂ in DETA solution can be described by following reactions [122]:



2.10. Reaction mechanism between CO₂ and 2MPZ

The reaction of CO₂ with 2MPZ is described by the zwitterion mechanism. Danckwerts [115] and Caplow [122] proposed that this mechanism can be used for the reaction between CO₂ and primary and secondary amines. Thus, it was assumed that zwitterion mechanism is valid for the 2MPZ – CO₂ – H₂O system. According to this mechanism, 2MPZ reacts with CO₂ to form a zwitterion intermediate (2MPZH⁺COO⁻), then consumed by a base B such as 2MPZ, 2MPZH⁺, H₂O or OH⁻.



2.11. Reaction mechanism between CO₂ and K₂CO₃

The reactions involved in the system of K₂CO₃ + H₂O + CO₂ can be represented as follows [123]:



Dissolution of K₂CO₃ (s) in water:



Hydrolysis of CO_3^{2-} :



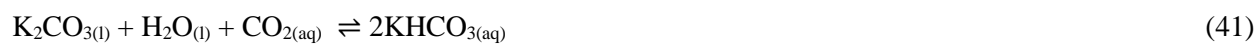
Bicarbonate formation:



Carbonate formation:



The carbonate formation reaction occurs rapidly, therefore the overall reaction of the K_2CO_3 solution with CO_2 is as follows:



EXPERIMENTAL SECTION

3.1. Materials

In this work, after a prescreening, different blended amine solutions were selected as a proposed chemical solvent for CO₂ capture. The chemical materials studied in this work are ((2-aminoethyl)amino)ethanol (AEEA), methyldiethanolamine (MDEA), piperazine (PZ), triethylenetetramine (TETA), 2-methylpiperazine (2-MPZ), monoethanolamine (MEA), trisodium phosphate (TSP), potassium carbonate (K₂CO₃), potassium salts of sarcosine (K-Sar), lysine (K-Lys), glycine (K-Gly), proline (K-Pro), alanine (K-Ala) and serine (K-Ser).

TSP and K₂CO₃ as inorganic solvents have some benefits in comparison to alkanolamines such as less solvent loss, lower toxicity, high stability towards thermal degradation, better resistance to degradation in the presence of oxygen and weak corrosivity. Due to these favorable properties, they were selected as base solvent in this work. Since the main drawback of TSP and K₂CO₃ solutions is their slow reaction rate with CO₂, it is necessary to add amine additive.

Three polyamines and six amino acid salts were selected as amine additives. Polyamines, including AEEA, 2MPZ and TETA have two or more than two amino groups in their structure which lead to a high CO₂ loading capacity and absorption rate.

Potassium salt of proline, sarcosine, serine, alanine, glycine and lysine with low concentration were also investigated as amine additive. Amino acid salt solutions gained interest as solvent due to their advantages over alkanolamines such as low volatility, less toxicity, high surface tension as well as being more environmentally friendly.

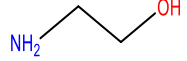
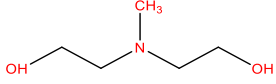
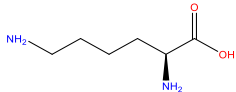
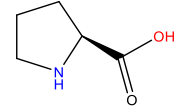
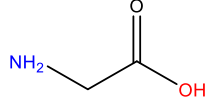
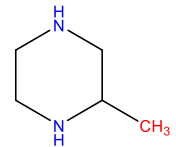
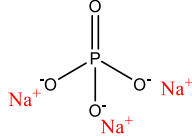
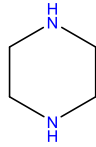
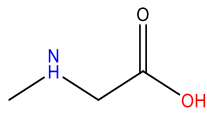
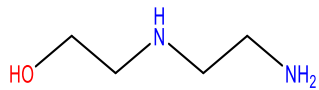
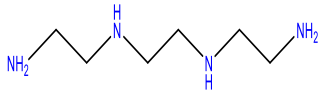
One of the objectives of this work is improvement of existing absorbents in the industrial application. In this regard, potassium salt of lysine was selected to add to MEA and MDEA to improve their CO₂ absorption characterization.

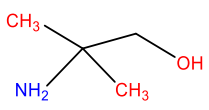
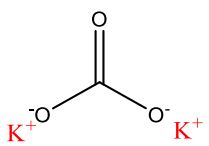
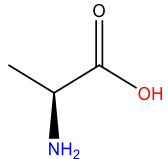
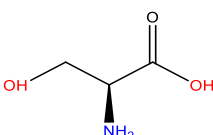
A detailed description of all used materials in this work and their molecular structures was given in Table 3.1. They were used without further purification.

The potassium salt of amino acids was prepared by the addition of an equimolar amount of KOH to amino acid dissolved in deionized water.

The N₂O, N₂ and CO₂ gases with purity >99% were also supplied by Air Liquid (Italy).

Table 3.1 Description of chemical samples used in present work.

Chemical name	Abbreviation	MW (g/mol)	Purity (%)	Source	Structure
Monoethanolamine	MEA	61.08	>99.0	Alfa Aesar	
Methyl-diethanolamine	MDEA	119.16	>98	Alfa Aesar	
Lysine	Lys	146.19	98	Acros	
Proline	Pro	115.13	>99	Sigma	
Glycine	Gly	75.06	98.5	Sigma	
2-methylpiperazine	2MPZ	100.16	98	Acros	
Trisodium phosphate	TSP	163.94	-	Alfa Aesar	
Piperazine	PZ	86.14	99	Alfa Aesar	
Sarcosine	Sar	89.09	98	Alfa Aesar	
Aminoethylethanolamine	AEEA	104.15	99	Alfa Aesar	
Triethylenetetramine	TETA	146.23	>97	Sigma	

2-amino-2-methyl-1-propanol	AMP	89.14	>95	Alfa Aesar	
Potassium carbonate	K ₂ CO ₃	138.20	>99	Acros	
Alanine	Ala	89.09	>98	Sigma	
Serine	Ser	105.09	99	Alfa Aesar	

3.2. Experimental gas-liquid contactors

The reaction kinetics between CO₂ and amine solutions can be studied by using different types of gas-liquid contactors such as wetted wall column, stopped flow technique, stirred cell reactor, laminar jet absorber, wetted sphere absorber and string of disc contactor. Many researchers used these techniques to measure absorption rate of CO₂ in different solutions.

For example, Knuutila et al. [124] and Hartono et al. [125] used string of discs contactor to study the reaction kinetics of CO₂ absorption in K₂CO₃ and DETA solutions, respectively. The advantage of this contactor is that the absorption surface area can be varied by addition of more the disc elements in the column [107].

The CO₂ absorption rate into solutions of EAE [126] and glycine [67] was measured using stopped flow technique. They pointed out that a conductivity measurement can only be done at low concentration of solution.

The kinetics of reaction of CO₂ in proline [72] and histidine [127] were also determined using wetted wall column. One of the limitations with this technique is possibility of creating ripples in the liquid film and inactive film at the bottom of the column [107].

The laminar jet absorber is an ideal contactor for fast reactions because of its short contact time. This equipment was used by Rinker et al. [128] and Aboudheir et al. [129] in order to investigate of CO₂ absorption rate in DEA and MEA, respectively.

The kinetics measurement experiments were carried out in a wetted sphere absorber by Seo et al. [130]. However, a fixed absorption surface area and inactive film at the bottom of the sphere are the main limitations of this technique [107].

The stirred cell reactor has been successfully performed by many researchers [109,131,132] because of its advantages. The most important advantage of this contactor is that chemical analysis of liquid is not necessary, and the fall-in-pressure versus time in the reactor is the only required parameter for measurement of absorption rate. Thus, this equipment is suitable for toxic gas or liquid [107]. Another advantage is that this contactor can also be used for measurement of CO₂ loading capacity of various solutions.

3.2.1. Stirred cell reactor apparatus

In this work, a stirred cell reactor with a smooth gas-liquid interface operating batch wise purchased from Buchiglas (Switzerland) was used in order to measure the reaction kinetics between CO₂ and different solutions. The experimental setup used was shown schematically in Figure 3.1.

The setup consists of three gas containers, two pressure transmitters, two temperature sensors, gas storage tank, a reactor, two water baths, vacuum pump and external magnetic motor. A pressure transmitter (Keller, Italy), a temperature sensor (DT100), an external magnetic motor (Huber, Italy) and a pressure release valve were placed on the cover plate of the reactor. The reactor was equipped with the glass heat jacket and an external water bath. The pressure transmitter was coupled with a converter to measure the pressure inside the reactor and record pressure changes versus time every second. Two impellers were equipped on a stirrer shaft in order to stir liquid and gas phases. To ensure that the interface of gas and liquid was undisturbed and liquid mass transfer coefficient is constant at a given temperature and concentration, the liquid volume and the impeller speed were kept constant in all experiments. A separate line on the cover plate of the reactor allows to evacuate the reactor by using an external vacuum pump. A stainless steel gas storage tank which immersed in a water bath was used in order to heat the gas before being charged inside the reactor. The temperature and pressure sensor were connected to gas storage tank to measure the values of pressure and temperature of gas in the gas storage tank.

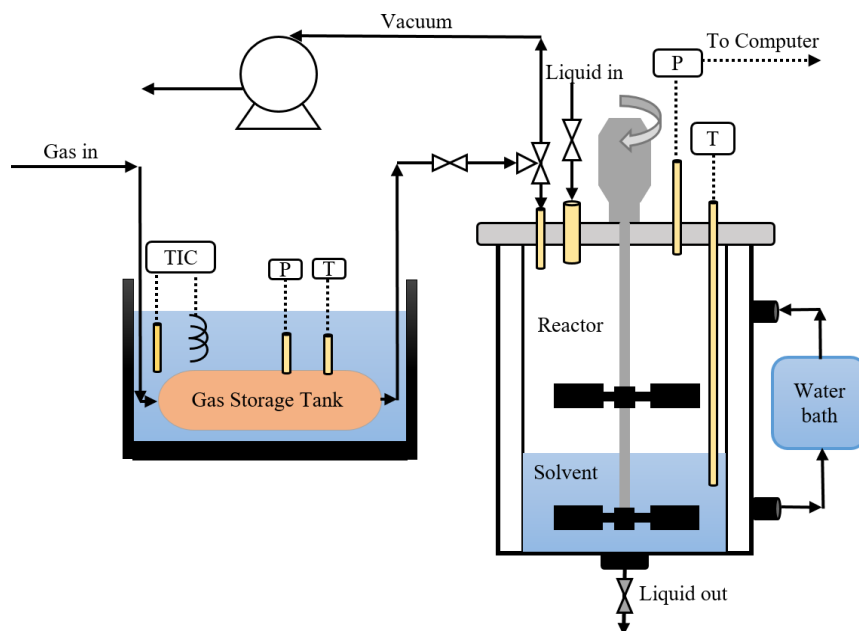


Figure 3.1 Schematic diagram of the vapor-liquid equilibrium equipment.

3.2.1.1. CO₂ loading capacity measurement

In each new experiment, the cell was purged with N₂ gas to eliminate air. After that, solvent was imported and the pressure of the equilibrium cell was set at vacuum by a vacuum pump to degas the solvent. Then, the valve of the vacuum line was closed and the temperature of the solution is set to the desired temperature, by using a water bath. CO₂ gas was supplied to the gas storage tank from a gas cylinder. After pre heating, CO₂ was introduced into the equilibrium cell for a very short time until the pressure in the reactor reached a selected value. The total moles of CO₂ transferred can be calculated from:

$$n_{\text{CO}_2}^i = \frac{[P_1 - P_2] V_s}{RT} \quad (42)$$

Where V_s , P_1 and P_2 are the volume, initial and final pressure of CO₂ in the gas storage tank, respectively. After the introduction of CO₂, the inlet valve is closed and the stirrer is turned on immediately to ensure homogeneous contact between gas and liquid and reach equilibrium quickly. The pressure in the reactor was decreased over time due to absorption of CO₂ in solvent. The temperature and pressure of cell were continuously recorded until equilibrium is reached. Equilibrium was assumed when the pressure in the reactor reached a constant value (after 3 hours).

The equilibrium partial pressure of CO₂ and moles of CO₂ remaining in reactor ($n_{\text{CO}_2}^f$) are calculated by:

$$P_{\text{CO}_2}^e = P_F - P_V \quad (43)$$

$$n_{\text{CO}_2}^f = \frac{V P_{\text{CO}_2}^e}{RT} \quad (44)$$

Where V , P_V and P_F are the reactor volume, vapor pressure of solution and final pressure of CO_2 in the reactor, respectively. The CO_2 loading capacity of solvent (α_{CO_2}) is defined as the total number of moles of CO_2 absorbed in reactor per one mole of solvent, and can be calculated by the following equation:

$$\alpha_{\text{CO}_2} = \frac{n_{\text{CO}_2}^i - n_{\text{CO}_2}^f}{n_{\text{solvent}}} \quad (45)$$

In order to check the reproducibility of the results, all the experiments in this work have been measured at least twice.

3.2.1.2. CO_2 absorption rate measurement

The CO_2 absorption rate experiments were conducted using the same setup discussed in the previous section. The measurement procedure of absorption rate is similar to CO_2 loading capacity measurement. Once CO_2 was injected in the reactor, the stirrer is switched on at a constant speed. The pressure inside the reactor because of reaction between CO_2 and solvent decreases. The pressure decrease versus time was recorded by pressure transmitter and slope of pressure changes versus time ($\frac{dP_{\text{CO}_2}}{dt}$) was used to calculate the CO_2 absorption rate:

$$N_{\text{CO}_2} = -\frac{V}{RTA} \frac{dP_{\text{CO}_2}}{dt} \quad (46)$$

3.3. Density and viscosity measurement

An Ubbelohde viscometer and Gay-Lussac pycnometer were used in this work to measure density (ρ) and viscosity (μ) of single and blended solutions, respectively. The measurements were performed at different concentrations and at a temperature range of 298.15 to 323.15 K. The pycnometer and viscometer were immersed in a water bath. The uncertainty of density and viscosity measurements are $0.001 \text{ g}\cdot\text{cm}^{-3}$ and $0.001 \text{ mPa}\cdot\text{s}$, respectively. The reported data in this work are the average of three measurements.

The density and viscosity of loaded and CO_2 unloaded viscous MEA solutions were measured using an Anton Paar DMA 4500 density meter and an Anton Paar Lovis 2000 ME rolling-ball viscometer, respectively. The measurement were conducted at the temperature range 25-70 °C and CO_2 loading up to 0.4 (mol CO_2 /mol solvent).

3.4. Absorption heat measurement (ΔH)

An important process parameter in a gas treating process using chemical absorbents, is calculation of absorption heat since it is directly related with energy consumption in the stripper for regeneration of absorbent.

The values of heat of CO₂ absorption can be obtained experimentally using a calorimeter or calculated on the basis of the following the Gibbs-Helmholtz equation:

$$-\frac{\Delta H}{R} = \left(\frac{\partial \ln P_{\text{CO}_2}}{\partial (1/T)} \right)_{\alpha} \quad (47)$$

Where R, T, α and ΔH are gas constant, temperature of system, CO₂ loading capacity and heat of absorption (kJ/mol CO₂), respectively. Carson et al. [133] measured heat of CO₂ absorption of DEA, MDEA and MEA solutions using a calorimeter. In order to check the validation of Gibbs-Helmholtz equation, Lee et al. [134], Rho et al. [135] and Li et al. [136] calculated heat of CO₂ absorption of these solutions using Gibbs-Helmholtz equation. They compared their results with values measured by Carson and found that Eq. (47) gives a good agreement with experimental results as given in Table 3.2. Thus, applying Gibbs-Helmholtz equation to calculate heat of absorption is reliable. Many researchers used this measurement method in their works [137,138].

Therefore, in this work, Gibbs-Helmholtz equation was used to estimate heat of CO₂ absorption of different solutions. The absorption heat was calculated directly from the slope of plot of $\ln P_{\text{CO}_2}$ versus $1/T$ at constant CO₂ solubility.

Table 3.2 Heat of CO₂ absorption in aqueous solutions of MEA, DEA and MDEA.

Solvent	- ΔH (kJ/mol CO ₂)	
	Experimental [133]	Estimated [134-136]
MEA	82	84.3
DEA	69	66.9
MDEA	49	54.6

3.5. pH measurement

The pH of several solvents before and after CO₂ absorption was measured using Benchtop pH meter (AE150, Italy). These data can be used for predicting of concentration of H⁺ in the solution.

$$\text{pH} = -\log [\text{H}^+] \quad (48)$$

3.6. Corrosion rate

In order to study of the corrosion rate of solvent, a potentiostat unit (AUTO LAB, 302N, Metrohm, Germany) was used according to ASTM G5-94 [139] on the carbon steel. Ag/AgCl (3 M KCl) and a rod of Pt was used as reference electrode and counter electrode, respectively. The experiments were conducted on carbon steel coupons (spherical shape, surface area of 1.13 cm²) at 313.15 K.

RESULTS AND DISCUSSION

This section is mainly a collection of our published or submitted papers.

4.1. Preliminary reliability test

Before measuring the CO₂ absorption capacity of selected solvents, the experimental procedure and reliability of the apparatus have been checked first by measuring the loading capacity of CO₂ in an aqueous solutions of 15 wt% and 30 wt% MEA at 313.15 K and CO₂ partial pressure up to 40 kPa. The results were compared with those published in the literature [43,140,141] as shown in Figure 4.1 and a good accuracy was observed.

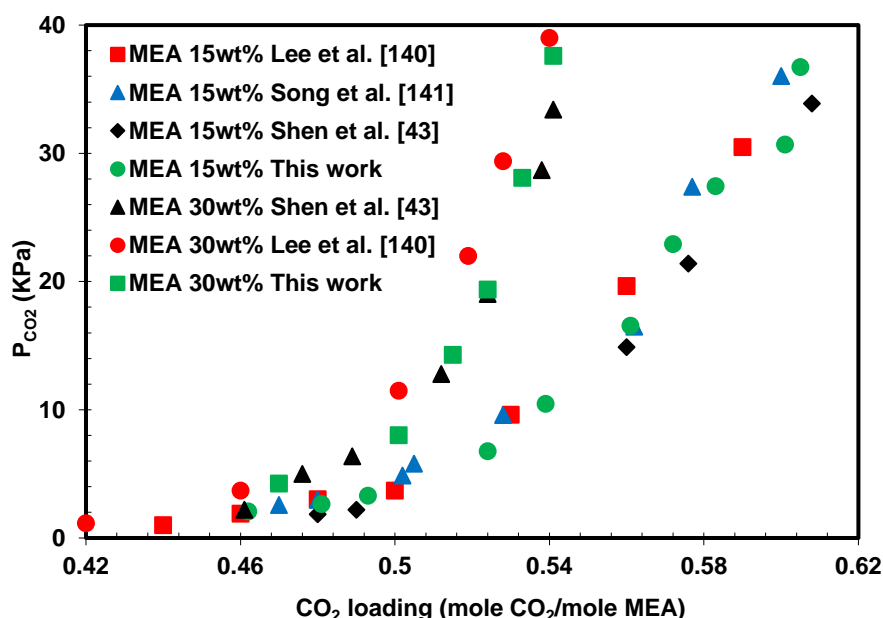


Figure 4.1 Comparison of experimental CO₂ loading data of MEA obtained in this work with literature at 313 K.

4.2. Absorption characterization of CO₂ in TSP solution

4.2.1. CO₂ loading capacity of TSP

After validating the methodology, the CO₂ loading (α) of trisodium phosphate (TSP) solution was measured using stirred cell reactor and the results were presented in Table 4.1 to 4.3. The effect of CO₂ partial pressure, temperature and concentration of TSP on CO₂ absorption capacity was investigated. Figure 4.2 and 4.3 show the experimental values of CO₂ loading of aqueous TSP solution at different concentrations and at 313 K and 323 K, respectively. It was found that CO₂ loading increases with

increasing CO₂ partial pressure, TSP concentration and temperature. The reason why a higher temperature can increase the CO₂ loading capacity in TSP solution is that the dissolution of more trisodium phosphate occurs with increasing temperature. As a result, more TSP is present in the solution and thus absorb more CO₂ which leads to a higher CO₂ solubility. In addition, CO₂ loading of 2 kmol/m³ TSP obtained in this work was compared with data reported by Balsora et al. [99], a good agreement was observed as shown in Figure 4.2.

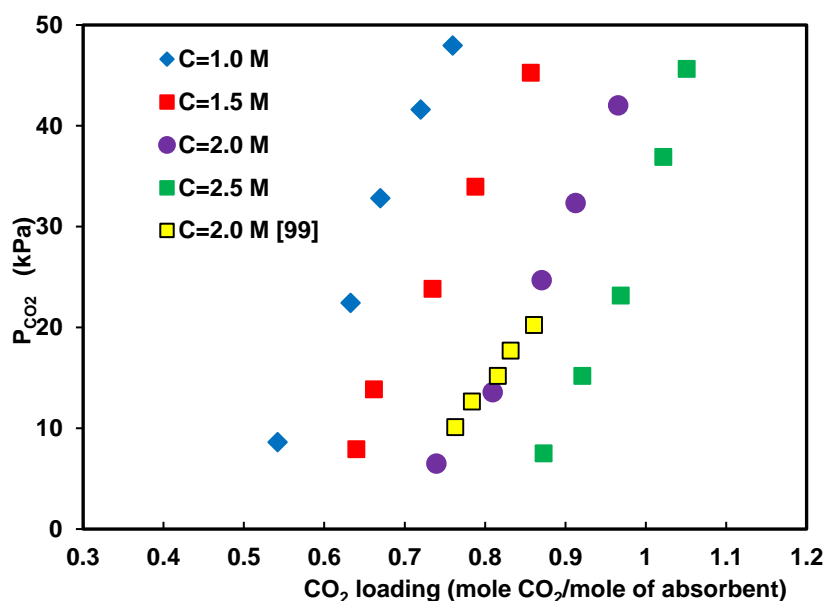


Figure 4.2 CO₂ loading capacity of TSP solution at 313.15 K and different concentrations

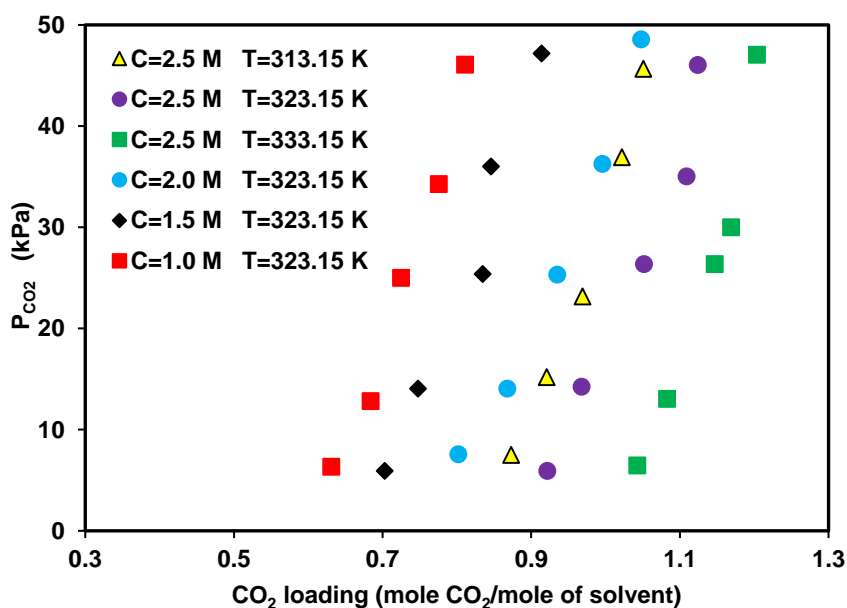


Figure 4.3 CO₂ loading capacity of TSP solution at 323.15 K and different concentrations.

Table 4.1 CO₂ loading capacity of TSP solution at 313.15 K and different concentrations

1 M TSP		1.5 M TSP		2 M TSP		2.5 M TSP	
P _{CO₂} (kPa)	α	P _{CO₂} (kPa)	α	P _{CO₂} (kPa)	α	P _{CO₂} (kPa)	α
08.63	0.542	07.93	0.641	06.48	0.740	07.52	0.873
22.46	0.633	13.86	0.662	13.57	0.809	15.2	0.921
32.84	0.670	23.84	0.735	24.69	0.871	23.17	0.969
41.63	0.719	33.97	0.788	32.35	0.913	36.92	1.022
47.97	0.758	45.28	0.857	42.01	0.966	45.67	1.051

α (mole CO₂/mole of absorbent) is the moles of CO₂ absorbed per one mole of solvent

Table 4.2 CO₂ loading capacity of TSP solution at 323.15 K and different concentrations

1 M TSP		1.5 M TSP		2 M TSP		2.5 M TSP	
P _{CO₂} (kPa)	α	P _{CO₂} (kPa)	α	P _{CO₂} (kPa)	α	P _{CO₂} (kPa)	α
06.35	0.631	05.92	0.703	07.59	0.802	05.93	0.922
12.84	0.684	14.05	0.748	14.05	0.868	14.26	0.968
25.01	0.725	25.38	0.835	25.31	0.935	26.38	1.052
34.28	0.776	36.02	0.846	36.28	0.996	35.04	1.109
46.07	0.811	47.18	0.914	48.59	1.048	46.05	1.124

α (mole CO₂/mole of absorbent) is the moles of CO₂ absorbed per one mole of solvent

Table 4.3 CO₂ loading capacity of 2.5 kmol/m³ TSP solution at different temperatures

T=313.15 K		T=323.15 K		T=333.15 K	
P _{CO₂} (kPa)	α	P _{CO₂} (kPa)	α	P _{CO₂} (kPa)	α
07.52	0.873	05.93	0.922	06.48	1.043
15.2	0.921	14.26	0.968	13.05	1.083
23.17	0.969	26.38	1.052	26.38	1.147
36.92	1.022	35.04	1.109	30.01	1.169
45.67	1.051	46.05	1.124	47.06	1.204

α (mole CO₂/mole of absorbent) is the moles of CO₂ absorbed per one mole of solvent

4.3. Absorption characterization of CO₂ in TSP + amine additives

4.3.1. CO₂ loading capacity of TSP + additive (1)

It is essential to determine CO₂ solubility of new absorbents at different pressures and temperatures because it supplies useful information about loading capacity of acid gases and has an important role at the efficient design of the gas absorption process [15]. In practice, a higher CO₂ solubility of the solvent leads to a smaller amount of solvent and a smaller plant size, resulting in a lower cost of CO₂ removal.

The CO₂ solubility in TSP blended with five amine additives, including triethylenetetramine (TETA), 2-amino-2-methylpropanol (AMP), potassium proline (K-Pro), potassium glycinate (K-Gly) and 2-methylpiperazine (2MPZ) was studied. Experiment measurements were conducted at temperatures 303.15 to 323.15 K, additive mole fractions (R) 0.2 to 0.4 and total concentration 2.5 kmol/m³, and the results were compared with 2.5 kmol/m³ MEA solution, which is the most important used alkanolamines in conventional plants. The loading capacity of CO₂ at temperatures 303, 313 and 323 K was tabulated in Tables 4.4 to 4.8, however, loading capacity only for temperature 313.15 K was illustrated in Figure 4.4 to 4.6 because the similar trend was observed for the other temperatures.

Table 4.4 CO₂ loading capacity of TSP + TETA solution

T=303.15 K		T=313.15 K		T=323.15 K	
P _{CO₂} (kPa)	α	P _{CO₂} (kPa)	α	P _{CO₂} (kPa)	α
R=0.2					
02.05	1.051	04.24	0.988	06.48	0.943
09.36	1.103	11.26	1.042	13.47	0.986
17.94	1.147	21.49	1.089	24.03	1.039
31.27	1.199	33.42	1.139	37.16	1.088
42.11	1.238	47.14	1.184	44.02	1.127
R=0.3					
03.91	1.124	06.14	1.083	10.25	1.059
10.27	1.168	13.62	1.128	16.04	1.103
21.04	1.209	23.93	1.191	27.61	1.156
31.26	1.257	35.28	1.232	39.07	1.204
42.35	1.302	46.13	1.279	48.13	1.252
R=0.4					
07.27	1.226	02.35	1.161	05.37	1.141
14.06	1.259	10.02	1.207	16.03	1.196
25.35	1.303	17.85	1.251	22.36	1.228
36.48	1.328	30.62	1.277	31.25	1.259
47.23	1.354	43.91	1.316	45.69	1.287

α (mole CO₂/mole of absorbent) is the moles of CO₂ absorbed per one mole of solvent

Table 4.5 CO₂ loading capacity of TSP + K-Gly solution

T=303.15 K		T=313.15 K		T=323.15 K	
P _{CO₂} (kPa)	α	P _{CO₂} (kPa)	α	P _{CO₂} (kPa)	α
R=0.2					
10.04	0.902	04.31	0.814	07.35	0.778
16.92	0.948	09.48	0.854	13.06	0.826
29.13	1.003	20.81	0.916	24.91	0.882
38.85	1.047	29.74	0.961	33.12	0.935
44.06	1.061	38.71	1.005	47.08	0.987
R=0.3					
03.37	0.834	08.02	0.803	06.94	0.752
11.06	0.883	16.74	0.869	14.49	0.798
23.58	0.946	29.05	0.922	27.44	0.857
32.71	0.984	40.15	0.969	38.89	0.906
43.62	1.031	48.29	1.013	46.04	0.953
R=0.4					
02.99	0.791	04.01	0.756	07.88	0.706
09.15	0.843	11.63	0.802	14.11	0.754
17.73	0.887	21.94	0.866	25.09	0.811
28.36	0.944	32.74	0.922	36.77	0.867
41.04	0.991	45.06	0.974	48.12	0.924

α (mole CO₂/mole of absorbent) is the moles of CO₂ absorbed per one mole of solvent

Table 4.6 CO₂ loading capacity of TSP + AMP solution

T=303.15 K		T=313.15 K		T=323.15 K	
P _{CO₂} (kPa)	α	P _{CO₂} (kPa)	α	P _{CO₂} (kPa)	α
R=0.2					
08.02	0.814	05.91	0.768	02.38	0.729
16.25	0.874	14.63	0.816	11.42	0.766
29.33	0.925	27.87	0.869	24.39	0.821
38.06	0.951	39.02	0.904	36.42	0.844
46.12	0.959	48.25	0.924	44.18	0.852
R=0.3					
07.11	0.786	06.37	0.731	03.31	0.698
20.47	0.852	13.27	0.773	09.04	0.729
31.05	0.869	24.61	0.808	18.36	0.768
37.88	0.898	35.06	0.853	27.64	0.784
44.26	0.907	47.95	0.878	39.07	0.802
R=0.4					
09.04	0.757	04.41	0.691	06.93	0.667

18.27	0.803	11.06	0.718	15.37	0.711
29.15	0.831	26.52	0.767	23.99	0.742
35.24	0.852	37.01	0.811	32.15	0.751
49.01	0.877	45.89	0.837	41.32	0.772

α (mole CO₂/mole of absorbent) is the moles of CO₂ absorbed per one mole of solvent

Table 4.7 CO₂ loading capacity of TSP + 2-MPZ solution

T=303.15 K		T=313.15 K		T=323.15 K	
P _{CO₂} (kPa)	α	P _{CO₂} (kPa)	α	P _{CO₂} (kPa)	α
R=0.2					
02.18	0.951	04.92	0.905	09.23	0.881
10.39	0.998	08.34	0.931	14.02	0.903
22.05	1.047	19.58	0.984	25.59	0.957
35.26	1.095	32.02	1.041	39.14	1.026
49.11	1.141	46.28	1.089	47.53	1.054
R=0.3					
03.39	1.024	06.88	0.983	09.01	0.951
08.02	1.044	12.59	1.014	15.35	0.988
21.67	1.098	25.37	1.072	28.24	1.042
33.29	1.139	38.14	1.109	41.03	1.083
46.15	1.177	49.02	1.137	49.18	1.103
R=0.4					
05.35	1.092	03.04	1.021	07.29	0.999
11.34	1.131	09.59	1.064	15.06	1.034
25.39	1.178	22.19	1.108	29.02	1.087
37.18	1.221	34.29	1.154	39.35	1.121
41.27	1.229	47.61	1.179	45.05	1.142

α (mole CO₂/mole of absorbent) is the moles of CO₂ absorbed per one mole of solvent

Table 4.8 CO₂ loading capacity of TSP + K-Pro solution

T=303.15 K		T=313.15 K		T=323.15 K	
P _{CO₂} (kPa)	α	P _{CO₂} (kPa)	α	P _{CO₂} (kPa)	α
R=0.2					
10.29	0.897	07.12	0.806	03.27	0.741
19.98	0.953	12.09	0.844	08.01	0.762
31.11	1.004	24.71	0.902	21.36	0.828
39.47	1.031	33.48	0.941	28.45	0.854
49.02	1.084	45.03	0.997	42.05	0.917
R=0.3					

06.24	0.852	05.06	0.768	02.24	0.702
21.04	0.932	13.79	0.824	09.81	0.743
32.27	0.986	23.31	0.861	18.27	0.785
38.92	1.007	36.07	0.927	31.43	0.839
49.01	1.053	42.11	0.953	45.11	0.893
R=0.4					
09.18	0.811	06.73	0.741	02.25	0.643
17.36	0.874	14.94	0.783	11.26	0.694
23.51	0.912	26.05	0.839	20.04	0.731
34.14	0.956	37.81	0.906	29.13	0.787
44.15	1.003	48.02	0.962	39.38	0.839

α (mole CO₂/mole of absorbent) is the moles of CO₂ absorbed per one mole of solvent

It is obvious from Figure 4.4 to 4.6, that the loading capacity of CO₂ into blend solutions of TSP + additive were much higher than MEA showing the high absorption ability of these blends. It can also be seen that, TSP + TETA blend reached the highest CO₂ loading of 1.316, compared to other additives. There are four functional groups at structure of TETA, including two primary amino groups and two secondary amino groups which can provide more available sites for reaction with CO₂, thus increase the CO₂ loading capacity considerably. However, working with TETA at higher concentration may be challenging due to high viscosity experienced. A similar effect, but with a slightly lower loading capacity, was also obtained in a blend of TSP and 2-MPZ solution. According to Figure 4.4 to 4.6, solution of TSP + 2-MPZ has a significantly higher solubility than TSP + K-Gly, TSP + K-Pro and TSP + AMP, but lower than TETA+TSP. Furthermore, it presented a higher loading capacity as compared to MEA. It also has been found that additives such as K-Gly, K-Pro and AMP have a negative impact on the CO₂ solubility of TSP solution. In other words, at a constant total concentration, CO₂ loading of solution decreases with addition of K-Gly, K-Pro and AMP. For similar relative composition the equilibrium solubility of CO₂ in TSP + K-Gly has been found to be higher than the solubility in TSP + K-Pro. Blend solution of TSP and K-Pro absorbs a slightly lower amount of CO₂ in comparison with TSP + K-Gly; however, it indicated a better performance than TSP + AMP. Among all the tested blends, TSP + AMP absorbs the least amount of CO₂, but still higher than MEA. In summary, the loading capacity of CO₂ in blended systems can be ranked in the following order: TSP + TETA > TSP + 2-MPZ > TSP > TSP + K-Gly > TSP + K-Pro > TSP + AMP > MEA.

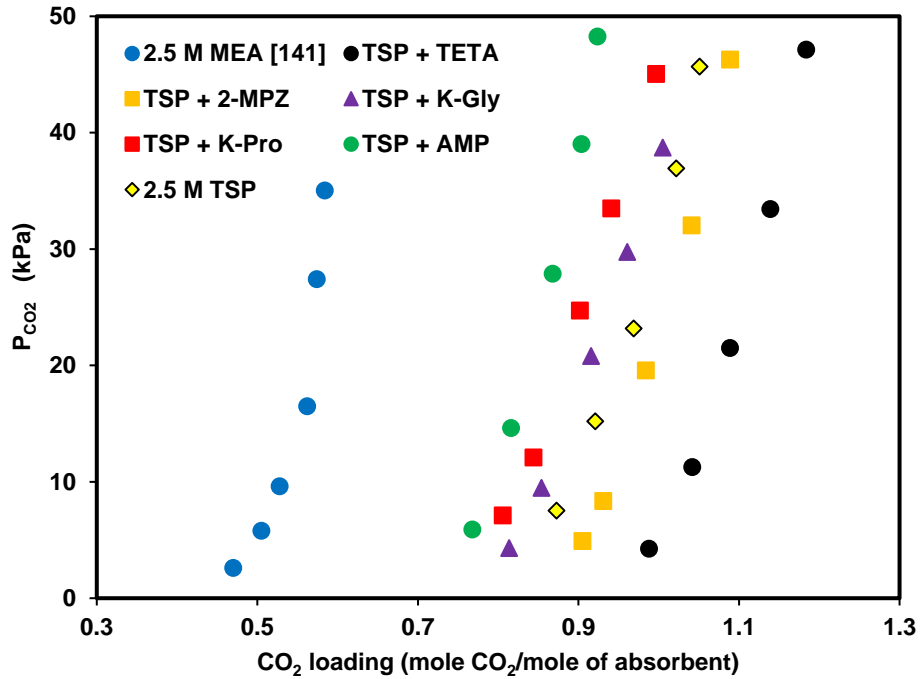


Figure 4.4 The effect of addition of different additives on CO₂ loading of TSP at 313.15 K and mole fraction 0.2.

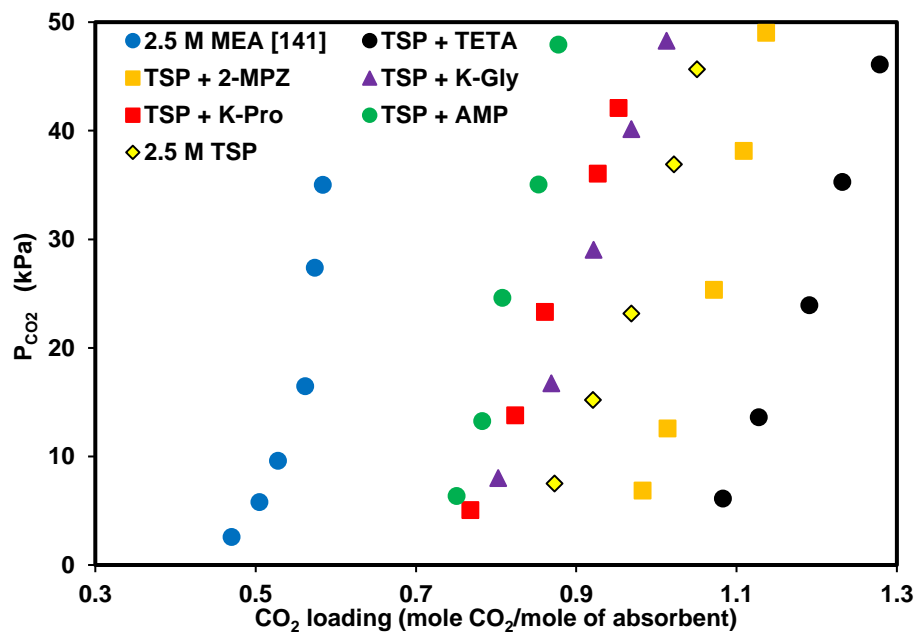


Figure 4.5 The effect of addition of different additives on CO₂ loading of TSP at 313.15 K and mole fraction 0.3.

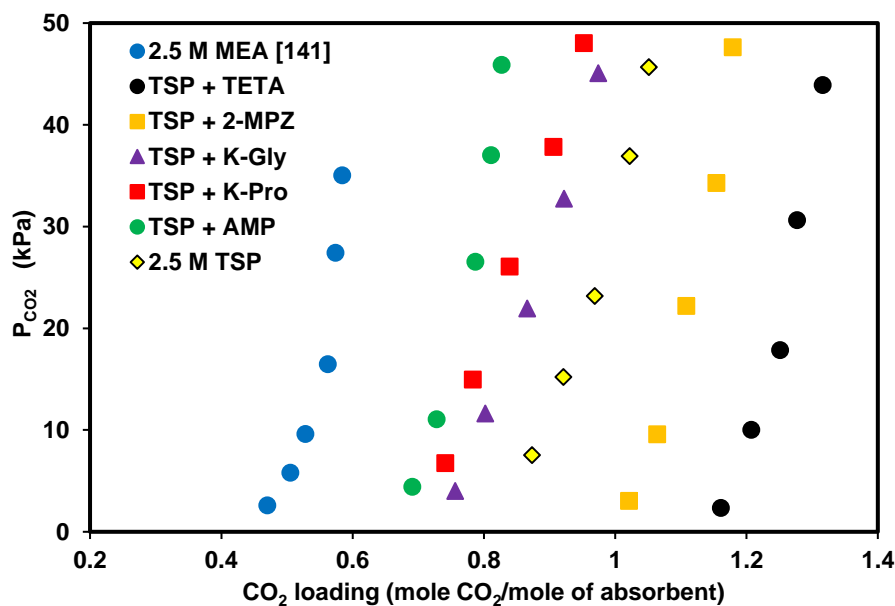


Figure 4.6 The effect of addition of different additives on CO₂ loading of TSP at 313.15 K and mole fraction 0.4.

The effect of temperature and mole fraction of additive on CO₂ loading of blended solutions was presented in Figure 4.7 to 4.11. Based on our observation, CO₂ loading of all the blend solutions decreases when temperature increases from 303.15 K to 323.15 K. It was found that CO₂ loading of TSP + TETA and TSP + 2MPZ increases with increasing concentration of additive while CO₂ loading of solutions of TSP + K-Gly, TSP + K-Pro and TSP + AMP showed a decreasing trend in loading capacity with increasing additive concentration.

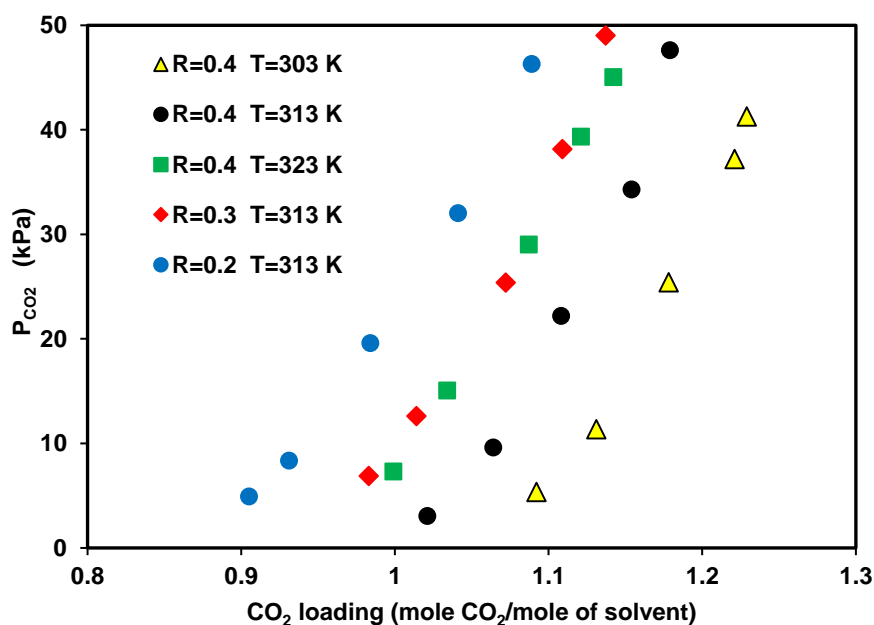


Figure 4.7 The effect of temperature and 2MPZ mole fraction on CO₂ loading capacity of TSP + 2MPZ solution.

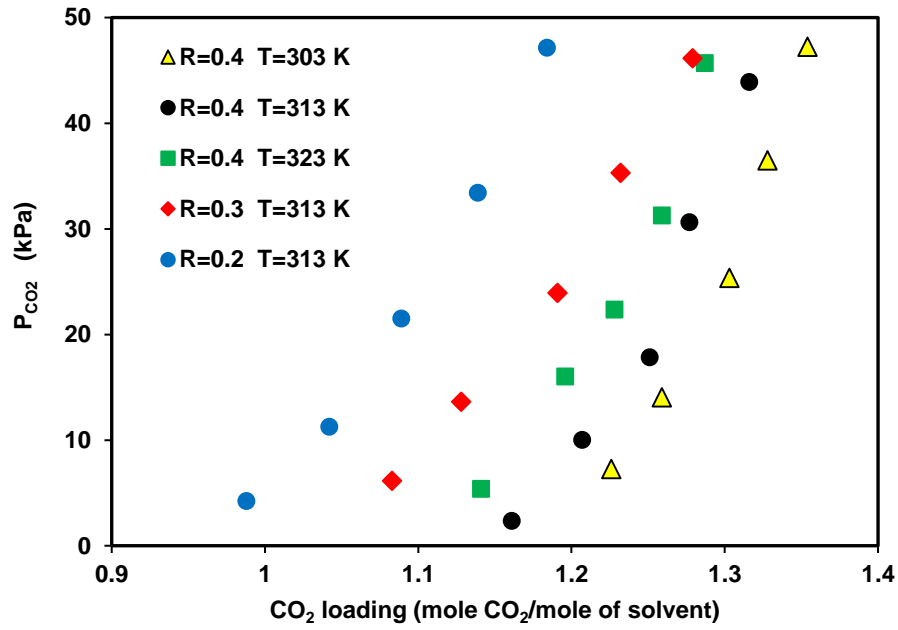


Figure 4.8 The effect of temperature and TETA mole fraction on CO₂ loading capacity of TSP + TETA solution.

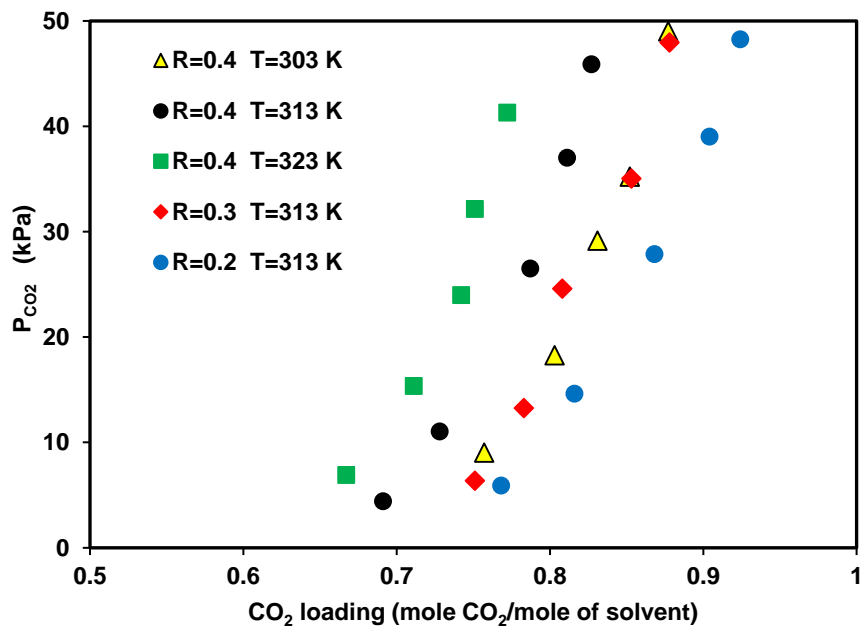


Figure 4.9 The effect of temperature and AMP mole fraction on CO₂ loading capacity of TSP + AMP solution.

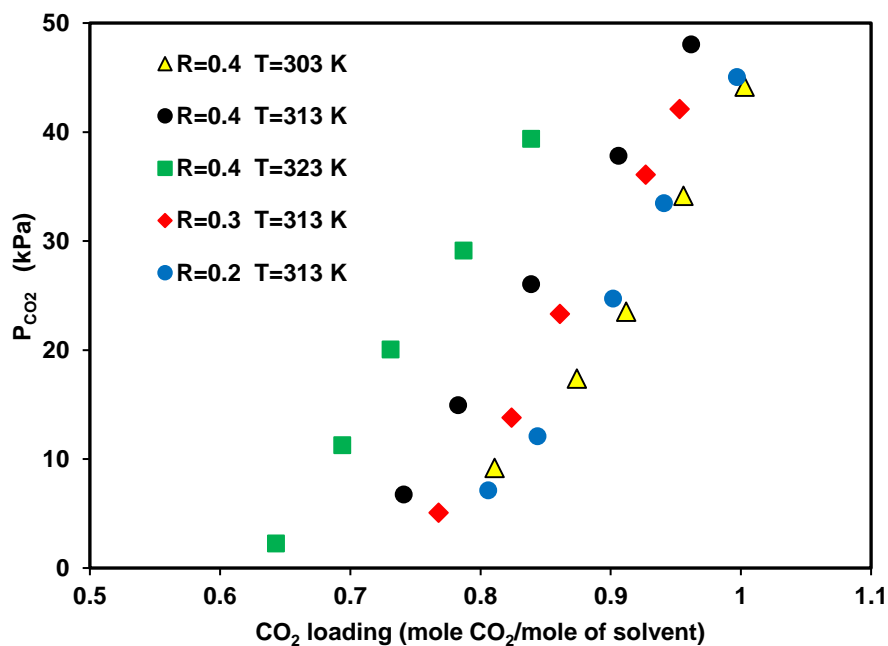


Figure 4.10 The effect of temperature and K-Pro mole fraction on CO₂ loading capacity of TSP + K-Pro solution.

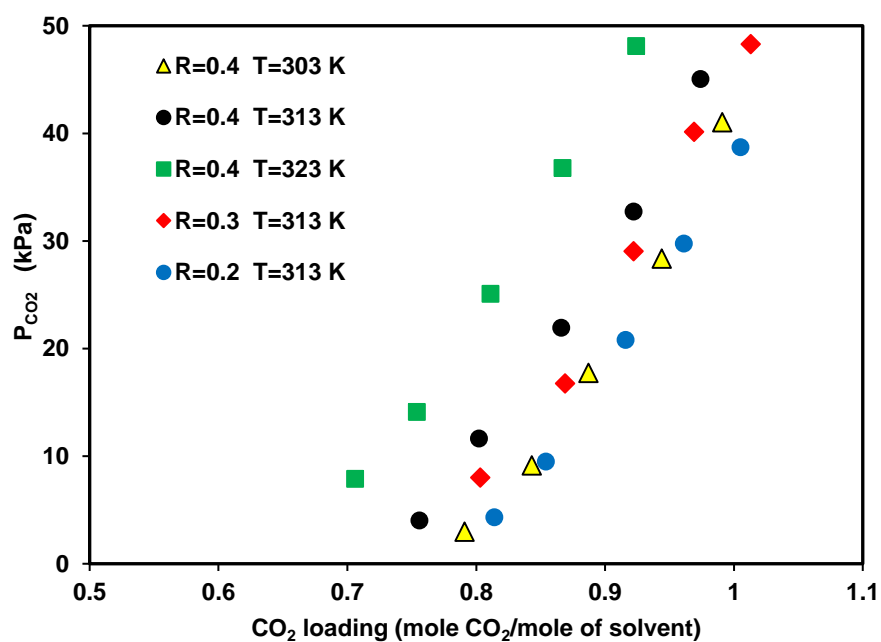


Figure 4.11 The effect of temperature and K-Gly mole fraction on CO₂ loading capacity of TSP + K-Gly solution.

4.3.2. Absorption rate of CO₂ in TSP + additive (1)

The high absorption rate as one of the parameters of solvent leads to the smaller size of the absorber and therefore reducing the processing cost. As mentioned in the previous sections, TSP as an inorganic solvent has a slower absorption kinetics than those of amine based solvents. Therefore, the different amine additives were added to TSP in order to improve the absorption rate of CO₂ in pure TSP solution. The CO₂ loading capacity versus time curves for different blend solutions are shown in Figure 4.12 to 4.14.

The absorption rate in this study determined from the initial slope of the loading curves over time in order to compare the performance of suggested additives. As shown in these figures, the absorption rate of CO₂ in single TSP solution was slowest. The absorption rate greatly improved with an increase of mole fraction TETA, 2MPZ, K-Pro, K-Gly and AMP, revealing the reinforcement of the amine additive on the absorption rate performance in pure TSP.

It was found that with an increasing mole fraction of TETA in the blend solution, the absorption rate significantly increases and TSP + TETA solution has the best absorption rate in comparison with other additives. It can be seen that the initial slope of TETA blended with TSP solution has a steeper ascend than that of pure TSP solution. Polyamines such as TETA are a category of potential amine absorbents. Thanks to their special structure, including two or more amino groups within one molecule, they exhibit high absorption capacity and fast absorption rate.

As presented in Figure 4.12 to 4.14, the addition of 2MPZ to TSP significantly accelerates the absorption rate in comparison with TSP solution. Moreover, it can be concluded that the absorption rate into TSP + 2MPZ is higher than into the other solvents except for TSP blended with TETA. Therefore, 2-MPZ as a diamine with two secondary amine sites could be a potential additive for gas absorption because of its high CO₂ solubility and absorption rate.

The small addition of K-Gly and K-Pro in TSP provides a significant impact on the enhancement of the absorption rate. From Figure 4.12 to 4.14, it is clear that the absorption rate in aqueous TSP + K-Pro is higher than TSP + K-Gly but slightly lower than TSP + 2-MPZ. Furthermore, it is clearly seen that the CO₂ absorption rate increases as mole fraction of AMP in the blend solution increases; however, it has a lower CO₂ absorption rate compared to TSP + K-Gly.

As an overall conclusion, it is found that the absorption rate increases significantly as the additives concentration increases, but this enhancement in blend solutions contained AMP was less than other type additives. In other words, all of the suggested additives showed a better CO₂ absorption rate than pure TSP in the order: TSP + TETA > TSP + 2MPZ > TSP + K-Pro > TSP + K-Gly > TSP + AMP > TSP.

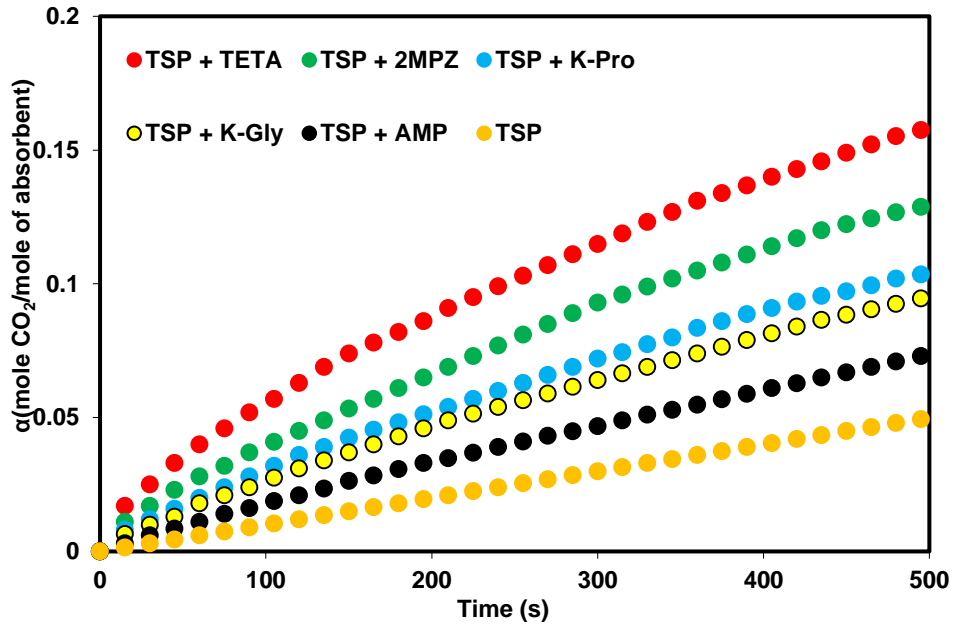


Figure 4.12 The effect of addition of additives to TSP solution on the CO₂ absorption rate at 313.15 K and additive mole fraction 0.2.

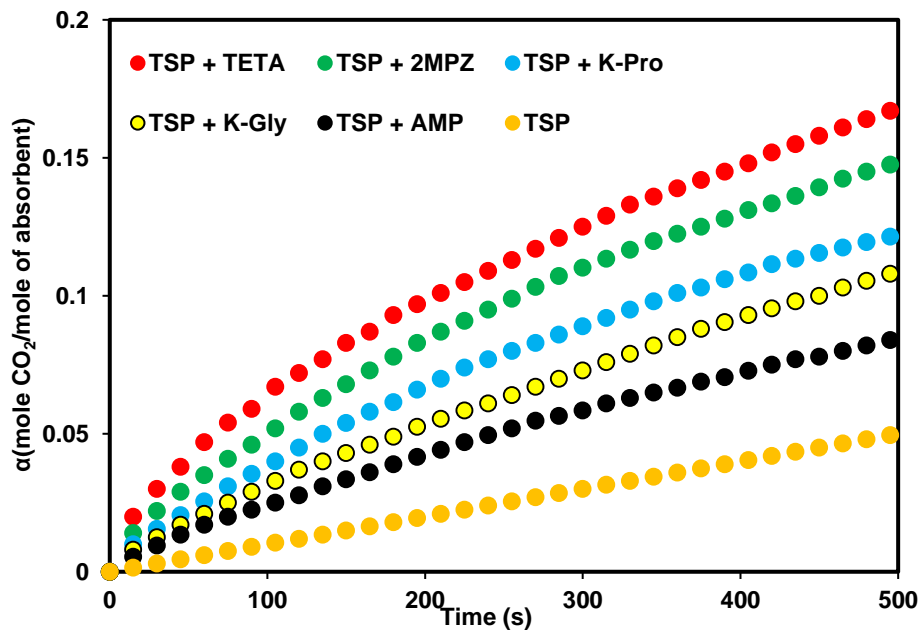


Figure 4.13 The effect of addition of additives to TSP solution on the CO₂ absorption rate at 313.15 K and additive mole fraction 0.3.

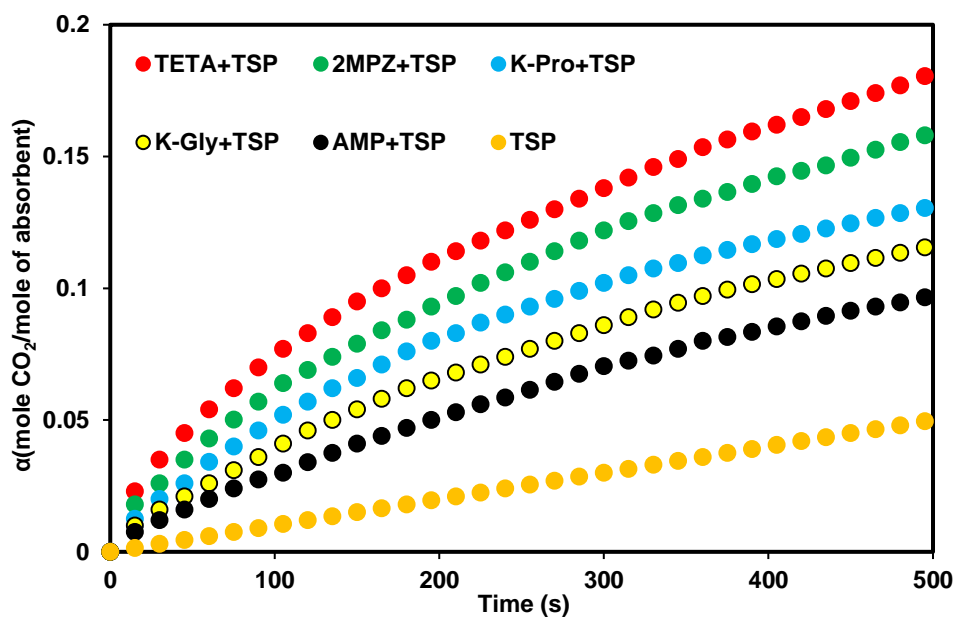


Figure 4.14 The effect of addition of additives to TSP solution on the CO₂ absorption rate at 313.15 K and additive mole fraction 0.4.

4.3.3. CO₂ loading capacity of TSP + additive (2)

Another group of amine additives, including potassium sarcosinate (K-Sar), potassium lysinate (K-Lys), piperazine (PZ), methyldiethanolamine (MDEA) and 2-(2-aminoethylamino)ethanol (AEEA) have been selected as additive to improve the loading capacity of CO₂ and the absorption rate into TSP solution. The CO₂ loading capacity of these blend solutions at 313 K and additive mole fractions of 0.2 to 0.5 was measured and the results were tabulated in Table 4.9 to 4.13.

Table 4.9 CO₂ loading capacity of TSP + K-Lys solution at 313.15 K.

R = 0.2		R = 0.4		R = 0.5	
P _{CO₂} (kPa)	α	P _{CO₂} (kPa)	α	P _{CO₂} (kPa)	α
08.25	0.921	06.24	0.941	07.21	0.972
19.76	0.977	18.50	0.992	17.68	1.014
28.64	1.011	30.76	1.036	28.34	1.055
37.42	1.045	38.26	1.068	37.64	1.079
48.18	1.069	47.19	1.077	49.23	1.102

α (mole CO₂/mole of absorbent) is the moles of CO₂ absorbed per one mole of solvent

Table 4.10 CO₂ loading capacity of TSP + PZ solution at 313.15 K.

R = 0.2		R = 0.4		R = 0.5	
P _{CO₂} (kPa)	α	P _{CO₂} (kPa)	α	P _{CO₂} (kPa)	α
07.32	0.901	08.74	0.921	06.32	0.935
21.37	0.972	17.64	0.971	22.58	1.013
31.28	1.008	28.37	1.004	34.67	1.042
39.52	1.032	36.57	1.036	41.86	1.064
47.34	1.051	48.21	1.059	48.62	1.073

α (mole CO₂/mole of absorbent) is the moles of CO₂ absorbed per one mole of solvent

Table 4.11 CO₂ loading capacity of TSP + AEEA solution at 313.15 K.

R = 0.2		R = 0.4		R = 0.5	
P _{CO₂} (kPa)	α	P _{CO₂} (kPa)	α	P _{CO₂} (kPa)	α
08.12	0.838	07.62	0.825	07.23	0.812
22.39	0.921	18.37	0.891	21.34	0.897
30.58	0.953	26.72	0.927	30.56	0.934
39.73	0.995	34.71	0.952	42.85	0.971
48.62	1.012	46.23	0.992	49.31	0.985

α (mole CO₂/mole of absorbent) is the moles of CO₂ absorbed per one mole of solvent

Table 4.12 CO₂ loading capacity of TSP + K-Sar solution at 313.15 K.

R = 0.2		R = 0.4		R = 0.5	
P _{CO₂} (kPa)	α	P _{CO₂} (kPa)	α	P _{CO₂} (kPa)	α
06.99	0.783	07.18	0.769	06.46	0.758
19.34	0.854	14.28	0.808	15.20	0.807
28.62	0.916	22.35	0.851	20.27	0.835
37.65	0.942	35.24	0.919	35.62	0.907
48.28	0.971	46.78	0.957	47.28	0.944

α (mole CO₂/mole of absorbent) is the moles of CO₂ absorbed per one mole of solvent

Table 4.13 CO₂ loading capacity of TSP + MDEA solution at 313.15 K.

R = 0.2		R = 0.4		R = 0.5	
P _{CO₂} (kPa)	α	P _{CO₂} (kPa)	α	P _{CO₂} (kPa)	α
07.24	0.728	08.27	0.702	09.31	0.709
16.52	0.785	15.29	0.763	18.66	0.761
25.31	0.824	24.37	0.807	25.37	0.794
34.28	0.881	36.71	0.872	36.82	0.865
46.18	0.923	45.94	0.911	44.78	0.889

The conditions for all experiments were set to a temperature of 313.15 K, a total blend concentration of 2.5 kmol/m³ and an additive mole fraction of 0.2, 0.4 and 0.5. It was found that a blend of the suggested additives with TSP has a significantly larger CO₂ loading capacity compared with MEA.

As seen from Figure 4.15 to 4.17, among the tested additives, K-Lys and PZ showed a positive effect on the CO₂ loading capacity of the pure TSP solution, while the effect of AEEA, K-Sar and MDEA was negative. The aqueous TSP + K-Lys solution presented the highest absorption capacity among all the absorbents tested.

In addition, the results showed that loading capacity of CO₂ into TSP + K-Lys increases with increasing molar fraction of amino acid salt in blend solution, but the loading capacity of CO₂ into TSP + K-Sar decreases. Thus, K-Lys shows a better performance than K-Sar on the solubility of CO₂ into TSP. This may be due to the two carbon-nitrogen bonds in the lysine structure which leads to an increase in the CO₂ loading capacity. This is because more sites available for reaction with carbon dioxide are provided with more amino groups.

It can also be observed in Figure 4.15 to 4.17 that the CO₂ loading capacity increases with increasing concentration of PZ in blend solutions. Furthermore, the solubility of CO₂ into TSP + PZ is higher than those into other absorbents, except for the TSP + K-Lys mixture. According to Figure 4.15 to 4.17, the solution AEEA + TSP exhibits a higher CO₂ solubility in comparison with K-Sar + TSP and MDEA + TSP, but the CO₂ solubility in this solution is lower than those in K-Lys + TSP and PZ + TSP. This might be due to the presence of one secondary and one primary amine group in the structure of AEEA. In summary, K-Lys+TSP has the highest CO₂ solubility than the additive + TSP solutions with the following ranking: K-Lys + TSP > PZ + TSP > TSP > AEEA + TSP > K-Sar + TSP > MDEA + TSP > MEA.

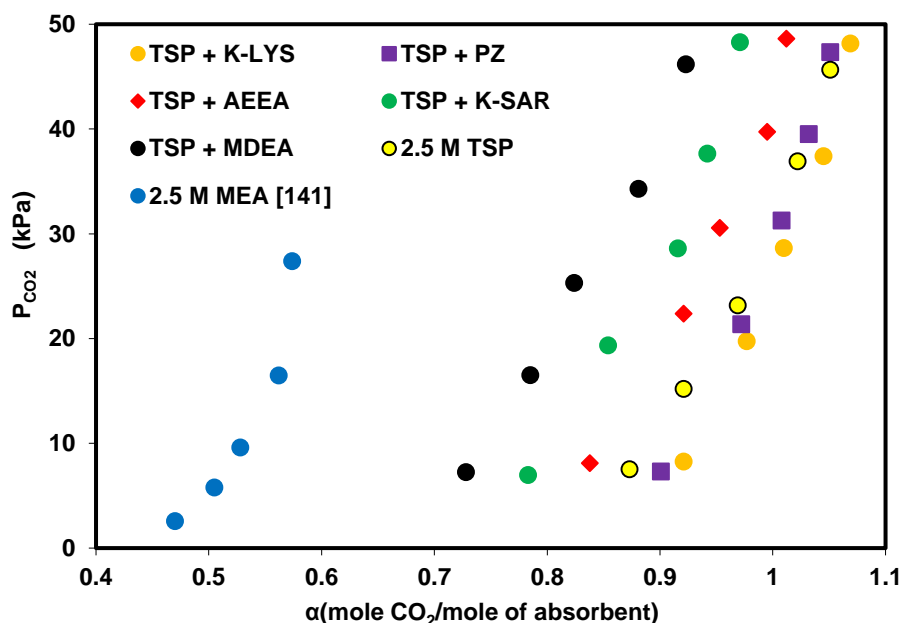


Figure 4.15 The effect of addition of additives on CO₂ loading of TSP at 313.15 K and mole fraction 0.2.

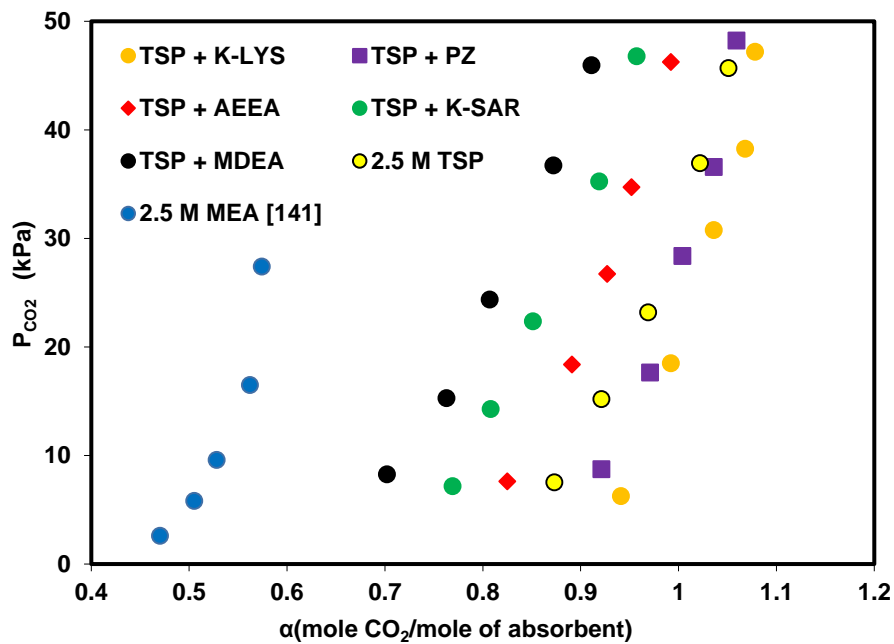


Figure 4.16 The effect of addition of additives on CO₂ loading of TSP at 313.15 K and mole fraction 0.4.

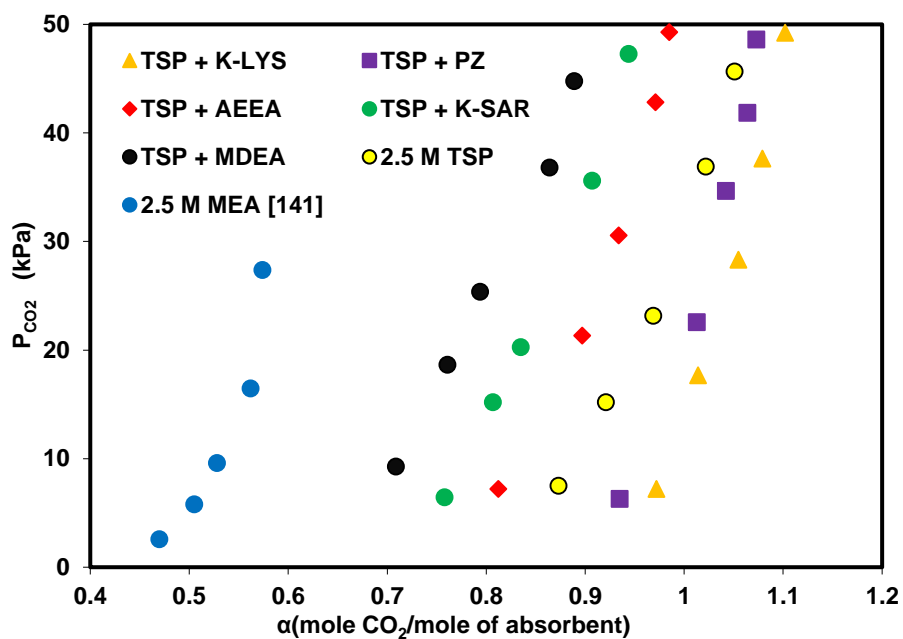


Figure 4.17 The effect of addition of additives on CO₂ loading of TSP at 313.15 K and mole fraction 0.5.

4.3.4. Absorption rate of CO₂ in TSP + additive (2)

In order to investigate and compare different additives in terms of absorption rate, CO₂ loading capacity is shown as a function of time in Figure 4.18 to 4.20. The initial slope of the solubility of CO₂ versus time is a key parameter for comparing the performance of various absorbents.

As can be observed in these figures, all the blended solutions show better CO₂ absorption rates than pure TSP. Furthermore, the absorption rate increases significantly as the additives concentration increases, but the enhancement in blend solutions containing MDEA is lower than other additives. The fastest absorption rate was achieved with TSP + PZ for all the three concentration levels of the activator. The initial slope of TSP + PZ has a steeper ascending trend than that of pure TSP. Piperazine as a diamine has several advantages, including a high loading capacity and fast chemical reactivity due to its cyclic diamine structure with two secondary amine sites.

It was found that MDEA has the weakest effect of activator on the absorption rate of CO₂ of TSP. After PZ, AEEA exhibits the strongest effect on the absorption rate. It can also be seen from Figure 4.18 to 4.20 that the addition of K-Lys and K-Sar to TSP accelerates the absorption of CO₂. K-Lys has a primary amino group (pK_a=9.16) and an aliphatic amino group in its side chain (pK_a=10.67), which has a different chemical structure from the other amino acid salts and results in a faster chemical reactivity with CO₂. Among the selected amino acid salts, K-Lys shows a higher reactivity with CO₂ than K-Sar.

According to our observation, a mixture of additive and TSP presents faster absorption rate than single TSP, in the order: PZ+TSP > AEEA+TSP > K-Lys+TSP > K-Sar+TSP > MDEA+TSP > TSP.

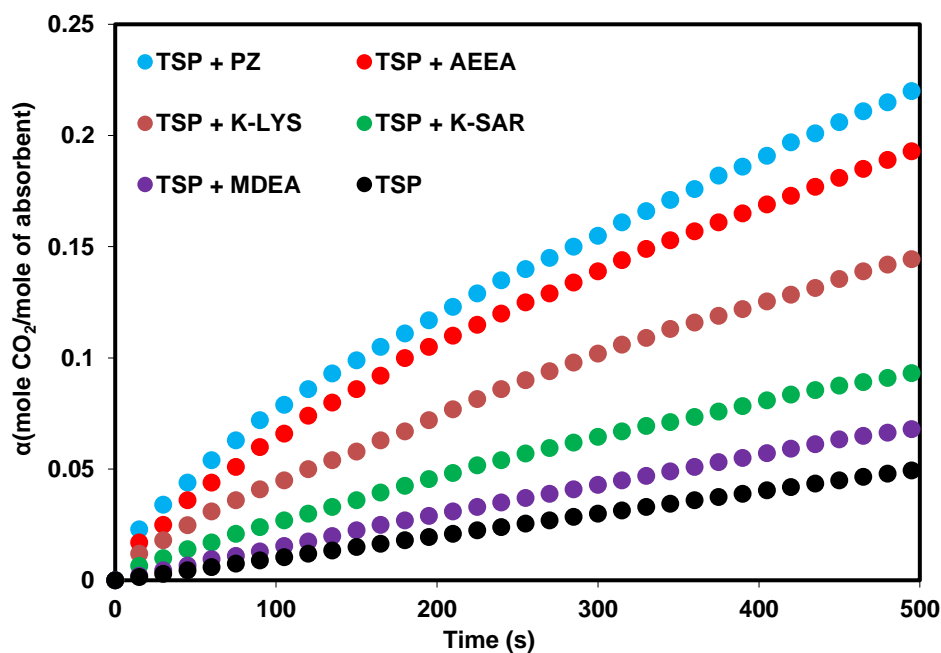


Figure 4.18 The effect of addition of additives on the CO₂ absorption rate of TSP at 313.15 K and additive mole fraction 0.2.

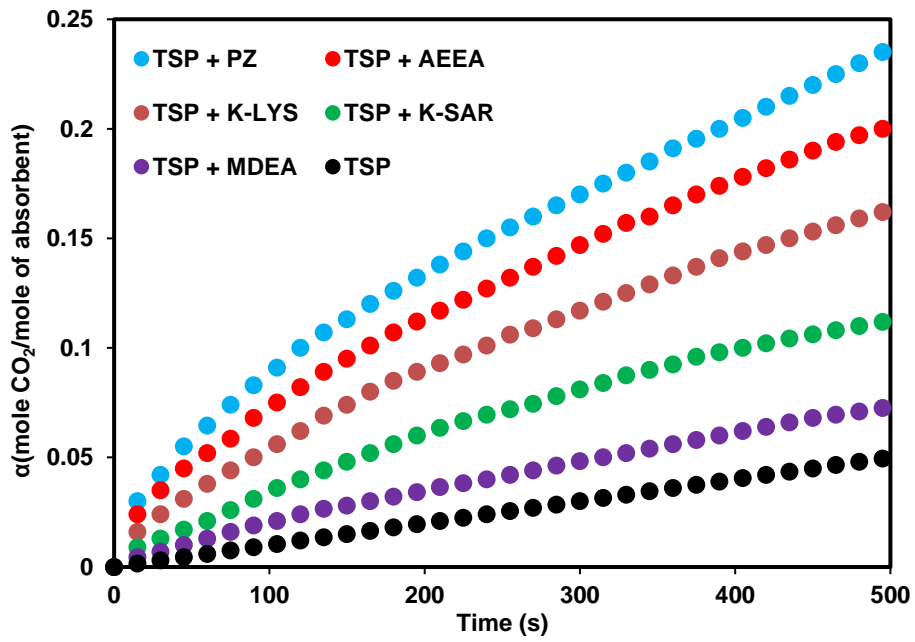


Figure 4.19 The effect of addition of additives on the CO₂ absorption rate of TSP at 313.15 K and additive mole fraction 0.4.

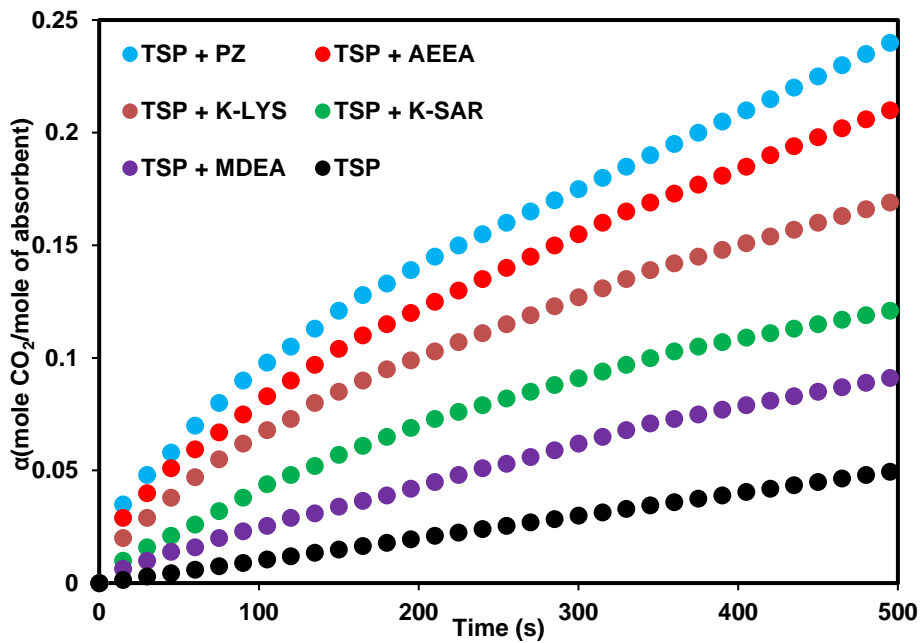


Figure 4.20 The effect of addition of additives on the CO₂ absorption rate of TSP at 313.15 K and additive mole fraction 0.5.

4.3.5. Corrosion rate of TSP + additive solution

The corrosion rate is one of the most important parameters of absorbent in the CO₂ absorption process because it reduces the equipment life and increases cost of the CO₂ capture [23]. Therefore, performance of solvent in terms of corrosion rate needs to be evaluated for its acceptability as a suitable solvent in industrial practice.

Performance of TSP solution blended with 10 amine additives was investigated in terms of CO₂ loading capacity and absorption rate in the previous sections. In order to further investigation of blend solutions in this work, the corrosion rate in TSP blended with amines was measured on carbon steel at temperature of 313.15 K according to ASTM G5-94 and the results was compared with MEA solution [142]. This investigation will allow to have a good understanding of absorbents in the application of gas absorption from acidic gases. Most corrosion studies in the literature are for single amines, and very few are for blended solutions.

The experimental data of corrosion rates of TSP + additive solutions at 313.15 K were given in Figure 4.21, with comparison to that of MEA. Apparently, TSP + TETA and TSP + PZ solution have the highest corrosion rate, while TSP + MDEA and TSP + AMP show the lowest corrosion rate among all the additives tested, although all of them have weaker corrosion than MEA. Usually, among the different types of amines, primary amines (such as MEA) exhibit the highest corrosion rate, while tertiary amines such as MDEA have the lowest corrosion rate.

Furthermore, the experimental results indicate that the corrosion rate using a TSP + amino acid salt solutions such as K-Lys, K-Sar, K-Pro and K-Gly is less than those using the TSP + cyclic amines such as 2MPZ and AEEA solutions.

According to Figure 4.21, the corrosiveness of carbon steel using a TSP + additive system was lower than that using the MEA system, and the experimental corrosion rates can be ranked as follows: MEA > TSP+TETA > TSP+PZ > TSP+2MPZ > TSP+AEEA > TSP+K-Gly > TSP+K-Pro > TSP+K-Sar > TSP+K-Lys > TSP+AMP > TSP+MDEA.

Overall, the major disadvantages of amines in general are their high heats of absorption and high corrosion rates, but accompanied by a high chemical reactivity toward CO₂, while the main benefits of using an inorganic solvent such as TSP are the lower corrosion rate, lower energy of regeneration and high stability. Thus, blending a fast reactant (such as amines), with a solvent (such as TSP) having a low corrosion rate and low regeneration energy could be a good option for improving the overall solvent performance in different ways.

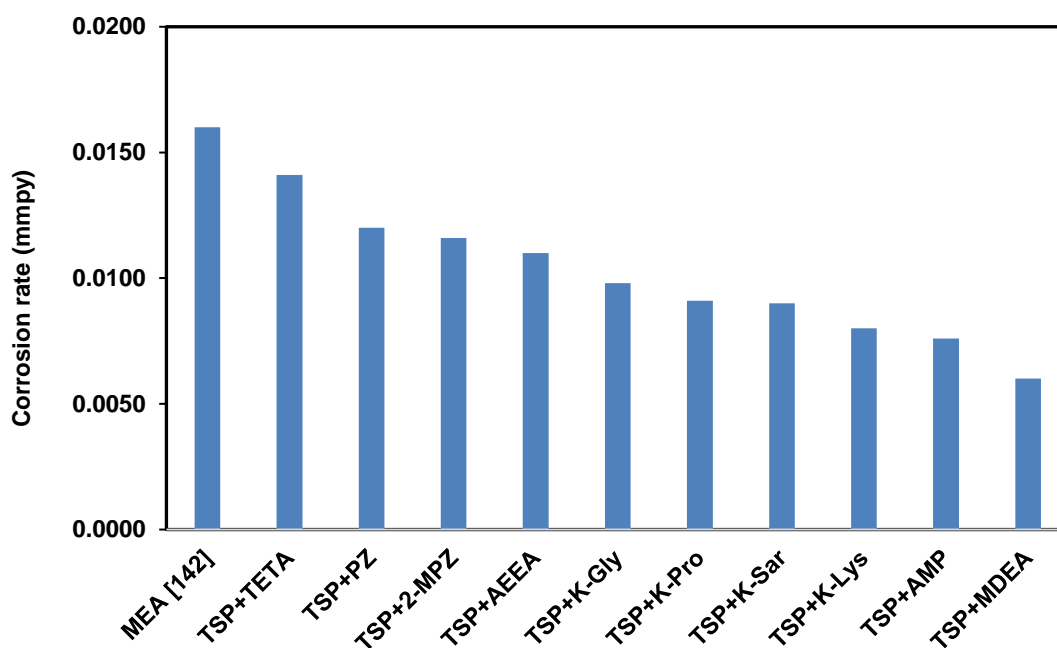


Figure 4.21 Comparison of corrosion rate between MEA and TSP + amine additives at 313.15 K.

4.3.6. Solvent toxicity

An ideal absorbent should have several desired characteristics, including fast kinetics, high absorption capacity and low regeneration energy. In addition, the low environmental and health risks are another characteristics of an ideal solvent for CO₂ capture process [24]. Therefore, the toxicity of solvent should be investigated. In this work, toxicity of studied solvents in this work was investigated.

A comparison between toxicity of different solvents was given in Figure 4.22. This figure shows values of lethal dose (LD₅₀) of several absorbents. The LD₅₀ is the amount of a material which causes the death of 50% of a group of tested animals in the certain time. Therefore, the lower values of LD₅₀ means more toxicity of solvent [24]. According to Figure 4.22, all of amino acids including serine, sarcosine, glycine, lysine, alanine and proline showed the least, and conventional amines such as MEA and PZ had the highest toxicity. Among the all of amino acids studied in this work serine indicated the lowest toxicity. The lower toxicity of amino acids in comparison to conventional amines is one of their advantages which make them attractive from point of view of environmental friendly.

It also can be seen from Figure 4.22, that MDEA presents higher toxicity than amino acids, but its value is still lower when compared to conventional amines. Inorganic solvents such as TSP and K₂CO₃ also showed good performance. However, MEA and PZ as most popular absorbents for CO₂ capture have high reaction rate, but they have high toxicity which limit their commercial viability.

As an overall conclusion, among all of the absorbents used in this study, amino acids seem to have a better performance in terms of toxicity in comparison with other amines, and therefore could be considered as an environmentally relatively acceptable absorbent.

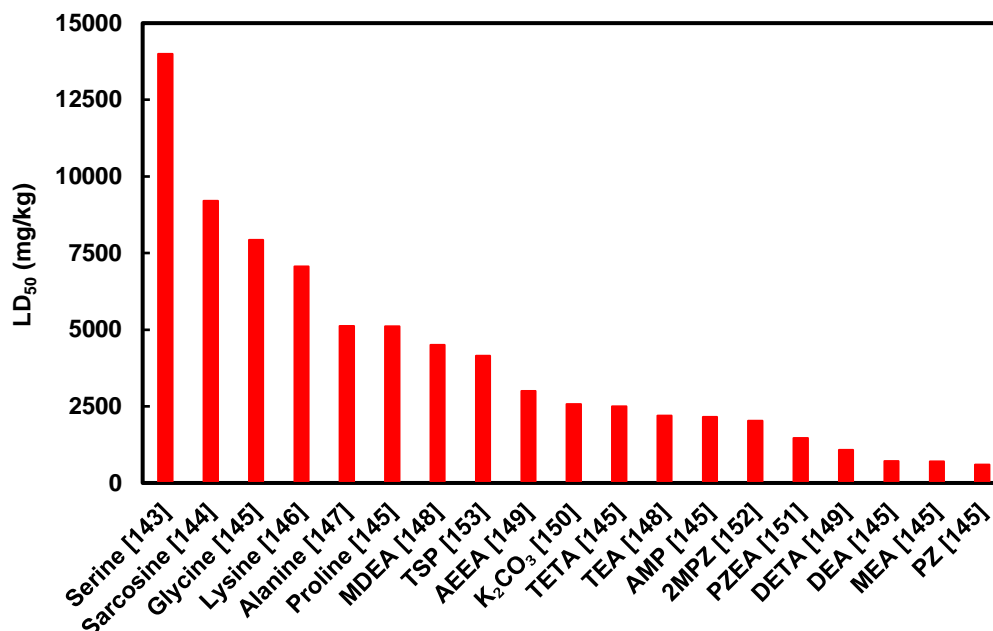


Figure 4.22 Values of toxicity of different types of chemical absorbents.

4.4. Absorption characterization of CO₂ in K₂CO₃ + AEEA, Ala, Ser

The performance of 10 different amine additives was evaluated in terms of CO₂ loading capacity, absorption rate, corrosion rate and toxicity in the previous section. According to the results obtained in the previous section, among all the tested amines, three amines including 2-methylpiperazine (2MPZ), potassium lysinate (K-Lys) and 2-(2-aminoethylamino)ethanol (AEEA) were selected as potential additives for further investigation. In addition, potassium salt of two amino acids including serine (K-Ser) and alanine (K-Ala) was chosen as additive.

4.4.1. CO₂ loading capacity of K₂CO₃ + AEEA, Ala, Ser

In this section, potassium carbonate, an inorganic solvent, was used as based solvent and three amines including AEEA, K-Ala and K-Ser were added as additive. The performance of 2MPZ and K-Lys will be evaluated in the next sections. The CO₂ absorption capacity of solutions of 2 M K₂CO₃ + (0.1-0.3) M additive was measured at 313 K and CO₂ partial pressures up to 25 kPa, the results was compared with results of single K₂CO₃ and MEA. The results of the measurement of CO₂ solubility were summarized in Table 4.14 to 4.16 and were presented in Figure 4.23 to 4.25.

Table 4.14 CO₂ loading capacity of K₂CO₃ + AEEA solution at 313.15 K.

2 M K₂CO₃+0.1 M AEEA		2 M K₂CO₃+0.2 M AEEA		2 M K₂CO₃+0.3 M AEEA	
P_{CO₂} (kPa)	α	P_{CO₂} (kPa)	α	P_{CO₂} (kPa)	α
02.07	0.569	02.18	0.641	02.44	0.721
04.27	0.621	04.64	0.686	05.59	0.762
07.14	0.652	07.33	0.723	10.07	0.804
12.36	0.702	11.03	0.743	13.81	0.827
16.83	0.714	15.12	0.767	16.50	0.831

α (mole CO₂/mole of absorbent) is the moles of CO₂ absorbed per one mole of solvent

Table 4.15 CO₂ loading capacity of K₂CO₃ + K-Ala solution at 313.15 K.

2 M K₂CO₃+0.1 M K-Ala		2 M K₂CO₃+0.2 M K-Ala		2 M K₂CO₃+0.3 M K-Ala	
P_{CO₂} (kPa)	α	P_{CO₂} (kPa)	α	P_{CO₂} (kPa)	α
03.31	0.548	02.04	0.578	02.06	0.622
05.26	0.587	05.11	0.626	04.77	0.649
08.99	0.611	08.25	0.663	09.93	0.694
11.47	0.630	13.94	0.711	13.26	0.717
15.08	0.659	16.55	0.719	17.41	0.728

α (mole CO₂/mole of absorbent) is the moles of CO₂ absorbed per one mole of solvent

Table 4.16 CO₂ loading capacity of K₂CO₃ + K-Ser solution at 313.15 K.

2 M K₂CO₃+0.1 M K-Ser		2 M K₂CO₃+0.2 M K-Ser		2 M K₂CO₃+0.3 M K-Ser	
P_{CO₂} (kPa)	α	P_{CO₂} (kPa)	α	P_{CO₂} (kPa)	α
02.37	0.470	03.01	0.539	02.10	0.563
05.88	0.542	07.22	0.592	07.33	0.625
08.02	0.571	10.25	0.633	11.18	0.649
13.28	0.619	14.30	0.651	13.06	0.668
16.31	0.642	17.55	0.672	15.42	0.685

α (mole CO₂/mole of absorbent) is the moles of CO₂ absorbed per one mole of solvent

As illustrated in Figure 4.23 to 4.25, all of the blend solutions showed a higher CO₂ loading capacity in comparison with pure MEA. In addition, the addition of amine additive to K₂CO₃ showed positive effect on CO₂ loading. This is because the amino groups in the AEEA, K-Ala and K-Ser are reactive and can absorb CO₂. It was also found that the CO₂ absorption capacity is the highest in K₂CO₃ + AEEA and the lowest in K₂CO₃ + K-Ser solution. This can be due to the fact that K-Ser has fewer amino groups than AEEA in its molecular structure. AEEA is a diamine with one secondary and one primary amine group in its structure. Thus, one mole of AEEA can absorb two moles of CO₂ which is higher than K-Ala and K-

Ser. In addition, solution of $K_2CO_3 + K\text{-Ala}$ presented a higher absorption capacity than $K_2CO_3 + K\text{-Ser}$ solution. This result can be explained mainly due to the fact that alanine as a sterically hindered amino acid has a methyl group in its α -carbon, which leads to an increase at CO_2 loading capacity in comparison with serine. As shown in Figure 4.23 to 4.25, with increasing CO_2 partial pressure, the CO_2 loading increases at constant temperature and concentration due to the increase in the driving force from the gas phase to the interface.

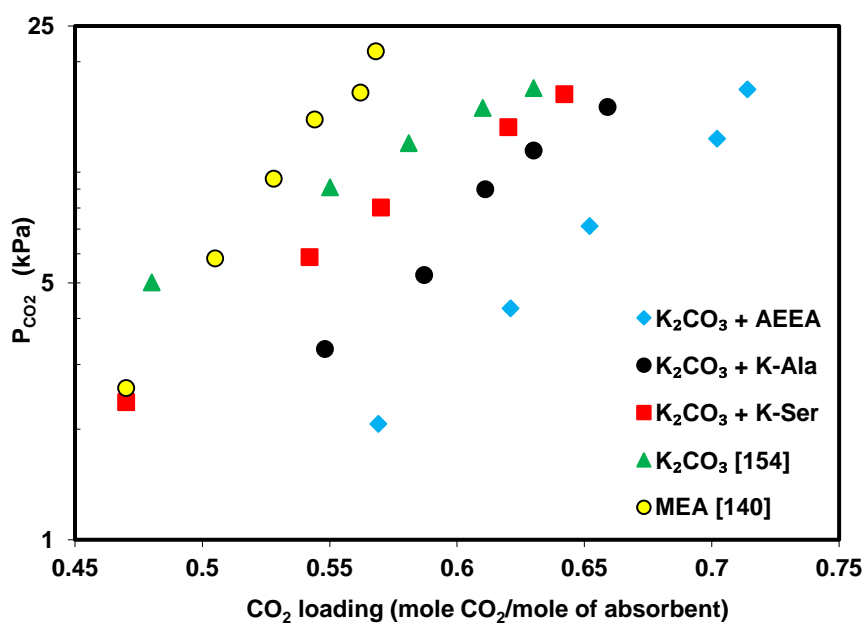


Figure 4.23 The values of CO_2 loading capacity of 2 M K_2CO_3 + 0.1 M additive at 313.15 K.

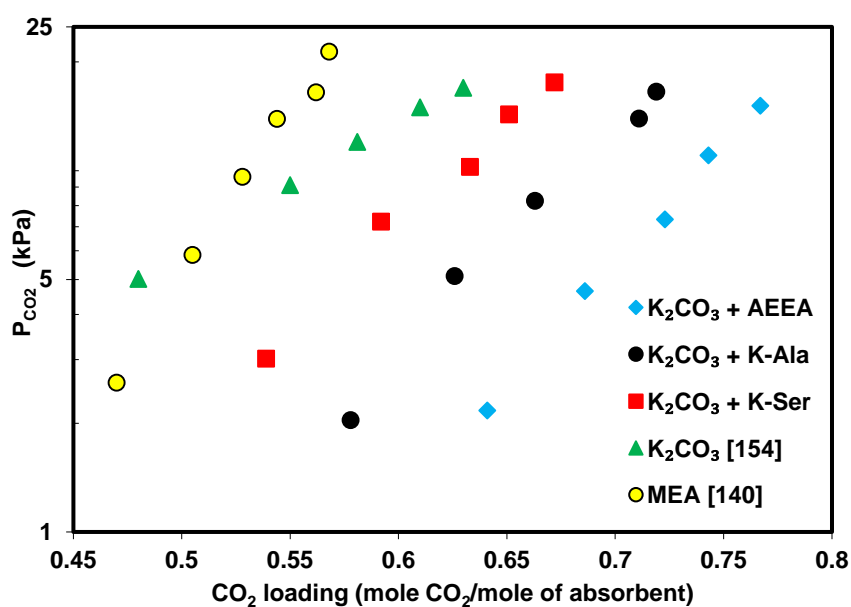


Figure 4.24 The values of CO_2 loading capacity of 2 M K_2CO_3 + 0.2 M additive at 313.15 K.

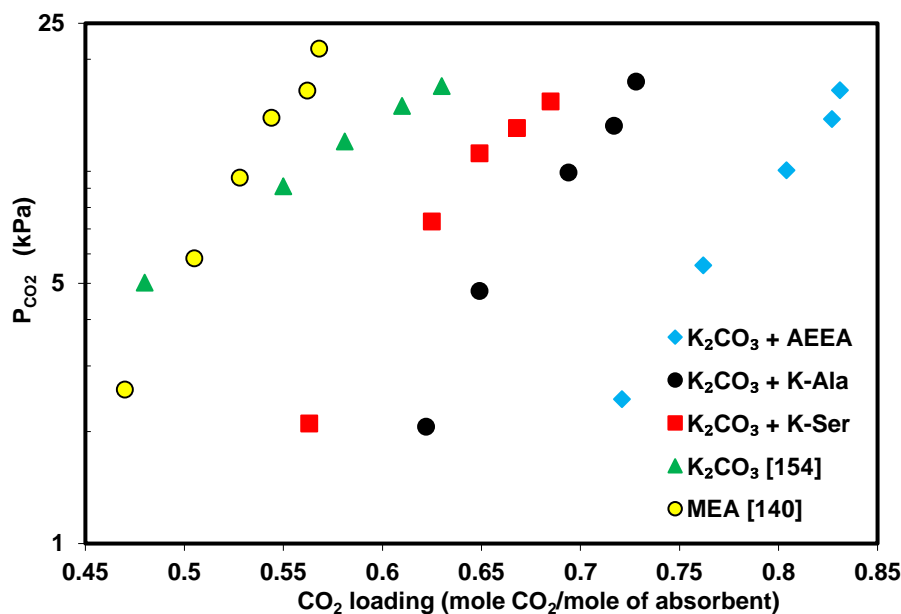


Figure 4.25 The values of CO₂ loading capacity of 2 M K₂CO₃ + 0.3 M additive at 313.15 K.

4.4.2. Absorption rate of CO₂ in K₂CO₃ + AEEA, Ala, Ser

As already mentioned, the main drawback with K₂CO₃ solution is the low absorption rate compared to amines, which leads to the larger absorber size. Thus, improving the absorption rate of K₂CO₃ as a suitable solvent is important for reducing absorber size and thus absorption process cost.

Pressure decay during absorption of CO₂ in the solutions at different temperatures and concentrations was determined using a pressure sensor and values of partial pressure of CO₂ versus time were recorded. Therefore, the CO₂ absorption rate of K₂CO₃ + additive can be calculated from the slope of the plot of pressure versus time according to Eq. (46).

The effect of temperature, concentration and type of additive on reactivity of CO₂ with K₂CO₃ + additive solution was studied and the results were listed in Table 4.17 to 4.19.

Table 4.17 Value of absorption rate of CO₂ in 2 M K₂CO₃ + 0.1 M additive

T (K)	K ₂ CO ₃	K ₂ CO ₃ + AEEA	K ₂ CO ₃ + K-Ser	K ₂ CO ₃ + K-Ala
	N _{CO₂} × 10 ⁶ (kmol/m ² .s)			
303.15	0.62	3.04	2.38	1.94
313.15	1.77	4.71	3.91	3.05
323.15	3.51	6.26	5.13	4.22

Table 4.18 Value of absorption rate of CO₂ in 2 M K₂CO₃ + 0.2 M additive

	K₂CO₃	K₂CO₃ + AEEA	K₂CO₃ + K-Ser	K₂CO₃ + K-Ala
T (K)	$N_{CO_2} \times 10^6$ (kmol/m ² .s)			
303.15	0.62	3.85	2.98	2.47
313.15	1.77	5.79	4.55	3.81
323.15	3.51	7.15	5.96	5.02

Table 4.19 Value of absorption rate of CO₂ in 2 M K₂CO₃ + 0.3 M additive

	K₂CO₃	K₂CO₃ + AEEA	K₂CO₃ + K-Ser	K₂CO₃ + K-Ala
T (K)	$N_{CO_2} \times 10^6$ (kmol/m ² .s)			
303.15	0.62	4.43	3.78	3.26
313.15	1.77	7.02	5.38	4.43
323.15	3.51	7.95	6.77	5.89

It was observed that the CO₂ partial pressure decreases with increasing time until a gas-liquid equilibrium is reached. The time required to obtain an equilibrium state is different for each solutions. This pressure reduction in the equilibrium cell shows the amount of gas absorption. It was also found that the addition of AEEA, K-Ala and K-Ser to K₂CO₃ has been led to a significant increase in the absorption rate that is favorable for the CO₂ capture process. In other words, CO₂ absorption rate can be accelerated remarkably when K₂CO₃ solution is promoted by the addition of small amounts of the suggested additives as shown in Figures 4.26 to 4.28. The pH of absorbent increases, when AEEA, K-Ala or K Ser are added to K₂CO₃. Therefore, rate of reaction CO₂ with OH⁻ increases which causes an enhancement in the overall absorption rate.

The K₂CO₃ + AEEA showed faster absorption rate compared to K₂CO₃ + K-Ala and K₂CO₃ + K-Ser. The reason is that primary and secondary amine groups in AEEA structure react with CO₂ and form primary and secondary carbamates with high pKa which leads to a significant enhancement in CO₂ absorption rate. In addition, rate in K₂CO₃ + K-Ser solution is higher than K₂CO₃ + K-Ala solution. Compared to K-Ala, K-Ser has a primary amino group and also a hydroxymethyl group which is attached to α-carbon, hence a fast reaction with CO₂ is expected.

According to the results, at constant concentration, absorption rate of CO₂ was accelerated when temperature increases due to the increase at reaction rate constant as given in Figure 4.29. It was observed that the CO₂ absorption rate has higher values at higher additive concentration due to reaction rate between CO₂ and additives increase, which leads to an enhancement at overall absorption rate.

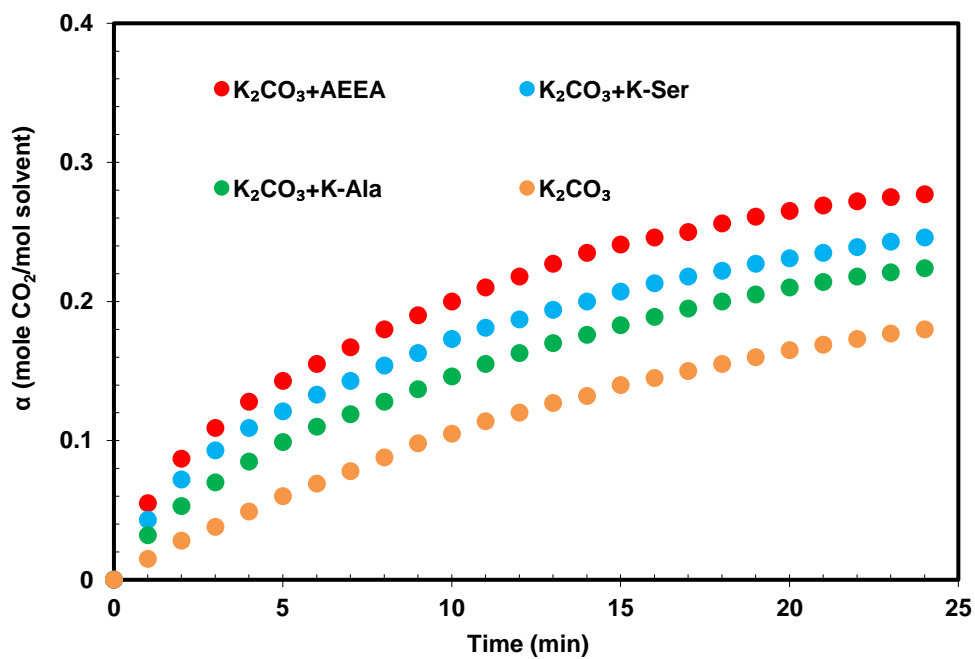


Figure 4.26 The effect of addition of 0.1 kmol/m^3 additives on the CO_2 absorption rate of K_2CO_3 at 313.15 K .

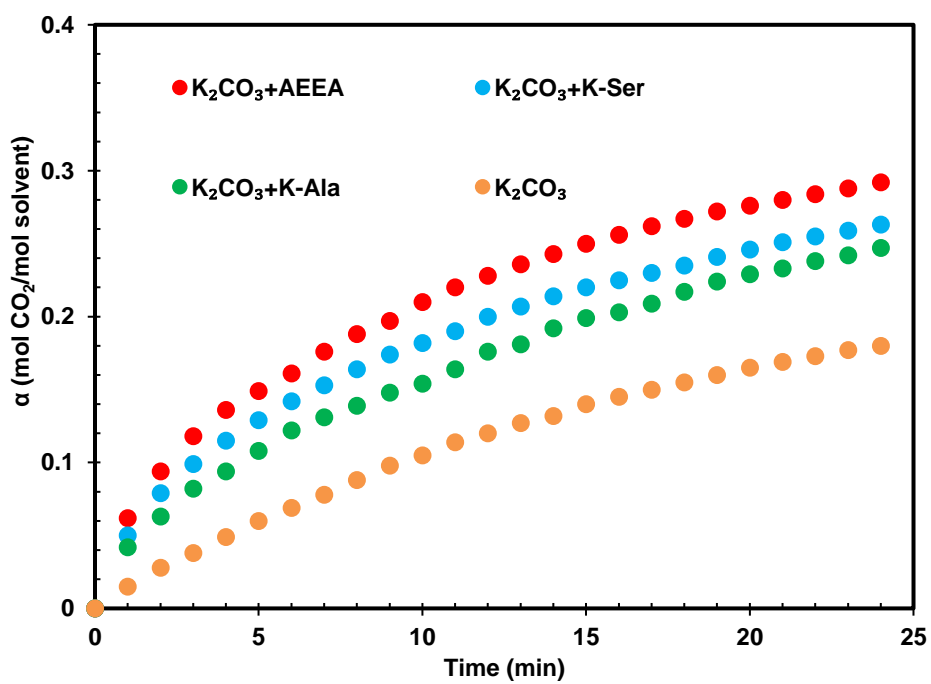


Figure 4.27 The effect of addition of 0.2 kmol/m^3 additives on the CO_2 absorption rate of K_2CO_3 at 313.15 K .

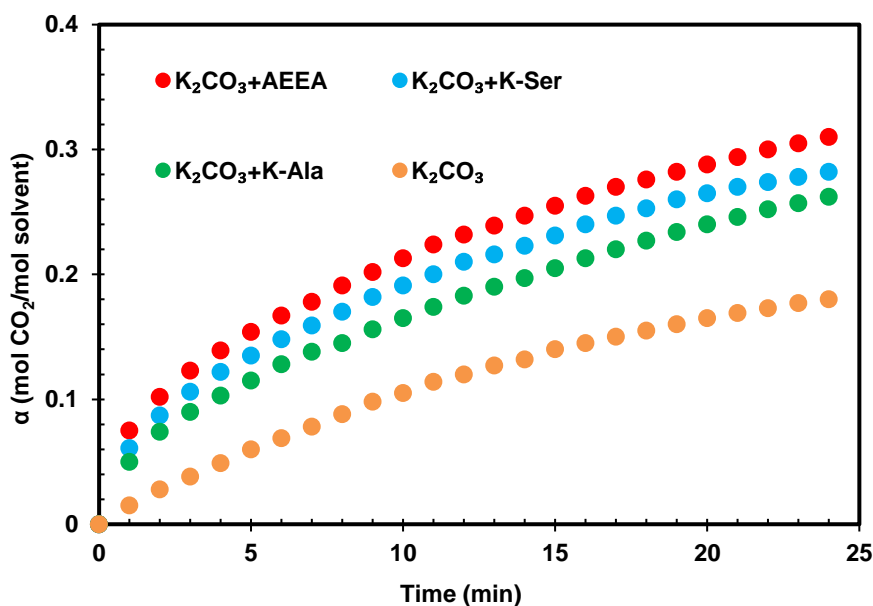


Figure 4.28 The effect of addition of 0.3 kmol/m^3 additives on the CO_2 absorption rate of K_2CO_3 at 313.15 K .

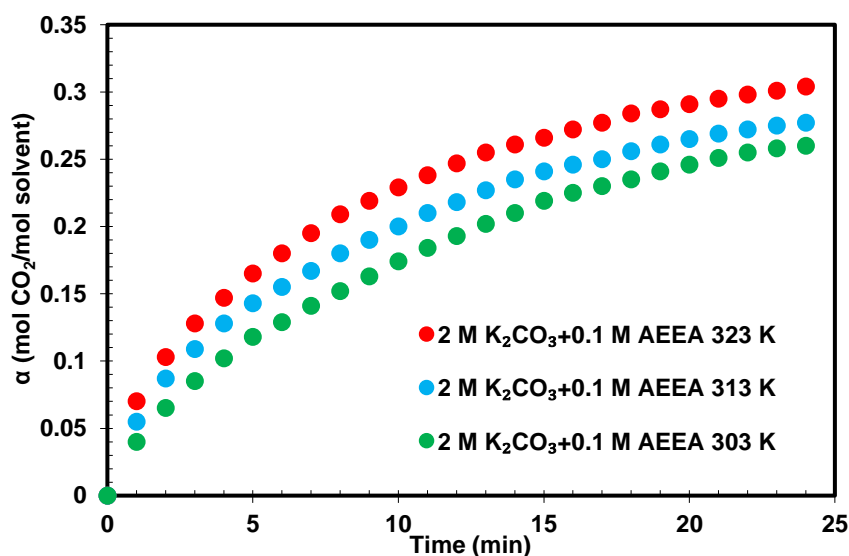


Figure 4.29 The effect of temperature on on the CO_2 absorption rate of $\text{K}_2\text{CO}_3 + \text{AEEA}$ solution.

4.4.3. Heat of CO_2 absorption of $\text{K}_2\text{CO}_3 + \text{AEEA}$, Ala, Ser

As it was mentioned before, one of main challenges in CO_2 capture process is high energy consumption in the stripper for regeneration of solvent which leads to an increase cost of absorption process. Therefore, investigation of performance of solvent in terms of absorption heat is necessary. The values of heat of CO_2 absorption can be calculated on the basis of the Gibbs-Helmholtz equation which was explained in section 3.4. In this work, CO_2 absorption heat of aqueous potassium carbonated promoted by

AEEA, K-Ala and K-Ser was determined directly from the slope of plot of $\ln P_{\text{CO}_2}$ versus $1/T$ at constant CO_2 solubility. The results were listed in Tables 4.20 to 4.22 and presented in Figure 4.30 to 4.32.

Table 4.20 Heat of CO_2 absorption in solution of 2 M K_2CO_3 + 0.1 M additive

	K_2CO_3 + AEEA	K_2CO_3 + K-Ala	K_2CO_3 + K-Ser
α	$-\Delta H$ (kJ/mol CO_2)	$-\Delta H$ (kJ/mol CO_2)	$-\Delta H$ (kJ/mol CO_2)
0.50	44.01	37.22	39.98
0.55	43.89	36.47	39.04
0.60	43.12	35.89	38.15
0.65	42.23	35.04	37.42
0.70	41.04	34.26	36.57
0.75	40.33	33.51	35.83
0.80	39.50	32.79	35.02

α (mole CO_2 /mole of absorbent) is the moles of CO_2 absorbed per one mole of solvent

Table 4.21 Heat of CO_2 absorption in solution of 2 M K_2CO_3 + 0.2 M additive

	K_2CO_3 + AEEA	K_2CO_3 + K-Ala	K_2CO_3 + K-Ser
α	$-\Delta H$ (kJ/mol CO_2)	$-\Delta H$ (kJ/mol CO_2)	$-\Delta H$ (kJ/mol CO_2)
0.50	45.79	39.02	41.65
0.55	45.24	38.44	40.86
0.60	44.65	37.53	40.04
0.65	43.72	36.88	39.13
0.70	42.54	36.03	38.27
0.75	41.31	35.46	37.53
0.80	40.67	34.97	36.79

α (mole CO_2 /mole of absorbent) is the moles of CO_2 absorbed per one mole of solvent

Table 4.22 Heat of CO_2 absorption in solution of 2 M K_2CO_3 + 0.3 M additive

	K_2CO_3 + AEEA	K_2CO_3 + K-Ala	K_2CO_3 + K-Ser
α	$-\Delta H$ (kJ/mol CO_2)	$-\Delta H$ (kJ/mol CO_2)	$-\Delta H$ (kJ/mol CO_2)
0.50	47.34	40.66	43.01
0.55	46.96	39.58	42.36
0.60	46.08	39.02	41.68
0.65	45.12	38.41	41.02
0.70	44.38	37.75	40.14
0.75	43.26	37.04	39.25
0.80	42.06	36.39	38.40

α (mole CO_2 /mole of absorbent) is the moles of CO_2 absorbed per one mole of solvent

As can be observed in Figure 4.30 to 4.32, an increase in CO₂ loading capacity leads to a decrease in heat of absorption in K₂CO₃ + additive system. This is because at higher loading capacity, the physical absorption dominates, and bicarbonate forms that leads to a reduction at heat of CO₂ absorption. It also can be seen from these figures that K₂CO₃ promoted by AEEA gives a higher value of heat of absorption over the entire CO₂ solubility in comparison with K₂CO₃ + K-Ala and K₂CO₃ + K-Ser due to the hydroxyl group in the structure of AEEA.

Furthermore, the K₂CO₃ + K-Ala showed the best performance in terms of heat of absorption. In other words, a mixture of K₂CO₃ with K-Ala has lowest heat of absorption and can be a favorable candidate for CO₂ capture. The structure similar to sterically hindered amines in alanine which causes a steric hindrance effect, and also the formation of an unstable carbamate can be reasons of reduction of the heat of absorption in comparison to serine. The easy of regeneration and high absorption capacity are the most important features of sterically hindered amines. Thus, the heat of CO₂ absorption can be ranked as follow: K₂CO₃ + K-Ala < K₂CO₃ + K-Ser < K₂CO₃+AEEA.

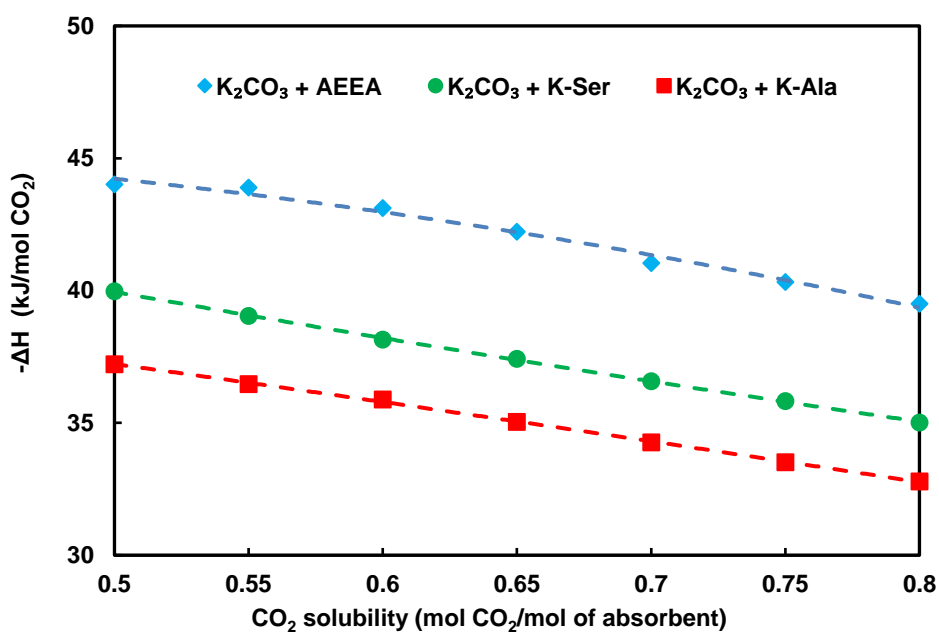


Figure 4.30 Heat of CO₂ absorption in solution of 2 M K₂CO₃ + 0.1 M additive

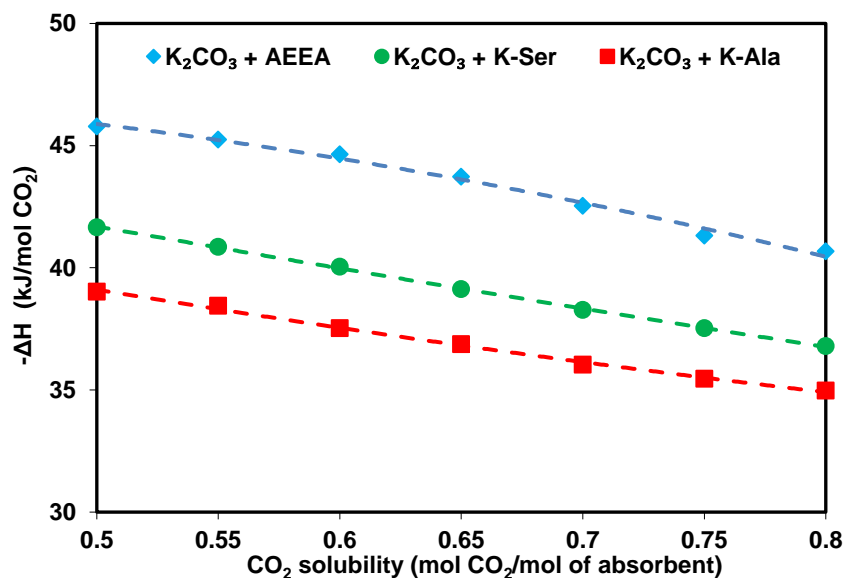


Figure 4.31 Heat of CO₂ absorption in solution of 2 M K₂CO₃ + 0.2 M additive

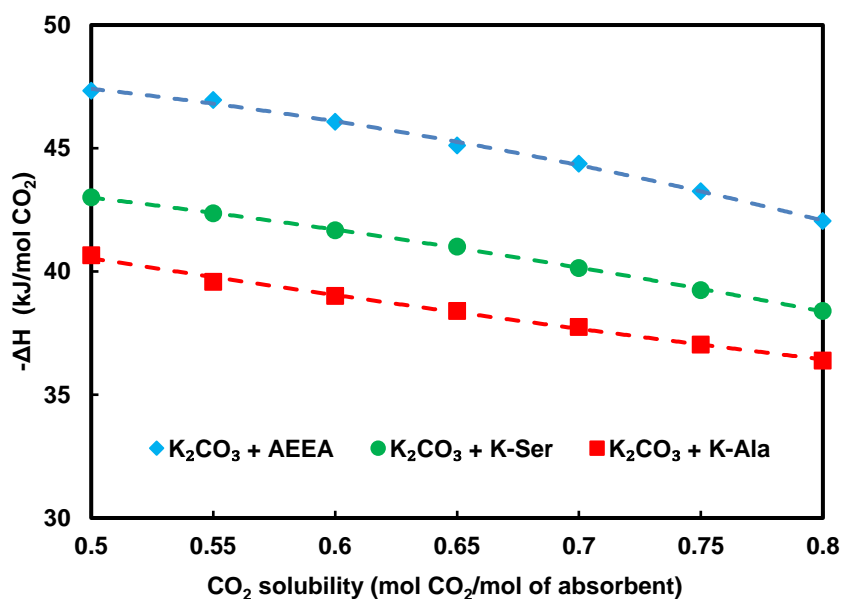


Figure 4.32 Heat of CO₂ absorption in solution of 2 M K₂CO₃ + 0.3 M additive

Absorption heat of K₂CO₃ + additive solutions tested in this work was compared to more commonly used solvents in the CO₂ absorption processes, such as MEA, AMP, PZ, DEA, MDEA and blend of K₂CO₃ with other additives such as K₂CO₃ + 2MPZ, K₂CO₃ + PZ and K₂CO₃ + DPTA as shown in Figure 4.33. It was found that a blend of K₂CO₃ with amine additives have lower heat of CO₂ absorption in comparison with pure MEA and other absorbents which means less energy is needed for CO₂ regeneration in stripper column. However, amines like MEA have fast reaction kinetics, but they have high absorption heat which increases CO₂ capture cost. MEA solution as a primary alkanolamine has highest value of heat of

absorption equal to 84.17 kJ/mol CO₂. This may be due to the fact that MEA reacts with CO₂ and form stable carbamates which causes an increase in heat of absorption. K₂CO₃ solution is an attractive absorbent because of its low regeneration energy requirement. Therefore, as expected, blend of K₂CO₃ as a base solvent with amine additives showed much better performance in terms of heat of absorption compared to conventional amines such as MEA, AMP, PZ, DEA and MDEA. Chowdhury et al. [155] observed that sterically hindered amines like AMP indicate a better absorption heat performance than MEA because of formation of unstable carbamate. In addition, Figure 4.33, shows that PZ solution as a secondary diamines has heat of absorption value lower than AMP and MEA, but higher than DEA and MDEA. It was also found that absorption heat of DEA solution is about 22% lower than MEA. Generally, secondary alkanolamines (DEA) have heats of absorption lower than primary alkanolamines (MEA) and higher than tertiary alkanolamines (MDEA). However, heat of absorption of MDEA is higher than K₂CO₃, but its value is still lower than other conventional amines such as AMP, DEA, PZ, PZEA and MEA because of formation of bicarbonates instead of carbamates in reaction of CO₂ with MDEA. A comparison of heat of absorption between K₂CO₃ solution and K₂CO₃ + PZ and K₂CO₃ + 2MPZ showed that the addition of these additives increase absorption heat because PZ and 2MPZ have primary and secondary amino groups, which form carbamate. As mentioned above, these carbamate ions increase absorption heat, however absorption heat of these blended solutions is still lower than MEA. According to the results, using K₂CO₃ blended with a potential additive such as AEEA, K-Ala and K-Ser for CO₂ absorption from flue gas is a right choice from the heat of absorption point of view.

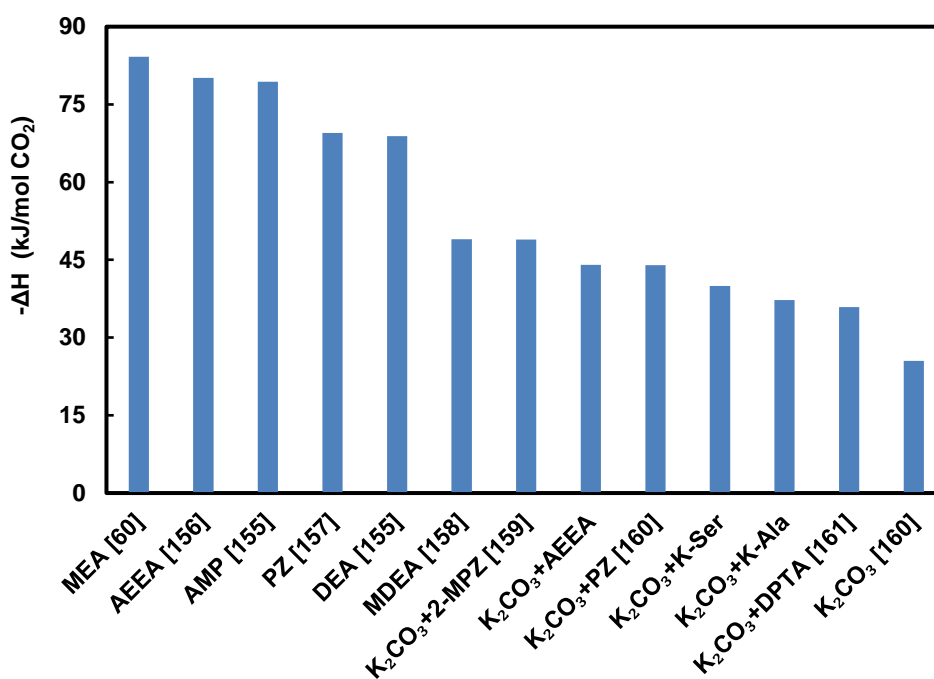


Figure 4.33 Comparison of heat of CO₂ absorption of K₂CO₃ + additive with the other absorbents.

4.5. Absorption characterization of CO₂ in K₂CO₃ + 2MPZ

4.5.1. CO₂ loading capacity of K₂CO₃ + 2MPZ

The CO₂ loading capacity of potassium carbonate promoted by 2MPZ was measured using stirred cell reactor and the results was listed in Table 4.23 and presented in Figure 4.34. As it can be seen, CO₂ loading capacity of K₂CO₃ + 2MPZ increases as the concentration of 2MPZ increases from 0.1 to 0.5 kmol/m³ at 313 K. This is due to the molecular structure of 2MPZ which is a cyclic diamine with two amino groups. These amino groups are reactive and can participate in the reactions of CO₂ absorption that means 2MPZ can absorb more CO₂. The obtained results in this work were compared with MEA (as the most widely used solvent in industrial absorption plant) and K₂CO₃ solutions. The CO₂ loading capacity of K₂CO₃ + 2MPZ solution is significantly higher than that of pure MEA and K₂CO₃. This indicates that K₂CO₃ + 2MPZ solution can be considered as a promising absorbent thanks to its high loading capacity. Generally, an absorbent with higher absorption capacity is preferred because it leads to a smaller amount of absorbent and reduce cost of CO₂ absorption process.

Table 4.23 CO₂ loading capacity of K₂CO₃ + (0.1-0.5) M 2MPZ solution at 313.15 K.

[2MPZ]=0.1 kmol/m ³		[2MPZ]=0.2 kmol/m ³		[2MPZ]=0.3 kmol/m ³		[2MPZ]=0.4 kmol/m ³		[2MPZ]=0.5 kmol/m ³	
P _{CO₂}	α	P _{CO₂}	α	P _{CO₂}	α	P _{CO₂}	α	P _{CO₂}	α
02.55	0.55	03.01	0.58	02.74	0.62	02.19	0.62	02.46	0.65
07.02	0.60	07.39	0.63	06.27	0.66	05.28	0.67	05.03	0.69
12.88	0.65	11.83	0.67	10.71	0.70	08.05	0.70	11.31	0.75
17.24	0.67	15.48	0.69	18.36	0.73	13.73	0.74	15.94	0.77
21.04	0.69	23.07	0.71	22.85	0.75	24.06	0.77	19.27	0.79

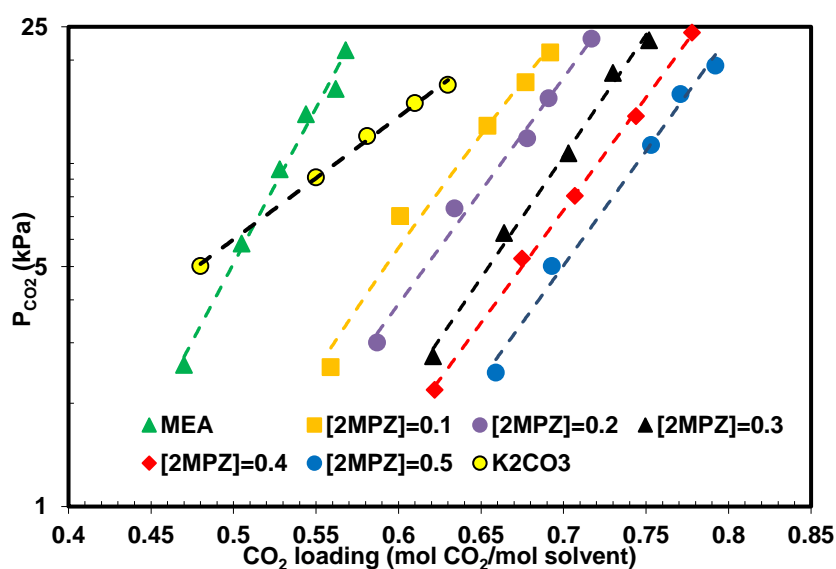


Figure 4.34 CO₂ loading capacity of K₂CO₃ + (0.1-0.5) M 2MPZ at 313.15 K.

4.5.2. Density and viscosity of $K_2CO_3 + 2MPZ$

It is necessary to measure density and viscosity of solvent at different temperatures and concentrations for calculations of diffusion coefficients and kinetics parameters. Before measurement of density and viscosity of $K_2CO_3 + 2MPZ$ solutions, density and viscosity of water were measured and compared with literature data [162,163] in order to validate the experimental procedures and devices used in this work. The given results in Table 4.24 showed that data obtained in this study are in good corresponding with the literature data.

Table 4.24 Comparison of experimental and literature data of density and viscosity of pure water.

T (K)	ρ (g.cm ⁻³)		μ (mPa.s ⁻¹)	
	Exp.	Lit. [162]	Exp.	Lit. [163]
303	0.9951	0.9957	0.7903	0.7975
313	0.9919	0.9922	0.6501	0.6532
323	0.9872	0.9880	0.5504	0.5471

After validation, density and viscosity of $K_2CO_3 + 2MPZ$ solutions were measured at temperatures between 303 and 323 K, with K_2CO_3 concentration of 2 kmol/m³ and 2MPZ concentration between 0.1 and 0.5 kmol/m³, and results were listed in Table 4.25 and plotted in Figure 4.35 and 4.36. As can be seen in these figures, both of density and viscosity of $K_2CO_3 + 2MPZ$ solution increase as the 2MPZ concentration increases and decrease when temperature increases from 303 to 323 K.

Table 4.25 Density and viscosity of 2 M $K_2CO_3 + (0.1-0.5)$ M 2MPZ solutions.

T (K)	[2MPZ]=0.1 kmol/m ³	[2MPZ]=0.2 kmol/m ³	[2MPZ]=0.3 kmol/m ³	[2MPZ]=0.4 kmol/m ³	[2MPZ]=0.5 kmol/m ³
ρ (g.cm ⁻³)					
303	1.0985	1.0987	1.0990	1.0991	1.0993
313	1.0940	1.0942	1.0945	1.0950	1.0953
323	1.0897	1.0899	1.0902	1.0904	1.0908
μ (mPa.s ⁻¹)					
303	1.1289	1.1670	1.2190	1.2540	1.3010
313	0.9211	0.9463	0.9852	1.0188	1.0552
323	0.7714	0.8102	0.8230	0.8446	0.8799

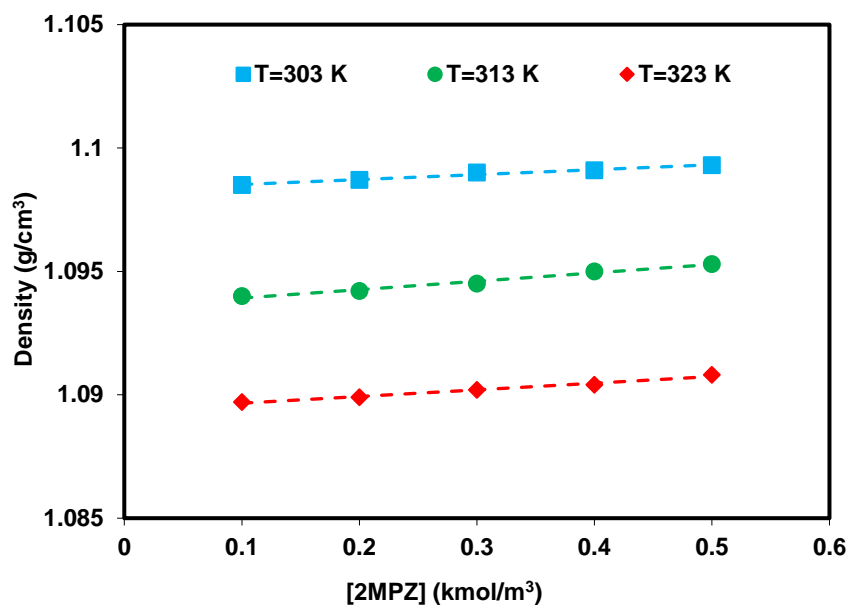


Figure 4.35 Density of 2 M K_2CO_3 + (0.1–0.5) M 2MPZ solutions

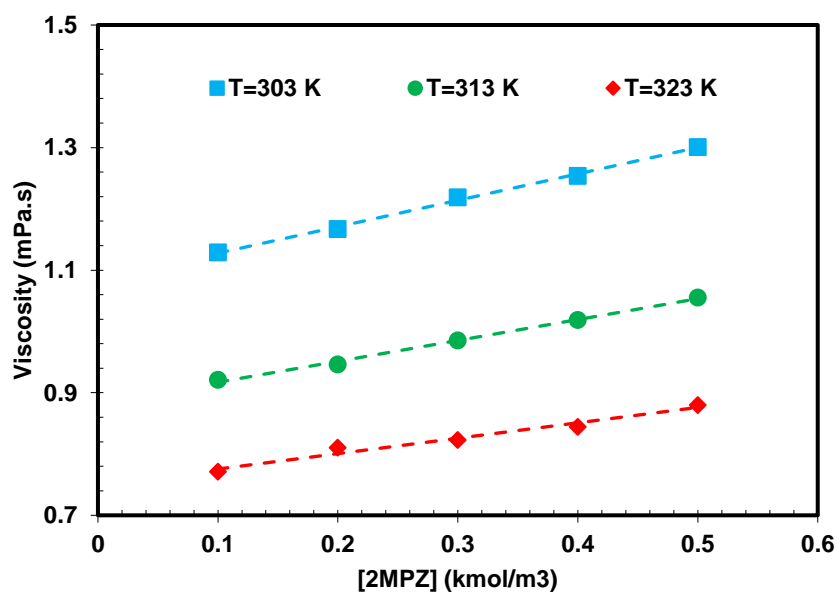


Figure 4.36 Viscosity of 2 M K_2CO_3 + (0.1–0.5) M 2MPZ solutions

4.5.3. Diffusivity of CO_2 in K_2CO_3 + 2MPZ

The values of solubility and diffusivity of CO_2 in solution are also required to obtain the kinetics parameters and to analyze the results of CO_2 absorption rate. The diffusivity of CO_2 and the physical solubility of CO_2 in K_2CO_3 + 2MPZ solution cannot be measured directly since CO_2 undergoes chemical reactions with solvent, and thus determining its physical solubility and the free molecular diffusivity is not possible [164].

Therefore, it is first necessary to measure diffusivity of N_2O and the physical solubility of N_2O in $K_2CO_3 + 2MPZ$ solution. Then, using N_2O analogy and modified Stokes-Einstein equation, and with the help of the physical properties of N_2O in solution, diffusivity and the physical solubility of CO_2 in $K_2CO_3 + 2MPZ$ solution can be calculated. This method was originally suggested by Clarke [165] and modified by Laddha et al. [166]. They used N_2O gas instead of CO_2 since N_2O gas does not react chemically with these solutions and also has similar molecular volume, configuration and electronic structure as CO_2 [167]. According to N_2O analogy, the ratio of the diffusivity or the physical solubility of CO_2 to N_2O in $K_2CO_3 + 2MPZ$ is equal to that in water. This N_2O analogy method was used extensively by researchers to estimate these properties in different solutions.

Therefore, in this work, the diffusion coefficient of CO_2 in $K_2CO_3 + 2MPZ$ was determined using Eqs. (50-53) and the obtained results were listed in Table 4.26 and presented in Figure 4.37.

$$H_{CO_2, \text{solvent}} = \exp \left(20.2669 - \frac{13830.6}{T} + \frac{6913000}{T^2} - \frac{15.589 \times 10^8}{T^3} + \frac{1.2 \times 10^{11}}{T^4} \right) \quad (49)$$

$$\left(\frac{D_{CO_2}}{D_{N_2O}} \right)_{\text{solvent}} = \left(\frac{D_{CO_2}}{D_{N_2O}} \right)_{H_2O} \quad (50)$$

$$D_{CO_2, H_2O} = 2.35 \times 10^{-6} \exp \left(\frac{-2119}{T} \right) \quad (51)$$

$$D_{N_2O, H_2O} = 5.07 \times 10^{-6} \exp \left(\frac{-2371}{T} \right) \quad (52)$$

From our viscosity measurements and using Eq. (53), we can obtain the values of the diffusion coefficients of N_2O in $K_2CO_3 + 2MPZ$:

$$D_{N_2O, \text{solvent}} = D_{N_2O, H_2O} \times \left(\frac{\mu_{H_2O}}{\mu_{\text{solvent}}} \right)^{0.6} \quad (53)$$

Where μ_{H_2O} and μ_{solvent} are the viscosity of water and $K_2CO_3 + 2MPZ$, respectively. According to the results, the diffusivity of CO_2 in mixture of K_2CO_3 and $2MPZ$ decreases as the concentration of $2MPZ$ increases and increases from approximately 16 to 27×10^{-10} (m^2/s) when temperature increases from 303 to 323 K. This is because the variation of diffusivity of CO_2 in the solution is opposite to that of viscosity. At higher temperature and lower concentration, viscosity of solution decreases which leads to increase diffusivity of CO_2 in solvent.

Table 4.26 The diffusivity of CO_2 in 2 M $K_2CO_3 + (0.1-0.5)$ M $2MPZ$ solutions.

T (K)	[2MPZ]=0.1 kmol/m ³	[2MPZ]=0.2 kmol/m ³	[2MPZ]=0.3 kmol/m ³	[2MPZ]=0.4 kmol/m ³	[2MPZ]=0.5 kmol/m ³
$D_{CO_2} \times 10^{10}$ (m^2/s)					
303	17.47	17.01	16.66	16.31	15.98
313	21.74	21.32	20.92	20.54	20.16
323	26.99	26.53	26.08	25.65	25.23

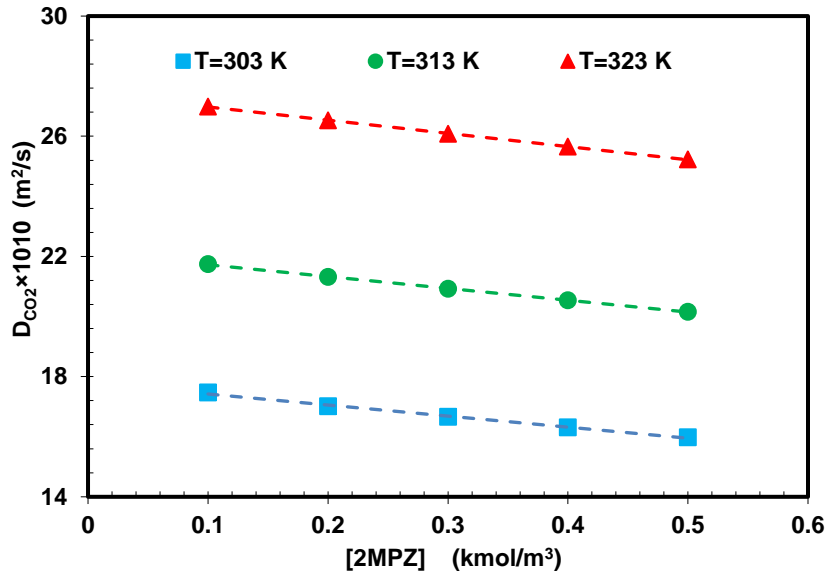


Figure 4.37 The diffusivity of CO₂ in 2 M K₂CO₃ + (0.1-0.5) M 2MPZ solutions.

4.5.4. Kinetics study of CO₂ absorption in K₂CO₃ + 2MPZ

This section focuses on reaction kinetics between CO₂ and aqueous K₂CO₃ + 2MPZ solution. The general expression for CO₂ absorption rate is described by the following equation [168]:

$$N_{\text{CO}_2} = E_A K_L ([\text{CO}_2]_i - [\text{CO}_2]_b) \quad (54)$$

Where E_A , K_L , $[\text{CO}_2]_i$ and $[\text{CO}_2]_b$ are enhancement factor, liquid mass transfer coefficient, interfacial CO₂ concentrations and concentration of CO₂ in the solution, respectively. Since absorbent used in all experiments was not initially loaded with CO₂, the bulk concentration of CO₂ ($[\text{CO}_2]_b$) is equal to zero. In order to study the kinetics of CO₂ with K₂CO₃ + 2MPZ solution, it is important that CO₂ absorption occurs in the fast pseudo-first-order reaction regime [169], and its necessary condition was given in Eq. (55):

$$3 < H_a \ll E_\infty \quad (55)$$

Where E_∞ and H_a are the enhancement factor for an instantaneous reaction and Hatta number, respectively, and can be obtained by the following equations:

$$H_a = \frac{\sqrt{K_{OV} D_{\text{CO}_2}}}{K_L} \quad (56)$$

$$E_\infty = 1 + \frac{D_{\text{solvent}} C_{\text{solvent}}}{b D_{\text{CO}_2} [\text{CO}_2]_i} \quad (57)$$

Where D_{CO_2} , D_{solvent} , b and K_{OV} are CO₂ diffusion coefficient, solvent diffusion coefficient the stoichiometric coefficient of solvent and the overall pseudo-first-order reaction rate constant, respectively. The enhancement factor and Hatta number are equal if condition at Eq. (55) is satisfied. The validity of

this assumption is checked experimentally in the next sections and discussed in more detail. Thus, Eq. (54) is rearranged to:

$$N_{\text{CO}_2} = \sqrt{K_{\text{OV}} D_{\text{CO}_2}} [\text{CO}_2]_i \quad (58)$$

According to Eq. (58), in the fast pseudo-first-order regime, CO_2 absorption flux is not depend on liquid mass transfer coefficient. Therefore, N_{CO_2} should be independent of the stirring speed. According to Henry's law, the interfacial concentration of CO_2 can be determined by Eq. (59):

$$[\text{CO}_2]_i = \frac{P_{\text{CO}_2}}{H_{\text{CO}_2}} \quad (59)$$

Consequently, Eq. (58) is changed to:

$$N_{\text{CO}_2} = \sqrt{K_{\text{OV}} D_{\text{CO}_2}} \frac{P_{\text{CO}_2}}{H_{\text{CO}_2}} \quad (60)$$

With using experimental values of absorption rate of CO_2 in the solution, CO_2 diffusivity, partial pressure of CO_2 and Henry constant, the overall reaction rate constant can be calculated for each system:

$$K_{\text{OV}} = \frac{\left(\frac{N_{\text{CO}_2} H_{\text{CO}_2}}{P_{\text{CO}_2}}\right)^2}{D_{\text{CO}_2}} \quad (61)$$

In the case CO_2 absorption in $\text{K}_2\text{CO}_3 + 2\text{MPZ}$ solution, it is necessary to consider reaction K_2CO_3 and CO_2 in parallel with the reaction between CO_2 with 2MPZ .

$$R_{\text{OV}} = R_{\text{CO}_2-2\text{MPZ}} + R_{\text{CO}_2-\text{OH}^-} \quad (62)$$

In CO_2 absorption process, where pH is greater than 9, reaction between H_2O and CO_2 can be neglected. Therefore, the reaction of CO_2 and OH^- is the rate-limiting reaction. A first-order reaction with respect to both carbon dioxide and OH^- was found by Astarita et al. [170]:

$$R_{\text{CO}_2-\text{OH}^-} = k_{\text{OH}^-} [\text{CO}_2] [\text{OH}^-] \quad (63)$$

Where k_{OH^-} can be determined from the equation given by Danckwerts et al. [115]:

$$\log k_{\text{OH}^-} = 13.635 - \frac{2895}{T} \quad (64)$$

According to zwitterion mechanism, the reaction rate between CO_2 and 2MPZ can be presented by Eq. (65):

$$R_{\text{CO}_2-2\text{MPZ}} = \frac{k_1 [2\text{MPZ}] [\text{CO}_2]}{1 + \frac{k_{-1}}{\sum k_B [B]}} \quad (65)$$

When the deprotonation of the zwitterion is very fast or $\left(\frac{k_{-1}}{\sum k_B [B]} \ll 1\right)$, the reaction rate of CO_2 with 2MPZ reduces to simple second-order reaction.

$$R_{\text{CO}_2-2\text{MPZ}} = k_1 [2\text{MPZ}] [\text{CO}_2] \quad (66)$$

When zwitterion deprotonation is rate-limiting or ($\frac{k_{-1}}{\sum k_B[B]} \gg 1$), then, the overall reaction order varies between two and three:

$$R_{\text{CO}_2-2\text{MPZ}} = k_1[2\text{MPZ}]^n [\text{CO}_2] \quad (67)$$

Consequently, Eq. (62) is changed to:

$$R_{\text{OV}} = [\text{CO}_2] (k_{\text{OH}^-}[\text{OH}^-] + k_1[2\text{MPZ}]^n) \quad (68)$$

$$R_{\text{OV}} = [\text{CO}_2] k_{\text{OV}} \quad (69)$$

$$k_{\text{OV}} = k_{\text{OH}^-}[\text{OH}^-] + k_1[2\text{MPZ}]^n \quad (70)$$

Then, the apparent reaction rate constant can be obtained as follows:

$$k_{\text{app}} = k_{\text{OV}} - k_{\text{OH}^-}[\text{OH}^-] = k_1 [2\text{MPZ}]^n \quad (71)$$

By plotting of $\log(k_{\text{app}})$ vs. $\log[2\text{MPZ}]$, values of k_1 and reaction order with respect to 2MPZ can be determined.

As mentioned before, a limitation associated with potassium carbonate solvent is its slow absorption rate with CO_2 . Therefore, 2MPZ was added as a potential promoter to improve the absorption rate. The absorption rate of CO_2 in 2 kmol/m³ potassium carbonate containing 0.1-0.5 kmol/m³ 2MPZ was measured at the temperature range between 303 and 323 K. The effect of temperature and concentration of 2MPZ on the absorption rate of $\text{K}_2\text{CO}_3 + 2\text{MPZ}$ was studied.

It can be seen from Figure 4.38 that with increasing concentration of 2MPZ from 0.1 to 0.5 kmol/m³, CO_2 absorption rate increases significantly, which is favorable for the CO_2 capture process. This can be due to the fact that with increasing concentration of 2MPZ, the reaction rate between CO_2 and 2MPZ increases, which results in an increase in overall absorption rate. Furthermore, the absorption rate of CO_2 in $\text{K}_2\text{CO}_3 + 2\text{MPZ}$ solution is higher than pure potassium carbonate solution (1.47×10^{-6} kmol/m²s) at 303 K.

Therefore, it can be concluded that 2MPZ acts as an efficient rate promoter for potassium carbonate solution. The reason for that is that K_2CO_3 is an inorganic solvent which reacts with CO_2 through the formation of a bicarbonate ($\text{CO}_2 + \text{OH}^- \leftrightarrow \text{HCO}_3^-$) with slower reaction rate compared to carbamate formation in 2MPZ. Thanks to 2MPZ molecular structure with two secondary amine sites, it has rapid carbamate formation, which can increase the kinetics. When 2MPZ is added to potassium carbonate solution, pH of solution increases, and results in an increase in the rate of reaction of CO_2 with OH^- , which leads to an increase in the overall absorption rate.

The effect of temperature on CO_2 absorption rate of $\text{K}_2\text{CO}_3 + 2\text{MPZ}$ solution was also shown in Figure 4.38. As expected, temperature actually has a positive effect on absorption rate, which is evident because the reaction rate constant (according to the Arrhenius expression) increases with increasing temperature. Moreover, lower viscosity and higher diffusivity at higher temperatures can be another reason for enhancement of absorption rate of CO_2 in solution.

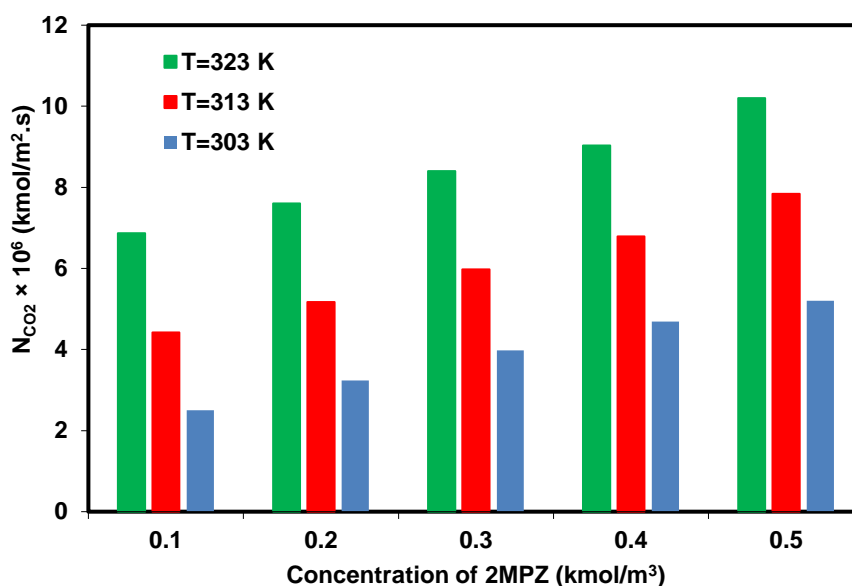


Figure 4.38 The absorption rate of CO₂ in 2 M K₂CO₃ + (0.1–0.5) M 2MPZ solutions

The values of overall reaction rate constant (k_{ov}) and apparent reaction rate constant (k_{app}) for K₂CO₃ + 2MPZ system were determined from Eq. (61) and Eq. (71), respectively. The reaction order and reaction rate constant can be calculated from the plot of $\log(k_{app})$ versus $\log(2MPZ)$ as shown in Figure 4.39. According to slope of this graph and Eq. (71), it was found that the reaction of CO₂ with K₂CO₃ + 2MPZ solution is first order with respect to the 2MPZ. The obtained reaction rate constant was plotted as a function of $1/T$ in order to determine the activation energy and Arrhenius expression as shown in Figure 4.40.

$$k_2 = A \exp\left(\frac{-E}{RT}\right) \quad (72)$$

The activation energy and Arrhenius constant for K₂CO₃ + 2MPZ system have been found to be 62.45 kJ/mol and 8.92×10^{14} m³/kmol.s, respectively.

$$k_2 = 8,92 \times 10^{14} \exp\left(\frac{-7511,8}{T}\right) \quad (73)$$

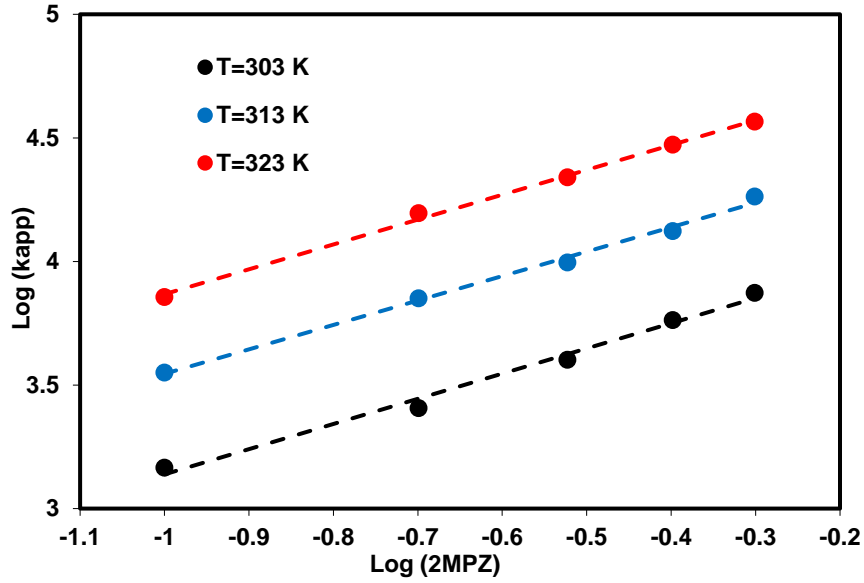


Figure 4.39 Plot of $\log(k_{app})$ versus \log of concentration of 2MPZ

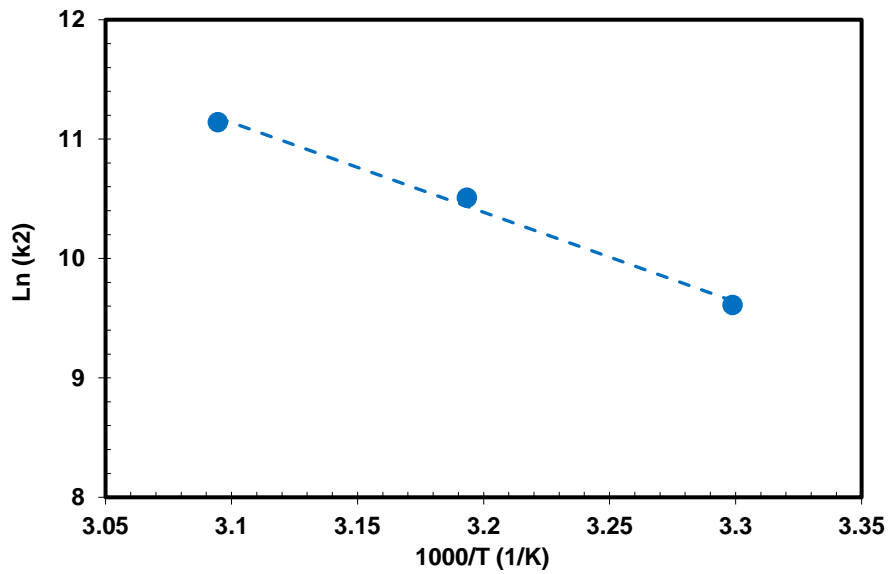


Figure 4.40 Arrhenius plot for the $\text{CO}_2 + \text{K}_2\text{CO}_3 + 2\text{MPZ}$ system.

The liquid mass transfer coefficient (K_L) was also obtained using a mass transfer correlation given by Kierzkowska-Pawlak et al. [171]. This parameter is necessary to calculate Hatta number and enhancement factor.

$$\frac{K_L d_s}{D_{\text{CO}_2}} = 0.3929 \left(\frac{n_s d_s^2 \rho}{\mu} \right)^{0.6632} \left(\frac{\mu}{\rho D_{\text{CO}_2}} \right)^{0.33} \quad (74)$$

Where d_s is dimension of impeller and n_s is the stirrer speed. Using the values of D_{CO_2} , K_{OV} , K_L and H_{CO_2} , the Hatta number and enhancement factor were calculated using Eqs. (56) and (57) to check the validity of condition given by Eq. (55). It is clear from Figure 4.41 that all Hatta number values are greater than 3 and lower than infinite enhancement factor, which ensures the fast pseudo-first-order reaction regime condition.

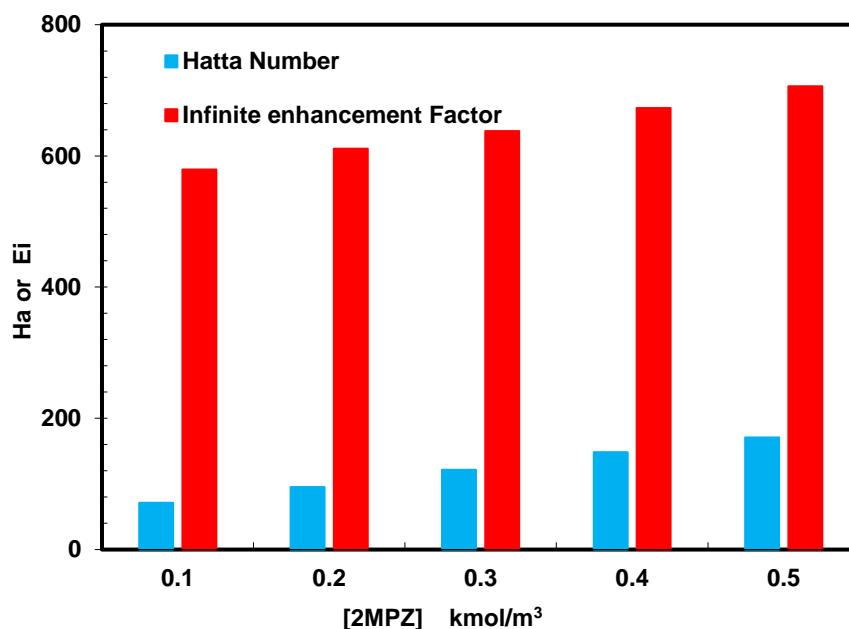


Figure 4.41 Effect of 2MPZ concentration on Ha and Ei at 303 K for $K_2CO_3 + 2MPZ$ system.

4.6. Absorption characterization of CO_2 in MEA + K-Lys

In order to have more attractive absorbents, it is essential to improve the existing absorbents or synthesize and screen new ones. This actually motivated us to select a blend of MEA and potassium lysinate (K-Lys) as a solvent for the CO_2 absorption process. MEA was chosen as a base solvent because of its wide use in CO_2 capture, and its advantages such as low solvent cost and suitability for low CO_2 partial pressures.

In the previous sections, potassium salt of lysine showed an excellent performance in terms of toxicity, CO_2 loading capacity and absorption rate. Knowledge of the reaction kinetics and physicochemical properties of absorbents are important for the design and modeling of CO_2 capture processes.

In this section, a comprehensive study of CO_2 absorption in MEA + K-Lys solution in terms of reaction kinetics, CO_2 loading capacity, absorption rate, thermodynamic modeling, absorption heat and physical properties was carried out.

4.6.1. CO₂ loading capacity of MEA + K-Lys

After validating of experimental setup and method by MEA solution, the CO₂ loading capacity of 2 kmol/m³ MEA blended with (0.2-0.5) kmol/m³ K-Lys was measured by stirred cell reactor at temperatures of 303, 313 and 323 K, and the results were listed in Tables 4.27 to 4.29.

Table 4.27 CO₂ loading capacity of 2 M MEA + (0.2-0.5) M K-Lys solution at 303 K.

+ 0.2 M K-Lys		+ 0.3 M K-Lys		+ 0.4 M K-Lys		+ 0.5 M K-Lys	
P _{CO₂} (kPa)	α	P _{CO₂} (kPa)	α	P _{CO₂} (kPa)	α	P _{CO₂} (kPa)	α
01.77	0.552	01.54	0.553	01.82	0.581	00.69	0.581
03.04	0.572	04.01	0.598	03.66	0.618	02.37	0.616
07.25	0.609	06.93	0.615	07.29	0.632	05.04	0.632
10.59	0.627	09.72	0.636	12.08	0.667	09.55	0.659
15.13	0.645	14.88	0.657	16.84	0.683	14.72	0.681

Table 4.28 CO₂ loading capacity of 2 M MEA + (0.2-0.5) M K-Lys solution at 313 K.

+ 0.2 M K-Lys		+ 0.3 M K-Lys		+ 0.4 M K-Lys		+ 0.5 M K-Lys	
P _{CO₂} (kPa)	α	P _{CO₂} (kPa)	α	P _{CO₂} (kPa)	α	P _{CO₂} (kPa)	α
00.77	0.472	01.29	0.508	00.98	0.501	01.53	0.547
03.05	0.526	04.26	0.550	03.47	0.555	05.83	0.598
06.68	0.560	08.04	0.578	07.33	0.583	08.30	0.613
10.24	0.582	11.25	0.594	11.62	0.606	10.42	0.624
14.55	0.598	14.61	0.607	15.25	0.622	13.04	0.635

Table 4.29 CO₂ loading capacity of 2 M MEA + (0.2-0.5) M K-Lys solution at 323 K.

+ 0.2 M K-Lys		+ 0.3 M K-Lys		+ 0.4 M K-Lys		+ 0.5 M K-Lys	
P _{CO₂} (kPa)	α	P _{CO₂} (kPa)	α	P _{CO₂} (kPa)	α	P _{CO₂} (kPa)	α
02.52	0.484	01.96	0.476	02.06	0.481	01.39	0.474
06.64	0.523	05.03	0.518	04.25	0.514	04.06	0.525
09.21	0.542	08.79	0.541	07.75	0.543	07.22	0.552
13.68	0.565	12.55	0.559	10.82	0.561	11.43	0.571
16.77	0.576	16.08	0.572	15.31	0.575	16.95	0.592

The effect of temperature, CO₂ partial pressure and K-Lys concentration on CO₂ loading capacity of MEA + K-Lys solution was studied and presented in Figure 4.42 to 4.46. As shown in these figures, MEA + K-Lys solution has higher CO₂ loading at high CO₂ partial pressures due to an enhancement of the concentration gradient. In addition, temperature indicated a negative effect on the CO₂ loading capacity. In the other words, an increase in the temperature from 303 to 323 K leads to a decrease in loading

capacity. This reduction can be explained by the fact that the equilibrium would shift in the backward direction with the increasing temperature and thus reducing the CO₂ loading.

It can also be seen from Figure 4.46 that by increasing the concentration of K-Lys in the blend solution from 0.2 to 0.5 M at 313.15 K, the CO₂ loading increased by about 15%. This positive effect can be explained by the fact that MEA has one amine group, while lysine has two amine groups in its molecular structure, which leads to more CO₂ loading for higher lysine concentrations. The reactivity of these amine groups and their contributions in the CO₂ absorption reactions, could be another reason for this positive effect. Similar trends were also observed for temperatures of 303 and 323 K.

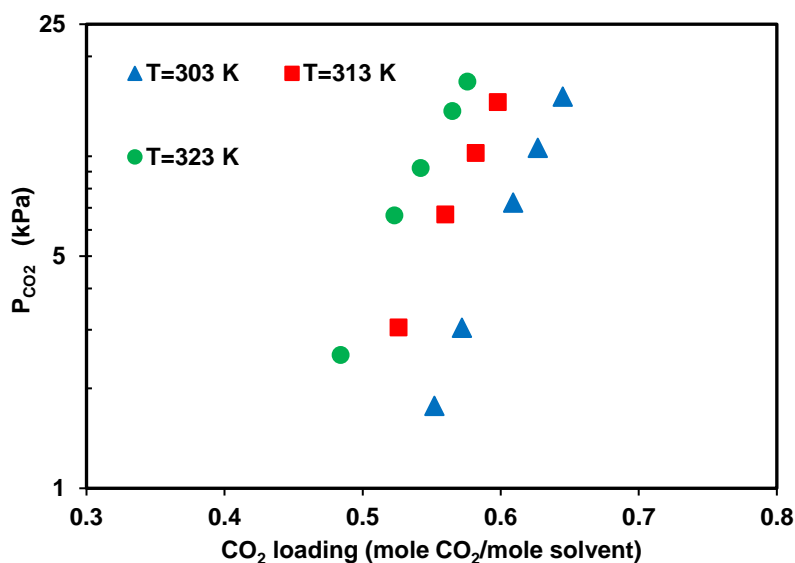


Figure 4.42 Partial pressure of CO₂ as a function of CO₂ loading capacity of 2 M MEA + 0.2 M K-Lys solution.

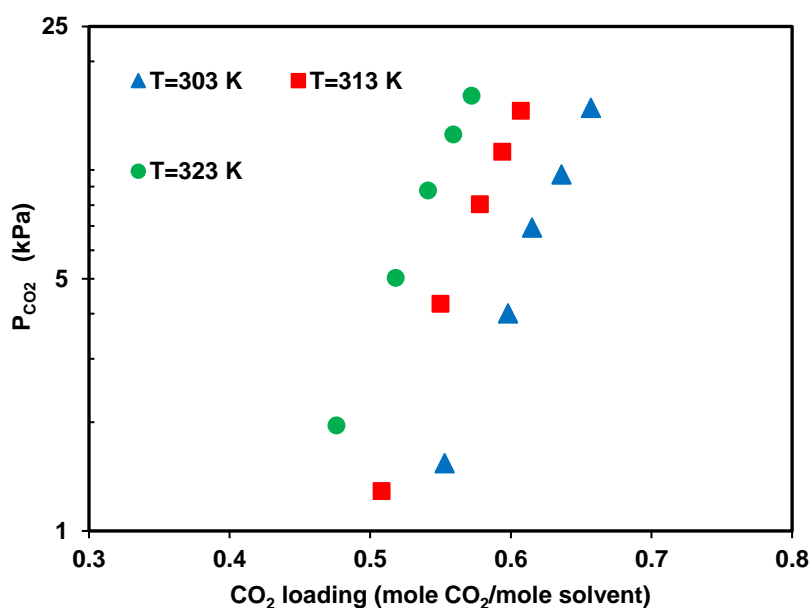


Figure 4.43 Partial pressure of CO₂ as a function of CO₂ loading capacity of 2 M MEA + 0.3 M K-Lys solution.

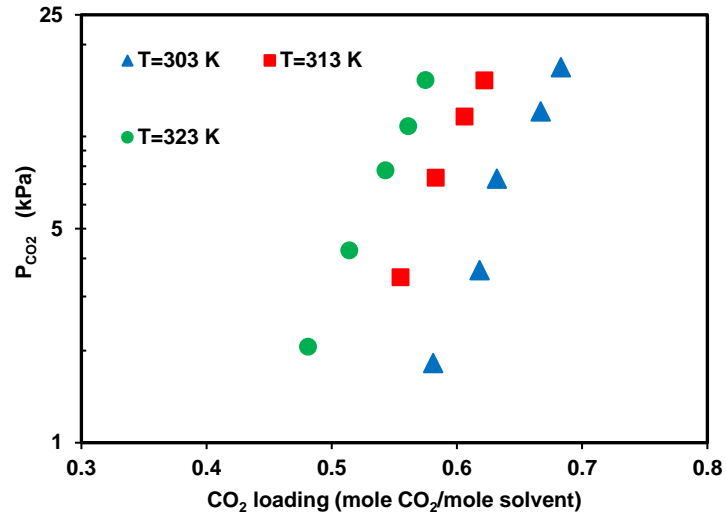


Figure 4.44 Partial pressure of CO₂ as a function of CO₂ loading capacity of 2 M MEA + 0.4 K-Lys solution.

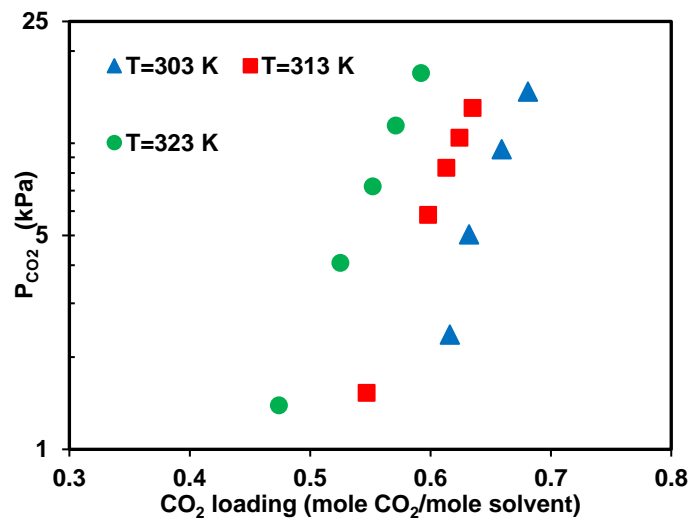


Figure 4.45 Partial pressure of CO₂ as a function of CO₂ loading capacity of 2 M MEA + 0.5 K-Lys solution.

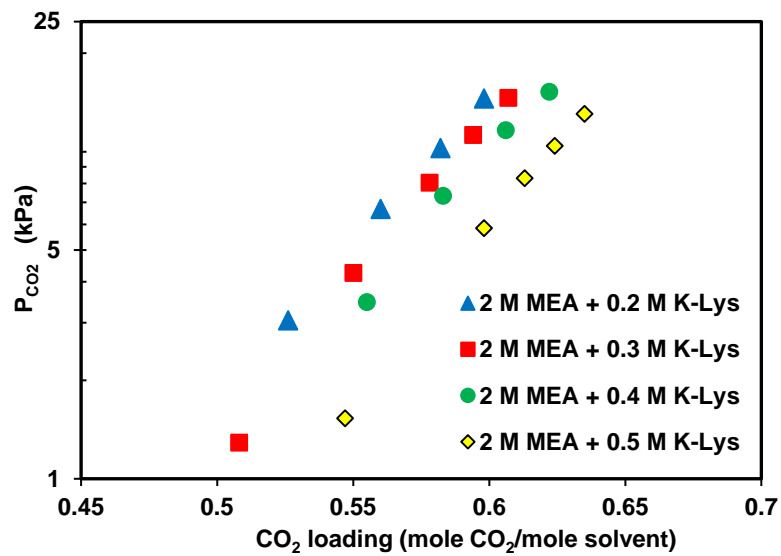


Figure 4.46 The effect of addition of K-Lys on CO₂ loading capacity of MEA solution.

A comparison of CO₂ loading capacity of an MEA + K-Lys solution was made with a pure MEA solution, as a widely used absorbent, MEA-based blends and other blended absorbents available in the literature. A blend solution with concentration of 2 M MEA + 0.5 M K-Lys was considered for comparison because it showed the highest CO₂ loading in the previous section. According to Figure 4.47, solvent studied in this work shows a higher CO₂ loading capacity compared with single MEA and the other solvents at 313.15 K which suggests MEA + K-Lys as an alternative absorbent to those traditionally used for post-combustion CO₂ capture process.

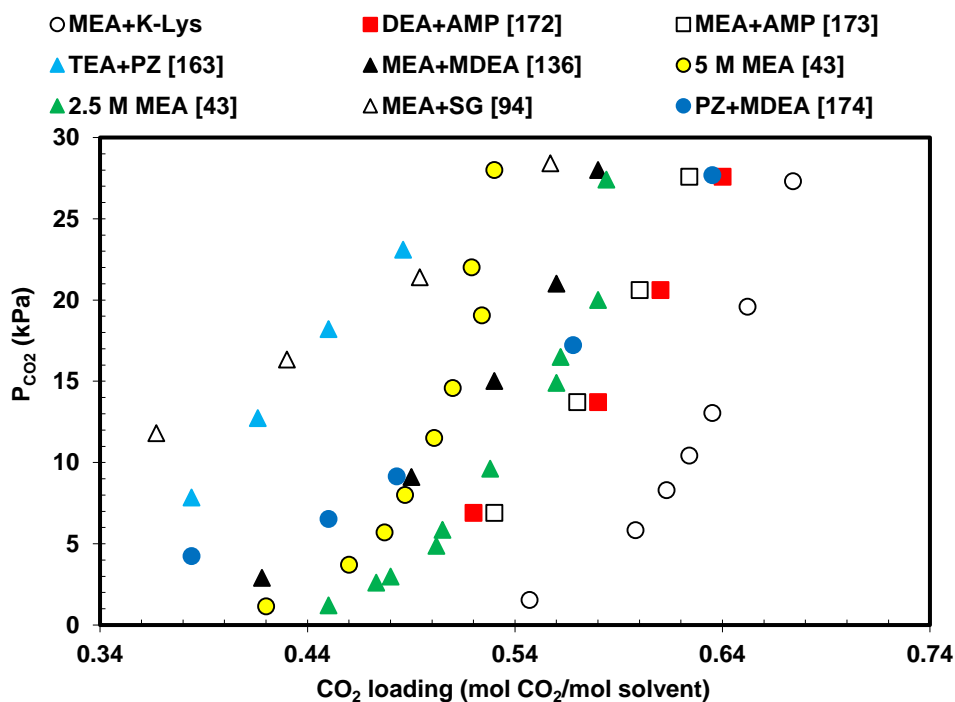


Figure 4.47 Comparison of CO₂ loading of solution of MEA + K-Lys with the other solvents at 313.15 K.

4.6.2. Density and viscosity of MEA + K-Lys

To confirm the reliability of density and viscosity measurements, density and viscosity of MEA and water at 303 to 323 K were measured and compared with the existing literature values [15,175]. A comparison between these values was given in Table 4.30. It is clear that the values determined in this study agree with the data in the literature very well.

After validating, density and viscosity 2 M MEA blended with K-Lys were measured at temperatures of 303-323 K and at K-Lys concentrations of 0.2-0.5 M, and the results were presented in Table 4.31 and Figure 4.48 and 4.49. The results show that both viscosity and density of MEA + K-Lys increase with an increase of K-Lys concentration and decrease as temperature increases.

Table 4.30 Comparison of experimental data of density and viscosity of MEA and water with literature.

	T (K)	Density (g cm ³)		Viscosity (mPa.s)	
		This work	Ref. [15,175]	This work	Ref. [15,175]
MEA	303.15	1.0093	1.0097	14.978	15.105
	313.15	1.0022	1.0027	9.8329	10.028
	323.15	0.9925	0.9944	6.9054	6.9463
Water	303.15	0.9951	0.9957	0.7903	0.7975
	313.15	0.9919	0.9922	0.6501	0.6532
	323.15	0.9872	0.9880	0.5504	0.5471

Table 4.31 Density and viscosity of solution of 2 M MEA + (0.2–0.5) M K-Lys.

T (K)	[K-Lys]=0.2 M	[K-Lys]=0.3 M	[K-Lys]=0.4 M	[K-Lys]=0.5 M
ρ (g.cm ⁻³)				
303	1.1226	1.1232	1.1237	1.1245
313	1.1149	1.1156	1.1161	1.1168
323	1.1072	1.1076	1.1082	1.1089
μ (mPa.s ⁻¹)				
303	1.182	1.221	1.259	1.294
313	1.085	1.119	1.153	1.187
323	1.002	1.032	1.064	1.091

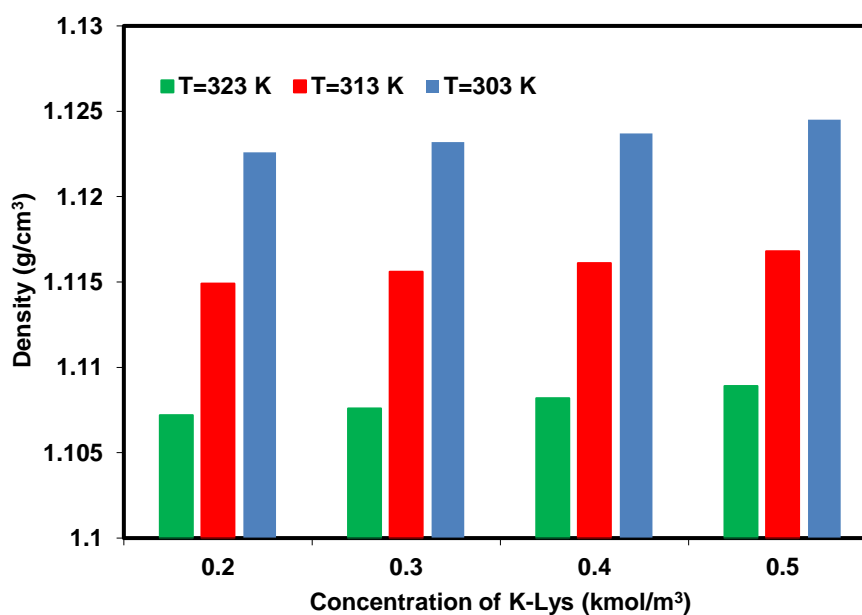


Figure 4.48 Density of solution of MEA blended with K-Lys as a function of K-Lys concentration.

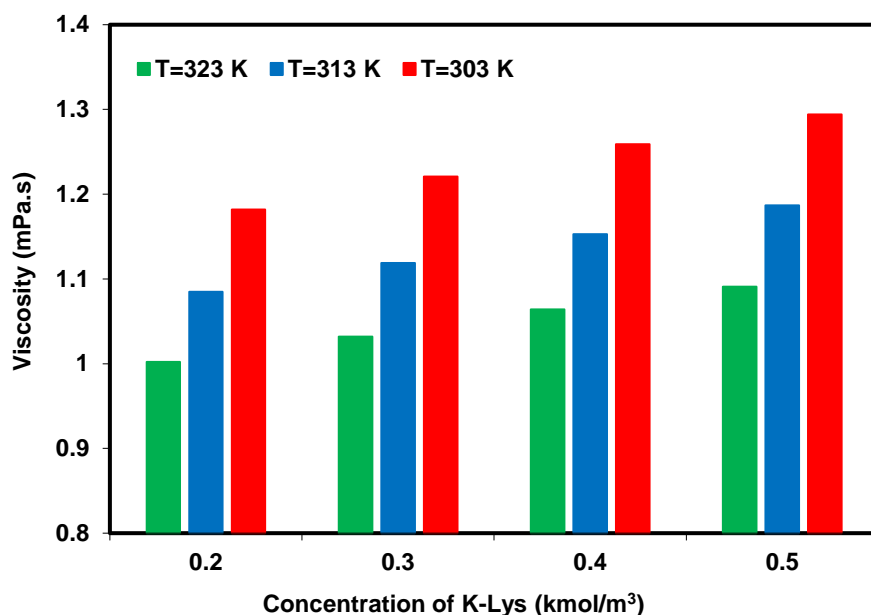


Figure 4.49 Viscosity of solution of MEA blended with K-Lys as a function of K-Lys concentration.

4.6.3. Diffusivity of CO₂ in MEA + K-Lys

For measurement of kinetics parameters, it is necessary to obtain values of diffusivity and physical solubility of CO₂ in MEA + K-Lys solution. A detailed description of the measurement method of these two parameters can be found in previous sections and therefore only the main details will be mentioned here. As mentioned before, since CO₂ reacts with the MEA + K-Lys solution, diffusivity and physical solubility of CO₂ cannot be found directly. These properties can be obtained using the N₂O analogy method:

$$D_{\text{CO}_2, \text{H}_2\text{O}} = 2.35 \times 10^{-6} \exp\left(\frac{-2119}{T}\right) \quad (75)$$

$$D_{\text{N}_2\text{O}, \text{H}_2\text{O}} = 5.07 \times 10^{-6} \exp\left(\frac{-2371}{T}\right) \quad (76)$$

The diffusivity of N₂O in the blend solution of 2 M MEA and (0.2-0.5) M K-Lys at temperatures of 303, 313 and 323 K can be determined by:

$$D_{\text{N}_2\text{O}, \text{MEA}+\text{Lys}} = D_{\text{N}_2\text{O}, \text{H}_2\text{O}} \times \left(\frac{\mu_{\text{H}_2\text{O}}}{\mu_{\text{MEA}+\text{KLys}}}\right)^{0.6} \quad (77)$$

Then, the diffusivity and physical solubility of CO₂ in a mixed amine solution can be estimated using the modified Stokes-Einstein.

$$\left(\frac{D_{\text{CO}_2}}{D_{\text{N}_2\text{O}}}\right)_{\text{MEA}+\text{KLys}} = \left(\frac{D_{\text{CO}_2}}{D_{\text{N}_2\text{O}}}\right)_{\text{H}_2\text{O}} \quad (78)$$

$$H_{\text{CO}_2, \text{solvent}} = \exp\left(20.2669 - \frac{13830.6}{T} + \frac{6913000}{T^2} - \frac{15.589 \times 10^8}{T^3} + \frac{1.2 \times 10^{11}}{T^4}\right) \quad (79)$$

The diffusivity of CO₂ obtained in MEA + K-Lys system were listed in Table 4.32 and shown graphically in Figure 4.50. It was found that the diffusivity of CO₂ in MEA + K-Lys solution increases at higher temperatures and lower concentrations of K-Lys due to the fact that the viscosity of solution increases with an increase in concentration of K-Lys in solution and, as expected, decreases with temperature.

Table 4.32 The diffusivity of CO₂ in solutions 2 M MEA + (0.2-0.5) M K-Lys.

T (K)	[K-Lys]=0.2 M	[K-Lys]=0.3 M	[K-Lys]=0.4 M	[K-Lys]=0.5 M
	$D_{\text{CO}_2} \times 10^{10} \text{ (m}^2/\text{s)}$			
303	1.70	1.66	1.64	1.61
313	1.98	1.95	1.91	1.88
323	2.32	2.28	2.24	2.21

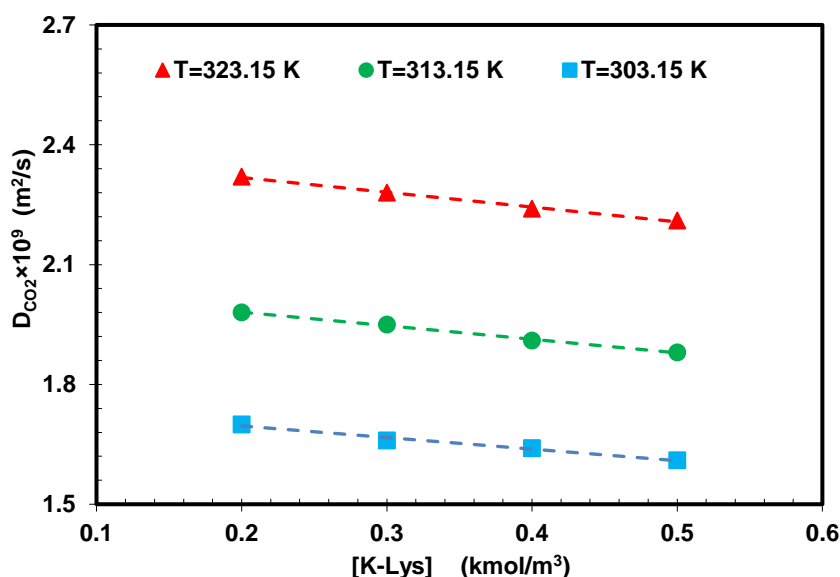


Figure 4.50 The diffusion coefficients of CO₂ in MEA + K-Lys solution.

4.6.4. Kinetics study of CO₂ absorption in MEA + K-Lys

The zwitterion mechanism can be used for reaction of CO₂ with alkanolamines and amino acids [115]. According to this mechanism, the overall absorption rate for the CO₂ + MEA + K-Lys + H₂O system can be determined from Eq. (80):

$$R_{\text{OV}} = R_{\text{CO}_2\text{-Lys}} + R_{\text{CO}_2\text{-MEA}} + R_{\text{CO}_2\text{-OH}^-} \quad (80)$$

The reaction of hydration of CO₂ has a very slow rate and can be neglected. However, the reaction of bicarbonate formation is fast and should be considered in the overall reaction rate:



$$R_{\text{CO}_2-\text{OH}^-} = k_{\text{OH}^-}[\text{CO}_2][\text{OH}^-] \quad (82)$$

$$\log k_{\text{OH}^-} = 13,635 - \frac{2895}{T} \quad (83)$$

Sanchez et al. [109] showed that the reaction of CO₂ with MEA is a first-order reaction with respect to MEA:

$$R_{\text{CO}_2-\text{MEA}} = k_{\text{MEA}}[\text{CO}_2][\text{MEA}] \quad (84)$$

The reaction rate constant (k_{MEA}) can be calculated from Eq. (85) [76]:

$$k_{\text{MEA}} = 4.14 \times 10^{11} \exp\left(\frac{-5399}{T}\right) \quad (85)$$

However, the value of k_{MEA} was again determined in this work and compared to the literature in the next section. The reaction kinetics of CO₂ and K-Lys can be described using from the zwitterion mechanism:

$$R_{\text{CO}_2-\text{Lys}} = \frac{k_{\text{Lys}}[\text{Lys}][\text{CO}_2]}{1 + \frac{k_{-1}}{\sum k_B[\text{B}]}} \quad (86)$$

Where $\sum k_B[\text{B}]$ shows the contribution of the bases present in solution for proton transfer. Depending on the zwitterion deprotonation, the reaction order with respect to concentration of K-Lys varies between one and two. When deprotonation is instantaneous ($\frac{k_{-1}}{\sum k_B[\text{B}]} \ll 1$), the reaction is first order with respect to K-Lys concentration:

$$R_{\text{CO}_2-\text{Lys}} = k_{\text{Lys}}[\text{Lys}][\text{CO}_2] \quad (87)$$

When zwitterion deprotonation is rate-limiting ($\frac{k_{-1}}{\sum k_B[\text{B}]} \gg 1$), the overall reaction order varies between two and three:

$$R_{\text{CO}_2-\text{Lys}} = k_{\text{Lys}}[\text{CO}_2][\text{Lys}]^n \quad (88)$$

As a result, the overall reaction rate of CO₂ in MEA + K-Lys and the overall reaction rate constant (k_{OV}) can be expressed by:

$$R_{\text{OV}} = k_{\text{OH}^-}[\text{CO}_2][\text{OH}^-] + k_{\text{MEA}}[\text{CO}_2][\text{MEA}] + k_{\text{Lys}}[\text{CO}_2][\text{Lys}]^n \quad (89)$$

$$R_{\text{OV}} = [\text{CO}_2] k_{\text{OV}} \quad (90)$$

$$k_{\text{OV}} = k_{\text{OH}^-}[\text{OH}^-] + k_{\text{MEA}}[\text{MEA}] + k_{\text{Lys}}[\text{Lys}]^n \quad (91)$$

As mentioned before, the CO₂ absorption in lean amine solutions can be obtained from Eq. (92):

$$N_{\text{CO}_2} = E_A K_L ([\text{CO}_2]_i - [\text{CO}_2]_b) \quad (92)$$

Where K_L and E_A are the liquid mass transfer coefficient and the enhancement factor, respectively. The interfacial CO₂ concentration $[\text{CO}_2]_i$ can be calculated using Eq. (59). The concentration of CO₂ in the bulk of the liquid $[\text{CO}_2]_b$ is negligible (approximately zero) because the solution used in all the experiments was not initially loaded with CO₂. Thus, the flux expression can be written as:

$$N_{\text{CO}_2} = E_A K_L [\text{CO}_2]_i \quad (93)$$

If the condition of Eq. (94) is satisfied, then the reaction belongs to a fast pseudo-first order regime.

$$3 < H_a \ll E_\infty \quad (94)$$

The calculation method of infinite enhancement factor and Hatta number was explained before. In the regime of fast pseudo-first order, enhancement factor is equal to Hatta number. Therefore, the flux expression is converted to Eq. (95):

$$N_{\text{CO}_2} = \frac{\sqrt{k_{\text{OV}} D_{\text{CO}_2}}}{K_L} K_L [\text{CO}_2]_i \quad (95)$$

Then,

$$N_{\text{CO}_2} = \sqrt{k_{\text{OV}} D_{\text{CO}_2}} [\text{CO}_2]_i \quad (96)$$

In addition, $[\text{CO}_2]_i$ can be substituted from $\frac{P_{\text{CO}_2}}{H_e}$ which leads to Eq. (97):

$$N_{\text{CO}_2} = \sqrt{k_{\text{OV}} D_{\text{CO}_2}} \frac{P_{\text{CO}_2}}{H_e} \quad (97)$$

Therefore, k_{ov} can be obtained from Eq. (97), knowing the values of D_{CO_2} , P_{CO_2} , N_{CO_2} and H_e . The apparent reaction rate constant (k_{app}) can be calculated from Eq. (98):

$$k_{\text{app}} = k_{\text{ov}} - k_{\text{OH}^-}[\text{OH}^-] - k_{\text{MEA}}[\text{MEA}] = k_{\text{Lys}}[\text{Lys}]^n \quad (98)$$

By plotting $\log k_{\text{app}}$ vs. $\log[\text{Lys}]$, values of the reaction order with respect to potassium lysinate and reaction rate constant can then be determined. To verify the reliability of the results and also measurement method for kinetics study, initial runs were made for the CO_2 absorption rate in single MEA solution and compared with the literature. Many researchers have studied the kinetics of $\text{CO}_2 + \text{MEA}$ and presented values of second-order rate constant (k_2). For example, Ying et al. [76] and Horng et al. [176] showed that second-order rate constant for $\text{MEA} + \text{CO}_2 + \text{H}_2\text{O}$ system at 303.15 K is equal to 6215 and 5986 $\text{m}^3/\text{kmol.s}$, respectively. The rate of absorption of CO_2 in 2 M MEA was measured by stirred cell reactor at 303.15 K and second-order rate constant was found to be 6144 $\text{m}^3/\text{kmol.s}$ which is in excellent agreement with the data reported in the literature, and thus ensures the accuracy of measurement used in this work. It is now possible to study the kinetics of CO_2 absorption in $\text{MEA} + \text{K-Lys}$. The absorption rates of CO_2 in 2 M MEA + (0.2-0.5) M K-Lys were measured over a temperature range 303.15-323.15 K to obtain the reaction order and k_{lys} using stirred cell reactor. It can clearly be seen in Figure 4.51 that the addition of K-Lys to MEA solution resulted in an increase in the absorption rate. This is because the amine group of the lysine can react quickly with CO_2 to form zwitterions which transfer protons to MEA and hence accelerate the overall absorption rate. The enhancement of the reaction rate between CO_2 and K-Lys with increasing concentration of K-Lys may be another reason for rate enhancement.

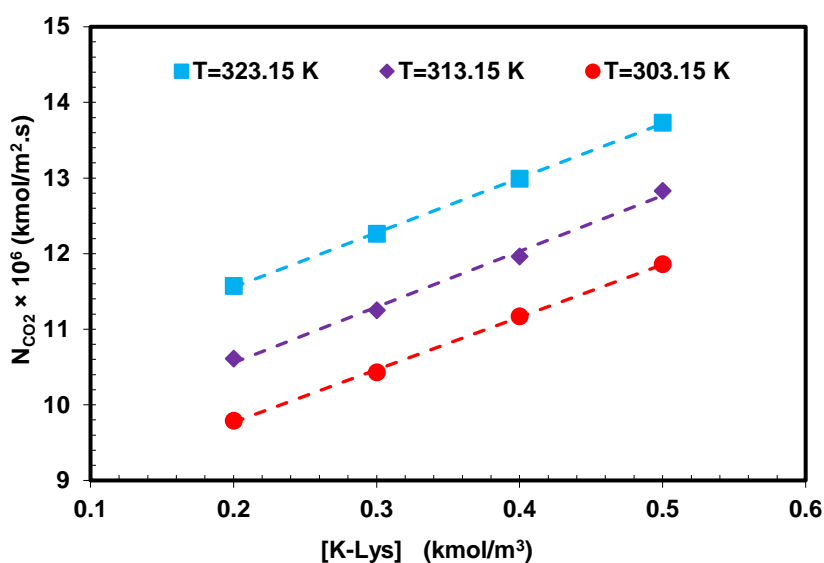


Figure 4.51 The CO₂ absorption rate in MEA + K-Lys at different temperatures and concentrations.

The k_{ov} was calculated from Eq. (97) and using the values of the absorption rate, the diffusivity, solubility and partial pressure of CO₂, and the results were listed in Table 4.33. Eq. (98) was also used to calculate k_{app} and the results were plotted in Figure 4.52. It was found that the k_{app} increases as K-Lys concentration and temperature increase.

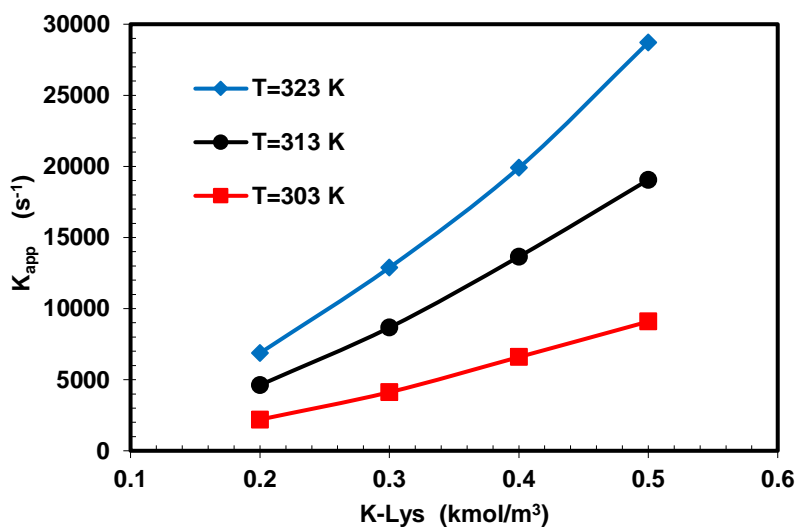


Figure 4.52 Plot of the apparent reaction rate constant versus K-Lys concentration.

In order to obtain the order of reaction with respect to K-Lys and the reaction rate constant (k_{Lys}), logarithmic plots of k_{app} vs. concentrations of K-Lys were demonstrated in Figure 4.53. It should be mentioned that the values of order of reaction with respect to K-Lys and k_{Lys} were determined from the

slope and intercept of these plots. As can be seen from Figure 4.53, order of reaction with respect to K-Lys was found to be 1.55.

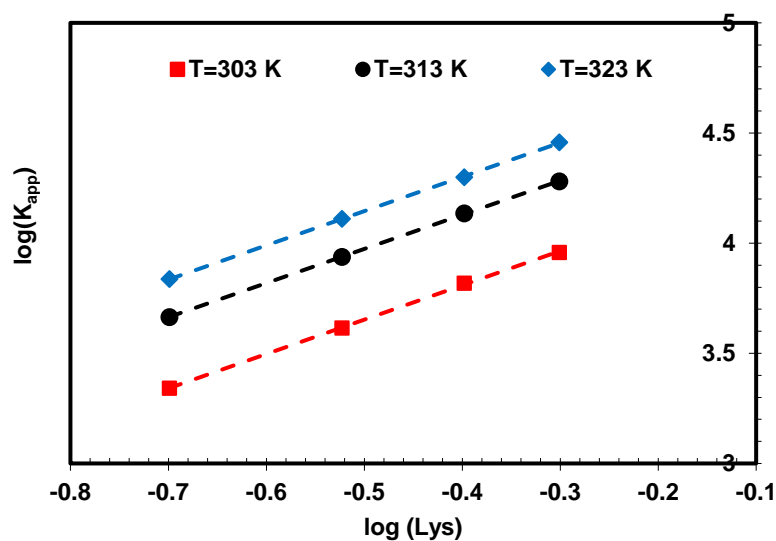


Figure 4.53 Plot of the $\log(k_{app})$ versus \log of concentration of K-Lys.

The k_{Lys} can be expressed by Arrhenius's law as shown in Eq. (99):

$$k_{Lys} = A \exp\left(\frac{-E}{RT}\right) \quad (99)$$

The Arrhenius plot of the k_{Lys} values at different temperatures was made in Figure 4.54. The activation energy was found to be 48.45 kJ/mol. The k_{Lys} was correlated as a function of temperature:

$$k_{Lys} = 6.23 \times 10^{12} \exp\left(\frac{-5827.7}{T}\right) \quad (100)$$

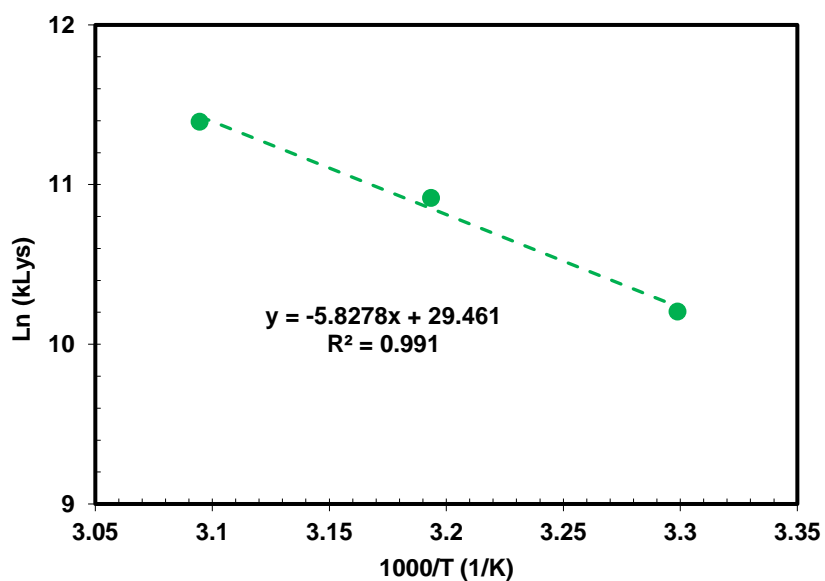


Figure 4.54 Arrhenius plot for the $\text{CO}_2 + \text{MEA} + \text{K-Lys}$ system.

The liquid mass transfer coefficient was calculated using the same method which explained in the previous section.

$$\frac{K_L d_s}{D_{CO_2}} = 0.3929 \left(\frac{n_s d_s^2 \rho}{\mu} \right)^{0.6632} \left(\frac{\mu}{\rho D_{CO_2}} \right)^{0.33} \quad (101)$$

The values of liquid mass transfer coefficient at different experimental conditions were reported in Table 4.33. It is now possible to validate the pseudo first-order regime by checking the conditions given in Eq. (94). Hatta number and infinite enhancement factor can be calculated from Eqs. (56) and (57) and with the help of the kinetics parameters obtained in the previous sections. The obtained values for these two parameters at temperatures 303-323 K and K-Lys concentrations of 0.2-0.5 M were also listed in Table 4.33. It can clearly be seen from this table and Figure 4.55 that in all cases the Ha values are all greater than three and smaller than infinite enhancement factor, which satisfies the condition of Eq. (94).

Table 4.33 Kinetic data for the CO₂ + MEA + K-Lys system.

T (K)	[MEA] kmol/m ³	[K-Lys] kmol/m ³	N _{CO₂} × 10 ⁶ (kmol/m ² , s)	k _{OV} (1/s)	K _L × 10 ⁵ (m/s)	Ha	Ei
303	2	0.2	09.79	15556	2.18	234	709
303	2	0.3	10.43	17478	2.13	252	747
303	2	0.4	11.17	19948	2.09	273	782
303	2	0.5	11.86	22446	2.04	293	824
313	2	0.2	10.61	32440	2.48	321	804
313	2	0.3	11.25	36483	2.43	345	839
313	2	0.4	11.96	41468	2.38	373	879
313	2	0.5	12.83	46873	2.33	401	923
323	2	0.2	11.57	56084	2.83	402	896
323	2	0.3	12.26	62097	2.77	428	937
323	2	0.4	12.99	69108	2.71	457	982
323	2	0.5	13.74	77930	2.67	491	1028

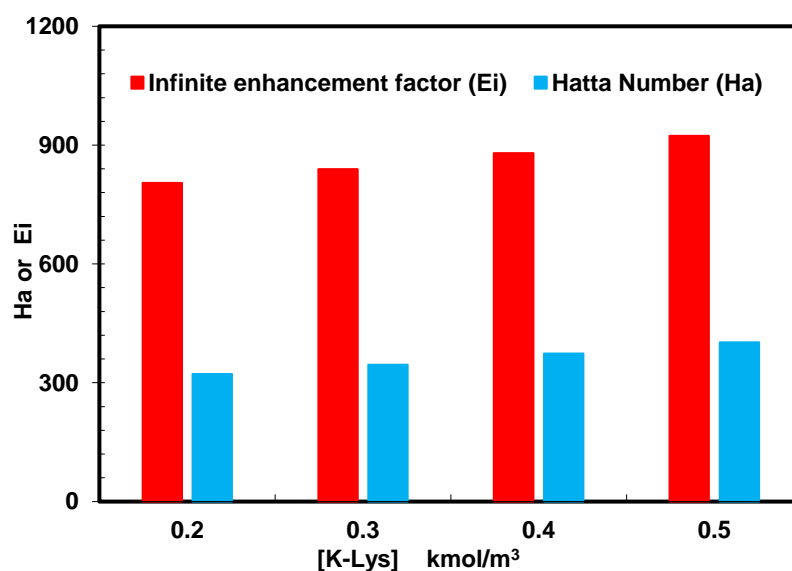


Figure 4.55 Effect of K-Lys concentration on Ha and Ei at 313 K for MEA + K-Lys system.

In the previous section, the highest CO₂ absorption rate was obtained using 2 M MEA + 0.5 M K-Lys solution. Therefore, this blend solution was chosen in this section in order to compare with other blended solutions at their best performance. Figure 4.56 shows a comparison of K_{ov} of 2 M MEA + 0.5 M K-Lys system with single 2.5 M MEA and other blended systems available in the literature at 313.15 K. The blend of 2 M MEA + 0.5 M K-Lys indicated the highest overall reaction rate constant among them because of two functional amino groups on its molecular structure. Lysine with an aliphatic amino group (pKa 10.67) and a primarily amino group (pKa 9.16) has rapid carbamate formation, which leads to a faster absorption rate in comparison with other conventional amines. It can also be concluded from Figure 4.52 that 2 M MEA + 0.5 M K-Lys showed a better performance than single 2.5 M MEA, while blend solutions of 0.4 M MEA + 1.7 M AMP, 0.5 M MEA + 1.5 M MDEA and 0.5 M MEA + 2 M TEA indicated a lower kinetic constant than 2.5 M MEA. Furthermore, the 2 M MDEA + 0.5 M DEA system was found to have the lowest kinetic constant.

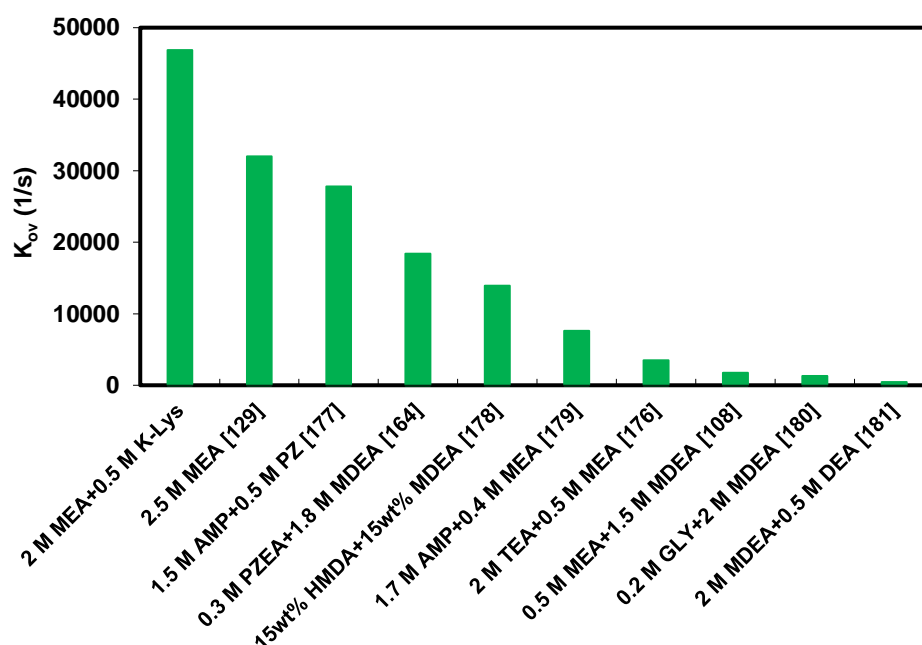


Figure 4.56 Comparison of the overall reaction rate constant of MEA + K-Lys with other blended systems at 313 K.

4.6.5. Heat of CO₂ absorption of MEA + K-Lys

The calculated heat of CO₂ absorption in solution of MEA + K-Lys was found to be equal to 72.8 kJ/mol using Gibbs-Helmholtz equation. Figure 4.57 shows a comparison between absorption heat of CO₂ in MEA + K-Lys solution and other conventional absorbents such as AEEA [137], MEA [136], PZ [138], AMP [137] and MDEA [135].

According to this figure, an aqueous MEA solution presents the highest absorption heat equal to 84.3 kJ/mol because of the formation of stable carbamate. The addition of K-Lys to MEA gives a decrease in

heat of absorption of CO₂ by approximately 15% which means a lower energy requirement for regeneration. In other words, MEA + K-Lys solution showed a better performance than MEA and other absorbents except MDEA. Therefore, a blend of MEA and K-Lys would be the right choice from the absorption heat point of view.

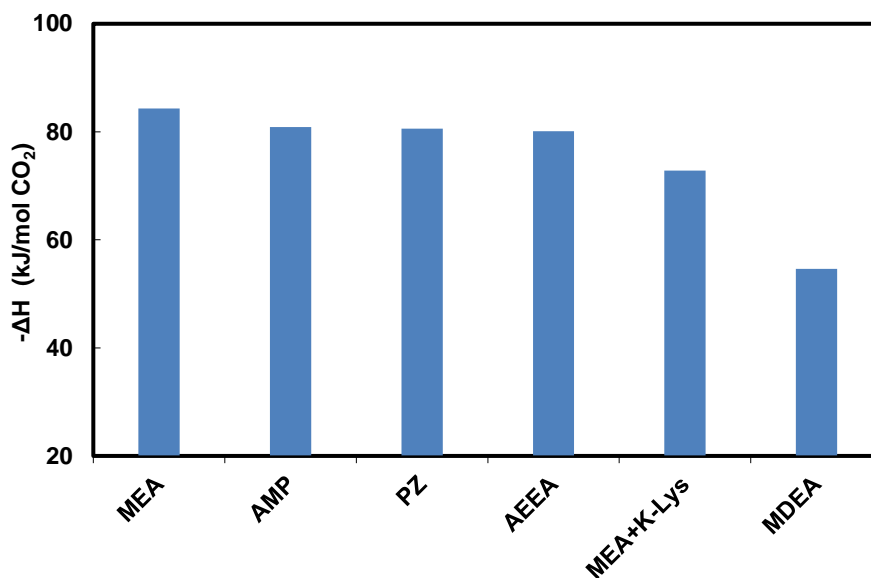


Figure 4.57 Comparison of heat of CO₂ absorption of MEA + K-Lys solution with the other absorbents.

4.7. Absorption characterization of CO₂ in MDEA + K-Lys

MDEA as a tertiary alkanolamines has advantages such as low heat of absorption, low vapor pressure, low corrosion rate and high solvent stability. These favorable factors of MDEA has made it an attractive candidate for CO₂ absorption process. However, the main challenge with MDEA is its slow reaction rate with CO₂, which can be increased by addition of small amount of a promoter.

In this work, lysine was selected to blend with MDEA to improve its performance. Therefore, CO₂ absorption into blends of MDEA and K-Lys was studied experimentally and theoretically. CO₂ solubility measurements were performed using a stirred batch reactor at temperatures of 298.15 to 313.15 K and at CO₂ partial pressure up to 25 kPa. The density, viscosity and pH of the blended solutions before and after CO₂ absorption were measured. A thermodynamic model was employed to predict measured CO₂ loading capacity data. The reaction kinetics between CO₂ and MDEA + K-Lys system was also investigated using zwitterion and base-catalyzed mechanisms. In addition, heat of CO₂ absorption was estimated by the Gibbs-Helmholtz correlation.

4.7.1. CO₂ loading capacity of MDEA + K-Lys

After validating the experimental setup, the CO₂ loading capacity of MDEA + K-Lys solution was

measured at different temperatures, concentrations and pressures as shown in Table 4.34 to 4.36. The three different blended solutions, 1.5 M MDEA + 0.2 M K-Lys, 1.5 M MDEA + 0.35 M K-Lys and 1.5 M MDEA + 0.5 M K-Lys were selected as absorbents.

Table 4.34 CO₂ loading capacity of MDEA + K-Lys solution at 298.15.

1.5 M MDEA + 0.2 M K-Lys		1.5 M MDEA + 0.35 M K-Lys		1.5 M MDEA + 0.5 M K-Lys	
P _{CO₂} (kPa)	α	P _{CO₂} (kPa)	α	P _{CO₂} (kPa)	α
3.7	0.600	3.2	0.651	2.4	0.724
7.8	0.633	6.3	0.675	4.7	0.753
14.9	0.662	14.27	0.709	8.9	0.780
18.4	0.677	19.91	0.732	19.89	0.808

α (mole CO₂/mole of absorbent) is the moles of CO₂ absorbed per one mole of solvent

Table 4.35 CO₂ loading capacity of MDEA + K-Lys solution at 303.15.

1.5 M MDEA + 0.2 M K-Lys		1.5 M MDEA + 0.35 M K-Lys		1.5 M MDEA + 0.5 M K-Lys	
P _{CO₂} (kPa)	α	P _{CO₂} (kPa)	α	P _{CO₂} (kPa)	α
2.01	0.488	2.9	0.608	1.55	0.678
6.5	0.560	6.9	0.639	3.7	0.705
10.98	0.592	13.77	0.680	8.3	0.749
16.4	0.607	24.09	0.727	12.9	0.768

α (mole CO₂/mole of absorbent) is the moles of CO₂ absorbed per one mole of solvent

Table 4.36 CO₂ loading capacity of MDEA + K-Lys solution at 313.15.

1.5 M MDEA + 0.2 M K-Lys		1.5 M MDEA + 0.35 M K-Lys		1.5 M MDEA + 0.5 M K-Lys	
P _{CO₂} (kPa)	α	P _{CO₂} (kPa)	α	P _{CO₂} (kPa)	α
5.3	0.427	04.30	0.558	3.51	0.665
7.2	0.481	09.01	0.598	6.39	0.704
12.4	0.530	14.4	0.628	13.65	0.747
20	0.607	19.62	0.656	21.36	0.772

α (mole CO₂/mole of absorbent) is the moles of CO₂ absorbed per one mole of solvent

It is seen that the CO₂ loading capacity increased with increasing CO₂ partial pressure due to an enhancement at the concentration gradient. As expected, CO₂ loading capacity decreased when temperature increased from 298.15 K to 313.15 K as illustrated in Figure 4.58 to 4.60. This negative impact of the temperature on CO₂ loading capacity can be due to the fact that the equilibrium shifts in the backward direction as temperature increases.

It can be clearly seen from Figure 4.61 that MDEA + K-Lys solution has higher CO₂ loading as K-Lys concentration increases from 0.2 to 0.5 M at 313.15 K. This is because the amino groups in the lysine are reactive and take part in CO₂ absorption reaction, thus improve the CO₂ loading capacity of MDEA. A

similar trend was also observed for temperatures 298.15 K and 303.15 K. Figure 4.62 presents a comparison between the performance of 1.5 M MDEA + 0.5 M K-Lys with other common blend solutions in the literature and with single MEA (as a widely used solvent) at 313.15 K. It can be seen that MDEA + K-Lys showed a better performance than other common absorbents and also has a much higher CO₂ loading compared to MEA. This higher absorption capacity of lysine in comparison to MEA is because of two active amine groups in its structure.

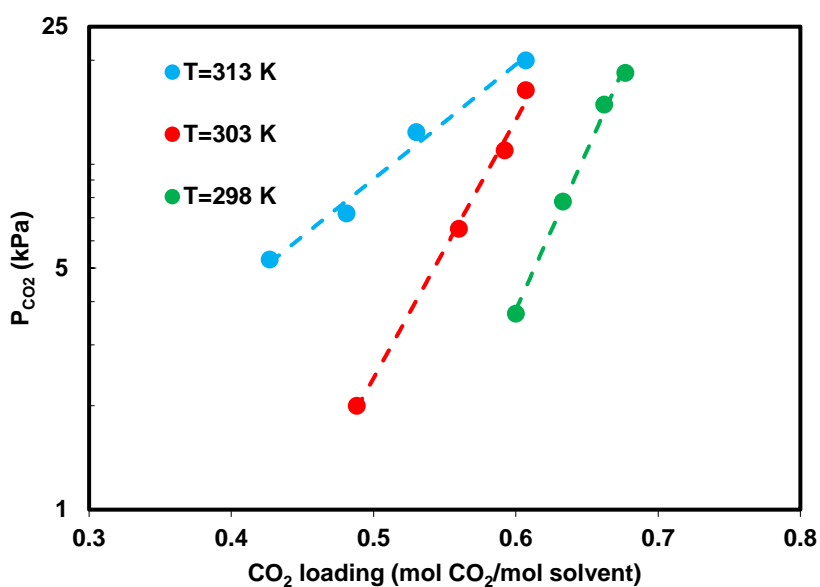


Figure 4.58 CO₂ loading of 1.5 M MDEA + 0.2 M K-Lys solution

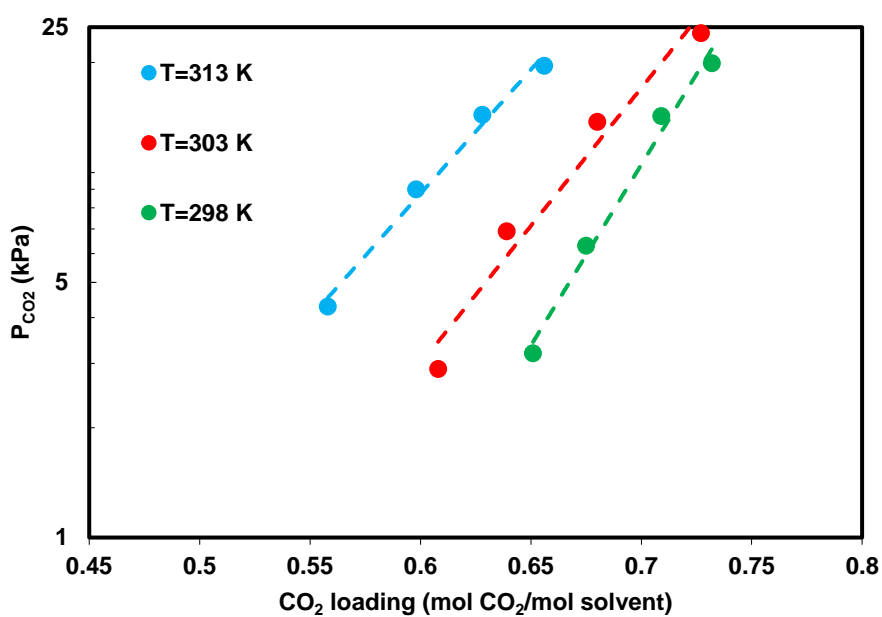


Figure 4.59 CO₂ loading of 1.5 M MDEA + 0.35 M K-Lys solution

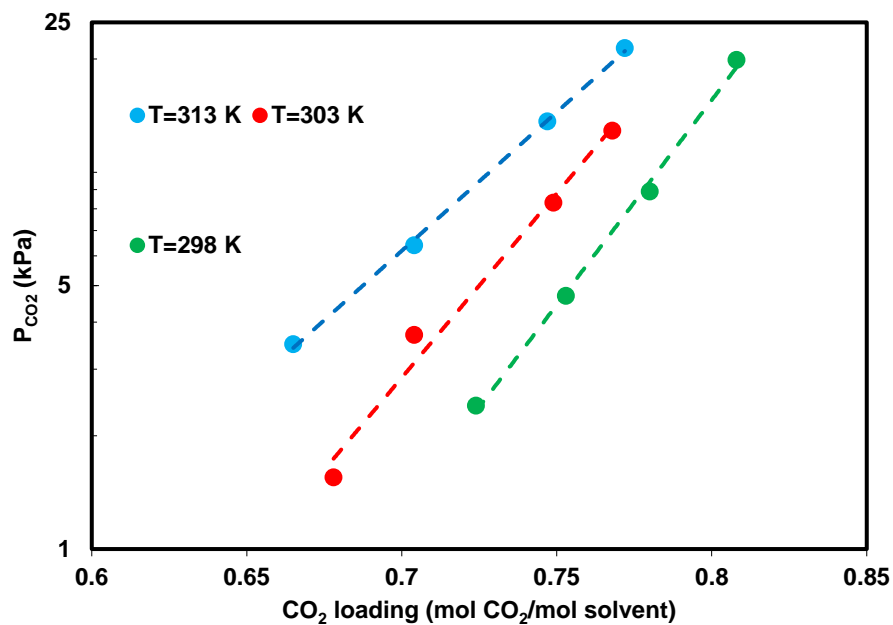


Figure 4.60 CO₂ loading of 1.5 M MDEA + 0.5 M K-Lys solution

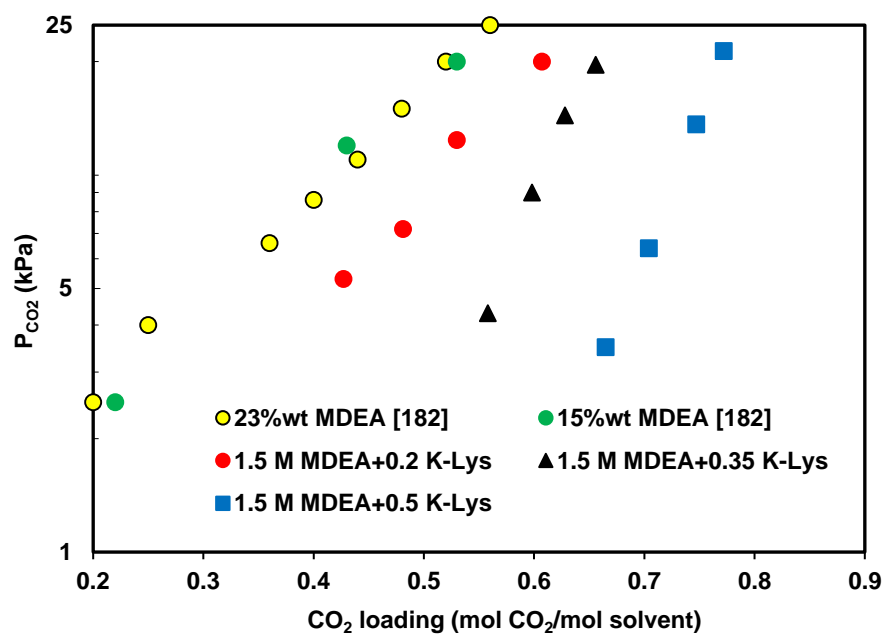


Figure 4.61 The effect of concentration of K-Lys on CO₂ loading capacity of MDEA at 313.15 K

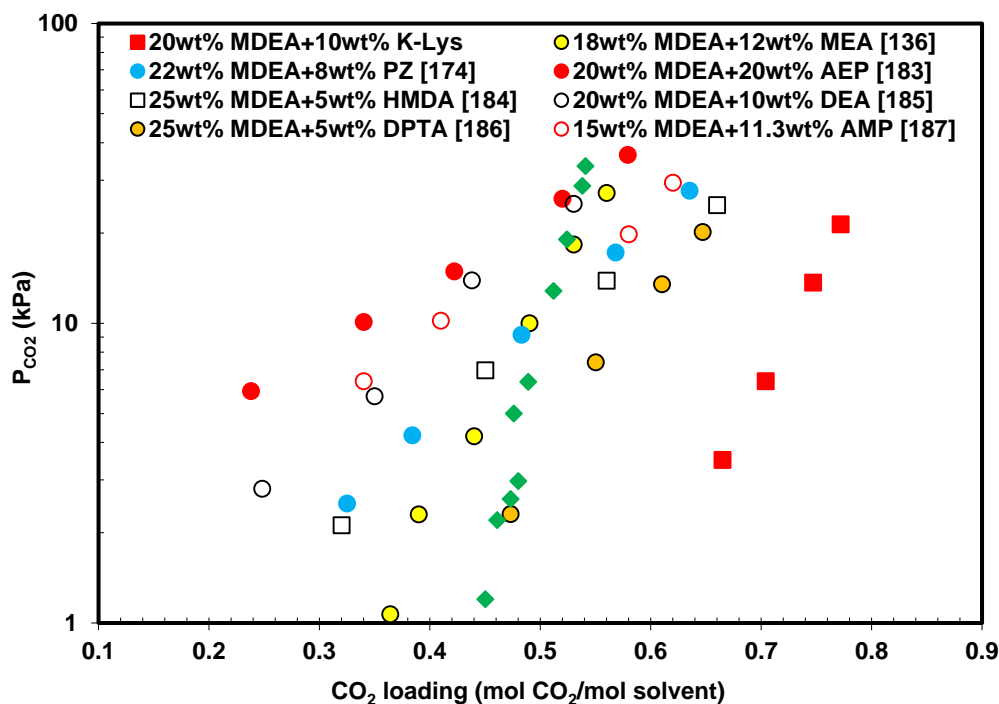


Figure 4.62 CO₂ loading capacity of MDEA + K-Lys and other blended solutions at 313 K.

Figure 4.63 presents a comparison between the performance of all of chemical absorbents studied in this work in terms of CO₂ loading capacity. It can be seen that TSP + TETA exhibits the highest CO₂ loading, while MEA + k-Lys solution presents the lowest. In addition, TSP + 2MPZ, TSP + AEEA, TSP + PZ showed the better performance than other solvents. This high CO₂ loading capacity of these solvents in comparison to others is due to more active amine groups in their structure.

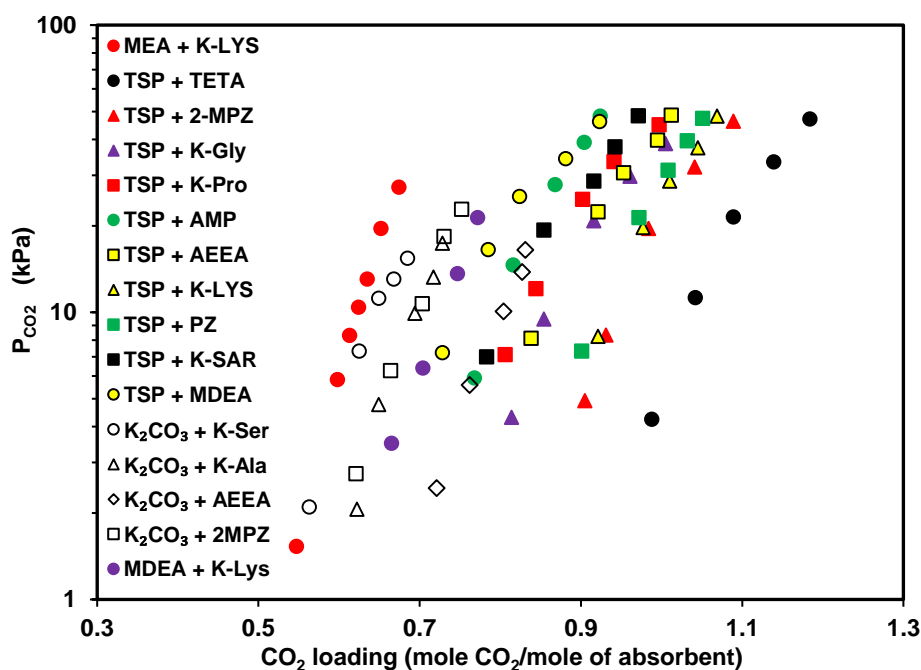


Figure 4.63 Comparison of CO₂ loading capacity of chemical solvents studied in this work at 313.15 K

4.7.2. Density, viscosity and pH of MDEA + K-Lys

The density, viscosity and pH of MDEA + K-Lys solutions before and after CO₂ absorption were measured using Gay-Lussac pycnometer, Ubbelohde viscometer (Fisherbrand, Italy) and Benchtop pH meter (AE150, Italy), respectively. The measurements were performed for 1.5 M MDEA + (0.2-0.5) M K-Lys and temperature range of 298-313 K. In order to test the reliability of the density and viscosity measurement setup, values of both of them for water and pure MDEA at 303 and 313 K were measured and compared with the data reported in the literature [188,189]. The results given in Table 4.37 shows a good agreement, which ensure the validity of the data.

Table 4.37 The values of density and viscosity of MDEA and water.

	T (K)	Density (g cm ⁻³)		Viscosity (mPa.s)	
		This work	Ref. [188]	This work	Ref. [189]
MDEA	303.15	1.0298	1.0341	56.11	56.30
	313.15	1.0269	1.0265	34.52	34.44
Water	303.15	0.9951	0.9957	0.7903	0.7975
	313.15	0.9919	0.9922	0.6501	0.6532

After validating the experimental data for density and viscosity measurement, these properties were measured for solutions of MDEA + K-Lys at 298.15 K to 313.15 K, and the results were listed in Table 4.38. According to this table, the density and viscosity of CO₂-unloaded MDEA + K-Lys solutions decrease with increasing temperature, and increase as concentration increases.

Table 4.38 Density and viscosity of MDEA + K-Lys solution at 298-313 K.

T (K)	1.5 M MDEA + 0.2 M K-Lys	1.5 M MDEA + 0.3 M K-Lys	1.5 M MDEA + 0.4 M K-Lys	1.5 M MDEA + 0.5 M K-Lys
ρ (g.cm⁻³)				
298	1.0221	1.0251	1.0272	1.0291
303	1.0202	1.0231	1.0254	1.0269
313	1.016	1.0187	1.0204	1.0222
μ (mPa.s⁻¹)				
298	2.1881	2.5456	2.8216	3.1322
303	1.8732	2.1667	2.3921	2.5445
313	1.4099	1.6141	1.7694	1.9417

The density and viscosity of CO₂-loaded 2 M MDEA + 0.5 M K-Lys solution at 298.15 to 313.15 were also measured, and the results were plotted in Figure 4.64 and 4.65. A small increase in density and

viscosity after CO₂ absorption was observed. For example, at 313.15 K, density and viscosity increased from 1.022 and 1.941 before CO₂ absorption ($\alpha = 0$) to 1.073 and 4.8 after CO₂ absorption ($\alpha = 0.8$), respectively.

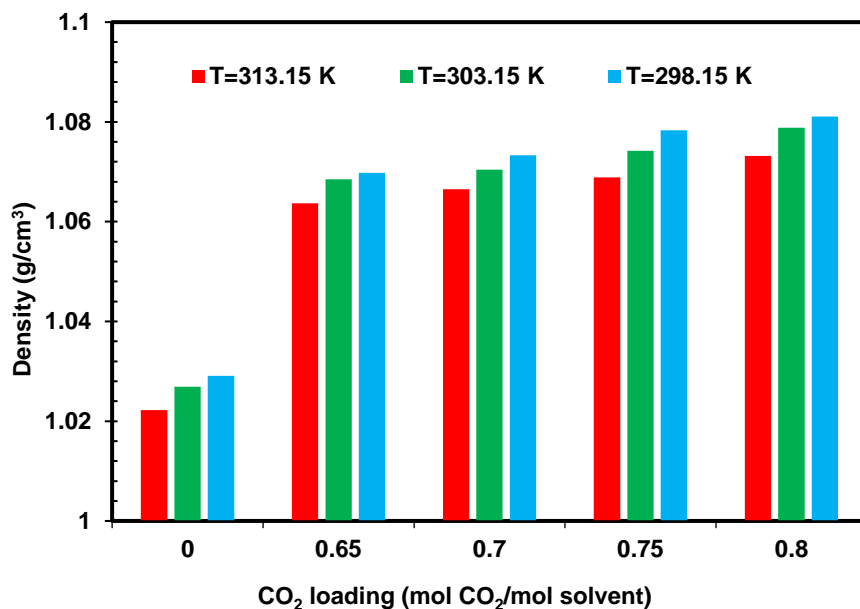


Figure 4.64 The density of 20 wt% MDEA + 10 wt% K-Lys solution after absorption at 298-313 K.

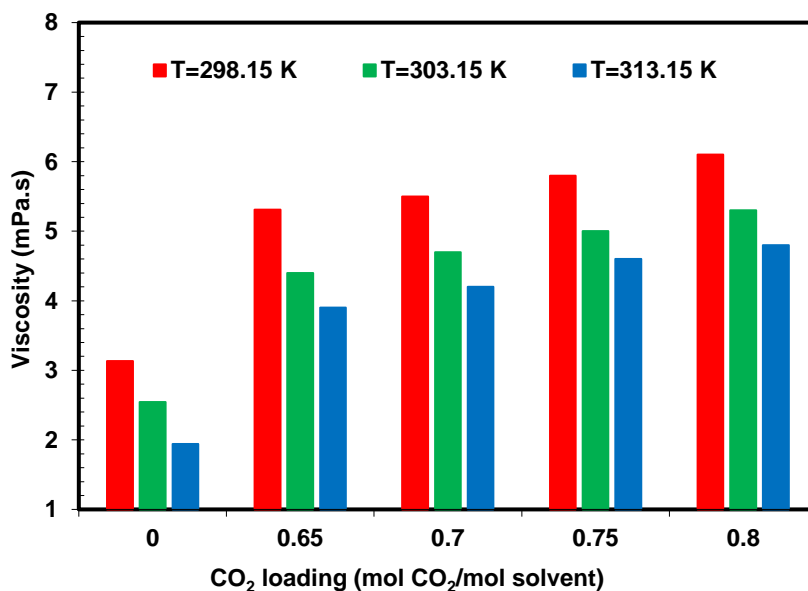


Figure 4.65 The viscosity of 20 wt% MDEA + 10 wt% K-Lys solution after absorption at 298-313 K.

The pH of MDEA + K-Lys solutions before and after CO₂ absorption was measured at temperatures of 298.15 to 313.15 K and (0.2-0.5) M K-Lys, and the results were compared to pH of 1.5 M MDEA

solution. The pH of MDEA + K-Lys solutions, before absorption, varies from 10.9 to about 11.7 depending on temperature and concentration of the solutions, as shown in Table 4.39. Moreover, addition of K-Lys to MDEA has been led to a rise in pH of solution.

Table 4.39 The pH of solutions of MDEA and MDEA + K-Lys before absorption at 298-313 K.

T (K)	1.5 M MDEA	2 M MDEA + 0.2 M K-Lys	2 M MDEA + 0.3 M K-Lys	2 M MDEA + 0.5 M K- Lys
pH				
298	11.29	11.48	11.65	11.72
303	11.21	11.37	11.53	11.61
313	10.98	11.15	11.27	11.37

The pH of 1.5 M MDEA + 0.5 M K-Lys solution after CO₂ absorption was also measured and presented in Figure 4.66. It is seen from this figure that pH of MDEA + K-Lys solution at studied temperatures decreases with the increase in CO₂ loading capacity due to an increase in acidity of solution. In addition, the results showed that the pH decreases when temperature increases from 298 to 313 K. This can be explained by the fact that [H⁺] concentration increases (due to more ionization) at higher temperatures which leads to reducing the pH.

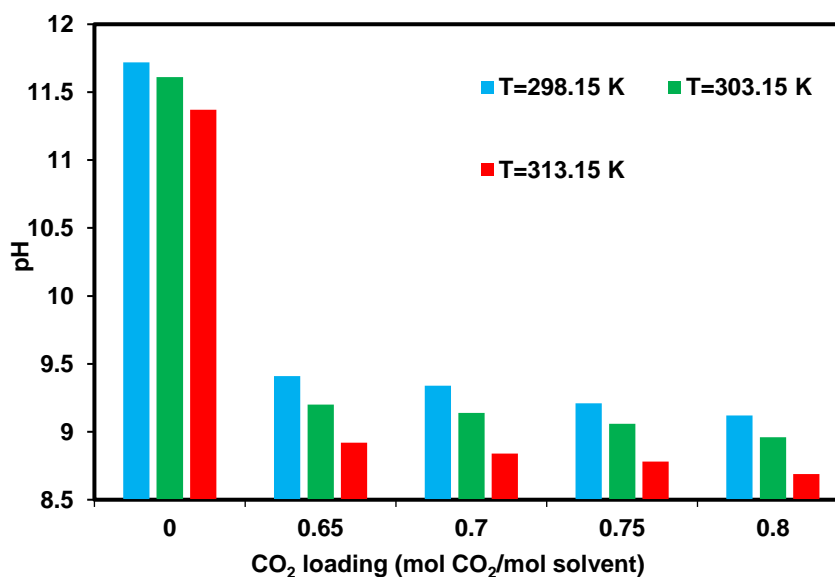


Figure 4.66 The pH of 20 wt% MDEA + 10 wt% K-Lys solution after absorption at 298-313 K.

4.7.3. Diffusivity of CO₂ in MDEA + K-Lys

The diffusion coefficient of CO₂ and physical solubility of CO₂ in MDEA + K-Lys solutions were obtained using the same method which explained in previous sections, and the results were illustrated in

Figure 4.67. It can be clearly seen that diffusion coefficient of CO₂ increases as temperature increases while decreases as K-Lys concentration increases. This behavior can be explained from variations of the solution viscosity relative to the temperature and concentration as mentioned before.

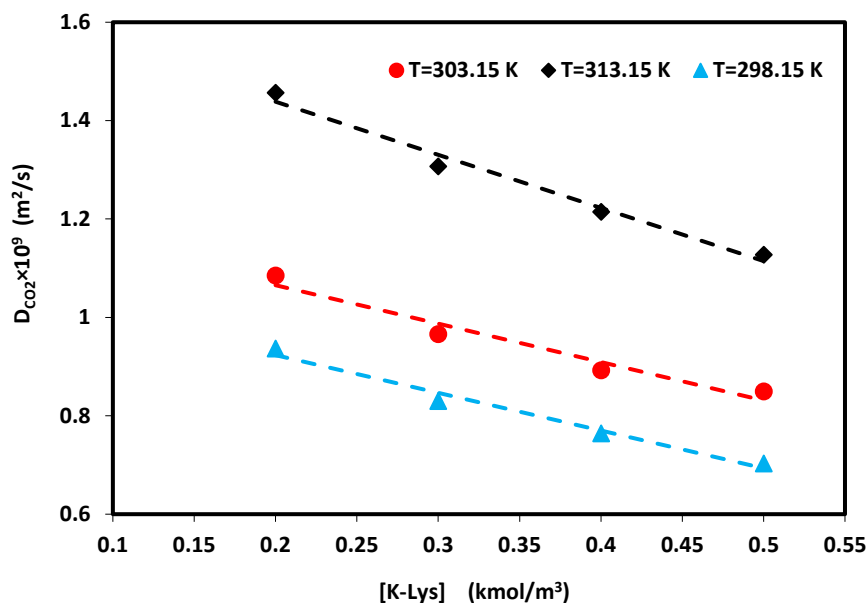


Figure 4.67 Diffusivity of CO₂ in MDEA + K-Lys as a function of K-Lys concentration

4.7.4. Kinetics study of CO₂ absorption in MDEA + K-Lys

The zwitterion mechanism is generally applied for the reactions between CO₂ with amino acids, primary and secondary alkanolamines, while reaction of CO₂ with tertiary alkanolamines can be described using the base-catalyzed mechanism. According to these mechanisms, the overall CO₂ absorption rate can be expressed as:

$$R_{OV} = R_{CO_2-MDEA} + R_{CO_2-Lys} + R_{CO_2-OH^-} \quad (102)$$

Some studies have shown that CO₂ absorption rate in MDEA solution is described by a pseudo-first order reaction kinetics:

$$R_{CO_2-MDEA} = k_{MDEA}[CO_2][MDEA] \quad (103)$$

Depending on the zwitterion deprotonation, the overall reaction order varies between two and three:

$$R_{CO_2-Lys} = \frac{k_{Lys}[Lys][CO_2]}{1 + \frac{k_{-1}}{\sum k_B[B]}} \quad (104)$$

When $\frac{k_{-1}}{\sum k_B[B]} \ll 1$, the reaction rate reduces to second order kinetics:

$$R_{CO_2-Lys} = k_{Lys}[Lys][CO_2] \quad (105)$$

When $\frac{k_{-1}}{\sum k_B[B]} \gg 1$, then Eq. (104) becomes:

$$R_{\text{CO}_2-\text{Lys}} = k_{\text{Lys}}[\text{CO}_2][\text{Lys}]^n \quad (106)$$

Consequently, the overall reaction rate (R_{OV}) can be represented by:

$$R_{\text{OV}} = k_{\text{OH}^-}[\text{CO}_2][\text{OH}^-] + k_{\text{MDEA}}[\text{CO}_2][\text{MDEA}] + k_{\text{Lys}}[\text{CO}_2][\text{Lys}]^n \quad (107)$$

$$R_{\text{OV}} = [\text{CO}_2] k_{\text{OV}} \quad (108)$$

Then, k_{ov} is simplified as:

$$k_{\text{ov}} = k_{\text{OH}^-}[\text{OH}^-] + k_{\text{MEA}}[\text{MEA}] + k_{\text{Lys}}[\text{Lys}]^n \quad (109)$$

The CO_2 absorption rate into MDEA + K-Lys solution can be also described by Eq. (110) according to Danckwert et al.:

$$N_{\text{CO}_2} = E_A K_L ([\text{CO}_2]_i - [\text{CO}_2]_b) \quad (110)$$

The values of experimental enhancement factor can be obtained by Eq. (111):

$$[E_A]_{\text{exp}} = \frac{N_{\text{CO}_2}}{K_L([\text{CO}_2]_i - [\text{CO}_2]_b)} \quad (111)$$

The value of theoretical enhancement factor can also be calculated by Eq. (112):

$$[E_A]_{\text{the}} = 1 + \frac{\text{Ha}}{A} [1 - \exp(-0.65 \times \text{Ha} \times \sqrt{A})] \quad (112)$$

$$A = \frac{\text{Ha}}{E_{\infty}-1} + \exp\left(\frac{0.68}{\text{Ha}} - \frac{0.45 \times \text{Ha}}{E_{\infty}-1}\right) \quad (113)$$

The measurement method for calculation of experimental absorption flux, concentration of CO_2 and liquid mass transfer coefficient, Hatta number and infinite enhancement factor was explained in the previous sections. Since obtained values of experimental and theoretical enhancement factor must be equal ($[E_A]_{\text{exp}} = [E_A]_{\text{the}}$), the value of Hatta number can be found. Then, overall reaction rate constant is determined as follows:

$$\text{Ha} = \frac{\sqrt{K_{\text{OV}} D_{\text{CO}_2}}}{K_L} \quad (114)$$

$$K_{\text{OV}} = \frac{(\text{Ha} \times K_L)^2}{D_{\text{CO}_2}} \quad (115)$$

Then, the apparent reaction rate constant can be obtained by Eq. (116):

$$k_{\text{app}} = k_{\text{ov}} - k_{\text{OH}^-}[\text{OH}^-] - k_{\text{MDEA}}[\text{MDEA}] = k_{\text{Lys}}[\text{Lys}]^n \quad (116)$$

By plotting $\log k_{\text{app}}$ vs. $\log[\text{Lys}]$, values of the reaction order with respect to potassium lysinate and reaction rate constant can be determined. Before studying kinetics of CO_2 absorption in MDEA + K-Lys system, it is essential to check the reliability of the experimental method. The CO_2 absorption in MDEA solution was studied at various temperatures by many researchers and values of reaction rate constant (k_{MDEA}) were reported. These data were used in this work in order to validate the experimental setup and procedures. The absorption flux of CO_2 in MDEA solution was measured at 298.15 K to 313.15 K using

stirred batch reactor, and the values of reaction rate constant were calculated. Figure 4.68 shows the comparison of reaction rate constant data for MDEA + CO₂ + H₂O system obtained in this study with those published in the literature. It can be observed that a well accordance was found between our results and data reported in the literature.

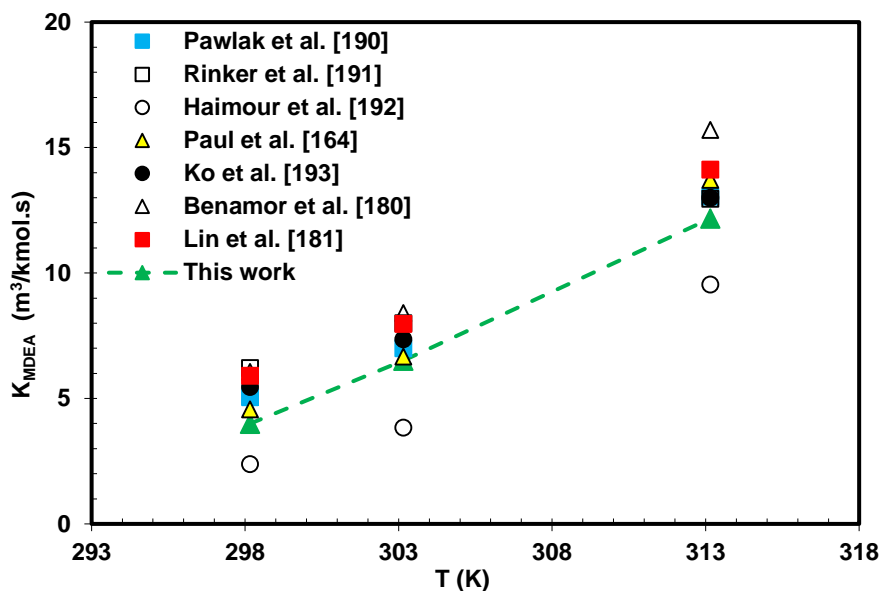


Figure 4.68 Comparison of the second-order rate constant calculated in this work with those obtained in the literature.

After validating the experimental setup and calculation method, the reaction kinetics of CO₂ absorption in CO₂ loaded and CO₂ unloaded solutions of MDEA, K-Lys and MDEA + K-Lys were studied. In this regards, the absorption flux of CO₂ in these solutions was measured at low and high partial pressure of CO₂. Figure 4.69(a-c) shows the pressure decay during absorption of CO₂ in the solutions of 1.5 M MDEA, 0.2 M K-Lys and 1.5 M MDEA + 0.2 M K-Lys at 298.15 K and at different partial pressure of CO₂. This pressure reduction in the equilibrium cell which is recorded by using a pressure transmitter shows the amount of gas absorption in the liquid. The partial pressure of CO₂ in the reactor decreases with increasing time until a gas-liquid equilibrium is reached. The time required to reach an equilibrium state is different for each solvents. It was found that K-Lys solution reaches the equilibrium state at less time in comparison to MDEA and MDEA + K-Lys. The reason for different equilibrium times is faster reaction rate of K-Lys with CO₂ than other solutions.

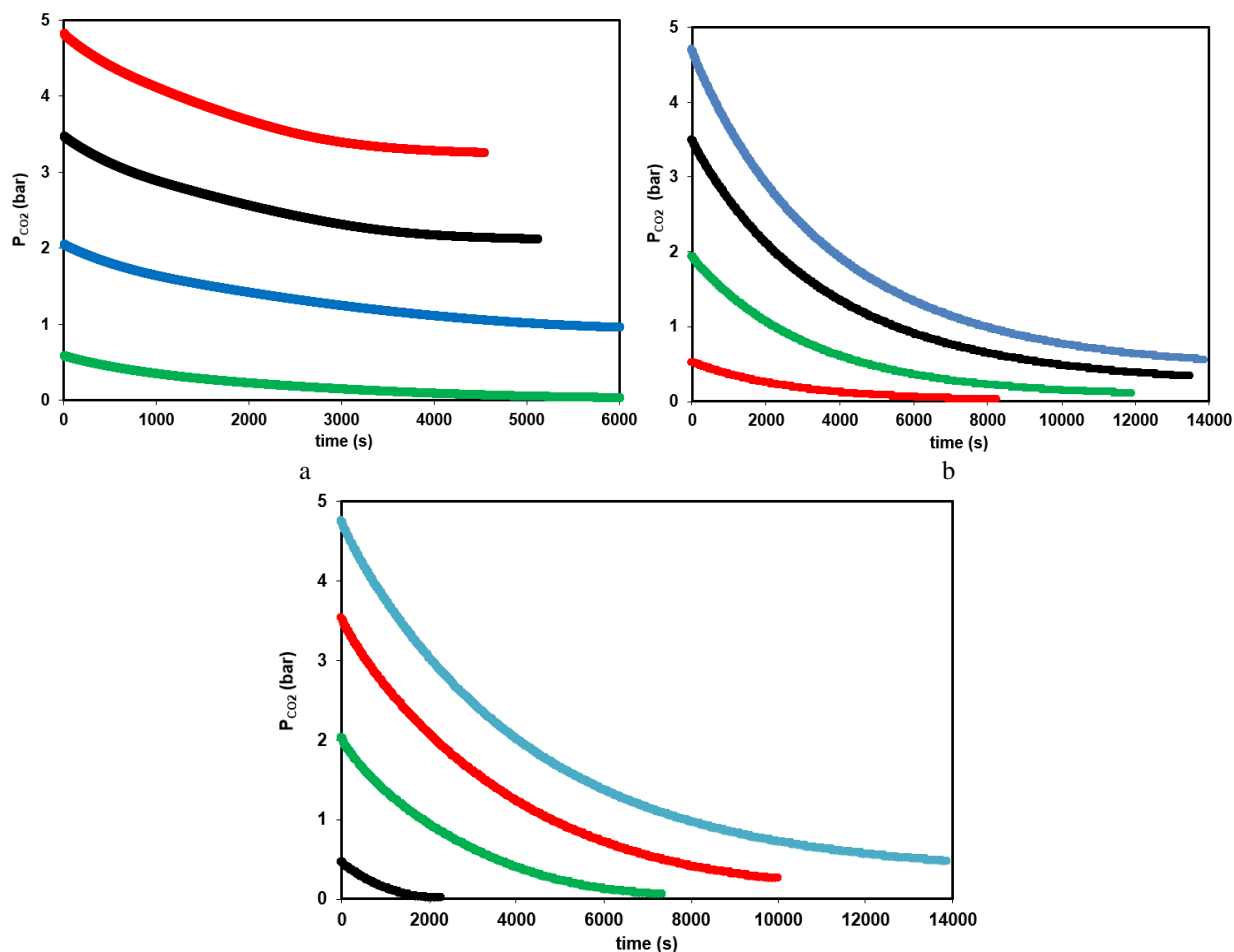


Figure 4.69(a-c) Pressure decay during CO₂ absorption in solutions of a) 1.5 M MDEA; b) 0.2 M K-Lys; c) 1.5 M MDEA + 0.2 M K-Lys.

The experimental CO₂ absorption flux can be calculated using Eq. (46) and from the slope of the plot of pressure versus time. The CO₂ absorption flux in solutions of MDEA, K-Lys and MDEA + K-Lys versus time at CO₂ partial pressure up to 500 kPa and at 298.15 was given in Figure 4.70(a-c). It is clear that the absorption flux of CO₂ in tested solvents decreases with absorption time. At the beginning, the CO₂ absorption flux is high. With the continued absorption of CO₂, pH of solution decreases and CO₂ loading increases which lead to lower absorption rate.

The experimental results also showed that the CO₂ absorption flux increases when partial pressure of CO₂ increases from around 50 to 480 kPa for all the solutions. This could be due to the fact that the driving force between gas phase and gas-liquid interface increases by increasing the CO₂ partial pressure, and thus results a higher absorption rate of CO₂.

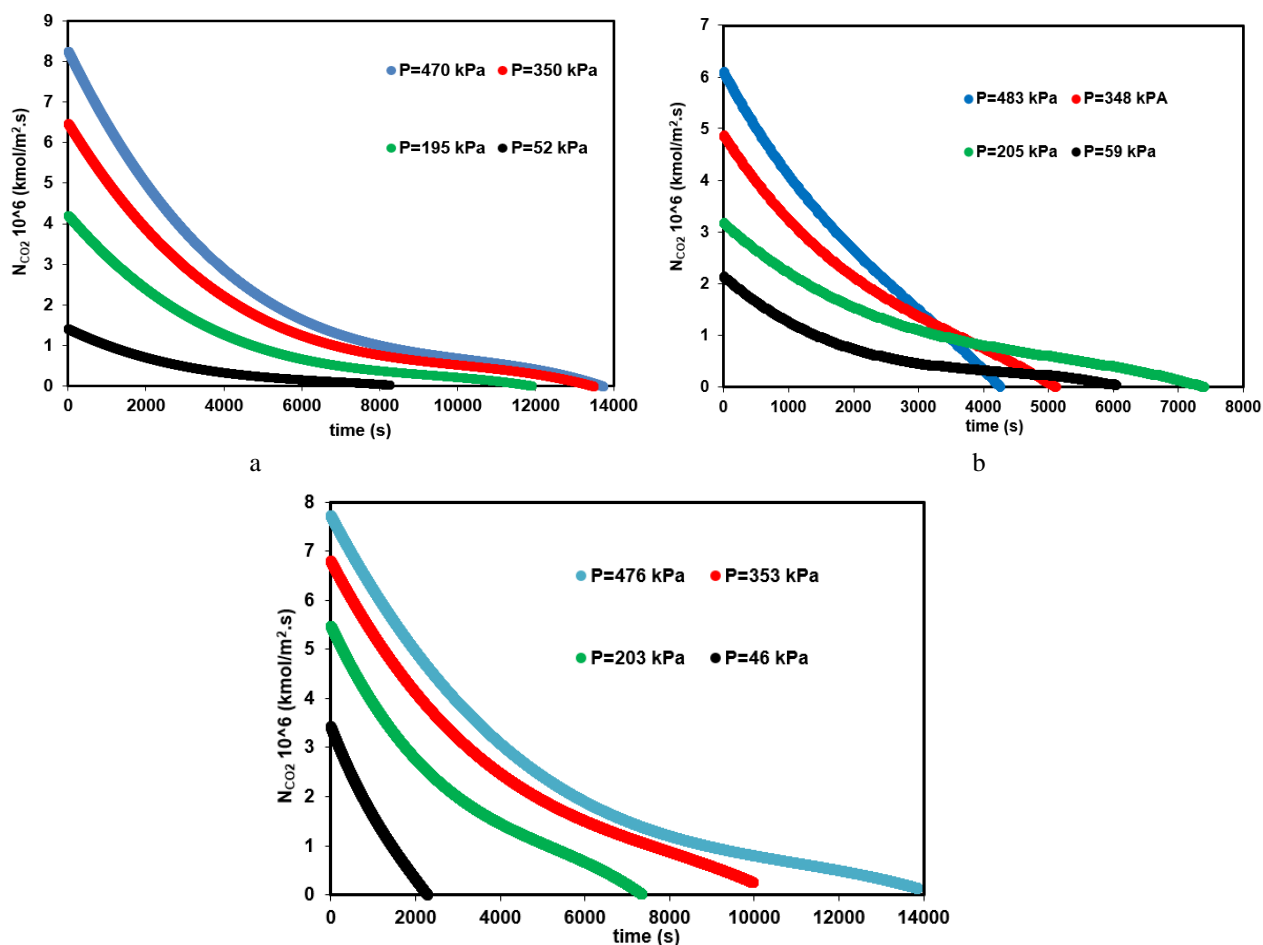


Figure 4.70(a-c) CO₂ absorption flux vs. absorption time at different CO₂ partial pressures for a) 1.5 M MDEA; b) 0.2 M K-Lys; c) 1.5 M MDEA + 0.2 M K-Lys.

The profiles of CO₂ absorption flux as a function of CO₂ loading of MDEA, K-Lys and MDEA + K-Lys solutions at 298.15 K were also presented in Figure 4.71(a-c). It can be clearly seen that the CO₂ absorption flux decrease when CO₂ loading capacity of solution increases. This can be explained that free concentration of solvent decreases when CO₂ loading capacity of solution increases. The less free concentration of solvent mean there are less free amine molecules available to react with CO₂ which will lead to a decrease of effective collisions.

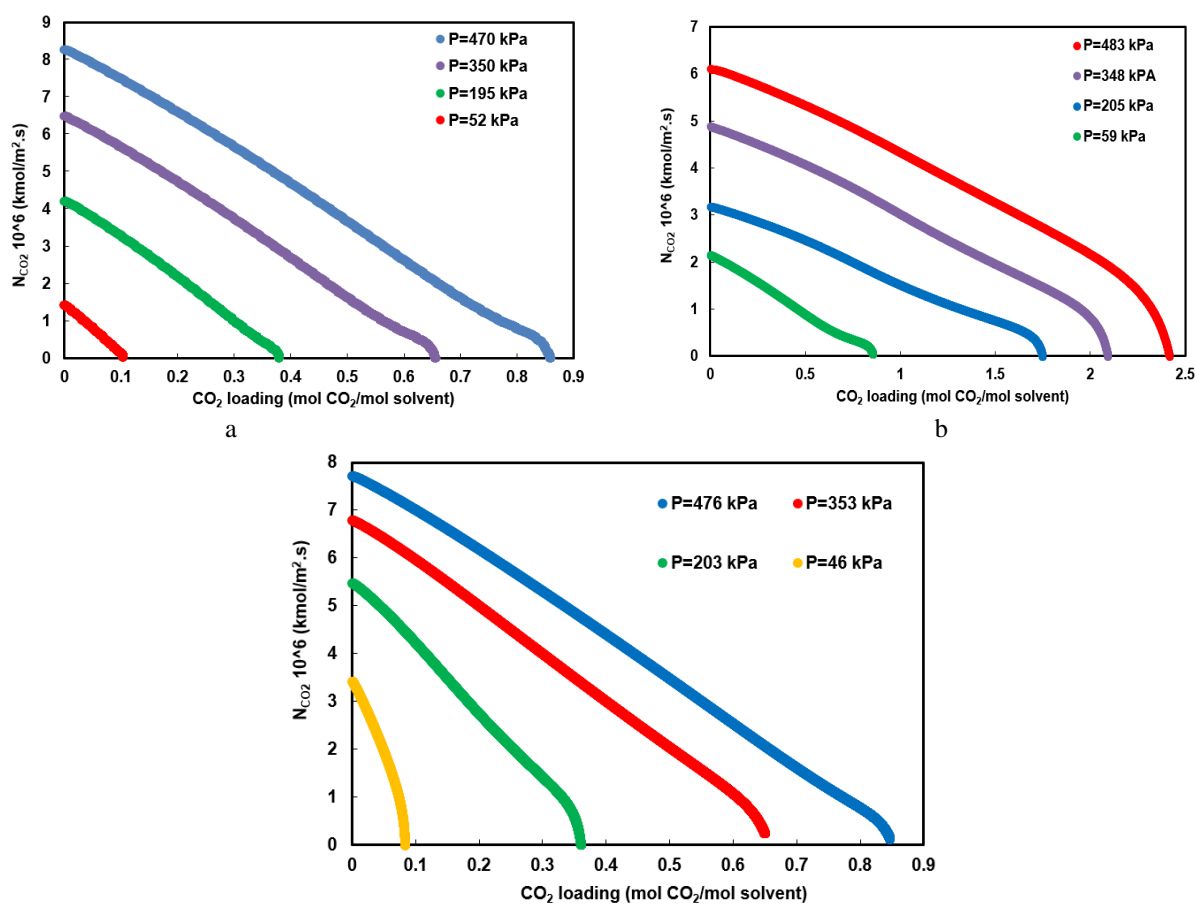


Figure 4.71(a-c) CO₂ absorption flux vs. CO₂ loading at different CO₂ partial pressures for a) 1.5 M MDEA; b) 0.2 M K-Lys; c) 1.5 M MDEA + 0.2 M K-Lys.

The effect of temperature on absorption rate of CO₂ in 1.5 M MDEA + 0.5 K-Lys solution was studied and the results were illustrated in Figure 4.72(a-c). As can be observed in this figure, the absorption rate increases when temperature increases from 298.15 K to 313.15 K. The reasons for this result could be due to the reduction of solution viscosity, and increase in reaction rate constant (according to Arrhenius law) with increase in temperature.

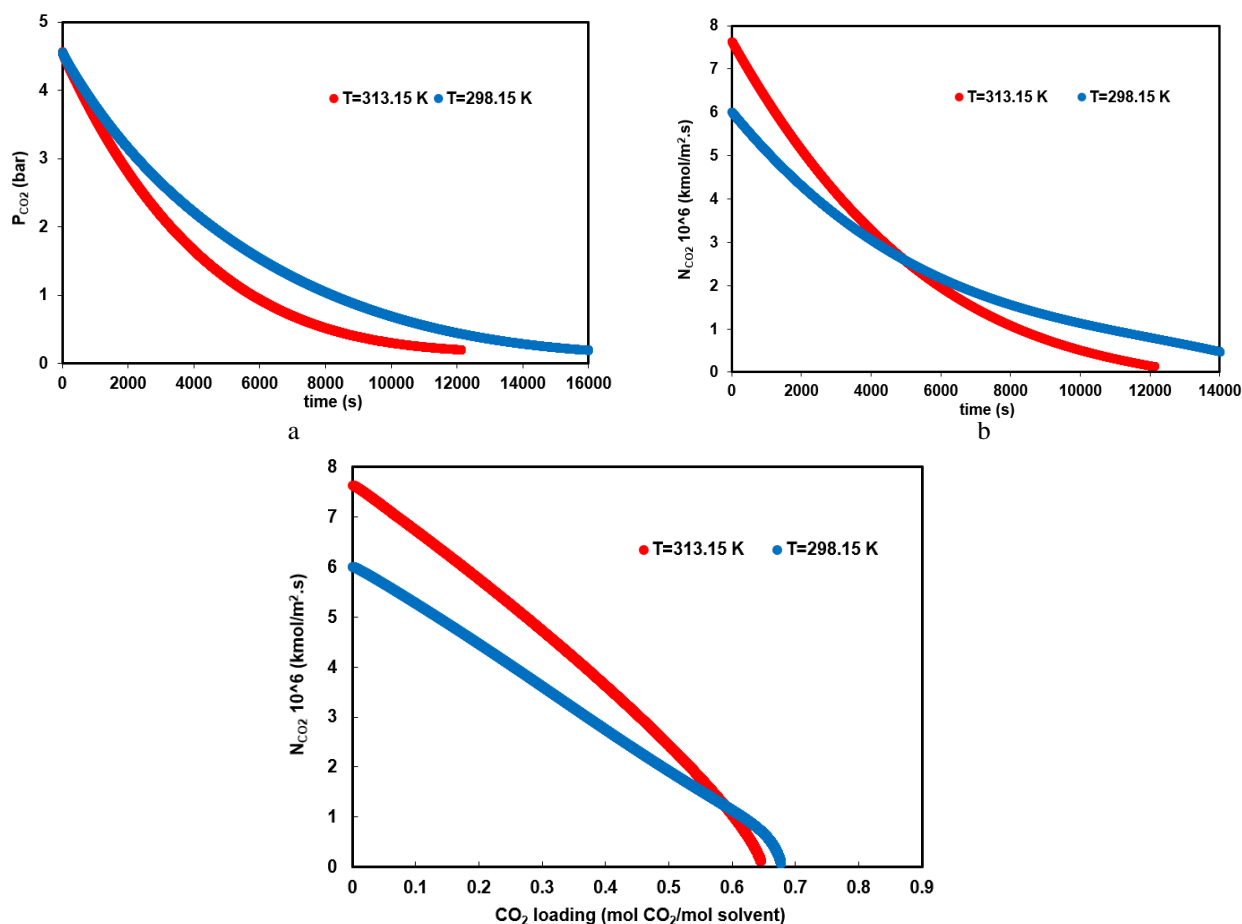


Figure 4.72(a-c) The effect of temperature on absorption flux of CO₂ in MDEA + K-Lys solution, a) P_{CO_2} vs. time; b) flux vs. time and c) flux vs. CO₂ loading.

The effect of addition of 0.2 M K-Lys to 1.5 M MDEA solution was studied at low, moderate and high CO₂ partial pressure as given in Figure 4.73 to 4.76(a-c). It can be seen from these figures that MDEA takes too much time to reach equilibrium state in comparison to single K-Lys. The reason for this behavior of MDEA is the formation of bicarbonates by CO₂ hydrolysis which is slower when compare with formation of carbamate by K-Lys and CO₂. The carbamate formation by primary amino group in K-Lys contributes to increasing the overall rate of absorption.

It was also found that at CO₂ partial pressure around 50 kPa, K-Lys has faster absorption flux than MDEA as shown in Figure 4.73 while at CO₂ partial pressure higher than 50 kPa, MDEA indicates better absorption flux than K-Lys as given in Figure 4.74 to 4.76. Therefore, the addition of K-Lys to MDEA at low partial pressure of CO₂ has been lead to a significant increase in CO₂ absorption rate of MDEA + K-Lys solution. In the other words, the addition of K-Lys at high pressure has no effect on absorption flux of CO₂ in MDEA + K-Lys. The reason for this behavior is due to the higher enhancement factor of K-Lys than MDEA at low partial pressure of CO₂ which will be discussed in next section.

It was also observed from absorption flux curves versus CO₂ loading that absorption flux of CO₂ shows a sudden decrease in high CO₂ loading capacity. One example can be for K-Lys solution at CO₂ loading higher than 2 and 2.25 for CO₂ partial pressure of 350 and 470 kPa, respectively. It should be noted that at this loading all the free amine molecules reacted with CO₂ and actually the absorption relied mainly on physical absorption and made chemical absorption secondary.

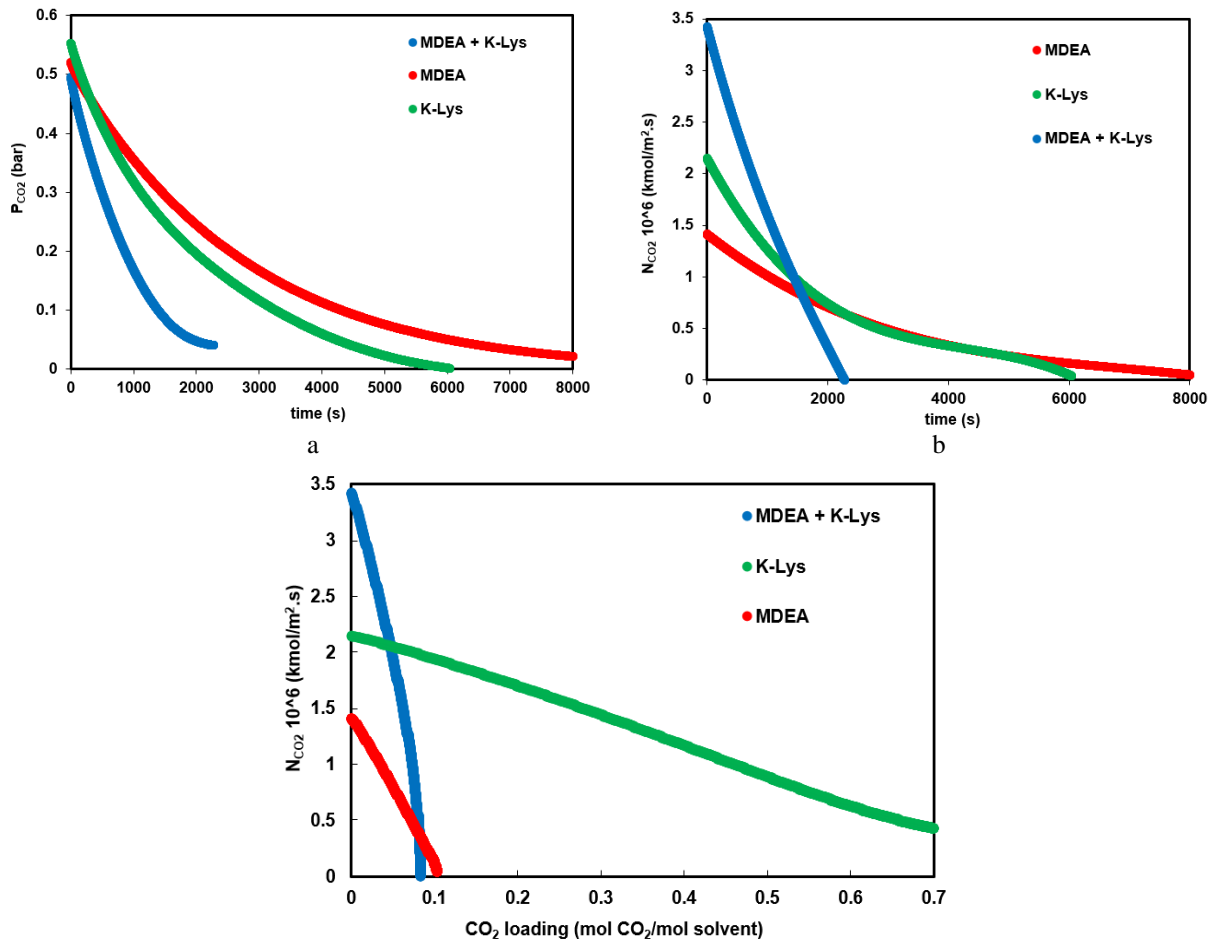


Figure 4.73(a-c) Comparison of performance of CO₂ absorption rate in different solutions at P_{CO₂}=50 kPa, a) P_{CO₂} vs. t ; b) flux vs. t and c) flux vs. CO₂ loading.

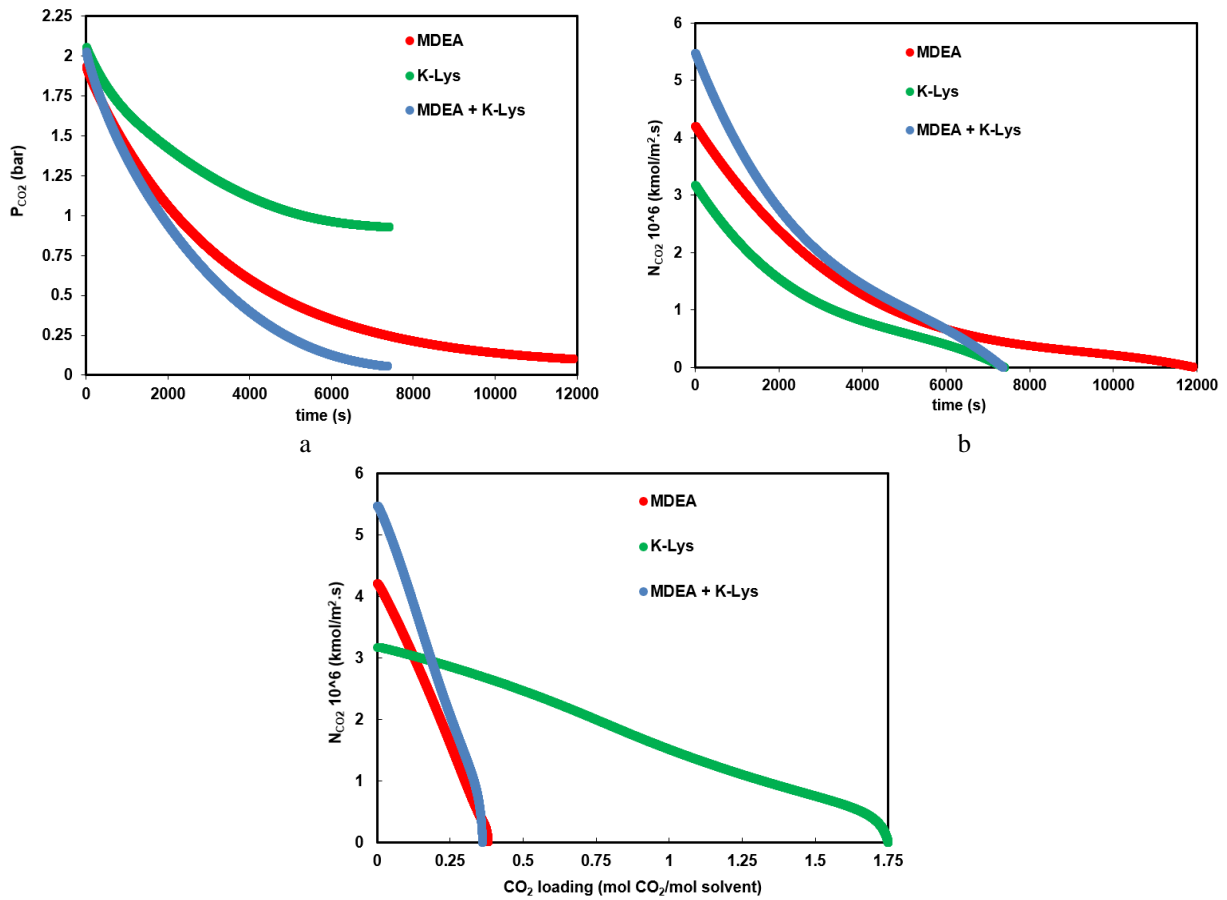


Figure 4.74(a-c) Comparison of performance of CO₂ absorption rate in different solutions at P_{CO₂}=200 kPa, a) P_{CO₂} vs. t ; b) flux vs. t and c) flux vs. CO₂ loading.

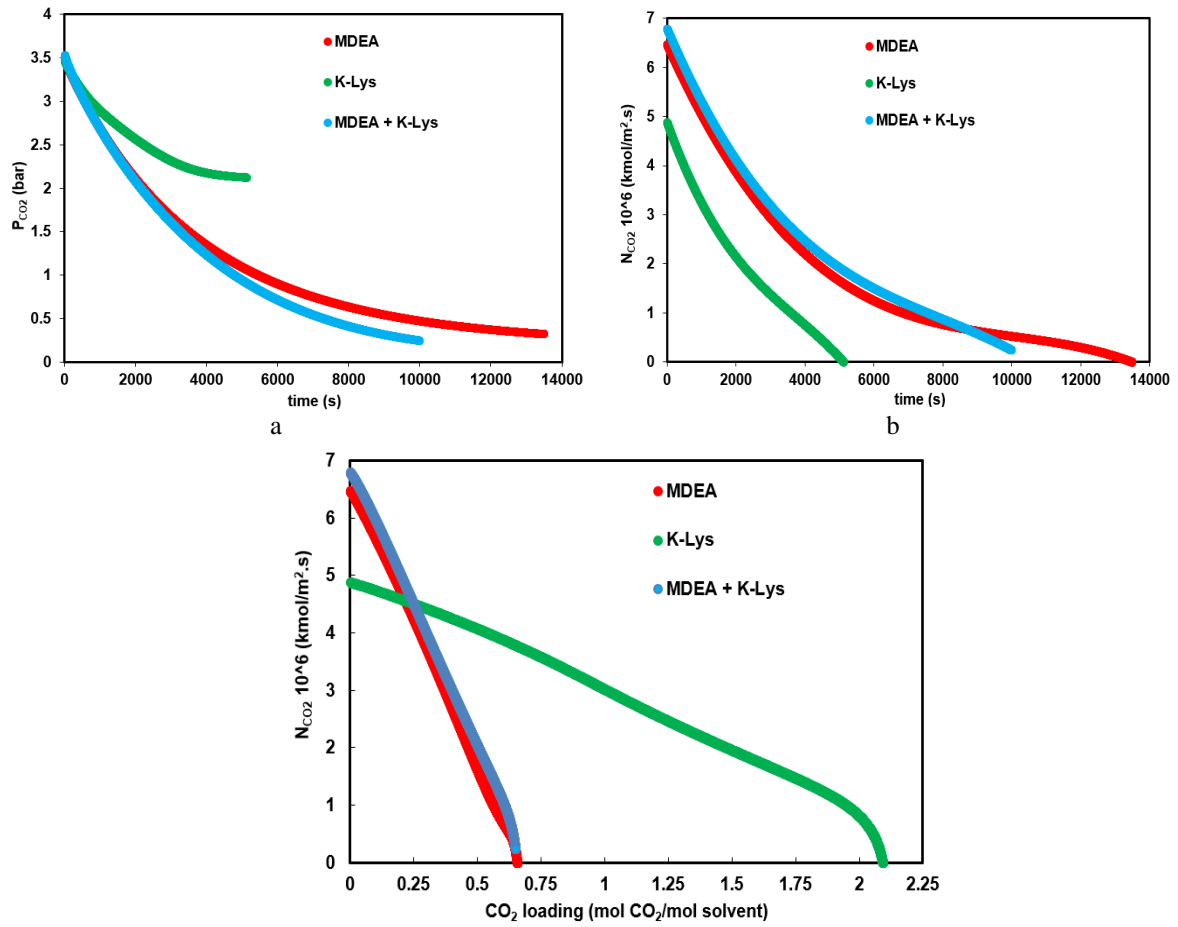


Figure 4.75(a-c) Comparison of performance of CO₂ absorption rate in different solutions at $P_{CO_2}=350$ kPa, a) P_{CO_2} vs. t ; b) flux vs. t and c) flux vs. CO₂ loading.

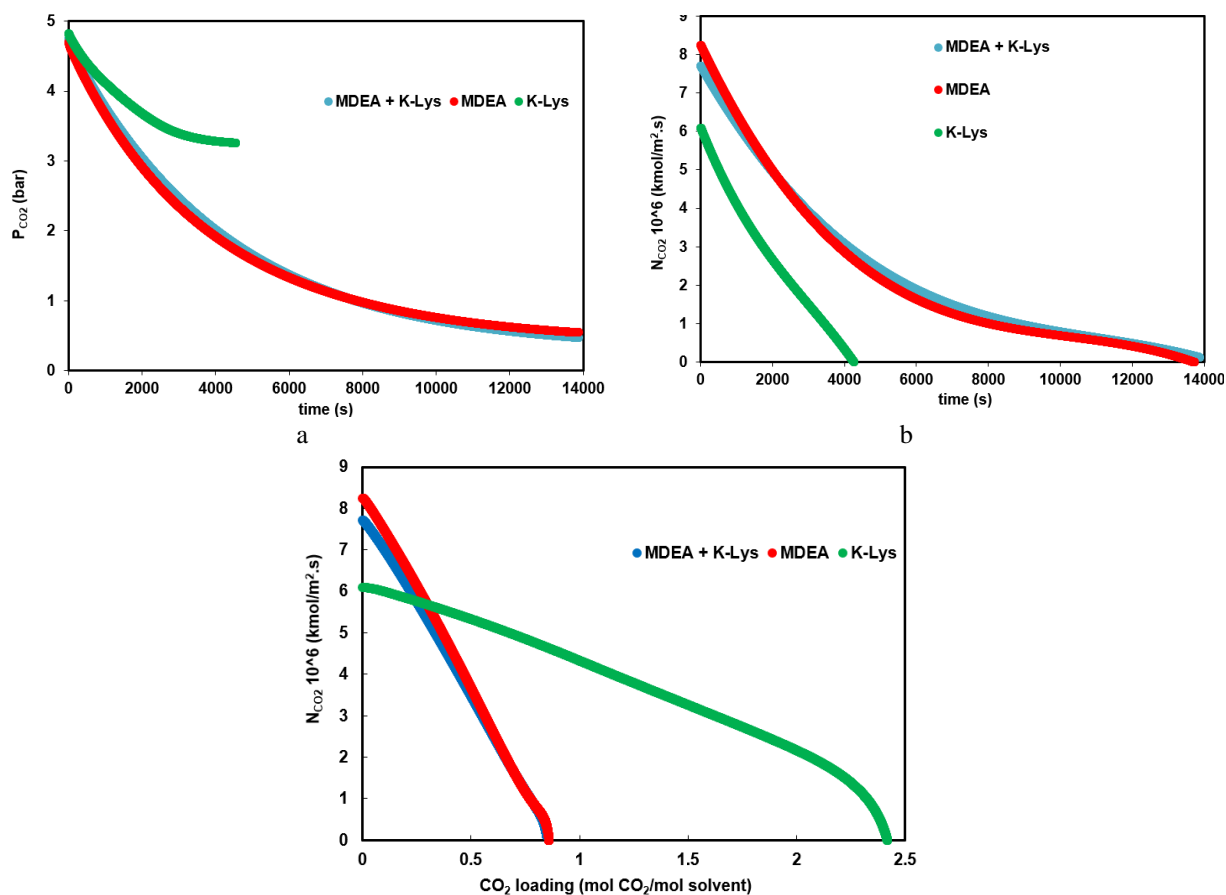


Figure 4.76(a-c) Comparison of performance of CO₂ absorption rate in different solutions at P_{CO₂}=500 kPa, a) P_{CO₂} vs. t ;b) flux vs. t and c) flux vs. CO₂ loading.

The enhancement factor as a function of partial pressure of CO₂ for 1.5 M MDEA and 0.2 M K-Lys solutions at 298.15 K was determined in order to investigate the effect of pressure. Generally, the enhancement factor is defined as the ratio between the CO₂ absorption flux with chemical reaction and the obtained flux of the CO₂ physical absorption with fluxes based on the same driving force [109], and thus can be calculated according to Eq. (117):

$$E_A = \frac{N_{\text{CO}_2 \text{ with reaction}}}{N_{\text{CO}_2 \text{ without reaction}}} \quad (117)$$

A comparison between experimental and predicted enhancement factor for MDEA and K-Lys solutions was presented in Figure 4.77. As is illustrated in this figure, the experimental enhancement factor data are in good agreement with predicted results.

It can also be seen that the enhancement factor has greater values at lower CO₂ partial pressure (CO₂ interfacial concentration). The reason for this behavior is that as partial pressure of CO₂ decreases, the contribution of physical absorption to the overall absorption of CO₂ decreases and the contributions of the chemical reactions between CO₂ and amine increases [109].

In addition, it was found that K-Lys shows a different behavior at high and low partial pressure of CO₂. Actually, K-Lys seems to offer better performance than MDEA only at low partial pressure of CO₂. In the other words, when CO₂ partial pressure is lower than 60 kPa, 0.2 M K-Lys exhibits higher enhancement factor than 1.5 M MDEA which lead to a faster absorption rate. However, with a further increase in CO₂ partial pressure, K-Lys shows lower enhancement factor than MDEA which can explained its slower absorption rate than MDEA as discussed before.

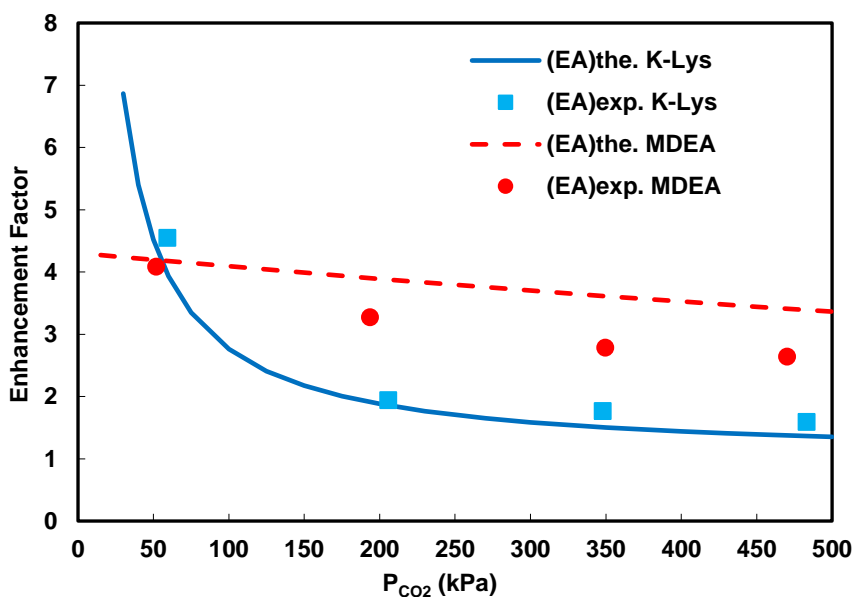


Figure 4.77 Comparison of experimental and predicted enhancement factor for CO₂ absorption in MDEA and K-Lys solutions.

To further analyze the absorption process, the absorption kinetic model was used to predict the experimental absorption data. The absorption flux of CO₂ in MDEA and K-Lys solutions was predicted by obtained enhancement factor values in previous section. The experimental and predicted CO₂ absorption rates versus CO₂ loading for CO₂ loaded and unloaded solutions of MDEA and K-Lys at 298.15 K were presented in Figure 4.78 and 4.79, respectively.

In addition, CO₂ partial pressure decay in the reactor during absorption was predicted with predicted absorption rate and the results were plotted in Figure 4.80. As can be seen from these figures, the experimental results are in good agreement with model calculations.

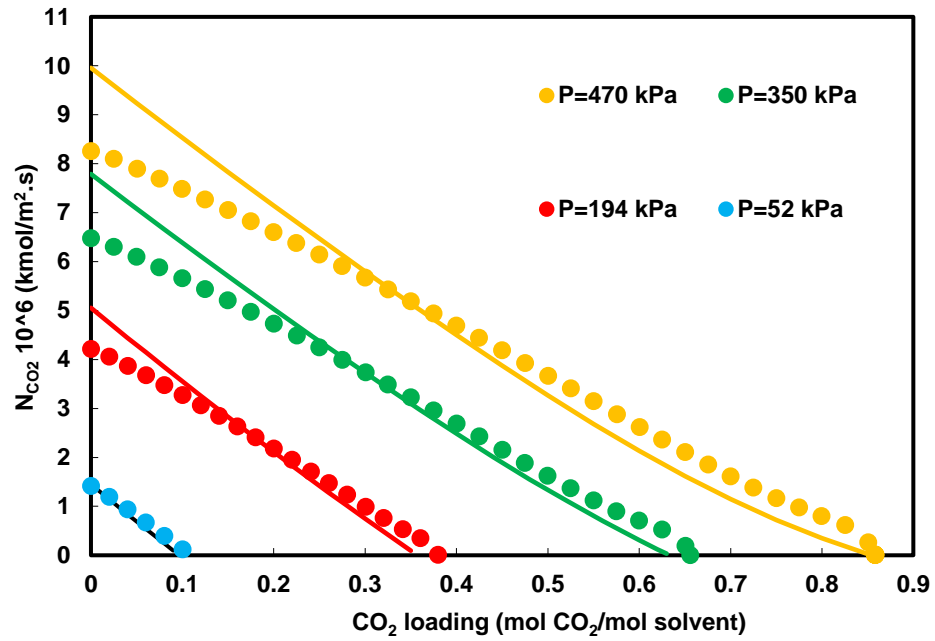


Figure 4.78 Comparison of experimental and predicted CO₂ absorption flux in MDEA solution.

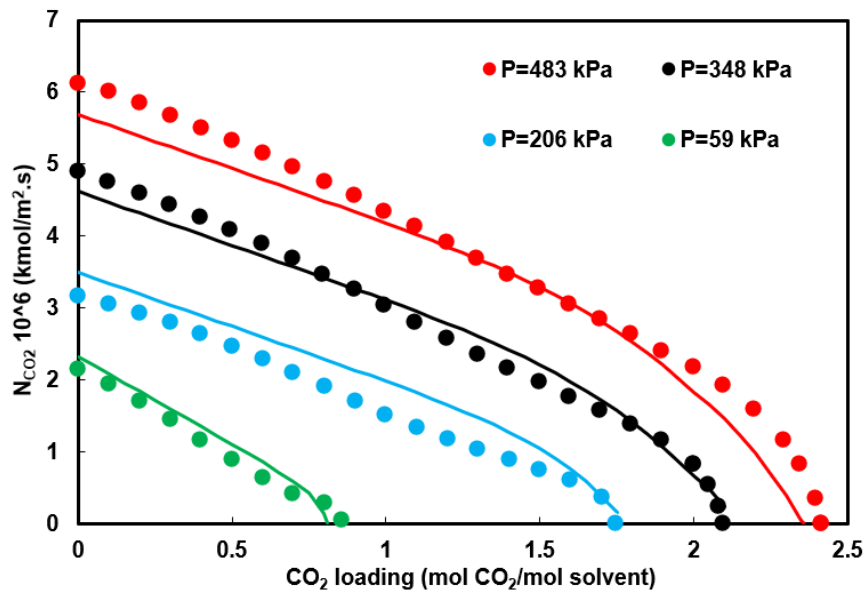


Figure 4.79 Comparison of experimental and predicted CO₂ absorption flux in K-Lys solution.

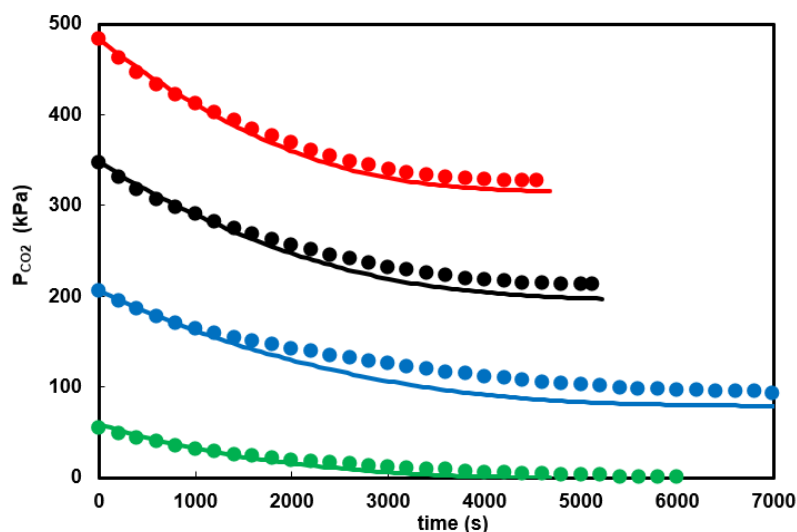


Figure 4.80 Comparison of experimental and predicted pressure decay for CO₂ absorption in K-Lys solution.

4.7.5. Heat of CO₂ absorption of MDEA + K-Lys

As mentioned before, the heat of absorption plays an important role in the selection of a suitable solvent because this parameter provides information about the energy requirements in the desorption column. The CO₂ absorption heat of MDEA + K-Lys was estimated by Eq. (47) and compared with other solvents as illustrated in Figure 4.81. The value of heat of absorption for MDEA + K-Lys was estimated to be around 59.7 kJ/mol which is lower than MEA and other studied amines, except single MDEA. This means that MDEA + K-Lys solution needs less energy to be regenerated in comparison to single MEA, and therefore is favorable for CO₂ capture. It also can be seen that heat of absorption of MDEA + K-Lys was about 10% higher than single MDEA. This may be due to the fact that lysine has primary amino groups, which produce stable carbamate ions and increases absorption heat. However, this value is still lower when compared with other blend solutions.

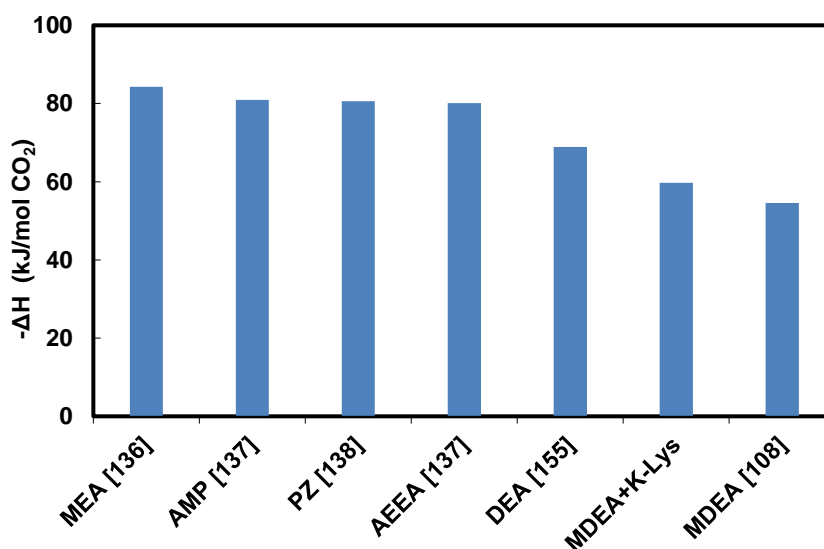


Figure 4.81 Comparison of heat of CO₂ absorption of MDEA + K-Lys solution with the other absorbents.

Figure 4.82 presents a comparison between CO₂ absorption heat of chemical absorbent investigated in this study. Single MEA presents the highest CO₂ absorption heat which means solvent need high energy for regeneration. However, the results show that MEA blended with K-Lys present lower absorption heat. In addition, K-Lys mixed with MDEA has lower absorption heat in comparison to K-Lys + MEA, which explained in previous sections. As can be seen in figure 4.82, K₂CO₃ solution promoted by 2MPZ, AEEA, K-Ser and K-Ala needs lower energy for regeneration according to results obtained in this work.

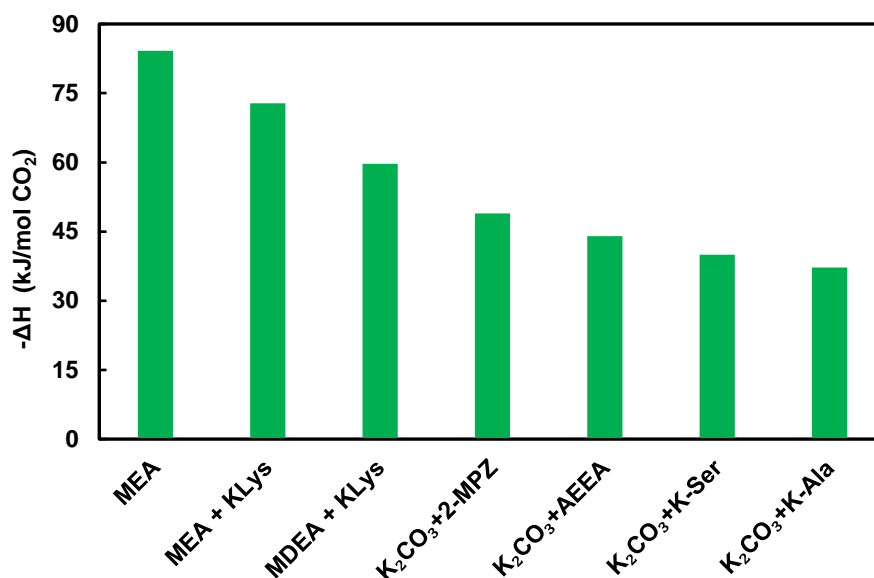


Figure 4.82 Comparison of heat of CO₂ absorption of chemical solvent studied in this work

4.8. Absorption characterization of CO₂ in MEA + Sugar

A good understanding and prediction of the mass transfer in viscous solutions is important for proper solvent selection and process design. In addition, post combustion processes normally work in the loading range between 0.2 and 0.5 (mol CO₂/mol solvent) and it is thus important to study the performance of loaded solutions. Therefore, a further study on the kinetics and the physicochemical properties of unloaded and CO₂ loaded viscous MEA solutions is necessary to give us a comprehensive understanding of mass transfer behavior of CO₂ absorption. In this regard, the CO₂ absorption performance in viscous MEA solutions was investigated in this work in collaboration with Norwegian University of Science and Technology. The main objective of this work was to study the effect of liquid viscosity on the mass transfer coefficient and absorption flux of CO₂ in MEA solution. In this work, the overall mass transfer coefficient in CO₂ loaded and unloaded solutions of MEA + sugar was measured using a string of discs contactor in the temperature range 25 to 70 °C and for CO₂ loading up to 0.4. In addition, the values of density and viscosity of solution at the same experimental condition were obtained and reported.

4.8.1. Density of MEA + Sugar

The density of CO₂ loaded and CO₂ unloaded solutions of 30 wt% MEA and 30 wt% MEA + (3-20) wt% sugar was measured using a density meter which explained in section 3.3. The values reported in this work are the average of two measurements. The obtained experimental results were plotted versus CO₂ loading in Figure 4.83 to 4.87. As shown in these figures, the density decreased with increasing temperature and increased with increasing CO₂ loading.

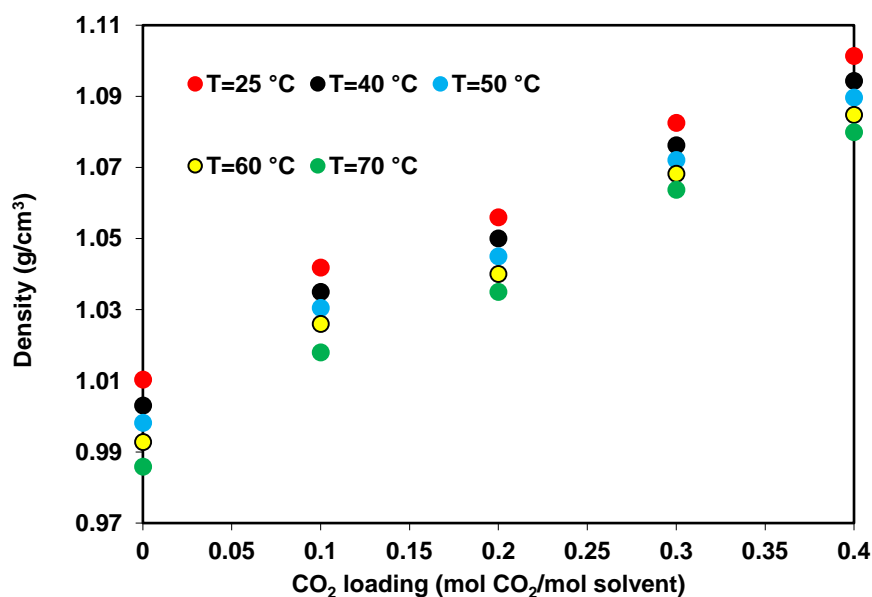


Figure 4.83 Density of unloaded and CO₂ loaded MEA solution at different temperatures

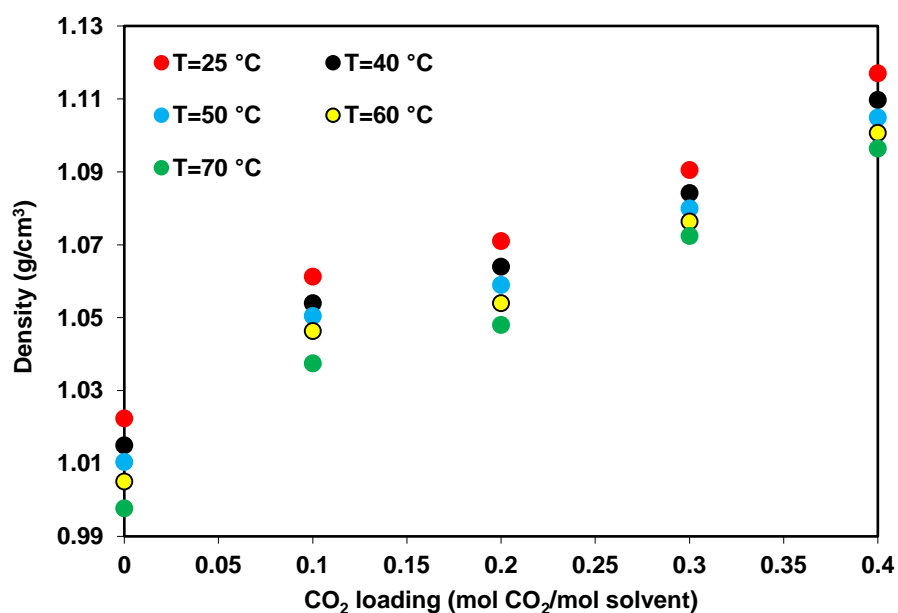


Figure 4.84 Density of unloaded and CO₂ loaded MEA + 3wt% sugar solution at different temperatures.

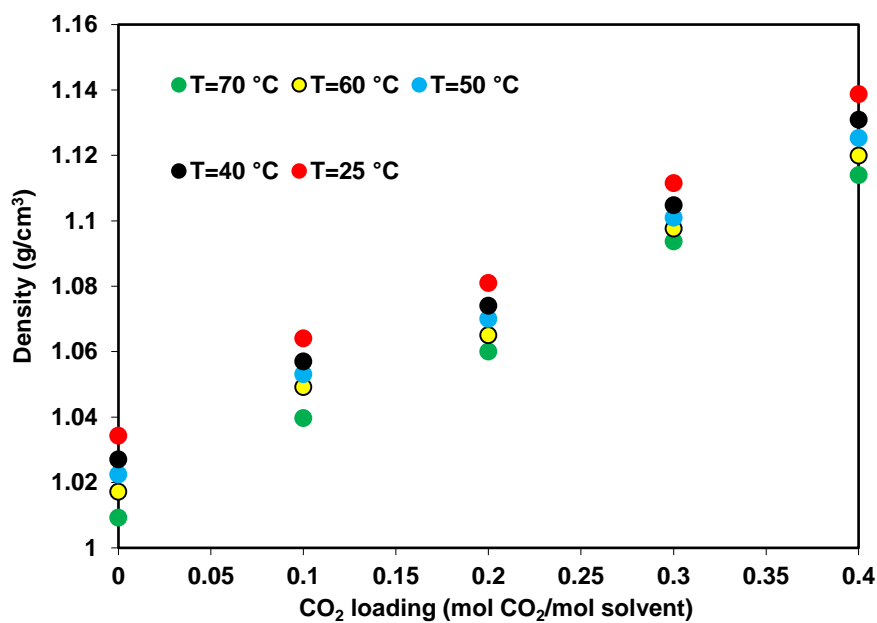


Figure 4.85 Density of unloaded and CO₂ loaded MEA + 6wt% sugar solution at different temperatures.

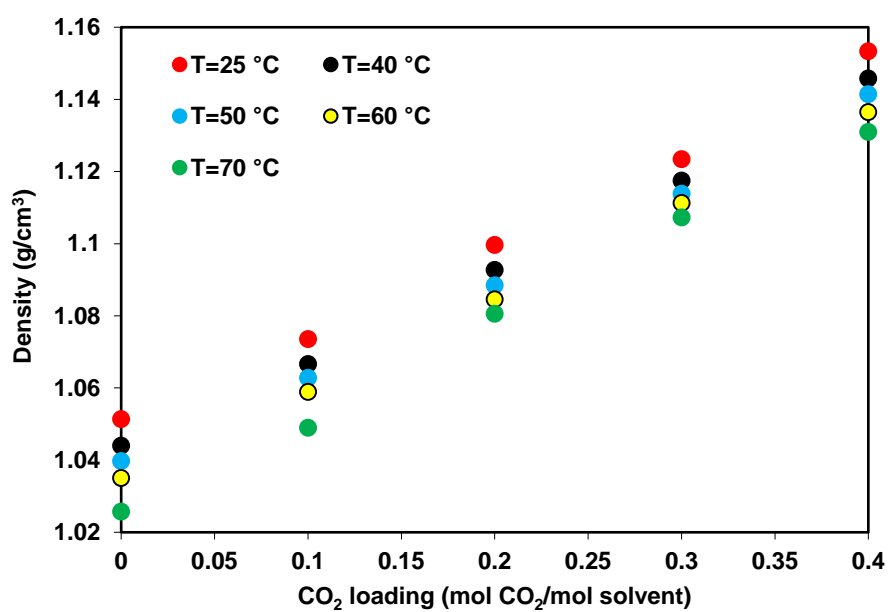


Figure 4.86 Density of unloaded and CO₂ loaded MEA + 10wt% sugar solution at different temperatures.

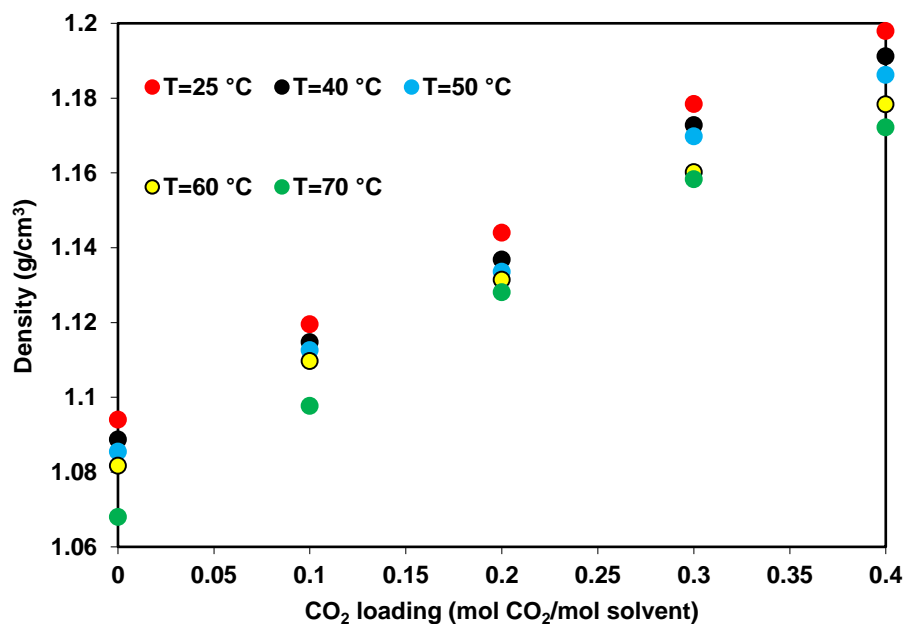


Figure 4.87 Density of unloaded and CO₂ loaded MEA + 20wt% sugar solution at different temperatures.

The effect of concentration of sugar on density of MEA + Sugar was investigated and presented in Figure 4.88 to 4.92. As seen from the results, the density of MEA blended with sugar increases when concentration of sugar increases from 3 wt% to 20 wt% at constant temperature and CO₂ loading.

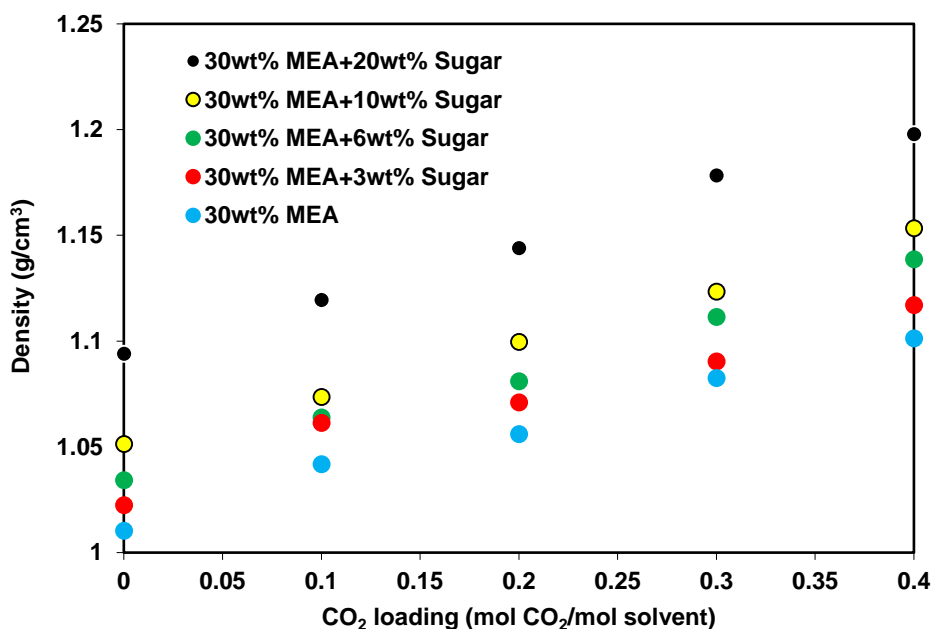


Figure 4.88 The effect of addition of sugar on density of MEA solution at 25 °C.

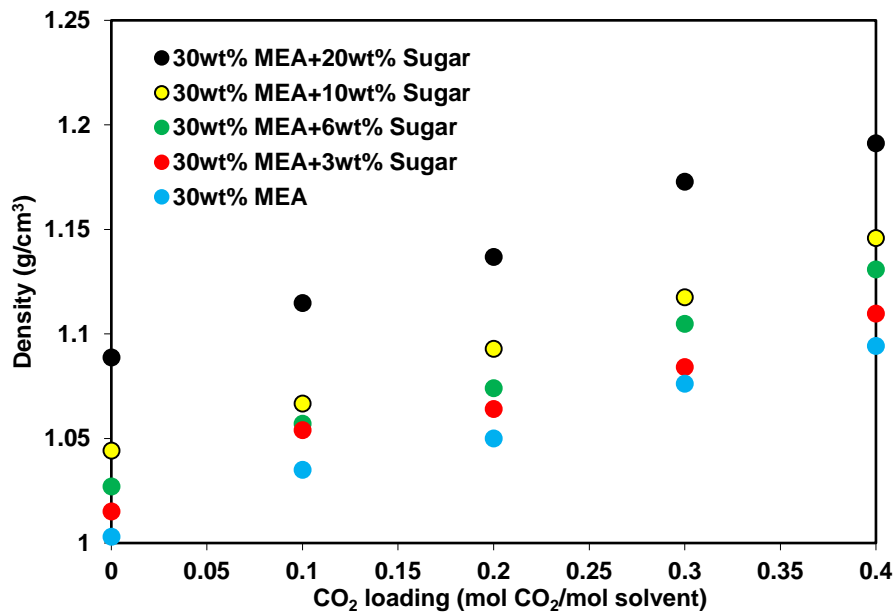


Figure 4.89 The effect of addition of sugar on density of MEA solution at 40 °C.

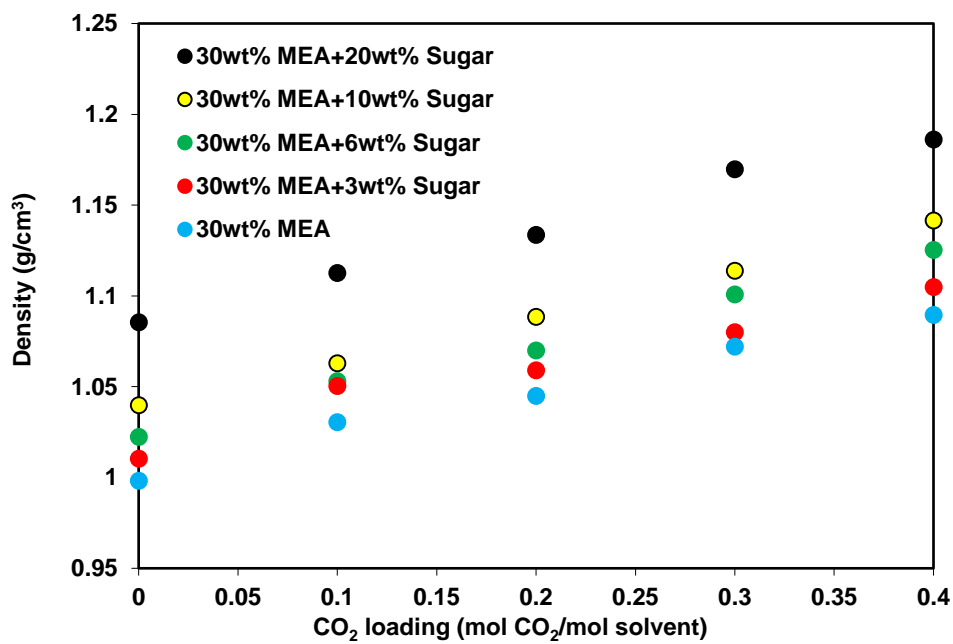


Figure 4.90 The effect of addition of sugar on density of MEA solution at 50 °C.

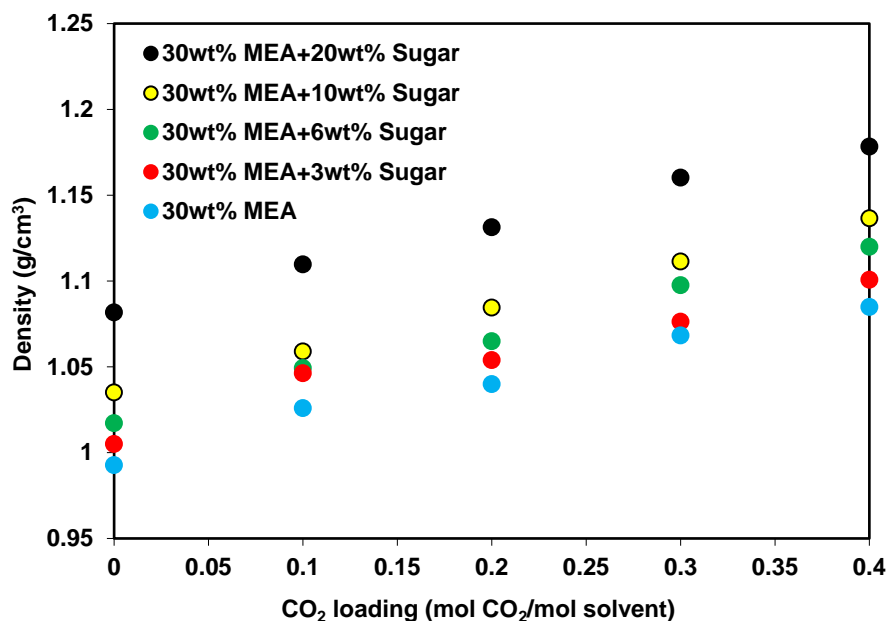


Figure 4.91 The effect of addition of sugar on density of MEA solution at 60 °C.

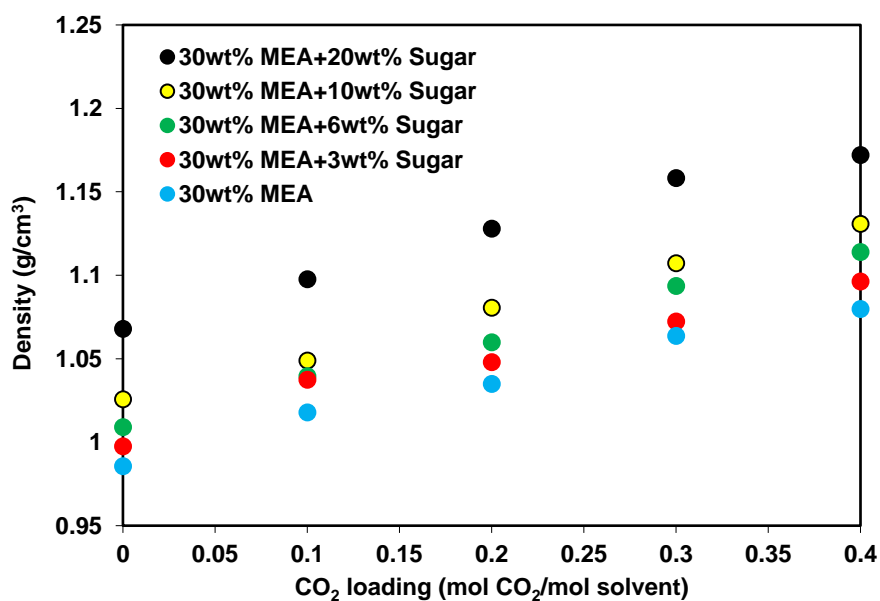


Figure 4.92 The effect of addition of sugar on density of MEA solution at 70 °C.

4.8.2. Viscosity of MEA + Sugar

The viscosity of CO₂ loaded and unloaded solutions of 30 wt% MEA, 30 wt% MEA + 3 wt% sugar, 30 wt% MEA + 6 wt% sugar, 30 wt% MEA + 10 wt% sugar and 30 wt% MEA + 20 wt% sugar was measured using a viscometer which explained in section 3.3. The viscosity data obtained in this work in the temperature range between 25 and 70 °C, and with a CO₂ loading range of 0 to 0.4 (mol CO₂/mol

solvent) was presented in Figure 4.93 to 4.97. The reported data are the average of two measurements. As can be observed from these figures, viscosity of solution increases with increasing CO₂ loading at all temperatures and decreases as temperature increases from 25 to 70 °C.

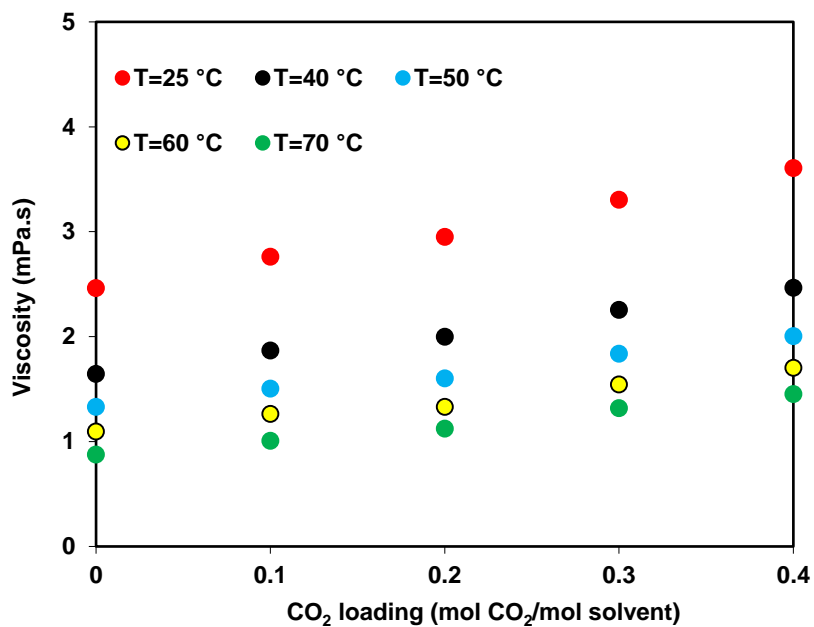


Figure 4.93 Viscosity of unloaded and CO₂ loaded MEA solution at different temperatures.

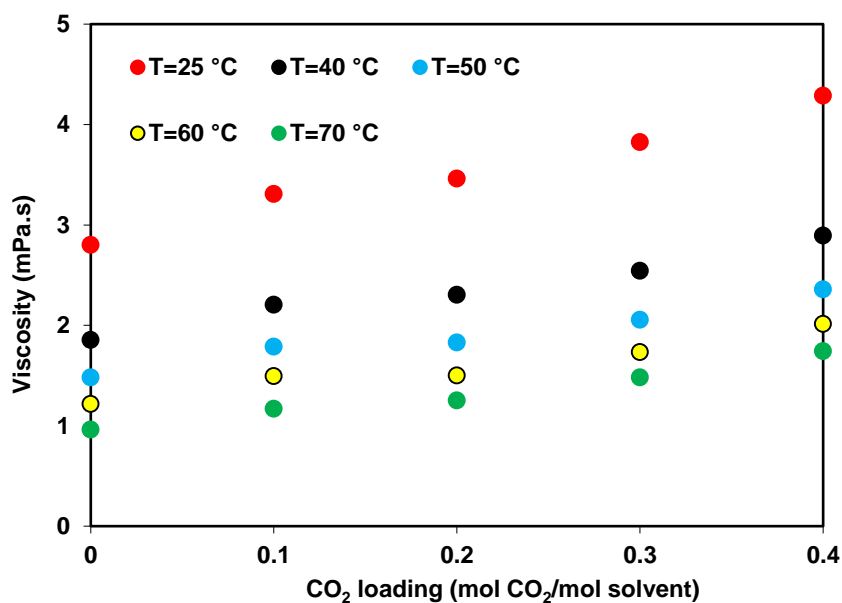


Figure 4.94 Viscosity of unloaded and CO₂ loaded MEA + 3wt% sugar solution at different temperatures.

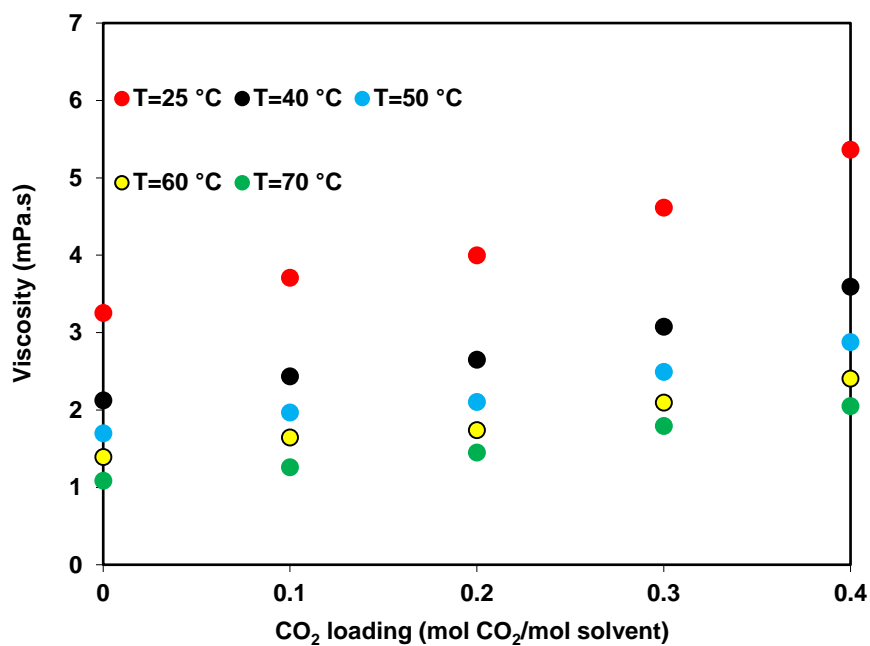


Figure 4.95 Viscosity of unloaded and CO₂ loaded MEA + 6wt% sugar solution at different temperatures.

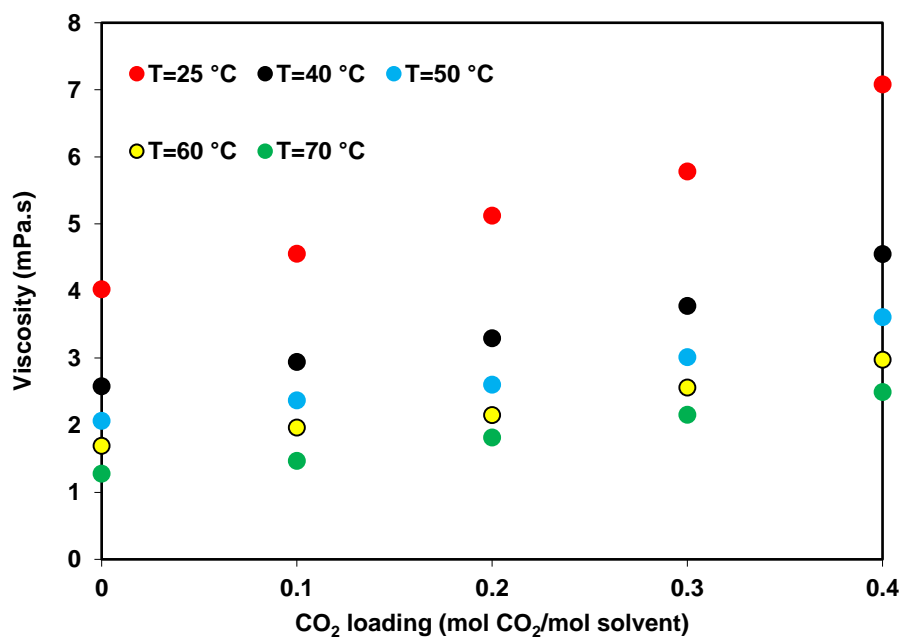


Figure 4.96 Viscosity of unloaded and CO₂ loaded MEA + 10wt% sugar solution at different temperatures.

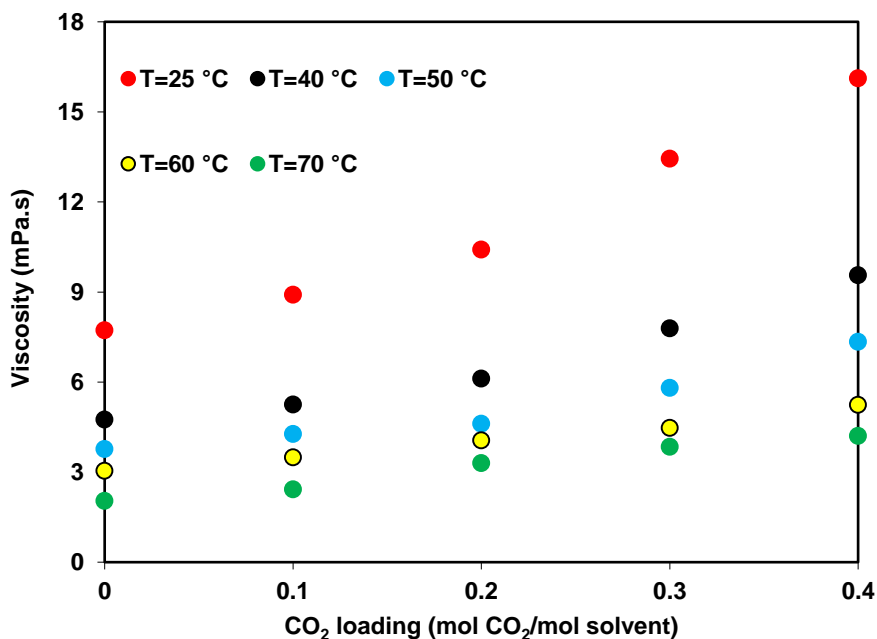


Figure 4.97 Viscosity of unloaded and CO₂ loaded MEA + 20wt% sugar solution at different temperatures.

The effect of addition of sugar on viscosity of MEA + Sugar was evaluated and the results were illustrated in Figure 4.98 to 4.102. It can be clearly seen that as expected, viscosity increases with addition of sugar.

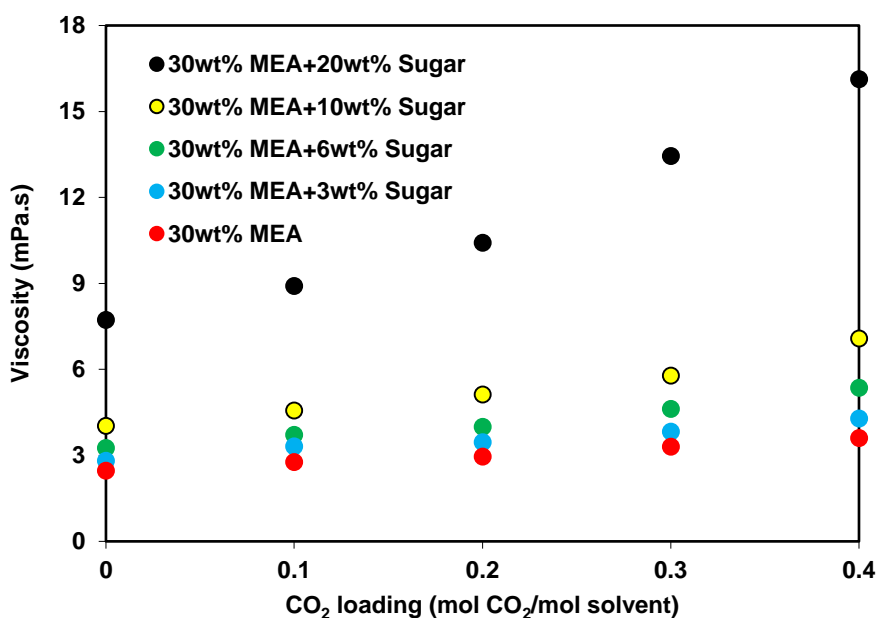


Figure 4.98 The effect of addition of sugar on viscosity of MEA solution at 25 °C.

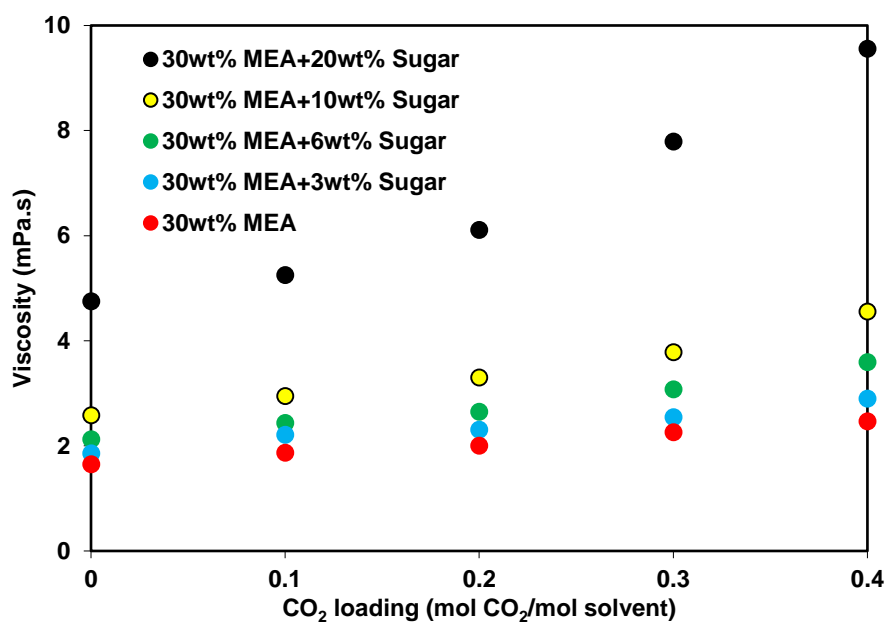


Figure 4.99 The effect of addition of sugar on viscosity of MEA solution at 40 °C.

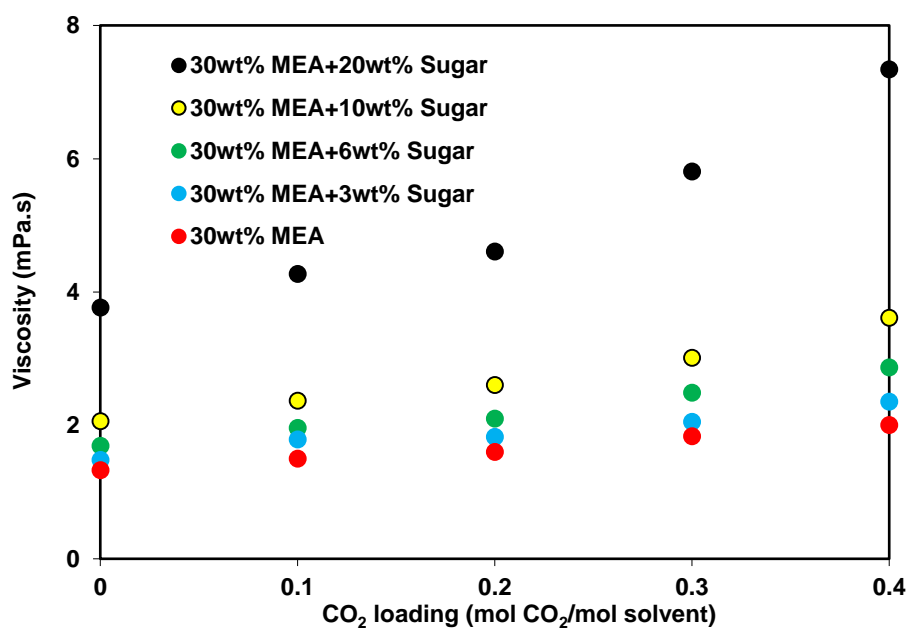


Figure 4.100 The effect of addition of sugar on viscosity of MEA solution at 50 °C.

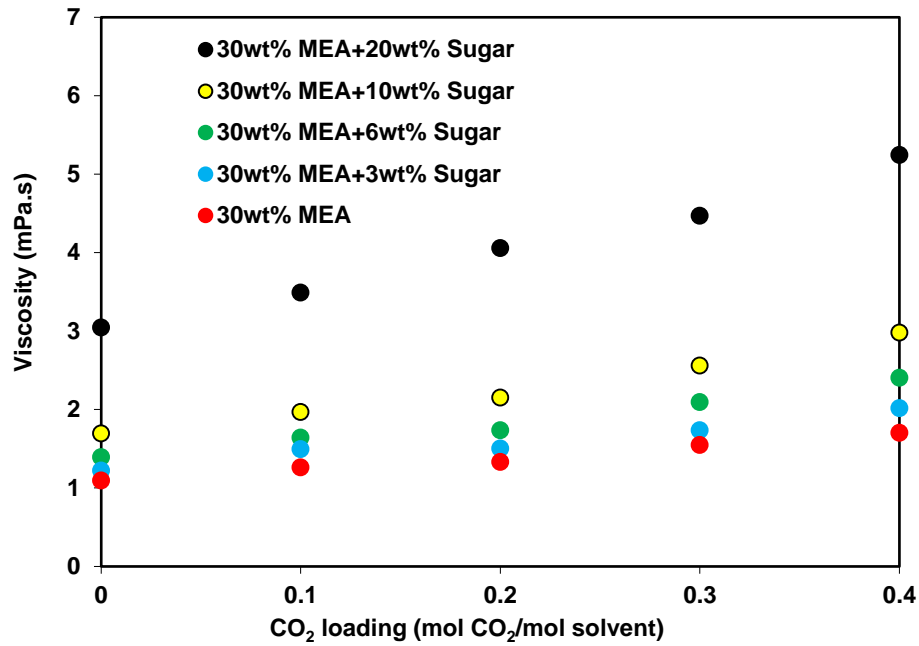


Figure 4.101 The effect of addition of sugar on viscosity of MEA solution at 60 °C.

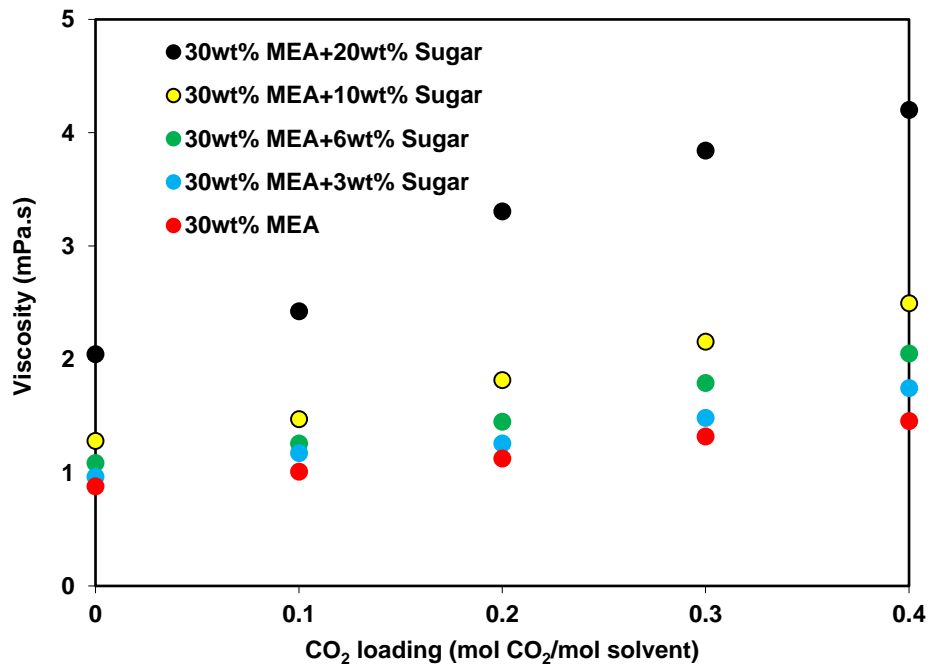


Figure 4.102 The effect of addition of sugar on viscosity of MEA solution at 70 °C.

4.8.3. Overall mass transfer coefficient of MEA + Sugar

A string of discs contactor apparatus was used in this section to measure the CO₂ absorption kinetics into an unloaded and CO₂ loaded MEA + sugar solution. The advantage of this contactor is that the absorption surface area can be varied by addition of more the disc elements in the column. However, the unknown hydrodynamics of both gas and liquid flows are the main drawback of this contactor.

A schematic diagram of the string of disc contactor used in this work was shown in Figure 4.103. The contactor which is placed in a heating chamber consists of 43 discs with a total column height of 64.5 cm. The contactor works in countercurrent mode with liquid flow from top to bottom and gas flow in the opposite direction. The temperature and pressure in inlet and outlet the liquid and gas phase were recorded by k-type thermocouples and pressure transmitter (DP cell from Druck). The inlet gas composition can be set by mass flow controllers while the outlet gas composition is recorded by using an IR analyzer.

The absorption flux of CO₂ in the solution is obtained by a mass balance over the entire system. Then, the overall mass transfer coefficient can be calculated from the ratio between the CO₂ absorption flux and the driving force as given in Eq. (118):

$$K_{OV} = \frac{N_{CO_2}}{\Delta P_{CO_2}} \quad (118)$$

Where ΔP_{CO_2} is the logarithmic mean of the CO₂ partial pressure difference between the outlet and the inlet stream.

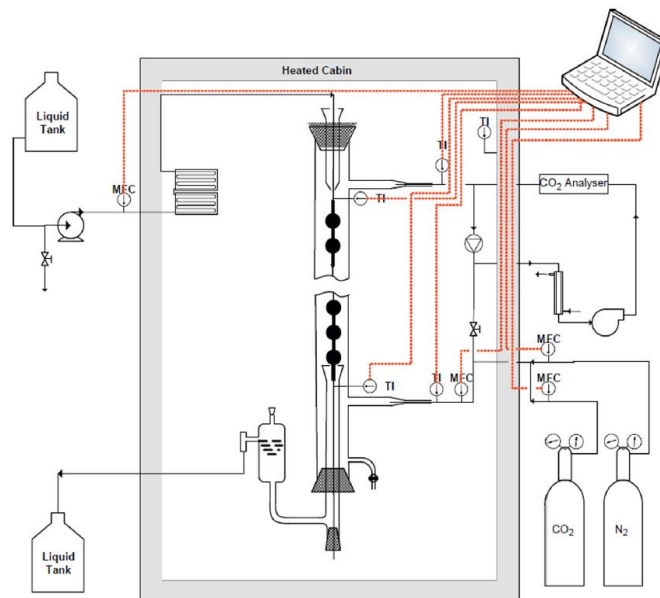


Figure 4.103 Schematic diagram of the string of discs contactor. The figure is retrieved from [194]

Before studying kinetics of CO₂ absorption in MEA + sugar, the string of discs contactor apparatus was validated by measuring the overall mass transfer coefficient into unloaded and CO₂ loaded 30 wt% MEA in the temperature range of 25-70 °C. A comparison between experimental results obtained in this work and the values of reported in the literature [125, 195, 196, 197] was given in Figure 4.104 in order to check the reliability of experimental data. It can be observed that a well accordance was found between our results and data reported in the literature.

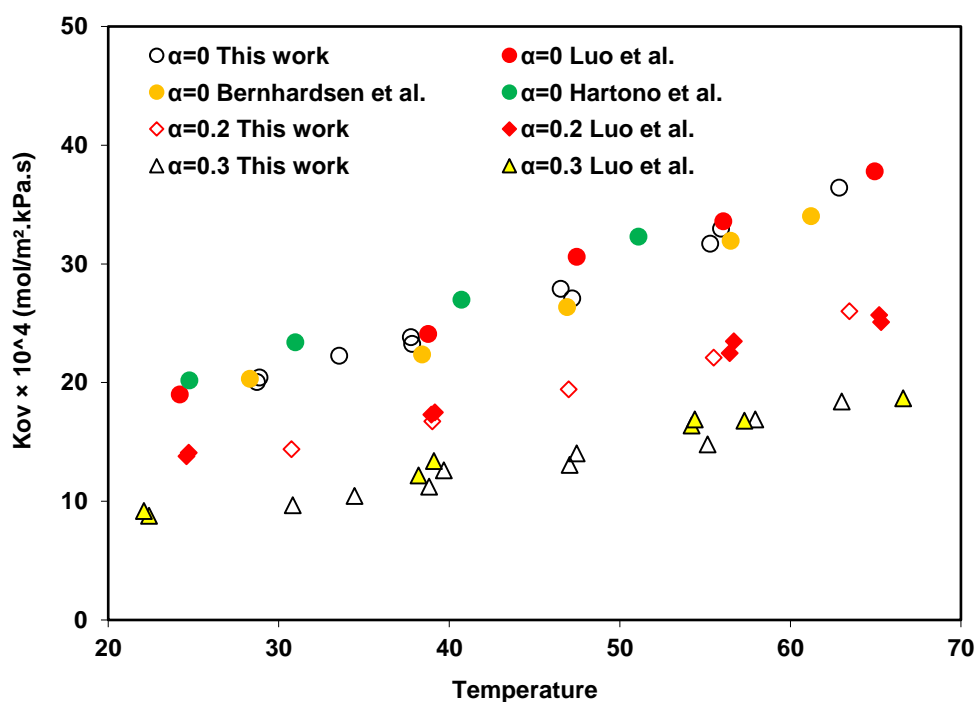


Figure 4.104 Comparison of overall mass transfer coefficient obtained in this work with literature.

Figure 4.105 to 4.109 show the effect of temperature and sugar concentration on the overall mass transfer coefficient of 30 wt% MEA + (0-20) wt% sugar. According to the results, overall mass transfer coefficient was found to be dependent of CO₂ loading, temperature and concentration. As seen from these figures, the overall mass transfer coefficient in MEA + sugar solution decreases with increasing concentration of sugar and enhanced when temperature increases from 25 to 70 °C. The higher viscosity of solution at high concentration of sugar and at lower temperature are reasons to explain this behavior.

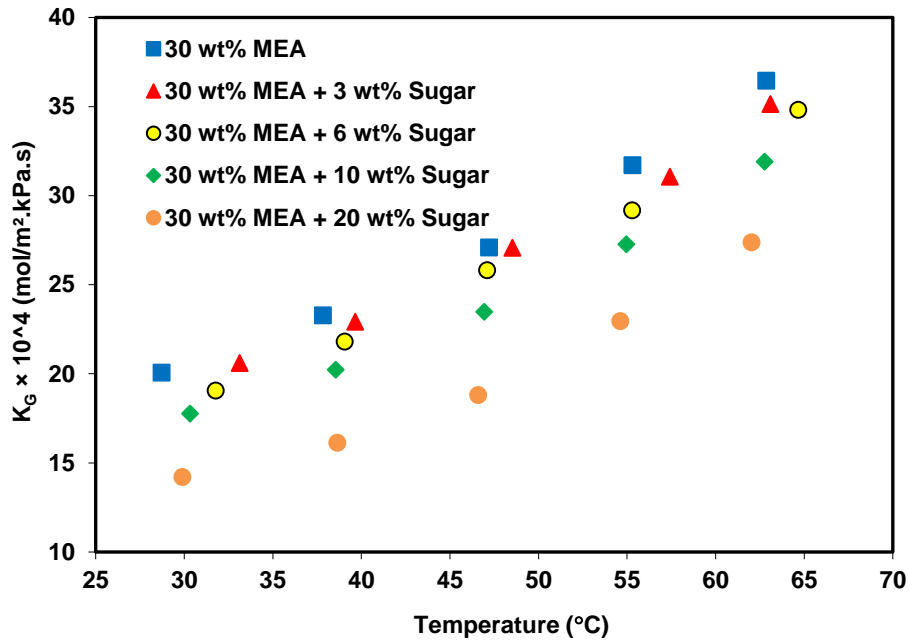


Figure 4.105 The overall mass transfer coefficient as a function of temperature at unloaded solutions.

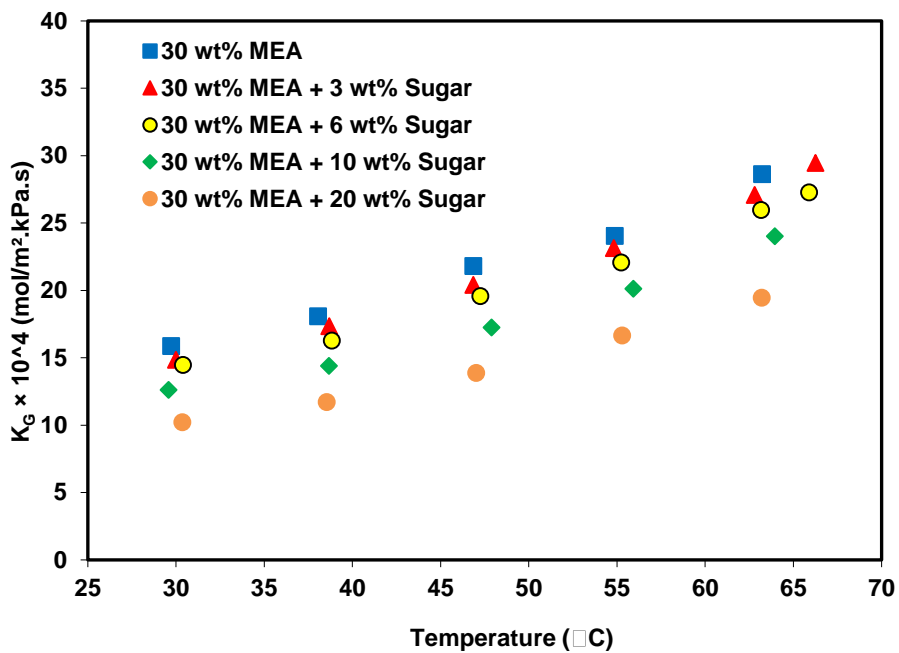


Figure 4.106 The overall mass transfer coefficient as a function of temperature at CO₂ loading of 0.1.

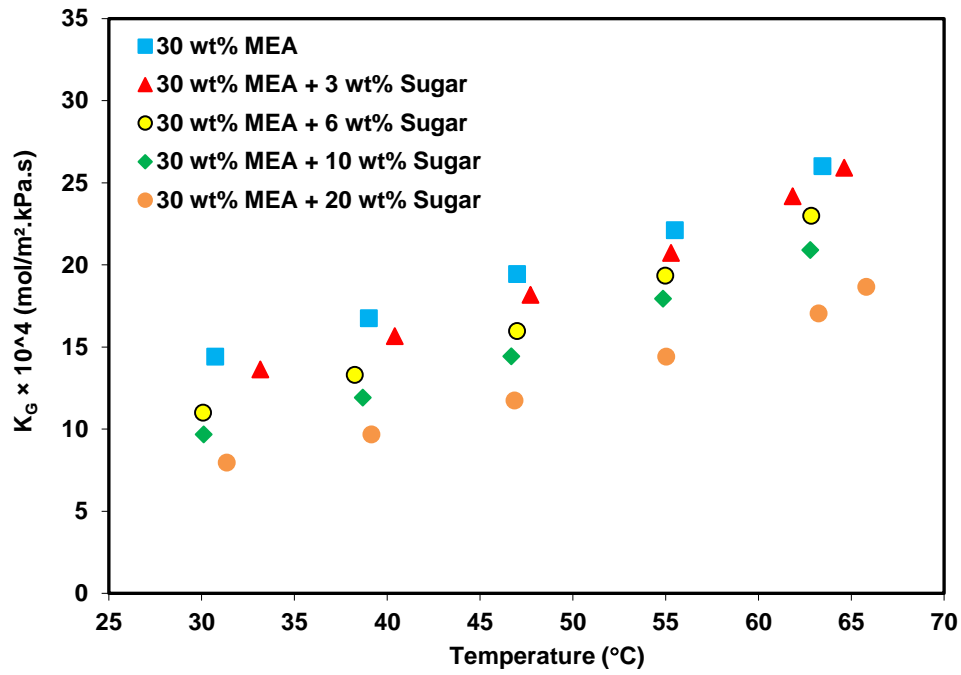


Figure 4.107 The overall mass transfer coefficient as a function of temperature at CO₂ loading of 0.2.

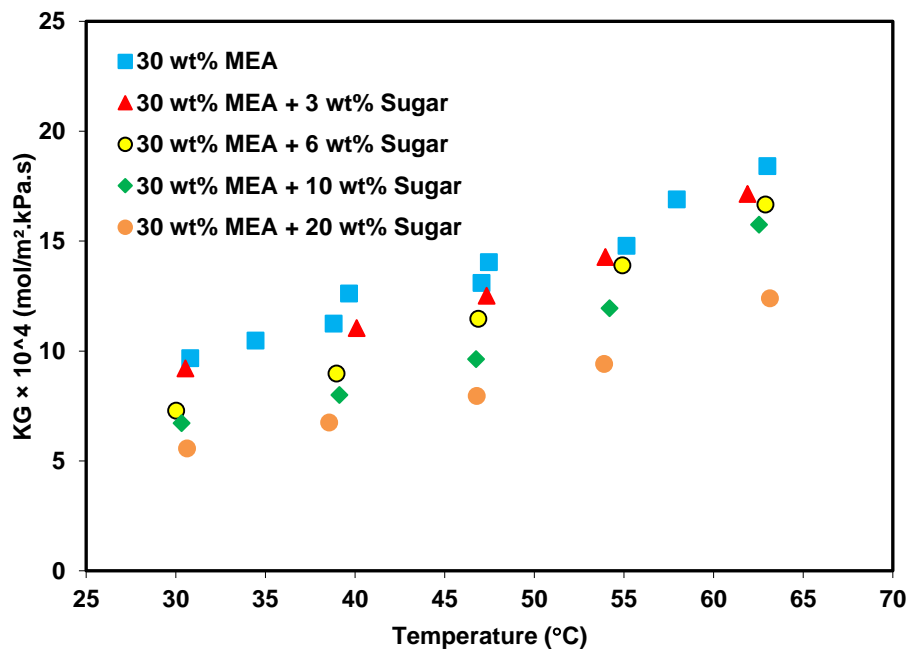


Figure 4.108 The overall mass transfer coefficient as a function of temperature at CO₂ loading of 0.3.

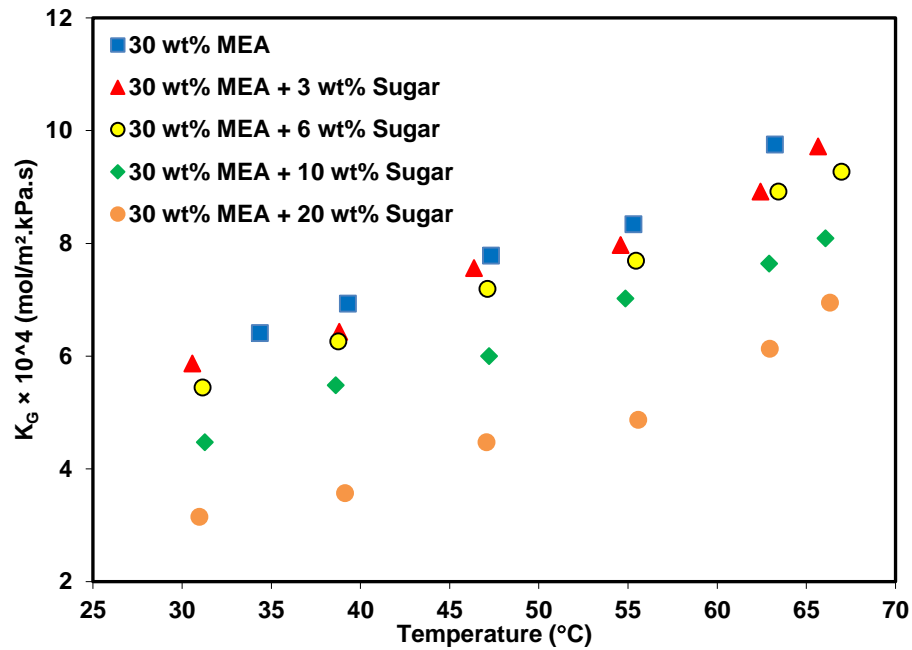


Figure 4.109 The overall mass transfer coefficient as a function of temperature at CO₂ loading of 0.4.

The overall mass transfer coefficient of CO₂ loaded and unloaded solutions of MEA and MEA blended with sugar as a function of CO₂ loading at different temperatures was plotted in Figure 4.110 to 4.114. It can be clearly seen that the mass transfer coefficient of the absorption of CO₂ in the solution decrease as CO₂ loading increases. The lower available free amine molecules (free concentration of solvent) at higher loading is the main reason for this reduction.

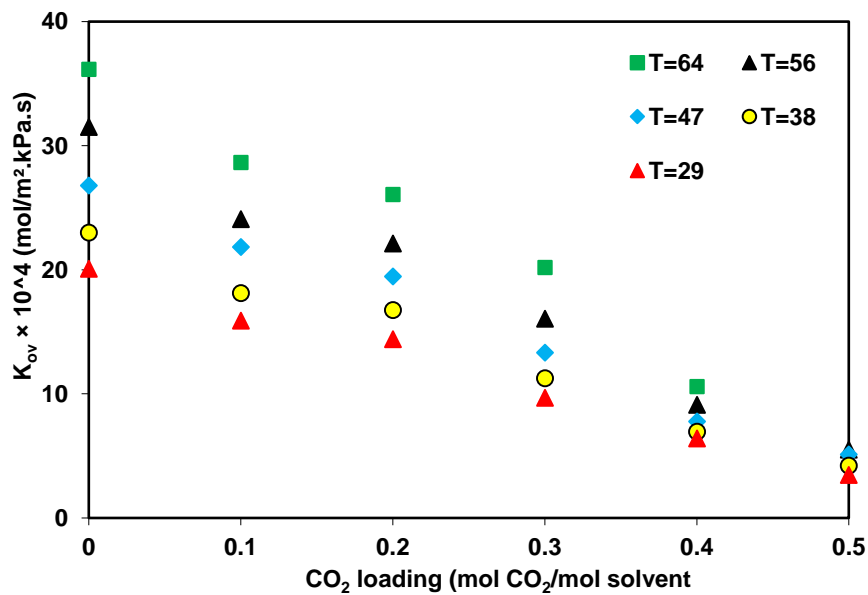


Figure 4.110 The effect of temperature and CO₂ loading on overall mass transfer coefficient of MEA.

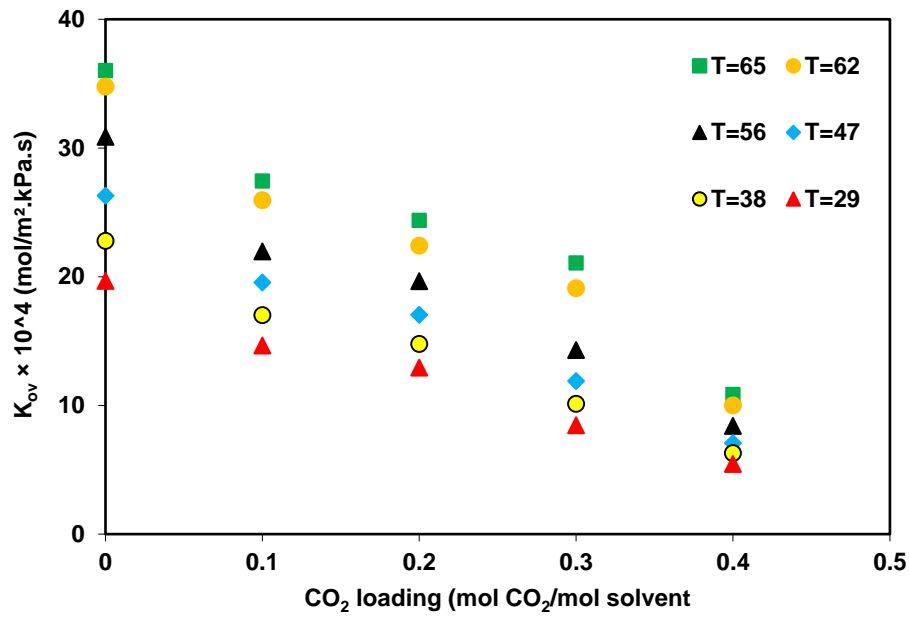


Figure 4.111 The effect of temperature and CO₂ loading on overall mass transfer coefficient of MEA+3wt% sugar.

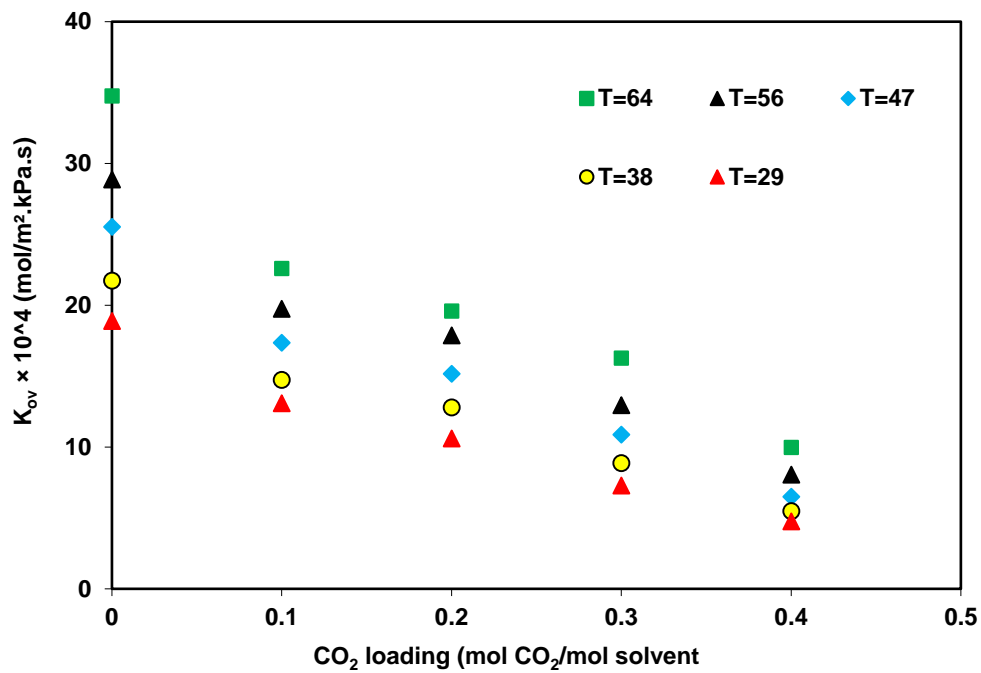


Figure 4.112 The effect of temperature and CO₂ loading on overall mass transfer coefficient of MEA+6wt% sugar.

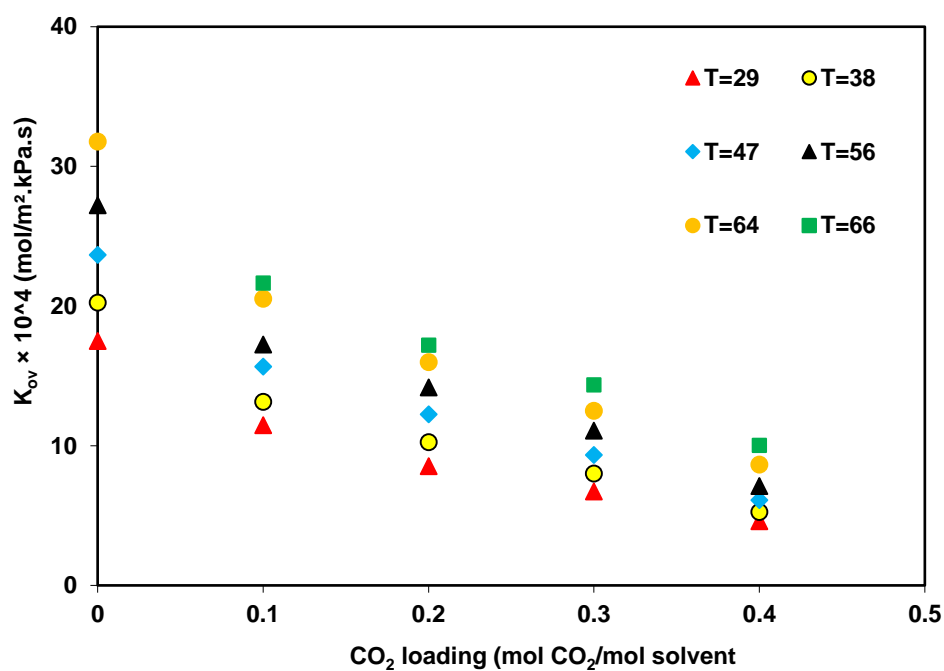


Figure 4.113 The effect of temperature and CO₂ loading on overall mass transfer coefficient of MEA+10wt% sugar.

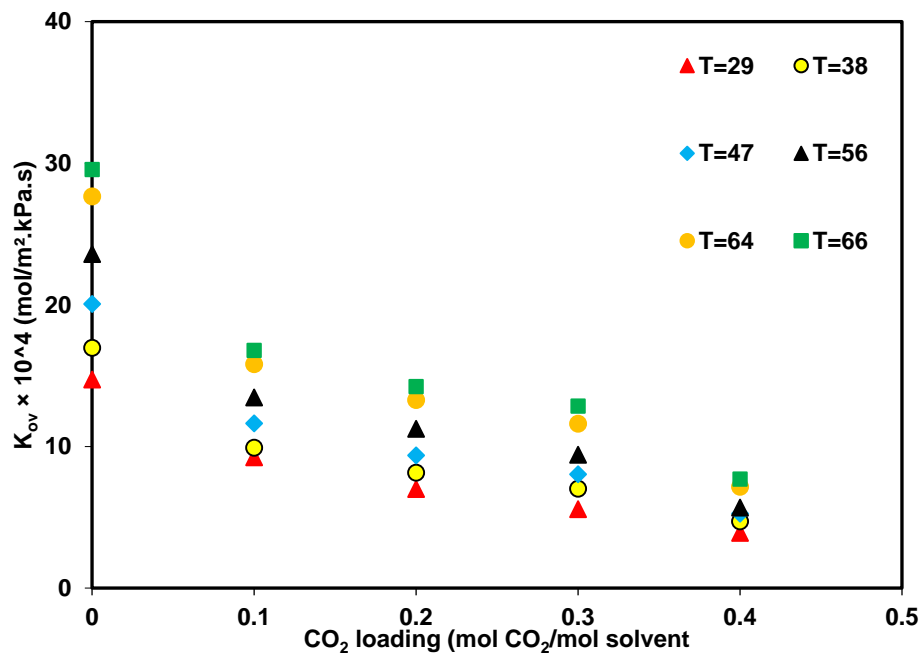


Figure 4.114 The effect of temperature and CO₂ loading on overall mass transfer coefficient of MEA+20wt% sugar.

THERMODYNAMIC MODELING OF CO₂ ABSORPTION

Thermodynamic modeling can be useful for optimization of industrial absorbers and description of the behavior of the experimental data. There are several thermodynamic models to represent loading capacity of CO₂ in amines which can be divided into three categories, including a) excess Gibbs energy models such as electrolyte-NRTL model, the Clegg-Pitzer and Austgen model, b) equation of state models (EOS) and c) empirical models like the Kent-Eisenberg model.

Among them, the Kent-Eisenberg (KE) model is one of the well-known models and is widely used in the literature because of its advantages, which include high speed of computation and low complexity. All coefficients of fugacity and activity in this model are considered to be equal to unity and the equilibrium constant (K) depends on temperature (T) as follows:

$$K = \exp \left(a_1 + \frac{a_2}{T} + \frac{a_3}{T^2} + \frac{a_4}{T^3} + \frac{a_5}{T^4} \right) \quad (119)$$

Jou et al. [198] and Posey et al. [199] developed this model and showed that equilibrium constants do not depend only on temperature but also on CO₂ loading (α) and solvent concentration (C) as follows:

$$K = \exp \left(a_1 + \frac{a_2}{T} + \frac{a_3}{T^3} + a_4 \times \alpha + \frac{a_5}{\alpha} + \frac{a_6}{\alpha^2} + a_7 \times \ln C \right) \quad (120)$$

The modified Kent-Eisenberg model was used by many researchers to predict the CO₂ absorption capacity in single and mixed amines. For example, Tong et al.[200], Fouad et al. [201], Sema et al.[202], Mondal et al. [184] and Chang et al. [203] used this model to predict the CO₂ loading capacity of AMP + PZ, TEA, DEAB, HMDA + MDEA and DETA + PZ, respectively. They showed that this model can provide a good fit between predicted and measured data.

Therefore, a modified KE model was chosen in this work to predict CO₂ loading capacity of single and blend absorbents.

5.1. Thermodynamic modeling of CO₂ absorption in MEA

The reactions between CO₂ and MEA solution can be expressed as follows:





Therefore, the equilibrium constants for CO₂ + MEA + H₂O system can be described as follows:

$$K_1 = \frac{[\text{RNH}_2] \times [\text{HCO}_3^-]}{[\text{RNHCOO}^-]} \quad (126)$$

$$K_2 = \frac{[\text{RNH}_2] \times [\text{H}^+]}{[\text{RNH}_3^+]} \quad (127)$$

$$K_3 = \frac{[\text{H}^+] \times [\text{HCO}_3^-]}{[\text{CO}_2]} \quad (128)$$

$$K_4 = [\text{H}^+] \times [\text{OH}^-] \quad (129)$$

$$K_5 = \frac{[\text{H}^+] \times [\text{CO}_3^{2-}]}{[\text{HCO}_3^-]} \quad (130)$$

In addition to the above equations, the overall material and charge balance equations are also considered:

MEA balance:

$$[\text{MEA}] = [\text{RNH}_2] + [\text{RNH}_3^+] + [\text{RNHCOO}^-] \quad (131)$$

CO₂ balance:

$$\alpha \times [\text{MEA}] = [\text{CO}_2] + [\text{HCO}_3^-] + [\text{CO}_3^{2-}] + [\text{RNHCOO}^-] \quad (132)$$

Charge balance:

$$[\text{H}^+] + [\text{RNH}_3^+] = [\text{RNHCOO}^-] + 2 \times [\text{CO}_3^{2-}] + [\text{OH}^-] + [\text{HCO}_3^-] \quad (133)$$

Henry's law relationship was used to estimate the concentration of CO₂:

$$[\text{CO}_2] = \frac{P_{\text{CO}_2}}{H_{\text{e}}} \quad (134)$$

The equilibrium constants of reactions (5-9) have been reported by many researchers and can be expressed in the form:

$$\ln K_i = a_1 + \frac{a_2}{T} + a_3 \ln T \quad (135)$$

where K_i is the equilibrium constant, T is temperature and a_{1-3} are constant coefficients. The equilibrium constants (K_1 - K_5) for reactions (5-9) were taken from the literature and given in Table 5.1.

Table 5.1 The equilibrium constants of K_1 to K_5 for Eqs. (121-125).

K_i (kmol/m^3)	a_1	a_2	a_3	Ref.
K_1	6.69425	-3090.83	0	[204]
K_2	-3.3636	-5851.11	0	[204]
K_3	235.485	-12092.1	-36.7816	[205]
K_4	140.932	-13445.9	22.4773	[205]
K_5	220.067	-12431.7	-35.4819	[205]

There are 8 unknown parameters for the CO_2 absorption in MEA solution, including $[\text{HCO}_3^-]$, $[\text{H}^+]$, $[\text{RNH}_2]$, $[\text{RNHCOO}^-]$, $[\text{RNH}_3^+]$, $[\text{CO}_3^{2-}]$, $[\text{OH}^-]$ and $[\text{CO}_2]$ which can be obtained by solving 8 algebraic equations (10-21). The combination of these nonlinear equations and their reduction to a single five-order polynomial equation for $[\text{H}^+]$ can be a suitable method for solving the mentioned equations:

$$A [\text{H}^+]^5 + B [\text{H}^+]^4 + C [\text{H}^+]^3 + D [\text{H}^+]^2 + E [\text{H}^+] + F = 0 \quad (136)$$

where:

$$A = -K_1^2 \quad (137)$$

$$B = K_1^2 \times (-K_2 - [\text{MEA}]) \quad (138)$$

$$C = K_1^2 K_4 + K_1^2 K_3 [\text{MEA}] - K_2 K_3 K_1 [\text{CO}_2] \quad (139)$$

$$D = K_1^2 K_2 K_4 + K_1^2 K_2 K_3 [\text{CO}_2] + 2K_1^2 K_5 K_3 [\text{CO}_2] - [\text{MEA}] [\text{CO}_2] K_2 K_3 K_1 \quad (140)$$

$$E = 2K_1^2 K_2 K_5 K_3 [\text{CO}_2] + K_2 K_3 K_4 K_1 [\text{CO}_2] + K_3^2 [\text{CO}_2]^2 K_1 K_2 \quad (141)$$

$$F = 2K_2 K_5 K_1 K_3^2 [\text{CO}_2]^2 \quad (142)$$

Then, CO_2 loading capacity of MEA solution can be determined using values of equilibrium constants and $[\text{H}^+]$ as given by:

$$\alpha = ([\text{CO}_2] + \left[\frac{K_5 K_3 [\text{CO}_2]}{[\text{H}^+]^2} \right] + \left[\frac{K_3 [\text{CO}_2]}{[\text{H}^+]} \right] + \left[\frac{K_2 K_3 [\text{CO}_2] M}{K_1 [\text{H}^+]^2} \right]) / [\text{MEA}] \quad (143)$$

where:

$$M = \frac{[\text{MEA}]}{N} \quad (144)$$

$$N = 1 + \frac{K_2}{[\text{H}^+]} + \frac{K_2 K_3 [\text{CO}_2]}{K_1 [\text{H}^+]^2} \quad (145)$$

Then, the modified KE model was employed to calculate the CO_2 loading capacity and concentrations of all chemical species for the MEA + CO_2 + H_2O system. The partial pressures of CO_2 was plotted against the experimental CO_2 loading capacity data of solutions of 2.5 M and 5 M MEA in Figure 5.1. The modeling curves for prediction of CO_2 loading of MEA solution were also demonstrated in this figure. The experimental CO_2 loading data reported by Lee et al. [140] and Shen et al. [43] for 2.5 and 5 M MEA

at 313.15 K were used for validation of the model. A comparison between experimental CO₂ loading data and the modeling results obtained in this work shows that the model is able to describe experimental data well and provides good prediction results.

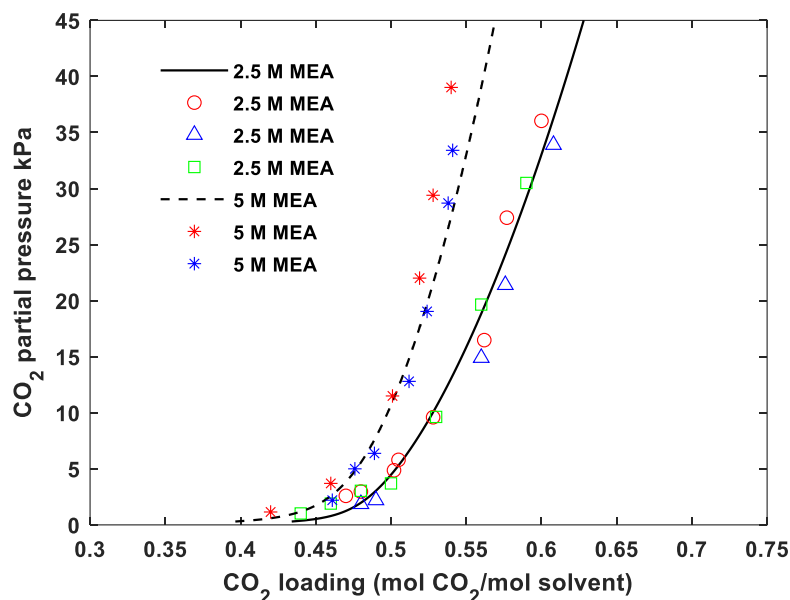


Figure 5.1 Experimental CO₂ loading of MEA solution compared with model predicted results.

The values of concentration of the different species in the 2.5 M MEA solution at 313.2 K were also obtained using the proposed model. The concentration profile versus CO₂ loading was plotted in Figure 5.2. It was found that the concentration of carbamate (RNHCOO⁻) reach to a maximum value at CO₂ loading 0.5, where MEA is nearly completely consumed. As CO₂ loading increases ($\alpha > 0.5$), carbamate concentration decreases while concentrations of HCO₃⁻ and RNH₃⁺ increase. In addition, at all value of CO₂ loading, concentration of carbonate (CO₃²⁻) is negligible.

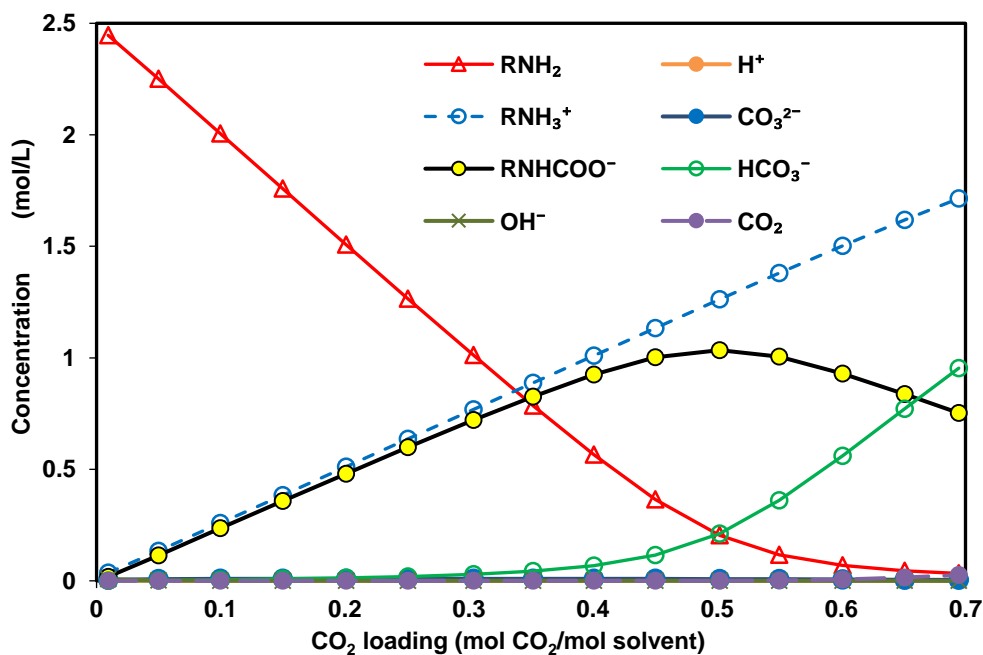


Figure 5.2 The profile of concentration of liquid-phase species in 2.5 M MEA solution.

5.2. Thermodynamic modeling of CO₂ absorption in K-Lys

The following liquid phase reactions are taking place when CO₂ is absorbed into K-Lys solution:



The equilibrium constants of reactions 146-152 are given as follows:

$$K_1 = \frac{[LysH] \times [HCO_3^-]}{[R_2LysR_1COO^-]} \quad (153)$$

$$K_2 = \frac{[LysH] \times [H^+]}{[LysH^+]} \quad (154)$$

$$K_3 = \frac{[Lys^-] \times [HCO_3^-]}{[^-OOCR_2LysR_1]} \quad (155)$$

$$K_4 = \frac{[\text{Lys}^-] \times [\text{H}^+]}{[\text{LysH}]} \quad (156)$$

$$K_5 = \frac{[\text{H}^+] \times [\text{HCO}_3^-]}{[\text{CO}_2]} \quad (157)$$

$$K_6 = [\text{H}^+] \times [\text{OH}^-] \quad (158)$$

$$K_7 = \frac{[\text{H}^+] \times [\text{CO}_3^{2-}]}{[\text{HCO}_3^-]} \quad (159)$$

Three balance equations are also necessary to be considered in order to calculate concentration of all chemical species.

Lys balance:

$$[\text{Lys}]_o = [\text{LysH}] + [\text{LysH}^+] + [\text{Lys}^-] + [\text{R}_2\text{LysR}_1\text{COO}^-] + [{}^-\text{OOCR}_2\text{LysR}_1] \quad (160)$$

CO₂ balance:

$$\alpha \times ([\text{Lys}]_o) = [\text{CO}_2] + [\text{HCO}_3^-] + [\text{CO}_3^{2-}] + [{}^-\text{OOCR}_2\text{LysR}_1] + [\text{R}_2\text{LysR}_1\text{COO}^-] \quad (161)$$

Charge balance:

$$[\text{H}^+] + [\text{K}^+] + [\text{LysH}^+] = [\text{R}_2\text{LysR}_1\text{COO}^-] + 2[{}^-\text{OOCR}_2\text{LysR}_1] + [\text{Lys}^-] + 2[\text{CO}_3^{2-}] + [\text{OH}^-] + [\text{HCO}_3^-] \quad (162)$$

The $[\text{HCO}_3^-]$, $[\text{H}^+]$, $[\text{CO}_3^{2-}]$, $[\text{OH}^-]$, $[\text{LysH}^+]$, $[\text{LysH}]$, $[\text{Lys}^-]$, $[\text{R}_2\text{LysR}_1\text{COO}^-]$, $[{}^-\text{OOCR}_2\text{LysR}_1]$, K_1 , K_2 , K_3 and K_4 are unknown parameters in this system. The values of concentration of liquid phase species and the equilibrium constants can be determined by solving above equations and using MATLAB software. The similar to previous section, the combination of nonlinear equations and their reduction to a single seven-order polynomial equation for $[\text{H}^+]$ was used to solve the mentioned equations:

$$A [\text{H}^+]^7 + B [\text{H}^+]^6 + C [\text{H}^+]^5 + D [\text{H}^+]^4 + E [\text{H}^+]^3 + F [\text{H}^+]^2 + G [\text{H}^+] + R = 0 \quad (163)$$

Where:

$$A = -K_1^2 K_3^2 \quad (164)$$

$$B = K_1^2 K_3^2 (-2[\text{LYS}] - K_2) \quad (165)$$

$$C = K_1 K_3^2 ((-[\text{LYS}]K_1 K_2) + (K_1 K_6) + ([\text{CO}_2]K_5 K_1) - (K_1 K_2 K_4) - ([\text{CO}_2]K_5 K_2)) \quad (166)$$

$$D = K_1^2 K_3^2 (K_2^2 K_6 K_4 [\text{LYS}] + [\text{CO}_2]K_2 K_5 + 2[\text{CO}_2]K_5 K_7 - [\text{LYS}]K_2 K_4) - K_1 K_3 [\text{CO}_2]K_1 K_5 \quad (167)$$

$$E = K_1^2 K_3^2 ((2K_2 K_5 K_7 [\text{CO}_2]) + (K_2 K_4 K_6) + ([\text{CO}_2]K_2 K_4 K_5)) + K_1 K_3 ((2K_1 K_2 K_5 K_6) + (K_2 K_5 [\text{CO}_2]) + (K_2 K_3 [\text{CO}_2]) - (K_1 K_2 K_4 K_5 [\text{LYS}])) \quad (168)$$

$$F = K_1 K_3 (2[\text{CO}_2]K_5 K_7 K_1 K_2 K_3 + 2K_2 K_3 K_5^2 + K_1 K_2 K_4 K_5 [\text{CO}_2] + K_1 K_2 K_4 [\text{CO}_2]^2) \quad (169)$$

$$G = 2K_7 K_4 K_2 K_3 K_5^2 [\text{CO}_2]^2 \quad (170)$$

$$R = 0 \quad (171)$$

Then, CO₂ loading capacity of K-Lys solution can be obtained using values of equilibrium constants and [H⁺] as given by:

$$\alpha = ([\text{CO}_2] + \frac{K_5 K_7 [\text{CO}_2]}{[\text{H}^+]^2} + \frac{K_5 [\text{CO}_2]}{[\text{H}^+]}) + \frac{[\text{LYS}]}{N} \left(\frac{K_2 K_5 [\text{CO}_2]}{K_1 [\text{H}^+]^2} + \frac{K_2 K_4 K_5 [\text{CO}_2]}{K_3 [\text{H}^+]^3} \right) / [\text{LYS}] \quad (172)$$

where:

$$N = 1 + \frac{K_2}{[\text{H}^+]} + \frac{K_2 K_4}{[\text{H}^+]^2} + \frac{K_4 K_2 K_5 \text{CO}_2}{[\text{H}^+]^3} + \frac{K_2 K_5 \text{CO}_2}{[\text{H}^+]^2} \quad (173)$$

The equilibrium constants (K₁ to K₄) obtained in this work at 313.15 K for K-Lys solution were listed in Table. 5.2. The values of K₁, K₃ and K₄ were assumed to be only dependent on temperature while K₂ was considered to be dependent on temperature and concentration of K-Lys.

Table 5.2 The equilibrium constants of K₁ to K₄ for Eqs. (153-156).

K _i (kmol/m ³)	0.5 M K-Lys	1 M K-Lys	1.5 M K-Lys	2.5 M K-Lys
K ₁	0.169	0.169	0.169	0.169
K ₂	17.87 × 10 ⁻¹⁰	12.67 × 10 ⁻¹⁰	10.24 × 10 ⁻¹⁰	10.08 × 10 ⁻¹⁰
K ₃	0.412	0.412	0.412	0.412
K ₄	1.38 × 10 ⁻¹¹	1.38 × 10 ⁻¹¹	1.38 × 10 ⁻¹¹	1.38 × 10 ⁻¹¹

The CO₂ loading capacity of 0.5 to 2.5 M K-Lys solution at 313.15 K was measured by Shen et al. [42]. A comparison between experimental CO₂ loading data from them and the modeling results obtained in this work was carried out in Figure 5.3. The calculated values from the model are presented as curved lines. It was found that the model presented here successfully represents experimental CO₂ loading data.

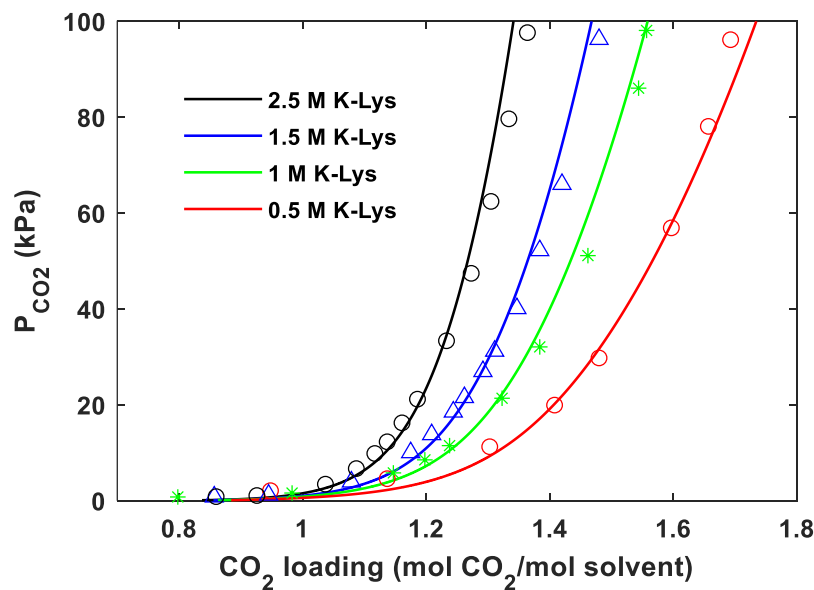


Figure 5.3 Comparison of experimental CO₂ loading capacity of K-Lys and model results.

In addition, performance of model in order to predict of CO₂ loading capacity was compared with model presented by Shen et al. [42]. The experimental CO₂ loading data, the model results from Shen model and the model results obtained in this work were plotted in Figure 5.4. The model results obtained in this work and from were shown as a dashed line and solid line, respectively. It can be clearly seen that the model presented in this work provided much better predicted results than the Shen model.

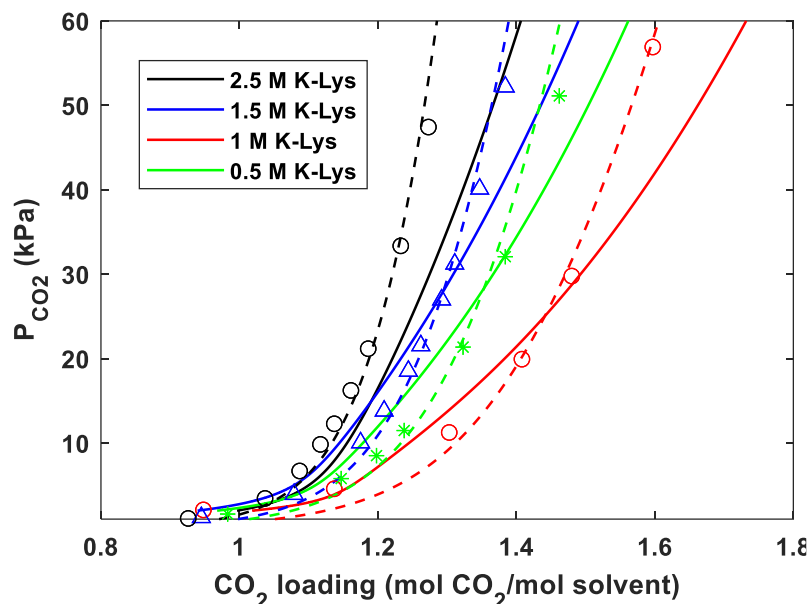


Figure 5.4 Comparison of modeling results between presented model in this work and model presented by in the literature.

The concentration of the liquid phase species in 0.5 M K-Lys and 2.5 M K-Lys solutions at 313.2 K were also obtained using the proposed model and presented in Figure 5.5 and 5.6, respectively, to provide a better understanding of the absorption process.

As seen from these figures, at CO₂ loading up to 0.7, values of both of carbamates, carbonate and LysH increases while Lys⁻ decreases. In addition, as the CO₂ loading increases, the LysH gradually decrease and the corresponding protonated lysine increases. The bicarbonate can be considered as one of main species formed at high CO₂ loading due to the hydrolysis of carbamates.

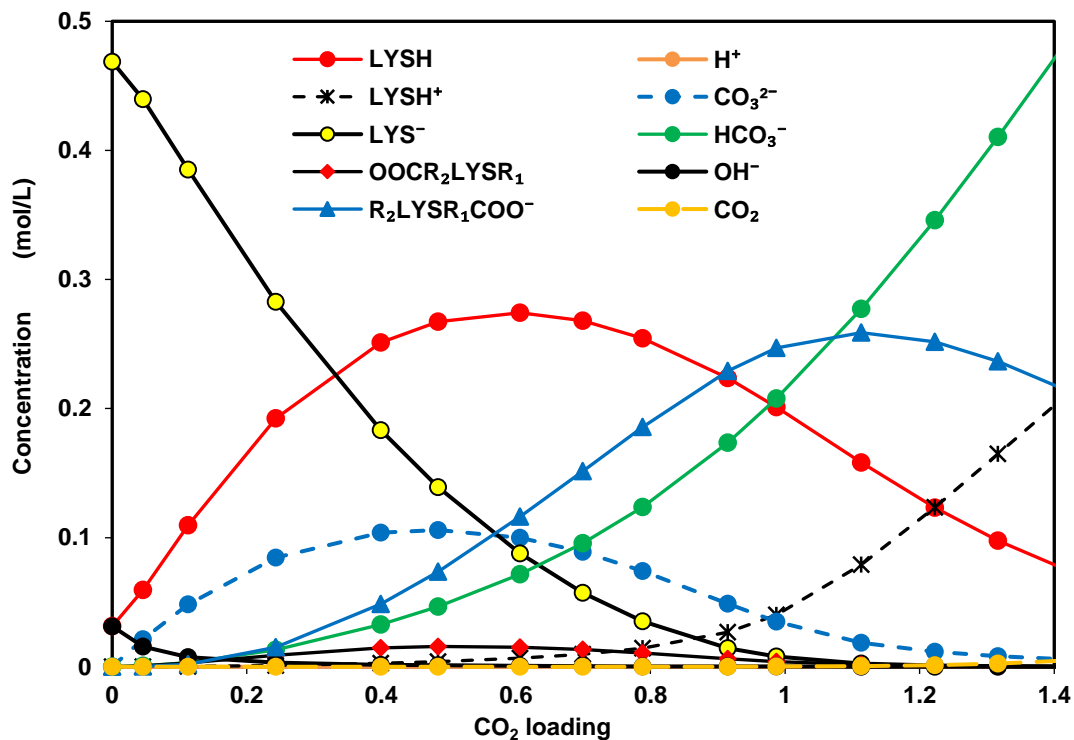


Figure 5.5 The profile of concentration of liquid-phase species in 0.5 M K-Lys solution.

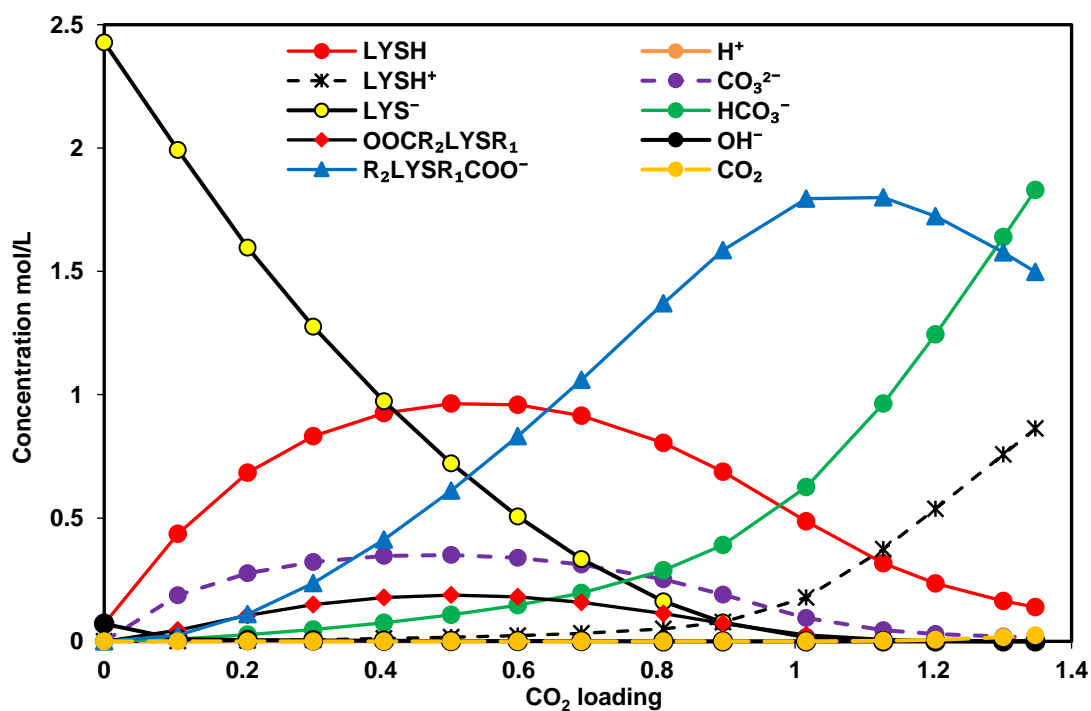


Figure 5.6 The profile of concentration of liquid-phase species in 2.5 M K-Lys solution.

In addition, the pH values of CO₂ loaded solution can be estimated by the equilibrium model and using Eq. (174):

$$\text{pH} = -\log[\text{H}^+] \quad (174)$$

The estimated pH of CO₂ loaded aqueous 2.5 M K-Lys solution as a function of CO₂ loading at 313.15 K was shown in Figure 5.7. It can be clearly seen that the pH of solution decreases with enhancing the CO₂ loading due to an increase in acidity of solution.

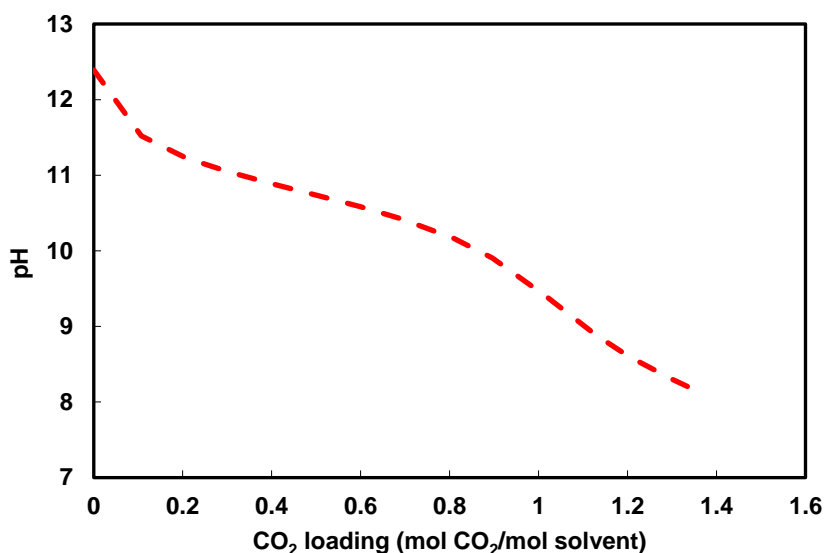
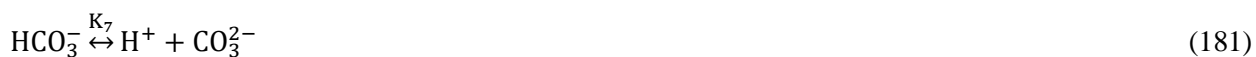


Figure 5.7 Model predicted pH of 2.5 M K-Lys solution at 313.15 K.

5.3. Thermodynamic modeling of CO₂ absorption in MEA+K-Lys

The reactions between CO₂ and MEA + K-Lys solution can be expressed as follows:



Therefore, the equilibrium constants for CO₂ + MEA + K-Lys system can be described as follows:

$$K_1 = \frac{[\text{LysH}] \times [\text{HCO}_3^-]}{[\text{R}_2\text{LysR}_1\text{COO}^-]} \quad (182)$$

$$K_2 = \frac{[\text{LysH}][\text{H}^+]}{[\text{LysH}^+]} \quad (183)$$

$$K_3 = \frac{[\text{RNH}_2][\text{HCO}_3^-]}{[\text{RNHCOO}^-]} \quad (184)$$

$$K_4 = \frac{[\text{RNH}_2][\text{H}^+]}{[\text{RNH}_3^+]} \quad (185)$$

$$K_5 = \frac{[\text{H}^+][\text{HCO}_3^-]}{[\text{CO}_2]} \quad (186)$$

$$K_6 = [\text{H}^+] \times [\text{OH}^-] \quad (187)$$

$$K_7 = \frac{[\text{H}^+][\text{CO}_3^{2-}]}{[\text{HCO}_3^-]} \quad (188)$$

In addition to the above equations, the overall material and charge balance equations are also considered:

MEA balance:

$$[\text{MEA}] = [\text{RNH}_2] + [\text{RNH}_3^+] + [\text{RNHCOO}^-] \quad (189)$$

Lys balance:

$$[\text{Lys}] = [\text{LysH}] + [\text{LysH}^+] + [\text{R}_2\text{LysR}_1\text{COO}^-] \quad (190)$$

CO₂ balance:

$$\alpha \times ([\text{MEA}] + [\text{Lys}]) = [\text{CO}_2] + [\text{HCO}_3^-] + [\text{CO}_3^{2-}] + [\text{RNHCOO}^-] + [\text{R}_2\text{LysR}_1\text{COO}^-] \quad (191)$$

Charge balance:

$$[\text{H}^+] + [\text{K}^+] + [\text{LysH}^+] + [\text{RNH}_3^+] = [\text{R}_2\text{LysR}_1\text{COO}^-] + [\text{RNHCOO}^-] + 2 \times [\text{CO}_3^{2-}] + [\text{OH}^-] + [\text{HCO}_3^-] \quad (192)$$

As mentioned in the previous section, a modified KE model was applied to model the experimental CO₂ loading data obtained in this study. The concentrations of all chemical species and values of equilibrium constants for all chemical reactions are required. There are 12 unknown parameters for the MEA + K-Lys system, including $[\text{LysH}]$, $[\text{HCO}_3^-]$, $[\text{R}_2\text{LysR}_1\text{COO}^-]$, $[\text{H}^+]$, $[\text{LysH}^+]$, $[\text{RNH}_2]$, $[\text{RNHCOO}^-]$, $[\text{RNH}_3^+]$, $[\text{CO}_3^{2-}]$, $[\text{OH}^-]$, K_1 and K_2 , which can be obtained by solving 12 algebraic equations. The single seven-order polynomial equation for $[\text{H}^+]$ concentration was obtained from combination of nonlinear equations as follows:

$$A [\text{H}^+]^7 + B [\text{H}^+]^6 + C [\text{H}^+]^5 + D [\text{H}^+]^4 + E [\text{H}^+]^3 + F [\text{H}^+]^2 + G [\text{H}^+] + M = 0 \quad (193)$$

where:

$$A = -K_3K_1 \quad (194)$$

$$B = K_3K_1(-K_2 - K_4 - 2C_2 - C_1) \quad (195)$$

$$C = K_5C_1(-K_1K_4 - K_2K_3 + K_1K_3) + K_1K_3(-C_1K_2 - 2C_2K_4 - C_2K_2 - K_2K_4 + K_6) \quad (196)$$

$$D = K_5C_2(-C_1K_2K_3 - C_2K_1K_4 - C_2K_2K_3 - K_2K_3K_4 - K_1K_2K_4 + K_7K_1K_3 + C_1K_1K_4 + C_2K_2K_3 + K_1K_2K_3 + K_1K_3K_4) + K_3K_1(-C_2K_4K_5 + K_2K_6 + K_4K_6 - C_2K_4K_2) \quad (197)$$

$$E = K_5^2 C_2^3 (-K_2 K_4 + K_2 K_3 + K_1 K_4) + K_5 C_1 (-C_2 K_1 K_2 K_4 + K_1 K_2 K_3 K_4 + K_1 K_4 K_6 + C_1 K_1 K_2 K_4 + 2K_7 K_1 K_2 K_3 + 2K_7 K_1 K_3 K_4 + K_6 K_2 K_3) \quad (198)$$

$$F = (K_5 C_2)^2 \times (K_2 K_3 K_4 + K_1 K_2 K_4 + K_7 K_1 K_4 + C_1 K_2 K_4 + K_7 K_2 K_3) + (K_5 C_2) \times (K_2 K_3 K_4 + K_1 K_2 K_4 + K_1 K_2 K_3 K_7) \quad (199)$$

$$G = (K_5 C_3)^2 \times (K_7 K_1 K_4 + K_7 K_2 K_3 + K_2 K_4 K_6 + K_5 K_2 C_2) \quad (200)$$

$$M = K_7 K_2 K_4 K_5^3 C_3^3 \quad (201)$$

Therefore, equilibrium constants K_1 and K_2 at different operating conditions, including pressure, CO₂ loading (α), temperature (T) and concentration (C) are determined. There are several correlations in the literature to fit the equilibrium constants of K_1 and K_2 with other variables. In this work, the modified form of the KE model was used to correlate K_1 and K_2 as follows:

$$K_i = \exp \left(a_1 + \frac{a_2}{T} + \frac{a_3}{T^3} + a_4 \times \alpha + \frac{a_5}{\alpha} + \frac{a_6}{\alpha^2} + a_7 \times \ln C \right) \quad (202)$$

The values of a_1 - a_7 are obtained by applying the least-squares fit to the experimental CO₂ loading of MEA + K-Lys solution. Then, CO₂ loading capacity of MEA + K-Lys can be predicted using values of equilibrium constants and $[H^+]$ as given by:

$$\alpha = \left(\frac{P_{CO_2}}{H_{CO_2}} \times \left(1 + \frac{K_5}{[H^+]} + \left(\frac{K_5 K_7}{[H^+]} \right) + \left(\frac{K_4 K_5 \frac{P_{CO_2}}{H_{CO_2}} C_2}{K_3 K_4 [H^+] + K_5 [H^+] + K_4 K_5 \frac{P_{CO_2}}{H_{CO_2}}} \right) \right) + \frac{K_2 K_5 \frac{P_{CO_2}}{H_{CO_2}} C_1}{K_1 K_2 [H^+] + K_1 [H^+]^2 + K_2 K_5 \frac{P_{CO_2}}{H_{CO_2}}} \right) / (C_1 C_2) \quad (203)$$

The values of carbamate hydrolysis constant (K_1) and amino acid deprotonation constant (K_2), which were calculated from the equilibrium model are summarized in Table 5.3.

Table 5.3 Model parameters fitted in Eq. (120) for the equilibrium constants K_1 and K_2 .

K_i (kmol/m ³)	a_1	a_2	a_3	a_4	a_5	a_6	a_7
K_1	-852.16	31075.2	089.42	43.26	86.32	-26.04	-0.35
K_2	2577.4	-118926	-327.17	-58.05	-110.1	27.53	0.18

The experimental CO₂ loading capacity of 2 M MEA + (0.2-0.5) M K-Lys solution as well as the modeling results were plotted in Figure 5.8(a-d). It was found that the model is able to describe experimental data well and provides good prediction results.

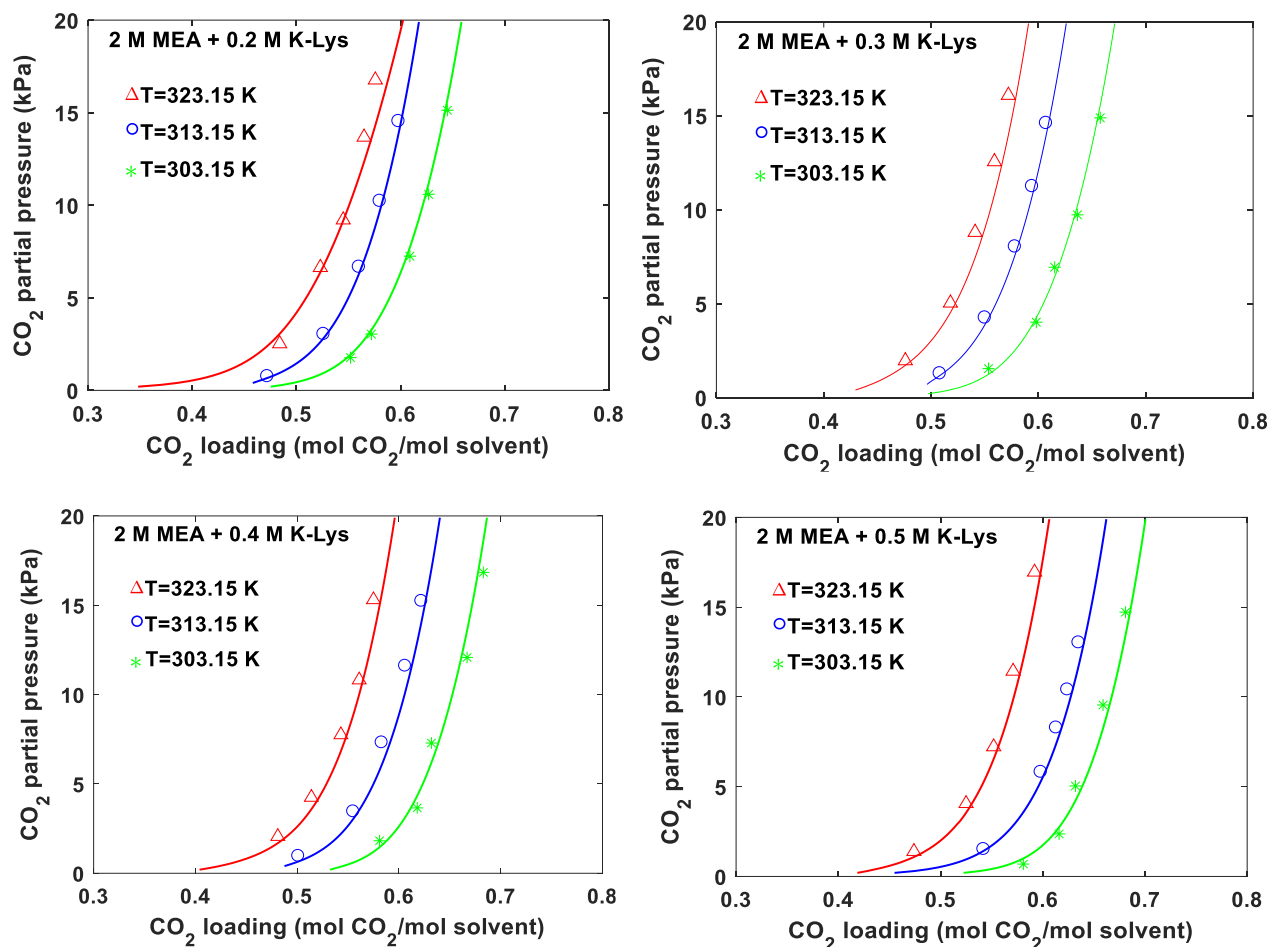


Figure 5.8 Comparison of experimental CO_2 loading capacity of 2 M MEA + (0.2-0.5) M K-Lys and model results at different temperatures.

The profile liquid-phase species for 2 M MEA + 0.5 M K-Lys as a function of CO_2 loading was presented in Figure 5.9. According to this figure, the concentration of MEA decreased rapidly while the concentration of K-Lys decreased slowly with loading. The formed carbamate from reaction of MEA and CO_2 increases until CO_2 loading 0.6 and then decreases with increasing CO_2 loading due to the carbamate hydrolysis reaction.

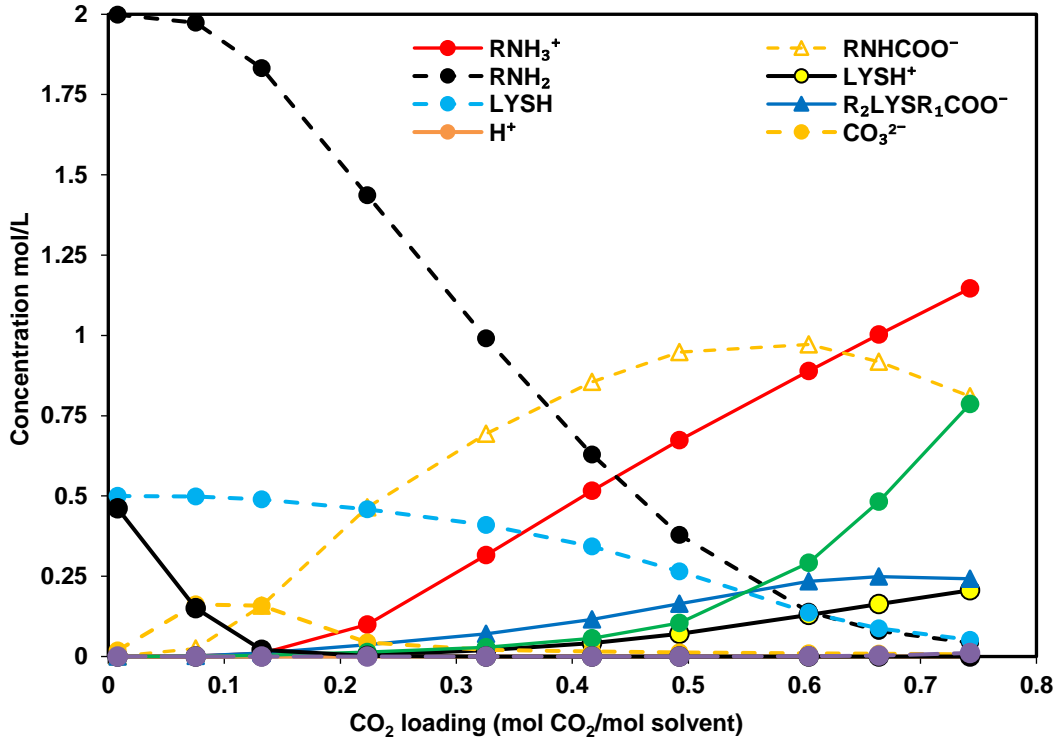
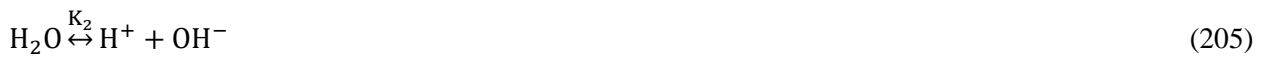


Figure 5.9 The profile of concentration of liquid-phase species in 2 M MEA + 0.5 M K-Lys solution.

5.4. Thermodynamic modeling of CO₂ absorption in MDEA + PZ

The thermodynamic model was applied to predict CO₂ loading capacity into MDEA solution promoted by piperazine (PZ). The following liquid phase reactions are taking place when CO₂ is absorbed into MDEA + PZ solution:



The equilibrium constants and balance equations are given as follows:

$$K_1 = \frac{[H^+][HCO_3^-]}{[CO_2]} \quad (212)$$

$$K_2 = [H^+] \times [OH^-] \quad (213)$$

$$K_3 = \frac{[H^+][CO_3^{2-}]}{[HCO_3^-]} \quad (214)$$

$$K_4 = \frac{[PZ][H^+]}{[PZH^+]} \quad (215)$$

$$K_5 = \frac{[H^+][PZCOO^-]}{[PZ][CO_2]} \quad (216)$$

$$K_6 = \frac{[H^+][PZCOO^-]}{[H^+PZCOO^-]} \quad (217)$$

$$K_7 = \frac{[H^+][PZCOO_2^-]}{[PZCOO^-][CO_2]} \quad (218)$$

$$K_8 = \frac{[MDEA] \times [H^+]}{[MDEAH^+]} \quad (219)$$

MDEA balance:

$$[MDEA]_o = [MDEA] + [MDEAH^+] \quad (220)$$

PZ balance:

$$[PZ]_o = [PZ] + [PZH^+] + [PZCOO^-] + [PZCOO_2^-] + [H^+PZCOO^-] \quad (221)$$

CO₂ balance:

$$\alpha \times ([MDEA]_o + [PZ]_o) = [CO_2] + [HCO_3^-] + [CO_3^{2-}] + [PZCOO^-] + 2[PZCOO_2^-] + [H^+PZCOO^-] \quad (222)$$

Charge balance:

$$[H^+] + [PZH^+] + [MDEAH^+] = [PZCOO^-] + 2[PZCOO_2^-] + 2[CO_3^{2-}] + [OH^-] + [HCO_3^-] \quad (223)$$

The equilibrium constants (K_1 - K_8) for Eqs. (212-219) were taken from the literature. The same method as explained in previous section was used here to determine the concentration of liquid phase species, including $[HCO_3^-]$, $[H^+]$, $[CO_2]$, $[PZ]$, $[PZH^+]$, $[PZCOO^-]$, $[PZCOO_2^-]$, $[H^+PZCOO^-]$, $[MDEA]$, $[MDEAH^+]$, $[CO_3^{2-}]$ and $[OH^-]$.

The profiles of concentration of liquid-phase species for MDEA, PZ and MDEA + PZ solutions against CO₂ loading were given in Figure 5.10 to 5.12. It can be seen that at low CO₂ loading, the protonated MDEA and bicarbonate are the main species which present in the solution. This can be explained by the fact that MDEA does not react with CO₂ and does not produce carbamate.

Piperazine concentration decreases rapidly with increasing in CO₂ loading because of reaction with CO₂ and formation of piperazine carbamate and protonated piperazine carbamate. Therefore, piperazine carbamate and protonated piperazine increase at low CO₂ loading and reach a maximum concentration

and then as CO₂ loading increases, they get converted to piperazine di-carbamate and protonated piperazine carbamate which leads to their reduction. Therefore, concentration of piperazine di-carbamate and protonated PZ carbamate enhanced at high CO₂ loading.

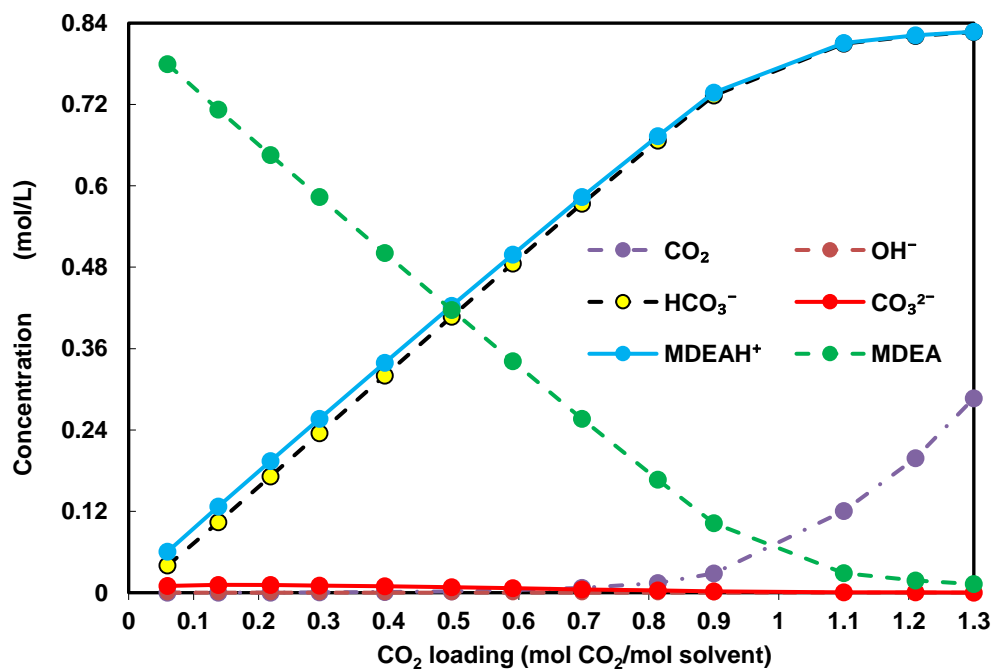


Figure 5.10 The profile of concentration of liquid-phase species in 0.84 M MDEA solution.

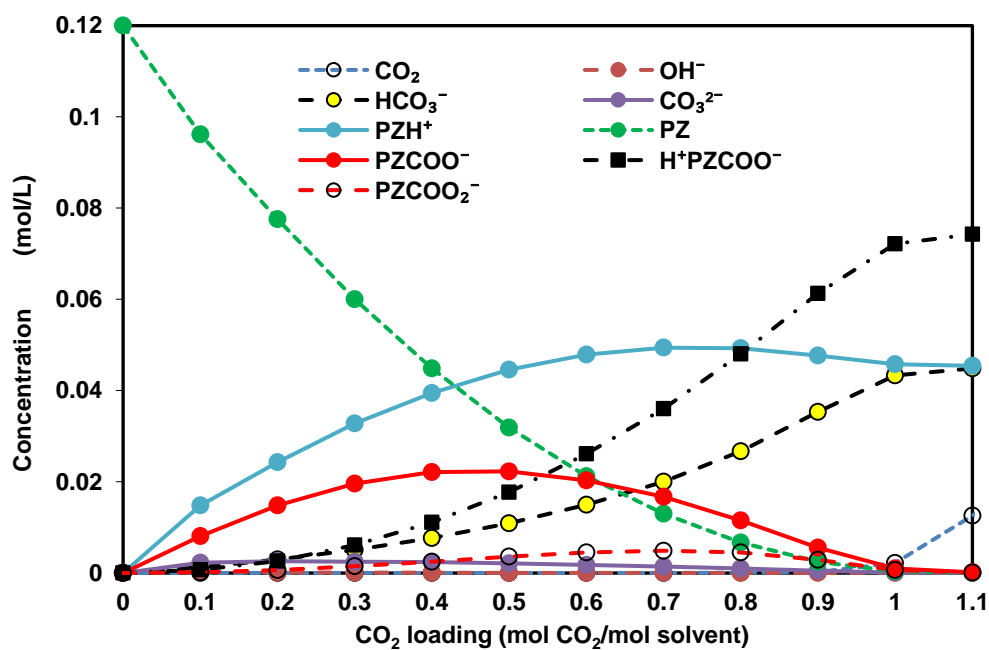


Figure 5.11 The profile of concentration of liquid-phase species in 0.12 M PZ solution.

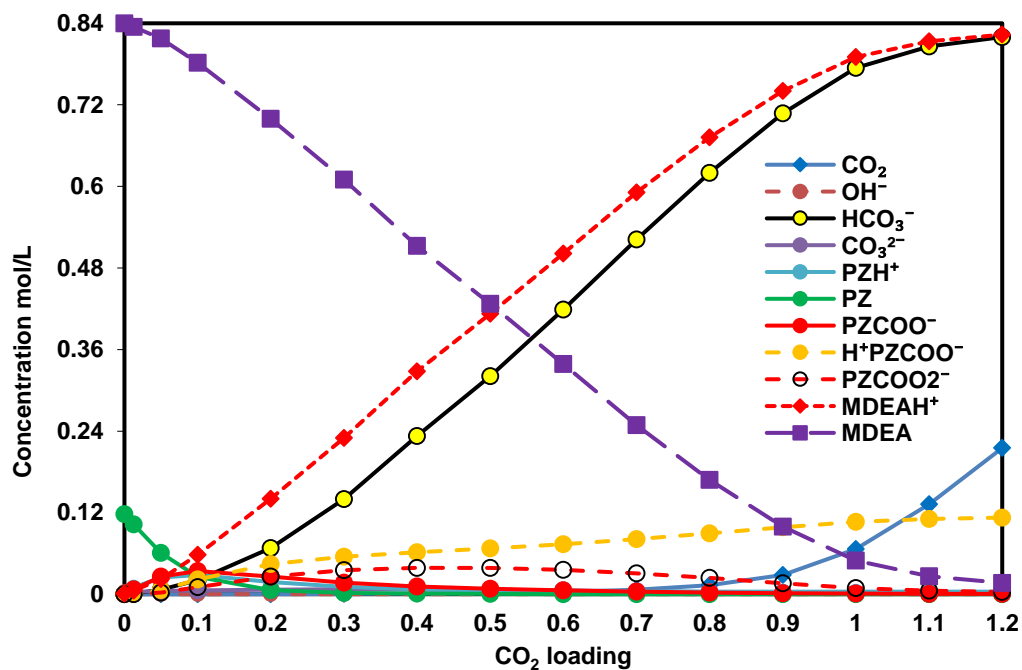


Figure 5.12 The profile of concentration of liquid-phase species in 0.84 M MDEA + 0.12 M PZ solution.

CONCLUSION AND RECOMMENDATION FOR FURTHER WORK

Post-combustion CO₂ capture using amine based chemical absorption is one of the main technologies to mitigate CO₂ emission into atmosphere. Although this technology has been widely deployed on a large scale across several industries for CO₂ absorption, but technical and operational improvements are still required to reduce the capital costs. Optimization of process, utilization of alternative process configurations and development of new chemical solvents can be considered as several activities which can reduce capital and operating cost of CO₂ absorption process. Since the efficiency and the overall cost of the process are directly affected by the solvent, the selection and development of novel solvents play a critical role in this process. Therefore, in this work, a comprehensive theoretical and experimental investigation on CO₂ absorption performance in different chemical solvents was performed. The absorption characterization of CO₂ in single and blended solutions was measured and discussed in details.

Based on the obtained results, key finding of the current study can be summarized as follow:

a. Density and viscosity

The density and viscosity of unloaded and CO₂ loaded chemical solvents were measured. It was revealed that both density and viscosity enhance as solvent concentration increases, and decrease as temperature increases. According to the results, density and viscosity of solvents increased when CO₂ loading of solution increases.

b. pH

The pH of solvent before and after CO₂ absorption was measured. It was found that pH of solution at decreases with the increase in CO₂ loading due to an increase in acidity of solution. In addition, the results showed that the pH decreases when temperature increases. This can be explained by the fact that [H⁺] concentration increases (due to more ionization) at higher temperatures which leads to reducing the pH.

c. Toxicity

It was found that amino acids present the least toxicity which make them attractive from point of view of environmental friendly, and therefore could be considered as an environmentally relatively acceptable absorbent. Among the all of amino acids studied in this work serine and sarcosine indicated the lowest toxicity. The conventional amines such as MEA and PZ exhibited the highest toxicity. Inorganic solvents such as TSP and K₂CO₃ also showed less toxicity when compared to conventional amines.

d. Corrosion rate

The corrosion rate of aqueous TSP solution blended with 10 different amines was measured. It was observed that TSP + TETA and TSP + PZ solutions have the highest corrosion rate, while TSP + MDEA and TSP + AMP show the lowest corrosion rate among all the additives tested, although all of them have weaker corrosion than MEA. Furthermore, the experimental results indicated that the corrosion rate using a TSP + amino acid salt solutions is less than those using the TSP + cyclic amines.

e. Heat of CO₂ absorption

According to the results, an increase in CO₂ loading led to a decrease in heat of absorption. At higher loading capacity, the physical absorption dominates, and bicarbonate forms that lead to a reduction in heat of CO₂ absorption. The experimental results also showed that K₂CO₃ promoted by AEEA gives a higher value of absorption heat over the entire CO₂ solubility in comparison with K₂CO₃ + K-Ala and K₂CO₃ + K-Ser. Furthermore, a mixture of K₂CO₃ with K-Ala indicated the lowest heat of absorption and can be a favorable candidate for CO₂ capture. It was also found that a blend of K₂CO₃ with amine additives has a lower heat of CO₂ absorption in comparison with pure MEA, which means less energy is needed for CO₂ regeneration in the stripper column and makes them a right choice from the heat of absorption point of view. The CO₂ absorption heat in K-Lys blended with MEA and MDEA was also determined. The calculated absorption heat in solutions of MEA + K-Lys and MDEA + K-Lys was found to be much lower than MEA with an absorption heat of 84.3 kJ/mol.

f. Mass transfer coefficient

A good understanding and prediction of the mass transfer in viscous solutions is important for proper solvent selection and process design. Therefore, the overall mass transfer coefficient of viscous MEA was measured using a string of discs contactor. According to the results, the overall mass transfer coefficient was found to be dependent on CO₂ loading, temperature, and concentration. The results indicated that the overall mass transfer coefficient in viscous MEA solution decreases with increasing viscosity and is enhanced when temperature increases from 25 to 70 °C. In addition, the overall mass transfer coefficient of absorption of CO₂ in the solution decreases as CO₂ loading increases. The lower available free amine molecules at higher loading is the main reason for this reduction.

g. CO₂ loading capacity

The stirred cell reactor was used to measure CO₂ loading capacity of single and blend solutions. It was found that K-Lys, PZ, TETA, and 2MPZ have a positive effect on the CO₂ loading of pure TSP, while the additive impact of AEEA, K-Sar, MDEA, K-Gly, K-Pro, and AMP is negative. Moreover, the results indicated that a blend of the TSP and amine additives has a better CO₂ loading as compared to MEA. In addition, the CO₂ loading of K₂CO₃ promoted by 2MPZ, K-Ala, K-Ser, and AEEA was obtained. It was found that all of the blend solutions showed a higher CO₂ loading capacity in comparison with pure

MEA. In addition, the addition of amine additive to K_2CO_3 showed positive effect on CO_2 loading. This is because the amino groups in the AEEA, 2MPZ, K-Ala and K-Ser are reactive and can absorb CO_2 . The CO_2 loading capacity of MEA + K-Lys and MDEA + K-Lys was also measured. It was observed that the CO_2 loading capacity increased with increasing CO_2 partial pressure due to an enhancement at the concentration gradient. As expected, temperature indicated a negative effect on the CO_2 loading capacity. This reduction in CO_2 loading can be explained by the fact that the equilibrium would shift in the backward direction with the increasing temperature and thus reducing the CO_2 loading. Based on the results, CO_2 loading of blend solution enhanced as concentration of K-Lys increased. The better absorption performance of MEA + K-Lys and MDEA + K-Lys in comparison to MEA make K-Lys an attractive additive to amines.

h. CO_2 absorption rate

The effect of addition of several amine additives on absorption rate of CO_2 in TSP and K_2CO_3 was studied. The experimental results showed the slower absorption rate of TSP and K_2CO_3 can be improved by addition of small amounts of amine additive. The small addition of TETA, PZ and 2MPZ in TSP provides a significant effect on the enhancement of the absorption rate. The absorption rate increases significantly as the additives concentration increases, but the enhancement in blend solutions containing MDEA is lower than other additives.

k. Reaction kinetics

The reaction kinetics between CO_2 and several solvents were studied using stirred cell reactor. The results showed that the investigated reactions belong to the pseudo-first-order fast reaction regime systems. The experimental results showed that the CO_2 absorption flux increases when partial pressure of CO_2 increases due to the fact that the driving force between gas phase and gas-liquid interface increases. Besides, it was found that the absorption flux of CO_2 decreases with absorption time and CO_2 loading due to the reduction of free concentration of solvent. In addition, at low CO_2 partial pressure, K-Lys showed faster absorption flux than MDEA while at high CO_2 partial pressure, MDEA indicates better absorption flux than K-Lys. Therefore, the addition of K-Lys at high pressure had no effect on absorption flux of CO_2 in MDEA + K-Lys. The absorption kinetic model was used to predict the absorption flux, enhancement factor and pressure decay in the reactor. A good agreement between experimental data and modeling results was observed.

m. Thermodynamic modeling

A thermodynamic model was successfully employed to predict measured CO_2 loading capacity of single and blend solution and description of the behavior of the experimental data. The values of concentration of liquid phase species were determined. A comparison between experimental CO_2 loading data and the modeling results showed that the model is able to describe experimental data well and provides good

prediction results. It was found, for MEA + CO₂ system, the concentration of carbamate reaches to a maximum value at CO₂ loading 0.5, and then as CO₂ loading increases, carbamate concentration decreases while concentrations of bicarbonate increase. For K-Lys + CO₂ system, it was observed that at low CO₂ loading, the carbamates, carbonate and LysH increase while Lys⁻ decreases. However, at high CO₂ loading, LysH gradually decrease and LysH⁺ increases. Since MDEA does not form carbamate, the protonated MDEA and bicarbonate are the main species in the solution. For PZ system, PZ carbamate and protonated PZ increase at low CO₂ loading and then as CO₂ loading increases, they get converted to PZ di-carbamate and protonated PZ carbamate.

The suggestions for this future work are as follows:

- a.** It is suggested to further work to measure absorption heat of CO₂ of solvent using calorimeter to determine the validity of reported absorption heat data. Actually, current efforts should be focused on the energy consumption of solvent to minimize total cost of process.
- b.** Since desorption is also an important process in CO₂ capture, it is necessary to study the performance of solvent in terms of desorption flux and desorption capacity. More experiments should be performed at desorption condition which means at high temperatures.
- c.** Another important parameter that needs to be considered when searching for new solvent is cyclic capacity. A solvent with high cyclic capacity is favorable for CO₂ capture because it reduce the size of the column, and then reduce absorbent circulation flow rate and process costs. Values of CO₂ cyclic capacity can be calculated from the difference between the CO₂ loading of solvent after absorption and the CO₂ loading of solvent after desorption. In this work the CO₂ loading of solvent after absorption for different solution was reported. Therefore, It is suggested to further work to measure CO₂ loading of solvent after desorption in order to determine cyclic capacity of solvent.
- d.** A systematic study is essential to investigate the volatility, surface tension, corrosion rate, amine degradation and thermal degradation of solvents at high temperature before applying of solvent to industrial use. These limitations such as the degradation of solvent not only decreases the CO₂ absorption rate and capacity but also increases the operation cost of CO₂ capture.
- e.** Although, amino acid showed a significant potential as a solvent for CO₂ capture, more work is needed to determine the long-term stability and amount of precipitation.
- f.** It is recommended that the performance of solvent should be evaluated under actual flue gas conditions. The effect of different impurities such as N₂, CH₄, O₂ on the CO₂ absorption need to be studied.
- g.** Since solvent in practical application are in CO₂ loaded state, more work is required to be conducted on CO₂ loaded solution. In the other words, future work should focus on physicochemical properties of CO₂ loaded absorbents to make better judgment about solvent.

List of symbols**Abbreviations**

AMP	2-amino-2-methylpropanol
AEEA	2-(2-aminoethylamino)ethanol
DEA	Diethanolamine
DEAE	2-diethylaminoethanol
EAE	Ethylaminoethanol
E-Glu	Ethyl-glutamate
DPTA	Dipropylenetriamine
DEEA	2-(diethylamino) ethanol
DETA	Diethylenetriamine
DEAB	4-(diethylamino)-2-butanol
Glu	Glutamate
His	Histidine
HMDA	Hexamethylenediamine
K-Ser	Potassium serinate
K-Pro	Potassium proline
K-Tau	Potassium taurate
K-Ala	Potassium alaninate
K-Lys	Potassium lysinate
K-Gly	Potassium glycinate
KOH	Potassium hydroxide
K ₂ CO ₃	Potassium carbonate
MEA	Monoethanolamine
MDEA	Methyldiethanolamine
MAPA	3-(methylamino) propylamine
PZEA	2-(1-piperaziny)-ethylamine
PZ	Piperazine
SG	Sodium glycinate
TEA	Triethanolamine
TSP	Trisodium phosphate
TETA	Triethylenetetramine
1-MPZ	1-methylpiperazine
2-MPZ	2-methylpiperazine

Greek symbols

α	CO ₂ loading capacity (mole CO ₂ /mole of absorbent)
ρ	Density (g/cm ³)
μ	Viscosity (mPa.s)

Alphabetical characters

A	Arrhenius constant (m ³ /kmol s)
A	Gas-liquid interfacial area
B	Base assisting in zwitterion deprotonation
b	Stoichiometric coefficient
D _{CO₂}	Diffusivity of CO ₂ (m ² /s)
D _{N₂O}	Diffusivity of N ₂ O (m ² /s)
D _{solvent}	Amine diffusion coefficient (m ² /s)
d _s	Stirrer dimension (m)
E _i	Enhancement factor
E	Activation energy (kJ/mol)
E _∞	Infinite enhancement factor
H _a	Hatta number
H _{CO₂}	Physical solubility of CO ₂ (kPa m ³ /kmol)
H _{N₂O}	Physical solubility of N ₂ O (kPa m ³ /kmol)
k _{OH⁻}	Reaction rate constant with hydroxide ion
k _{OV}	Overall pseudo-first-order reaction rate constant (1/s)
k ₁	Forward reaction rate constant (m ³ /kmol s)
k ₋₁	Reverse reaction rate constant (1/s)
k _{obs}	Observed reaction rate constant (1/s)
K _L	Liquid mass transfer coefficient (m/s)
k ₂	Second order rate constant (m ³ /kmol s)
K _i	Equilibrium constant
n _{solvent}	The moles of solvent in liquid phase
N ₂	Nitrogen
N ₂ O	Nitrous oxide
n	Order of the reaction with respect to amine
n _s	Speed of stirrer (1/s)
n _{solvent}	Mole of solvent in liquid phase
P _{CO₂}	Partial pressure of CO ₂ (kPa)
P _V	Vapor pressure of solution (kPa)

P_F	Final pressure of reactor (kPa)
P_1	Initial pressure in gas storage tank (kPa)
P_2	Final pressure in gas storage tank (kPa)
R_{OV}	Overall reaction rate of CO ₂ in solution
R	Mole fraction of additive
R	Gas constant (J/mol K)
V_R	Volumes of reactor
V_S	Volumes of solution
V_1	Volume of gas storage tank
V_2	Volume of reactor
$[CO_2]_i$	Interfacial concentration of CO ₂ (kmol/m ³)
$[CO_2]_b$	Concentration of CO ₂ in the bulk of liquid
T	Temperature (K)
t	Time (s)
ΔH	Heat of absorption (kJ/mol CO ₂)

List of publications

1. Camilla Costa, Renzo Di Felice, Paolo Moretti, Maddalena Oliva, Rouzbeh Ramezani, Piperazine and methyldiethanolamine interrelations in CO₂ absorption by aqueous amine mixture, *The Canadian Journal of Chemical Engineering*, 2020, (Accepted).
2. Rouzbeh Ramezani, Saeed Mazinani, Renzo Di Felice, A comprehensive kinetic and thermodynamic study of CO₂ absorption in blends of monoethanolamine and potassium lysinate: experimental and modeling, *Chemical Engineering Science*, 206 (2019) 187-202.
3. Rouzbeh Ramezani, Renzo Di Felice, Kinetics study of CO₂ absorption in potassium carbonate solution promoted by diethylenetriamine, *Green Energy & Environment*, 2020, (In Press)
4. Rouzbeh Ramezani, Saeed Mazinani, Renzo Di Felice, Characterization and kinetics of CO₂ absorption in potassium carbonate solution promoted by 2-methylpiperazine, *Journal of Environmental Chemical Engineering*, 6 (2018) 3262-3272.
5. Rouzbeh Ramezani, Saeed Mazinani, Renzo Di Felice, Potential of different additives to improve performance of potassium carbonate for CO₂ absorption, *Korean Journal of Chemical Engineering*, 35 (2018) 2065-2077.
6. Rouzbeh Ramezani, Saeed Mazinani, Renzo Di Felice, Experimental study of CO₂ absorption in potassium carbonate solution promoted by triethylenetetramine, *The Open Chemical Engineering Journal*, 12 (2018) 67-79.
7. Rouzbeh Ramezani, Saeed Mazinani, Renzo Di Felice, Siavash Darvishmanesh, Bart Van Der Bruggen, Selection of blended absorbents for CO₂ capture from flue gas: CO₂ solubility, corrosion and absorption rate, *International Journal of Greenhouse Gas Control*, 62 (2017) 61-68.
8. Rouzbeh Ramezani, Saeed Mazinani, Renzo Di Felice, Bart Van Der Bruggen, Experimental and correlation study of corrosion rate, absorption rate and CO₂ loading capacity in five blend solutions as new absorbents for CO₂ capture, *Journal of Natural Gas Science and Engineering*, 45 (2017) 599-608.

References

- [1] G. Hu, N. Nicholas, K. Smith, K. Mumford, S. Kentish, Carbon dioxide absorption into promoted potassium carbonate solutions: A review, *Int. J. Greenh. Gas Con.* 53 (2016) 28-40.
- [2] B. Zhao, W. Tao, M. Zhong, Y. Su, G. Cui, Process, performance and modeling of CO₂ capture by chemical absorption using high gravity: A review. *Renew. Sust. Energ. Rev.* 65 (2016) 44-56.
- [3] G. Capannelli, A. Comite, C. Costa, R. Di Felice, Effect of absorbent type and concentration on CO₂ capture from a gas stream into a liquid phase, *Ind. Eng. Chem. Res.* 52 (2013) 13128-13136.
- [4] https://19january2017snapshot.epa.gov/ghgemissions/overview-greenhouse-gases_.html
- [5] <http://www.ccsassociation.org/what-is-ccs/>
- [6] D. Jansen, M. Gazzani, G. Manzolini, E. Dijk, M. Carbo, Pre-combustion CO₂ capture, *Int. J. Greenh. Gas Con.* 40 (2015) 167-187.
- [7] <https://gcaptain.com>
- [8] R. Franca, A. Azapagic, Carbon capture, storage and utilisation technologies: A critical analysis and comparison of their life cycle environmental impacts, *Journal of CO₂ Utilization* 9 (2015) 82-102.
- [9] Ch. Nwaoha, T. Supap, R. Idem, Ch. Saiwan, P. Tontiwachwuthikul, Advancement and new perspectives of using formulated reactive amine blends for post-combustion carbon dioxide capture technologies. *Petroleum* 3 (2017) 10-36.
- [10] www.4cleanair.org
- [11] <http://www.zeroco2.no/introduction/what-is-ccs>
- [12] A. Setameteekul, A. Aroonwilas, A. Veawab, Statistical factorial design analysis for parametric interaction and empirical correlations of CO₂ absorption performance in MEA and blended MEA/MDEA processes, *Sep. Purif. Technol.* 64 (2008) 16-25.
- [13] Zh. Liang, W. Rongwong, H. Liu, K. Fu, H. Gao, Recent progress and new developments in post-combustion carbon-capture technology with amine based solvents, *International Journal of Greenhouse Gas Control* 40 (2015) 26-54.
- [14] J. Yu, Sh. Wang, Modeling analysis of energy requirement in aqueous ammonia based CO₂ capture process, *Int. J. Greenh. Gas Con.* 43 (2015) 33-45.
- [15] Sh. Shen, Y. Yang, Y. Wang, Sh. Ren, J. Han, CO₂ absorption into aqueous potassium salts of lysine and proline: density, viscosity and solubility of CO₂, *Fluid Phase Equilib* 399 (2015) 40-49.
- [16] Y.E. Kim, S.H. Yun, J.H. Choi, S.Ch. Nam, S.Y. Park, Comparison of the CO₂ absorption characteristics of aqueous solutions of diamines: absorption capacity, specific heat capacity, and heat of absorption, *Energy Fuels* 29 (2015) 2582-2590.
- [17] <http://www.frames-group.com/>
- [18] B. Mondal, A. Samanta, Equilibrium solubility and kinetics of CO₂ absorption in hexamethylenediamine activated aqueous sodium glycinate solvent, *Chem. Eng. J.* (2019).

- [19] T. Zarogiannis, A. Papadopoulos, P. Seferlis, Systematic selection of amine mixtures as post-combustion CO₂ capture solvent candidates, *J. Clean Prod.* 136 (2016) 159-175.
- [20] A. Lee, K.A. Mumford, Y. Wu, N. Nicholas, G.W. Stevens, Understanding the vapour-liquid equilibrium of CO₂ in mixed solutions of potassium carbonate and potassium glycinate, *Int. J. Greenh. Gas Con.* 47 (2016) 303-309.
- [21] M. Xiao, H. Liu, R. Idem, P. Tontiwachwuthikul, Zh. Liang, A study of structure-activity relationships of commercial tertiary amines for post-combustion CO₂ capture, *Applied Energy* 184 (2016) 219-229.
- [22] X. Luo, K. Fu, Zh. Yang, H. Gao, W. Rongwong, Experimental studies of reboiler heat duty for CO₂ desorption from triethylenetetramine and triethylenetetramine + methyldiethanolamine, *Ind. Eng. Chem. Res.* 54 (2015) 8554-8560.
- [23] M. Shaikh M, A. Shariff, M. Bustam, G. Murshid, Physical properties of aqueous blends of sodium glycinate (SG) and piperazine (PZ) as a solvent for CO₂ capture. *J. Chem. Eng. Data* 58 (2013) 634-638.
- [24] A. Shariff, M. Shaikh, Aqueous amino acid salts and their blends as efficient absorbents for CO₂ capture, Wojciech M. Budzianowski, *Energy Efficient Solvents for CO₂ capture by gas-liquid absorption*, (2016) 117-151.
- [25] G. Fytianos, U. Seniz, A. Grimstvedt, A. Hyldbakk, H. Svendsen, Corrosion and degradation in MEA based post-combustion CO₂ capture. *Int. J Greenh. Gas Con.* 46 (2016) 48-56.
- [26] G. Murshid, W. But, Investigation of thermophysical properties for aqueous blends of sarcosine with 1-(2-aminoethyl) piperazine and diethylenetriamine as solvents for CO₂ absorption. *J. Mol. Liq.* 278 (2019) 584-591.
- [27] H. Song, S. Park, H. Kim, A. Gaur, J. Park, Carbon dioxide absorption characteristics of aqueous amino acid salt solutions, *Int. J. Greenh. Gas Con.* 11 (2012) 64-72.
- [28] U. Aronu, K. Hoff, H. Svendsen, Vapor-liquid equilibrium in aqueous amine amino acid salt solution: 3-(methylamino)propylamine/sarcosine. *Chem. Eng. Sci.* 66 (2011) 3859-3867.
- [29] S. Garg, A. Shariff, M. Shaikh, B. Lal, Experimental data, thermodynamic and neural network modeling of CO₂ solubility in aqueous sodium salt of L-phenylalanine. *Journal of CO₂ Utilization* 19 (2017) 146-156.
- [30] A. Aftab, A. Shariff, S. Garg, B. Lal, M. Shaikh, Solubility of CO₂ in aqueous sodium alaninate: Experimental study and modeling using Kent Eisenberg model. *Chem. Eng. Res. Des.* 131 (2018) 385-392.
- [31] S. Garg, A. Shariff, M. Shaikh, B. Lal, A. Aftab, VLE of CO₂ in aqueous potassium salt of L-phenylalanine: Experimental data and modeling using modified Kent-Eisenberg model. *J. Nat. Gas Sci. Eng.* 34 (2016) 864-872.

- [32] P. Kumar, J. Hogendoorn, S. Timmer, P. Feron, G. Versteeg, Equilibrium solubility of CO₂ in aqueous potassium taurate solutions: Part 2. Experimental VLE data and model. *Ind. Eng. Chem. Res.* 42 (2003) 2841-2852.
- [33] C. Wei, G. Puxty, P. Feron, Amino acid salts for CO₂ capture at flue gas temperatures *Chem. Eng. Sci.* 107 (2014) 218-226.
- [34] H. Song, S. Lee, S. Maken, J. Park, J. Park, Solubilities of carbon dioxide in aqueous solutions of sodium glycinate. *Fluid Phase Equilibria* 246 (2006) 1-5.
- [35] A. Portugal, J. Sousa, F. Magalhães, A. Mendes, Solubility of carbon dioxide in aqueous solutions of amino acid salts. *Chem. Eng. Sci.* 64 (2009) 1993-2002.
- [36] Zh. Chen, Rh. Leron, M. Li, Equilibrium solubility of carbon dioxide in aqueous potassium Lasparaginate and potassium L-glutamate solutions. *Fluid Phase Equilibria* 400 (2015) 20-26.
- [37] M. Majchrowicz, D. Brillman, Solubility of CO₂ in aqueous potassium L-prolinate solutions-absorber conditions. *Chem. Eng. Sci.* 72 (2012) 35-44.
- [38] H. Song, M. Lee, H. Kim, A. Gaur, J. Park, Density, viscosity, heat capacity, surface tension, and solubility of CO₂ in aqueous solutions of potassium serinate, *J. Chem. Eng. Data* 56 (2011) 1371-1377.
- [39] J. Lim, D. Kim, Y. Yoon, S. Jeong, K. Park, Absorption of CO₂ into aqueous potassium salt solutions of alanine and proline. *Energy Fuels* 26 (2012) 3910-3918.
- [40] D. Kang, S. Park, H. Jo, J. Min, J. Park, Solubility of CO₂ in amino-acid-based solutions of (potassium sarcosinate), (potassium alaninate + PZ), and (potassium serinate + PZ) *J. Chem. Eng. Data* 58 (2013) 1787-1791.
- [41] Y. Chang, R. Leron, M. Li, Carbon dioxide solubility in aqueous potassium salt solutions of L-proline and aminobutyric acid at high pressures, *J. Chem. Thermodynamics* 83 (2015) 110-116.
- [42] Sh. Shen, Y. Zhao, Y. Bian, Y. Wang, H. Guo, CO₂ absorption using aqueous potassium lysinate solutions: Vapor-liquid equilibrium data and modelling, *J. Chem. Thermodynamics* 115 (2017) 209-220.
- [43] K. Shen, P. Li, Solubility of carbon dioxide in aqueous mixtures of monoethanolamine with methyldiethanolamine, *J. Chem. Eng. Data* 37 (1992) 96-100.
- [44] U. Aronu, H. Svendsen, K. Hoff, Investigation of amine amino acid salts for carbon dioxide absorption, *Int. J. Greenh. Gas Con* 4 (2010) 771-775.
- [45] Y. Zhao, Y. Bian, H. Li, H. Guo, S. Shen, J. Han, A comparative study of aqueous potassium lysinate and aqueous monoethanolamine for post-combustion CO₂ capture, *Energy Fuels* 31 (2017) 14033-14044.
- [46] Y. Bian, Y. Zhao, Sh. Shen, Characteristics of potassium prolinate + water + ethanol solution as a phase changing absorbent for CO₂ capture, *J. Chem. Eng. Data* 62 (2017) 3169-3177.

- [47] S. Garg, G. Murshid, F. Mjalli, A. Ali, W. Ahmad, Experimental and correlation study of selected physical properties of aqueous blends of potassium sarcosinate and 2-piperidineethanol as a solvent for CO₂ capture, *Chem. Eng. Res. Des.* 118 (2017) 121-130.
- [48] S. Garg, A. Shariff, M. Shaikh, B. Lal, A. Aftab, Selected physical properties of aqueous potassium salt of l-phenylalanine as a solvent for CO₂ capture, *Chem. Eng. Res. Des.* 113 (2016) 169-181.
- [49] M. Shaikh, A. Shariff, S. Garg, M. Bustam, Physical properties of aqueous solutions of potassium L-prolinate from 298.15 to 343.15 K at atmospheric pressure. *Chemical Papers* 71 (2017) 1185-1194.
- [50] M. Shaikh, A. Shariff, A. Bustam, G. Murshid, Physicochemical properties of aqueous solutions of sodium prolinate as an absorbent for CO₂ removal. *J. Chem. Eng. Data* 59 (2014) 362-368.
- [51] M. Shaikh, A. Shariff, M. Bustam, Physicochemical properties of aqueous solutions of sodium glycinate in the non-precipitation regime from 298.15 to 343.15 K. *Chin. J. Chem. Eng.* 23 (2015) 536-540.
- [52] C. Perinu, I. Bernhardsen, H. Knuutila, NMR speciation of aqueous MAPA, tertiary amines, and their blends in the presence of CO₂: influence of pK_a and reaction mechanisms. *Ind. Eng. Chem. Res.* 57 (2018) 1337-1349.
- [53] J. Holst, G. Versteeg, D. Brillman, J. Hogendoorn, Kinetic study of CO₂ with various amino acid salts in aqueous solution. *Chem. Eng. Sci.* 64 (2009) 59-68.
- [54] G. Hu, K. Smith, Y. Wu, S. Kentish, G. Stevens, Screening amino acid salts as rate promoters in potassium carbonate solvent for carbon dioxide absorption. *Energy Fuels* 31 (2017) 4280-4286.
- [55] S. Shen, Y. Yang, Y. Zhao, Y. Bian, Reaction kinetics of carbon dioxide absorption into aqueous potassium salt of histidine. *Chem. Eng. Sci.* 146 (2016) 76-87.
- [56] Sh. Shen, Y. Yang, Carbon dioxide absorption into aqueous potassium salt solutions of arginine for post-combustion capture, *Energy Fuels* 30 (2016) 6585-6596.
- [57] A. Portugal, P. Derks, G. Versteeg, F. Magalhaes, A. Mendes, Characterization of potassium glycinate for carbon dioxide absorption purposes *Chem. Eng. Sci.* 62 (2017) 6534-6547.
- [58] <https://www.sigmaaldrich.com>
- [59] Sh. Shen, Y. Yang, Y. Bian, Y. Zhao, Kinetics of CO₂ absorption into aqueous basic amino acid salt: potassium salt of lysine solution. *Environ. Sci. Technol.* 50 (2016) 2054-2063.
- [60] M. Kim, H. Song, M. Lee, H. Jo, J. Park, Kinetics and steric hindrance effects of carbon dioxide absorption into aqueous potassium alaninate solutions. *Ind. Eng. Chem. Res.* 51 (2012) 2570-2577.
- [61] M. Majchrowicz, S. Kersten, W. Brillman, Reactive absorption of carbon dioxide in prolinate salt solutions. *Ind. Eng. Chem. Res.* 53 (2014) 11460-11467.
- [62] P. Kumar, J. Hogendoorn, G. Versteeg, Kinetics of the reaction of CO₂ with aqueous potassium salt of taurine and glycine, *AIChE Journal* 49 (2003) 203-213.

- [63] K. Simons, W. Brilman, H. Mengers, K. Nijmeijer, Kinetics of CO₂ absorption in aqueous sarcosine salt solutions: influence of concentration, temperature, and CO₂ loading. *Ind. Eng. Chem. Res.* 49 (2010) 9693-9702.
- [64] A. Portugal, F. Magalhaes, A. Mendes, Carbon dioxide absorption kinetics in potassium threonate, *Chem. Eng. Sci.* 63 (2008) 3493-3503.
- [65] B. Yu, H. Yu, K. Li, Q. Yang, R. Zhang, L. Li, Characterisation and kinetic study of carbon dioxide absorption by an aqueous diamine solution, *Applied Energy* 208 (2017) 1308-1317.
- [66] N. Mahmud, A. Benamor, M. Nasser, M. Al-Marri, H. Qiblawey, P. Tontiwachwuthikul, Reaction kinetics of carbon dioxide with aqueous solutions of arginine, glycine & sarcosine using the stopped flow technique. *Int. J. Greenh. Gas Con.* 63 (2017) 47-58.
- [67] D. Guo, H. Thee, G. Tan, J. Chen, W. Fei, S. Kentish, G. Stevens, G. Silva, Amino acids as carbon capture solvents: chemical kinetics and mechanism of the glycine + CO₂ reaction. *Energy Fuels* 27 (2013) 3898-3904.
- [68] U. Aronu, A. Hartono, K. Hoff, H. Svendsen, Kinetics of carbon dioxide absorption into aqueous amino acid salt: potassium salt of sarcosine solution. *Ind. Eng. Chem. Res.* 50 (2011) 10465-10475.
- [69] G. Hu, K. Smith, Y. Wu, K. Mumford, S. Kentish, G. Stevens, Carbon dioxide capture by solvent absorption using amino acids: A review. *Chin. J. Chem. Eng.* 26 (2018) 2229-2237.
- [70] S. Park, Y. Son, D. Park, K. Oh, Absorption of carbon dioxide into aqueous solution of sodium glycinate. *Sep. Sci. Technol.* 43 (2008) 3003-3019.
- [71] Q. Xiang, M. Fang, H. Yu, M. Maeder, Kinetics of the reversible reaction of CO₂ and HCO₃⁻ with sarcosine salt in aqueous solution. *J. Phys. Chem. A* 116 (2012) 10276-10284.
- [72] S. Paul, K. Thomsen, Kinetics of absorption of carbon dioxide into aqueous potassium salt of proline, *Int. J. Greenh. Gas Con.* 8 (2012) 169-179.
- [73] K. Hwang, D. Park, K. Oh, S. Kim, S. Park, Chemical absorption of carbon dioxide into aqueous solution of potassium threonate, *Sep. Sci. Technol.* 45 (2010) 497-507.
- [74] G. Hu, K. Smith, L. Liu, S. Kentish, G. Stevens, Reaction kinetics and mechanism between histidine and carbon dioxide, *Chem. Eng. J.* 307 (2017) 56-62.
- [75] A. Sodiq, A. Rayer, A. Olanrewaju, M. Zhra, Reaction kinetics of carbon dioxide absorption in sodium salts of taurine and proline using a stopped-flow technique, *Int. J. Chem. Kinet.* 46 (2014) 730-745.
- [76] J. Ying, D. Eimer, Determination and measurements of mass transfer kinetics of CO₂ in concentrated aqueous monoethanolamine solutions by a stirred cell, *Ind. Eng. Chem. Res.* 52 (2013) 2548-2559.
- [77] S. Lee, S. Choi, S. Maken, H. Song, H. Shin, Physical properties of aqueous sodium glycinate solution as an absorbent for carbon dioxide removal, *J. Chem. Eng. Data* 50 (2005) 1773-1776.

- [78] S. Park, H. Song, J. Park, Selection of suitable aqueous potassium amino acid salts: CH₄ recovery in coal bed methane via CO₂ removal, *Fuel Process. Technol.* 120 (2014) 48-53.
- [79] F. He, T. Wang, M. Fang, Z. Wang, H. Yu, Screening test of amino acid salts for CO₂ absorption at flue gas temperature in a membrane contactor, *Energy Fuels* 31 (2017) 770-777.
- [80] H. Svendsen, E. Hessen, T. Mejdell, Carbon dioxide capture by absorption, challenges and possibilities, *Chem. Eng. J.* 171 (2011) 718-724.
- [81] M. Majchrowicz, W. Brilman, Amino acid salts for carbon dioxide capture: evaluating proline at desorber conditions, *Energy Fuels* 29 (2015) 3268-3275.
- [82] Y. Zhao, Sh. Shen, Y. Bian, Y. Yang, U. Ghosh, CO₂ solubility in aqueous potassium lysinate solutions at absorber conditions, *J. Chem. Thermodynamics* 111 (2017) 100-105.
- [83] U. Aronu, E. Hessen, T. Warberg, K. Hoff, H. Svendsen, Vapor-liquid equilibrium in amino acid salt system: Experiments and modeling, *Chem. Eng. Sci.* 66 (2011) 2191-2198.
- [84] V. Salazar, Y. Sanchez-Vincente, C. Pando, J. Renuncio, Enthalpies of absorption of carbon dioxide in aqueous sodium glycinate solutions at temperatures of (313.15 and 323.15) K, *J. Chem. Eng. Data* 55 (2010) 1215-1218.
- [85] U. Aronu, I. Kim, G. Haugen, Evaluation of energetic benefit for solid-liquid phase change CO₂ absorbents. *Energy Procedia* 63 (2014) 532-541.
- [86] M. Majchrowicz, D. Brilman, M. Groeneveld, Precipitation regime for selected amino acid salts for CO₂ capture from flue gases. *Energy Procedia* 1 (2009) 979-984.
- [87] M. Rabensteiner, G. Kinger, M. Koller, C. Hochenauer, PCC pilot plant studies with aqueous potassium glycinate. *Int. J. Greenh. Gas Con.* 42 (2015) 562-570.
- [88] P. Kumar, Development and design of membrane gas absorption processes. Ph.D. Thesis, University of Twente, Enschede, Netherlands, 2002.
- [89] Q. Huang, S. Bhatnagar, J. Remias, J. Selegue, K. Liu, Thermal degradation of amino acid salts in CO₂ capture. *Int. J. Greenh. Gas Con.* 19 (2013) 243-250.
- [90] N. Aldenkamp, P. Huttenhuis, N. Elk, E. Hamborg, Solubility of carbon dioxide in aqueous potassium salts of glycine and taurine at absorber and desorber conditions. *J. Chem. Eng. Data* 59 (2014) 3397-3406.
- [91] B. Epp, F. Hans, V. Monika, Degradation of solutions of monoethanolamine, diglycolamine and potassium glycinate in view of tail-end CO₂ absorption. *Energy Procedia* 4 (2011) 75-80.
- [92] S. Moiola, L. Pellegrini, M. Ho, D. Wiley, A comparison between amino acid based solvent and traditional amine solvent processes for CO₂ removal, *Chem. Eng. Res. Des.* 146 (2019) 509-517.
- [93] S. Mazinani, R. Ramazani, A. Jahanmiri, B. Van der Bruggen, Equilibrium solubility, density, viscosity and corrosion rate of carbon dioxide in potassium lysinate solution. *Fluid Phase Equilibria* 396 (2015) 28-34.

- [94] S. Mazinani, A. Samsami, A. Jahanmiri, Solubility, density, viscosity, and corrosion rate of carbon dioxide in blend solutions of monoethanolamine (MEA) and sodium glycinate (SG). *J. Chem. Eng. Data* 56 (2011) 3163-3168.
- [95] S. Ahn, H. Song, J. Park, I. Lee, K. Jang, Characterization of metal corrosion by aqueous amino acid salts for the capture of CO₂, *Korean J. Chem. Eng.* 27 (2010) 1576-1580.
- [96] A. Talkhan, A. Benamor, M. Nasser, H. Qiblawey, S. El-Tayeb, Corrosion study of carbon steel in CO₂ loaded solution of methyldiethanolamine and L-arginine mixtures. *J Electroanal. Chem.* 837 (2019) 10-21.
- [97] H. Balsora, M. Mondal, Solubility of CO₂ in an aqueous blend of diethanolamine and trisodium phosphate, *J. Chem. Eng. Data* 56 (2011) 4691-4695.
- [98] C. Anderson, T. Harkin, M. Ho, K. Mumford, A. Qader, G. Stevens, B. Hooper, *Energy Procedia* 37, 225 (2013).
- [99] H. Balsora, M. Mondal, Solubility of CO₂ in aqueous TSP, *Fluid Phase Equilib* 328 (2012) 21- 24.
- [100] Sh. Xu, Y. Wang, Kinetics of the reaction of carbon dioxide with 2-amino-2-methyl-1-propanol solutions, *Chem. Eng. Sci.* 51 (1996) 841-850.
- [101] Sh. Ma'mun, H. Svendsen, K. Hoff, O. Juliussen, Selection of new absorbents for carbon dioxide capture, *Energy Conversion and Management* 48 (2007) 251-258.
- [102] A. Rayer, Y. Armugam, A. Henni, P. Tontiwachwuthikul, High-pressure solubility of carbon dioxide in aqueous 1-methyl piperazine solution, *J. Chem. Eng. Data* 59 (2014) 3610-3623.
- [103] H. Thee, Y. A. Suryaputradinata, K. A. Mumford, K. H. Smith, G. da Silva, A kinetic and process modeling study of CO₂ capture with MEA-promoted potassium carbonate solutions, *Chem. Eng. J.* vol. 210 (2012) 271-279.
- [104] R. Muraleedharan, A. Mondal, B. Mandal, Absorption of carbon dioxide into aqueous blends of 2-amino-2-hydroxymethyl-1,3-propanediol and monoethanolamine, *Separation and Purification Technology* 94 (2012) 92-96.
- [105] A. Haghtalab, H. Eghbali, A. Shojaeian, Experiment and modeling solubility of CO₂ in aqueous solutions of Diisopropanolamine + 2-amino-2-methyl-1-propanol + Piperazine at high pressures, *J. Chem. Thermodynamics* 71 (2014) 71-83.
- [106] F. Camacho, S. Sanchez, R. Pacheco, A. Sanchez, M. La Rubia, Absorption of carbon dioxide at high partial pressures in aqueous solutions of di-isopropanolamine, *Ind. Eng. Chem. Res.* 44 (2005) 7451-7457.
- [107] T. Sema, A. Naami, Zh. Liang, H. Shi, A. Rayer, Part 5b: Solvent chemistry: reaction kinetics of CO₂ absorption into reactive amine solutions. *Carbon Management* 3 (2012) 201-220.
- [108] Ch. Liao, M. Li, Kinetics of absorption of carbon dioxide into aqueous solutions of monoethanolamine + methyldiethanolamine, *Chem. Eng. Sci.* 57 (2002) 4569-4582.

- [109] L. Sanchez, G. Meindersma, A. Haan, Kinetics of absorption of CO₂ in amino-functionalized ionic liquids. *Chem. Eng. J.* 166 (2011) 1104-1115.
- [110] Z. Wu, Z. Huang, Y. Zhang, Y. Qin, J. Ma, Kinetics analysis and regeneration performance of 1-butyl-3-methylimidazolium glycinate solutions for CO₂ capture, *Chem. Eng. J.* 295 (2016) 64-72.
- [111] S. Kumar Dash, A. Samanta, A. Samanta, S. Bandyopadhyay, Absorption of carbon dioxide in piperazine activated concentrated aqueous 2-amino-2-methyl-1-propanol solvent, *Chem. Eng. Sci.* 66 (2011) 3223-3233.
- [112] D. Fu, L. Wang, P. Zhang, Ch. Mi, Solubility and viscosity for CO₂ capture process using MEA promoted DEAE aqueous solution, *J. Chem. Thermodynamics* 95 (2016) 136-141.
- [113] U. Aronu, A. Hartono, H. Svendsen, Kinetics of carbon dioxide absorption into aqueous amine amino acid salt: 3-(methylamino)propylamine/sarcosine solution, *Chem. Eng. Sci.* 66 (2011) 6109-6119.
- [114] R. Hook, An investigation of some sterically hindered amines as potential carbon dioxide scrubbing compounds. *Ind. Eng. Chem. Res.* 36 (1997) 1779-1790.
- [115] P. Danckwerts, The reaction of CO₂ with ethanolamines. *Chem. Eng. Sci.* 34 (1979) 443-446.
- [116] S. Bishnoi, G.T. Rochelle, Absorption of carbon dioxide into aqueous piperazine: reaction kinetics, mass transfer and solubility, *Chem. Eng. Sci.* 22 (2000) 5531-5543.
- [117] V. Ermatchkov, A. Kamps, G. Maurer, Chemical equilibrium constants for the formation of carbamates in (carbon dioxide + piperazine + water) from NMR-spectroscopy, *J. Chem. Thermodyn.* 35 (2003) 1277-1289.
- [118] A.T. Zoghi, F. Feyzi, S. Zarrinpashneh, Equilibrium solubility of carbon dioxide in a 30 wt.% aqueous solution of 2-((2-aminoethyl)amino)ethanol at pressures between atmospheric and 4400 kPa: An experimental and modelling study, *J. Chem. Thermodyn.* 44 (2012) 66-74.
- [119] Donaldson TL, Nguyen YN. Carbon dioxide reaction kinetics and transport in aqueous amine membranes. *Ind. Eng. Chem. Fundam.* 10 (1980) 260-266.
- [120] J. G. Amann, Ch. Bouallou, Kinetics of the absorption of CO₂ in aqueous solutions of methyldiethanolamine + triethylenetetramine, *Ind. Eng. Chem. Res.* 48 (2009) 3761-3770.
- [121] Zh. Pei, Sh. Yao, W. Jianwen, Zh. Wei, Y. Qing, Regeneration of 2-amino-2-methyl-1-propanol used for carbon dioxide absorption, *J. Environ. Sci.* 20 (2008) 39-44.
- [122] M. Caplow, Kinetics of carbamate formation and breakdown. *J Am Chem Soc.* 90 (1968) 6795-6803.
- [123] K. Mumford, K. Smith, C. Anderson, S. Shen, W. Tao, Y. Suryaputradinata, *Energy Fuels* 26 (2012) 138.
- [124] H. Knuutila, O. Juliussen, H. F. Svendsen, Kinetics of the reaction of carbon dioxide with aqueous sodium and potassium carbonate solutions, *Chem. Eng. Sci.* 65 (2010) 6077-6088.

- [125] A. Hartonoa, E. daSilvab, H. F.Svendsen, Kinetics of carbon dioxide absorption in aqueous solution of diethylenetriamine (DETA), *Chem. Eng. Sci.* 64 (2009) 3205-3213.
- [126] B. Liu, X. Luo, H. Gao, R. Idem, P. Tontiwachwuthikul, W. Olson, Zh. Liang, Reaction kinetics of the absorption of carbon dioxide in aqueous solutions of sterically hindered secondary alkanolamines using the stopped-flow technique, *Chem. Eng. Sci.* 170 (2017) 16-25.
- [127] Sh. Shen, Y. Yang, Y. Zhao, Y. Bian, Reaction kinetics of carbon dioxide absorption into aqueous potassium salt of histidine, *Chem. Eng. Sci.* 146 (2016) 76-87.
- [128] E. Rinker, S. Ashour, O. Sandall, Kinetics and modeling of carbon dioxide absorption into aqueous solutions of diethanolamine. *Ind. Eng. Chem. Res.* 35 (1996) 1107-1114.
- [129] A. Aboudheir, P. Tontiwachwuthikula, A. Chakma, R. Idem, Kinetics of the reactive absorption of carbon dioxide in high CO₂-loaded, concentrated aqueous monoethanolamine solutions, *Chem. Eng. Sci.* 58 (2003) 5195-5210.
- [130] S. DJ, H. WH, Effect of piperazine on the kinetics of carbon dioxide with aqueous solutions of 2-amino-2-methyl-1-propanol. *Ind. Eng. Chem. Res.* 39 (2000) 2062-2067.
- [131] H. Kierzkowska-Pawlak, Kinetics of CO₂ absorption in aqueous diethylethanolamine and its blend with (2-aminoethyl)ethanolamine using a stirred cell reactor, *Int. J. Greenh. Gas Con.* 37 (2015) 76-84.
- [132] J. Nathalie, P. Elka, E. Hamborga, Kinetics of absorption of carbon dioxide in aqueous amine and carbonate solutions with carbonic anhydrase, *Int. J. Greenh. Gas Control* 12 (2013) 259-268.
- [133] J. Carson, K. Marsh, A. Mather, Enthalpy of solution of carbon dioxide in (water + monoethanolamine, or diethanolamine, or *N*-methyldiethanolamine) and (water+monoethanolamine +methyldiethanolamine) at $T=298$, *J. Chem. Thermodyn.* 32 (2000) 1285-1296.
- [134] J. Lee, F. Otto, A. Mather, Solubility of carbon dioxide in aqueous diethanolamine solutions at high pressures, *J. Chem. Eng. Data* 17 (1972) 465-468.
- [135] S. Rho, Y. Lee, J. Nam, S. Son, J. Min, Solubility of CO₂ in Aqueous Methyldiethanolamine Solutions, *J. Chem. Eng. Data* 42 (1997) 1161-1164.
- [136] M. Li, K. Shen, Calculation of equilibrium solubility of carbon dioxide in aqueous mixtures of monoethanolamine with methyldiethanolamine, *Fluid Phase Equilibria*, 85 (1993) 85, 129-140.
- [137] Ch. Nwaoha, R. Idem, T. Supap, Ch. Saiwan, P. Tontiwachwuthikul, Heat duty, heat of absorption, sensible heat and heat of vaporization of amino-2-Methyl-1-Propanol (AMP), Piperazine (PZ) and Monoethanolamine (MEA) tri-solvent blend for carbon dioxide (CO₂) capture, *Chem. Eng. Sci.* 170 (2017) 26-35.
- [138] N. Hadri, D. Quang, E. Goetheer, M. Abu Zahra, Aqueous amine solution characterization for post-combustion CO₂ capture process, *Applied Energy* 185 (2017) 1433-1449.

- [139] Standard reference test method for making potentiostatic and potentiodynamic anodic polarization measurements. in annual book of ASTM standards; American Society of Testing and Materials: West Conshohocken, PA, 2004.
- [140] J. Lee, I. Otto, Equilibrium between carbon dioxide and aqueous monoethanolamine solutions, *J. Appl. Chem. Bio. Techn*, 26 (1976) 541-549.
- [141] J.H. Song, J.H. Yoon, H. Lee, K. Lee, Solubility of carbon dioxide in monoethanolamine + ethylene glycol + water and monoethanolamine + poly(ethyleneglycol) + water, *J. Chem. Eng. Data*, 45 (1996) 497-499.
- [142] J. Kittel, S. Gonzalez, Corrosion in CO₂ Post-Combustion Capture with Alkanolamines-A Review, *Oil & Gas Science and Technology*, 69 (2014) 915-929.
- [143] Tada Y, Yano N, Takahashi H, Yuzawa K, Ando H, Kubo Y, A. Nagasawa J. *Toxicol. Pathol.* 23 (2010) 39.
- [144] <https://www.cir-safety.org/sites/default/files>
- [145] <http://www.sciencelab.com/msds>
- [146] PerkinElmer, <https://www.perkinelmer.com>
- [147] <http://www.cdhfinechemical.com/images/product/msds>
- [148] <https://onlinelibrary.wiley.com/doi/pdf/10.1002/3527600418.mb10559kske0009>
- [149] <https://pubchem.ncbi.nlm.nih.gov>
- [150] <https://www.caymanchem.com/msdss/700517m.pdf>
- [151] <http://www.merckmillipore.com>
- [152] <https://www.fishersci.com/>
- [153] <https://www.scribd.com/document/391127473/msds>
- [154] J. Tosh, J. Field, H. Benson, W. Haynes, U. S. Bureau of Mines Rept. Invest. 5484, 23 (1959).
- [155] F. Chowdhury, H. Okabe, H. Yamada, M. Onoda, Y. Fujioka, Synthesis and selection of hindered new amine absorbents for CO₂ capture, *Energy Procedia* 4 (2011) 201-208.
- [156] I. Kim, H. Svendsen, Heat of absorption of carbon dioxide (CO₂) in monoethanolamine (MEA) and 2-(aminoethyl)ethanolamine (AEEA) solutions, *Ind. Eng. Chem. Res.* 46 (2007) 5803-5809.
- [157] M. Hilliard, Ph.D. Dissertation, The University of Texas at Austin, 2008.
- [158] I. Kim, K. Hoff, E. Hessen, T. Haug-Warberg, H. Svendsen, Enthalpy of absorption of CO₂ with alkanolamine solutions predicted from reaction equilibrium constants, *Chem. Eng. Sci.* 64 (2009) 2027-2038.
- [159] Y. Kim, J. Choi, S. Yun, S. Nam, Y. Yoon, CO₂ capture using aqueous solutions of K₂CO₃+2-methylpiperazine and monoethanolamine: Specific heat capacity and heat of absorption *Korean J. Chem. Eng.* 33 (2016) 3465-3472.

- [160] J. Cullinane, G. Rochelle, Carbon dioxide absorption with aqueous potassium carbonate promoted by piperazine, *Chem. Eng. Sci.* 59 (2004) 3619-3630.
- [161] B. Mondal, S. Bandyopadhyay, A. Samanta, Equilibrium solubility and enthalpy of CO₂ absorption in aqueous bis(3-aminopropyl) amine and its mixture with MEA, MDEA, AMP and K₂CO₃, *Chem. Eng. Sci.* 170 (2017) 58-67.
- [162] H. Lia, Y. Moullec, J. Lu, J. Chen, J. Marcos, G. Chen, Solubility and energy analysis for CO₂ absorption in piperazine derivatives and their mixtures, *Int. J. Greenh. Gas Con.* 31 (2014) 25-32.
- [163] P. Chung, A. Soriano, R. Leron, M. Li, Equilibrium solubility of carbon dioxide in the amine solvent system of (triethanolamine+piperazine + water), *J. Chem. Thermodynamics* 42 (2010) 802-807.
- [164] S. Paul, A. Ghoshal, B. Mandal, Kinetics of absorption of carbon dioxide into aqueous blends of 2-(1-piperazinyl)-ethylamine and methyldiethanolamine, *Chem. Eng. Sci.* 64 (2009) 1618-1622.
- [165] J. K. Clarke, Kinetics of absorption of carbon dioxide in monoethanolamine solutions at short contact times. *Ind. Eng. Chem. Fundam.* 3 (1964) 239-245.
- [166] S. S. Laddha, J. M. Diaz, P. V. Danckwerts, The N₂O analogy: The solubilities of CO₂ and N₂O in aqueous solutions of organic compounds. *Chem. Eng. Sci.* 36 (1981) 228-229.
- [167] K. Fu, G. Chen, Zh. Liang, T. Sema, R. Idem, Analysis of mass transfer performance of monoethanolamine-based CO₂ absorption in a packed column using artificial neural networks, *Ind. Eng. Chem. Res.* 53 (2014) 4413-4423.
- [168] H. Kierzkowska-Pawlak, Kinetics of CO₂ absorption in aqueous diethylethanolamine and its blend with (2-aminoethyl)ethanolamine using a stirred cell reactor, *Int. J. Greenh. Gas Con.* 37 (2015) 76-84.
- [169] P. Danckwerts, 1970. *Gas-Liquid Reactions*. McGraw-Hill, New York.
- [170] G. Astarita, D.W. Savage, J.M. Longo, Promotion of carbon dioxide mass transfer in carbonate solutions, *Chem. Eng. Sci.* 36 (1981) 581-588.
- [171] H. Kierzkowska-Pawlak, A. Chacuk, Kinetics of CO₂ desorption from aqueous methyldiethanolamine solutions, *Chem. Eng. J.* 168 (2011) 367-375.
- [172] G. Kumar, T. Mondal, M. Kundu, Solubility of CO₂ in aqueous blends of (diethanolamine+2-amino-2-methyl-1-propanol) and (diethanolamine + methyldiethanolamine), *J. Chem. Eng. Data* 57 (2012) 670-680.
- [173] S. Park, K. Lee, J. Hyun, S. Kim, Correlation and prediction of the solubility of carbon dioxide in aqueous alkanolamine and mixed alkanolamine solutions, *Ind. Eng. Chem. Res.* 41 (2002) 1658-1665.

- [174] S. Dash, S. Bandyopadhyay, Studies on the effect of addition of piperazine and sulfolane into aqueous solution of methyldiethanolamine for CO₂ capture and VLE modelling using NRTL equation *J. Greenh. Gas Con.* 44 (2016) 227-237.
- [175] M.S. Shaikh, A. Shariff, M. Bustam, Gh. Murshid, Measurement and prediction of physical properties of aqueous sodium l-prolinate and piperazine as a solvent blend for CO₂ removal, *chemical engineering research and design* 102 (2015) 378-388.
- [176] Sh. Horng, M. Li, Kinetics of absorption of carbon dioxide into aqueous solutions of monoethanolamine + triethanolamine, *Ind. Eng. Chem. Res.* 41 (2002) 257-266.
- [177] W. Sun, Ch. Yong, M. Li, Kinetics of the absorption of carbon dioxide into mixed aqueous solutions of 2-amino-2-methyl-1-propanol and piperazine, *Chem. Eng. Sci.* 60 (2005) 503-516.
- [178] B. Mondal, S. Bandyopadhyay, A. Samanta, Kinetics of CO₂ absorption in aqueous hexamethylenediamine blended methyldiethanolamine, *Ind. Eng. Chem. Res.* 56 (2017) 14902-14913.
- [179] J. Xiao, Ch. Li, M. Li, Kinetics of absorption of carbon dioxide into aqueous solutions of 2-amino-2-methyl-1-propanol + monoethanolamine, *Chem. Eng. Sci.* 55 (2000) 161-175.
- [180] A. Benamor, M. Al-Marri, M. Khraisheh, M. Nasser, P. Tontiwachwuthikul, Reaction kinetics of carbon dioxide in aqueous blends of methyldiethanolamine and glycine using the stopped flow technique, *J. Nat. Gas Sci. Eng.* 33 (2016) 186-195.
- [181] Ch. Lin, A. Soriano, M. Li, Kinetics study of carbon dioxide absorption into aqueous solutions containing N-methyldiethanolamine + diethanolamine, *J. Taiwan Inst. Chem. E.* 40 (2009) 403-412.
- [182] F. Jou, A. Mather, F. Otto, Solubility of H₂S and CO₂ in aqueous methyldiethanolamine solutions, *Ind. Eng. Chem. Process Des. Dev.* 21 (1982) 539-544.
- [183] A. Dey, S. Dash, B. Mandal, Equilibrium CO₂ solubility and thermophysical properties of aqueous blends of 1-(2-aminoethyl) piperazine and methyldiethanolamine, *Fluid Phase Equilibria* 463 (2018) 91-105.
- [184] B. Mondal, S. Bandyopadhyay, A. Samanta, Equilibrium solubility measurement and Kent-Eisenberg modeling of CO₂ absorption in aqueous mixture of methyldiethanolamine and hexamethylenediamine, *Greenhouse Gas Sci. Technol.* 7 (2017) 202-214.
- [185] F. Murrieta, M. Rebolledo, A. Romero-Martínez, A. Trejo, Solubility of CO₂ in aqueous mixtures of diethanolamine with methyl diethanolamine and 2-amino-2-methyl-1-propanol, *Fluid Phase Equilib.* 150 (1998) 721-729.
- [186] B. Mondal, S. Bandyopadhyay, A. Samanta, Equilibrium solubility and enthalpy of CO₂ absorption in aqueous bis(3-aminopropyl) amine and its mixture with MEA, MDEA, AMP and K₂CO₃, *Chem. Eng. Sci.* 170 (2017) 58-67.

- [187] D. Silkenbäumer, B. Rumpf, R. Lichtenthaler, Solubility of carbon dioxide in aqueous solutions of 2-amino-2-methyl-1-propanol and n-methyldiethanolamine and their mixtures in the temperature range from 313 to 353 K and pressures up to 2.7 MPa. *Ind. Eng. Chem. Res.* 37 (1998) 3133-3141.
- [188] B. García, M. Estrada, Densities and excess molar volumes of aqueous solutions of methyldiethanolamine (MDEA) at temperatures from (283.15 to 363.15) K, *J. Chem. Eng. Data* 48 (2003) 1442-1445.
- [189] N. Ghani, N. Sairi, N. Aroua, Y. Alias, R. Yusoff, R. Density, surface tension, and viscosity of ionic liquids (1-ethyl-3-methylimidazolium diethylphosphate and 1,3-dimethylimidazolium dimethylphosphate) aqueous ternary mixtures with MDEA, *J. Chem. Eng. Data* 59 (2014) 1737-1746.
- [190] H. Pawlak, A. Chacuki, Kinetics of carbon dioxide absorption into aqueous MDEA solutions, *Ecol. Chem. Eng. S* 17 (2010) 463-475.
- [191] E. Rinker, S. Ashour, O. Sandall, Kinetics and modeling of carbon dioxide absorption into aqueous solutions of methyldiethanolamine, *Chem. Eng. Sci.* 50 (1995) 755-768.
- [192] N. Haimour, A. Bidarian, O. Sandall, Kinetics of the reaction between carbon dioxide and methyldiethanolamine, *Chem. Eng. Sci.* 42 (1987) 1393-1398.
- [193] J. Ko, M. Li, Kinetics of absorption of carbon dioxide into solutions of methyldiethanolamine + water, *Chem. Eng. Sci.* 55 (2000) 4139-4147.
- [194] I. Bernhardsen, H. Knuutila, Kinetics of CO₂ absorption into aqueous solutions of 3-dimethylamino-1-propanol and 1-(2-hydroxyethyl)pyrrolidine in the blend with 3-(methylamino)propylamine, *Chemical Engineering Science: X* 3 (2019) 100032.
- [195] I. Bernhardsena, L. Ansalonia, H. Betten, L. Deng, H. Knuutila, Effect of liquid viscosity on the performance of a non-porous membrane contactor for CO₂ capture, *Separation and Purification Technology* 222 (2019) 188-201.
- [196] X. Luo, A. Hartono, H. Svendsen, Comparative kinetics of carbon dioxide absorption in unloaded aqueous monoethanolamine solutions using wetted wall and string of discs columns, *Chem. Eng. Sci.* 82 (2012) 31-43.
- [197] X. Luo, A. Hartono, S. Hussain, H. Svendsen, Mass transfer and kinetics of carbon dioxide absorption into loaded aqueous monoethanolamine solutions, *Chem. Eng. Sci.* 123 (2015) 57-69.
- [198] F. Jou, A. Mather, F. Otto, Solubility of H₂S and CO₂ in aqueous methyldiethanolamine solutions, *Ind. Eng. Chem Process. Des. Dev.* 21 (1982) 539-544.
- [199] M. Posey, K. Tapperson, G. Rochelle, A simple model for prediction of acid gas solubilities in alkanolamines. *Gas. Sep. Purif.* 10 (1996) 181-186.
- [200] D. Tong, G. Maitland, M. Trusler, P. Fennell, Solubility of carbon dioxide in aqueous blends of 2-amino-2-methyl-1-propanol and piperazine, *Chem. Eng. Sci.* 101 (2013) 851-864.

- [201] W. Fouad, A. Berrouk, Prediction of H₂S and CO₂ solubilities in aqueous triethanolamine solutions using a simple model of Kent-Eisenberg type, *Ind. Eng. Chem. Res.* 51 (2012) 6591-6597.
- [202] T. Sema, A. Naami, R. Idem, P. Tontiwachwuthikul, Correlations for equilibrium solubility of carbon dioxide in aqueous 4-(diethylamino)-2-butanol solutions, *Ind. Eng. Chem. Res.* 50 (2011) 14008-14015.
- [203] Y. Chang, Rh. Leron, M. Li, Equilibrium solubility of carbon dioxide in aqueous solutions of (diethylenetriamine + piperazine), *J. Chem. Thermodynamics* 64 (2013) 106-113.
- [204] M. Wagner, I. Harbou, J. Kim, I. Ermatchkova, G. Maurer, Solubility of carbon dioxide in aqueous solutions of monoethanolamine in the low and high gas loading regions, *J. Chem. Eng. Data* 58 (2013) 883-895.
- [205] M.Z. Haji-Sulaiman, M.K. Aroua, A. Benamor, Analysis of equilibrium data of CO₂ in aqueous solutions of diethanolamine (DEA), methyldiethanolamine (MDEA) and their mixtures using the modified Kent-Eisenberg model, *Chem. Eng. Res. Des.* 76 (1998) 961-968.